Flexible optical transport networks : benefits of the combination of time and spectral domains to adapt the granularity of optical resources to the needs of operators

Bing Han

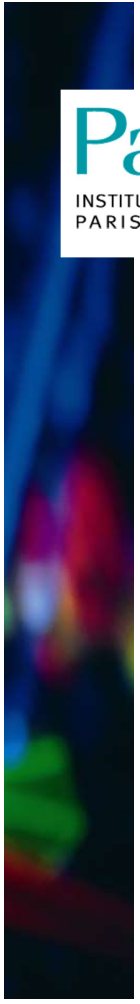

ParisTech
INSTITUT DES SCIENCES ET TECHNOLOGIES
PARIS INSTITUT OF TECHNOLOGY

TELECOM ParisTech

2018-ENST-0018

EDITE ED 130

Doctorat ParisTech

T H È S E

pour obtenir le grade de docteur délivré par

Télécom ParisTech

Spécialité “ Communications & Electronique ”

présentée et soutenue publiquement par

Bing HAN

le 05 Avril 2018

Réseaux de transport optique flexibles : apport de la combinaison des domaines temporel et spectral pour adapter la granularité des ressources optiques aux besoins de l’opérateur

Directeur de thèse : **Yves JAOUEN**

Jury

M. Philippe GRAVEY, IMT- Atlantique de Brest	Rapporteur
M. Nicola CALABRETTA, Eindhoven University of Technology	Rapporteur
M. Dominique CHIARONI, Nokia Bell Labs	Examinateur
Mme. Catherine LEPERS, Télécom Sud Paris	Examinateur
M. Laurent BRAMERIE, ENSSAT	Examinateur
M. Yves JAOUEN, Télécom ParisTech	Directeur de thèse
Mme. Paulette GAVIGNET, Orange Labs	Invité
M. Erwan PINCEMIN, Orange Labs	Invité

T H È S E

Télécom ParisTech
école de l’Institut Mines Télécom – membre de ParisTech
46, rue Barrault – 75634 Paris Cedex 13 – Tél. + 33 (0)1 45 81 77 77 – www.telecom-paristech.fr

Acknowledgements

First of all, I would like to deliver my gratitude to all my honorable jury members. I would like to thank Mr. Philippe GRAVEY from IMT- Atlantique de Brest and Mr. Nicola CALABRETTA from Eindhoven University of Technology, for accepting the role of reporters to review my thesis and for their constructive comments to improve the quality of this thesis. Moreover, I would like to thank Mrs. Catherine LEPERS from Télécom Sud Paris that has been the president of the thesis committee and Mr. Dominique CHIARONI from Nokia Bell Labs and Mr. Laurent BRAMERIE from ENSSAT for accepting to be a member of the jury committee.

I would like to express my sincere gratitude to my thesis supervisor Paulette Gavignet. I really appreciated your constructive advices, useful suggestions on my thesis and the large amount of time and effort that you dedicate to my PhD work.

I would like to extend my heartfelt gratitude to my thesis supervisor Erwan Pincemin. You deserve gratitude for the invaluable contribution and help you have made on my PhD work. I consider it an honor to work with you and I enjoyed the conference journey with you.

It is with immense gratitude that I acknowledge the support and help of my thesis director Yves Jaouen. Thank you very much for your continuous guide and encouragement in my PhD work. I am really grateful for your suggestions and advices on my thesis.

I would like to thank all my colleagues and my friends in SOAN team of Orange Labs and in COMELEC of Télécom ParisTech: Nicolas, Esther, Bernard, Thierry, Luay, Antoine, Clara, Mengdi, Heming … …, for their direct and indirect support and help. And also thanks for their kindness; with them the working environment is very amiable.

Résumé de la thèse

Introduction

L'augmentation du débit des interfaces de transmission à 100 Gbit/s et au-delà est maintenant une réalité. Cette nécessité de devoir transporter toujours plus de débit dans les réseaux cœur a été le moteur des avancées technologiques qui ont vu le jour et continuent à être étudiées chez les équipementiers et dans les laboratoires de recherche.

La contrepartie de cette augmentation de la granularité du débit des interfaces est que le remplissage peut être relativement inefficace si ce n'est au travers d'une agrégation électronique coûteuse en interfaces de conversion optique-électrique-optique (O-E-O) et peu économes en énergie.

Il existe cependant deux solutions optiques qui permettent d'accéder à la granularité sous la longueur d'onde conduisant ainsi à une meilleure utilisation des ressources en remplissant plus efficacement les canaux de transmission. La première utilise le domaine temporel : il s'agit de la solution SLPSN (Sub-Lambda Photonically Switched Networks) [1], la seconde utilise le domaine spectral, il s'agit de l'OFDM multi-bandes (Orthogonal Frequency Division Multiplexing) [2].

Etat de l'art

Solutions pour l'accès à la granularité sous la longueur d'onde

Les solutions SLPSN

Les solutions SLPSN (Sub-Lambda Photonically Switched Networks) [1] ont ainsi été identifiées comme permettant non seulement l'utilisation efficace de la ressource de transport [3] mais également comme une solution de partage des interfaces dans les réseaux cœur et métropolitain dans le domaine optique.

Ces solutions reposent sur la commutation photonique de tranches temporelles de longueurs d'onde appelées rafales (bursts), slots ou plus généralement SLPS Units (SLPSU). De ce fait les solutions SLPSN se démarquent des techniques TDM telles que OTN/SDH mais aussi des techniques paquets (ATM, Ethernet, IP, …) qui opèrent cette commutation dans le domaine électrique. Elles se

démarquent également des solutions Optical Circuit Switching (OCS), (utilisant des ROADMs : Reconfigurable Optical Add-Drop Multiplexers) qui réalisent la commutation de longueurs d'onde entières, pour de très longues durées et avec des temps de commutation/reconfiguration lents (de l'ordre de la dizaine de millisecondes).

L'agrégation optique réalisée avec les solutions SLPSN permet en effet de bénéficier du multiplexage statistique et ainsi obtenir un remplissage efficace des longueurs d'onde.

Le concept initial de commutation optique de rafales de données ou "Optical Burst Switching" (OBS) a été introduit en 1999 par C.M. Qiao et M.S. Yoo pour compenser le manque de flexibilité des réseaux optiques à commutation de circuits et l'immaturité des techniques de commutation de paquets optiques (Optical Packet Switching). Cette solution a notamment été poussée par l'augmentation des volumes de trafic et la généralisation du trafic IP, se traduisant par un trafic de plus en plus sporadique ("bursty") de nature « paquet ».

Contrairement à la commutation optique de paquets, l'OBS consiste à rassembler un certain nombre de paquets destinés au même nœud d'extrémité dans une seule rafale. Cette façon de faire permet d'avoir des rafales de durée plus longue que les paquets IP natifs, et ainsi de relâcher les contraintes techniques (vitesse de traitement) au niveau des nœuds. Comme la durée des rafales reste faible (quelques µs à quelques ms), l'OBS bénéficie d'un multiplexage statistique significatif qui améliore le remplissage des canaux. De ce point de vue, l'OBS est un bon compromis entre complexité technique et performance. Mais contrairement à la commutation électronique, l'OBS ne bénéficie pas de la possibilité d'avoir des mémoires optiques, et contourne ce problème ou bien en utilisant des méthodes de gestion de contentions de rafales ou bien en contrôlant finement les périodes d'émission au niveau des sources.

Outre la capacité des rafales optiques à améliorer l'efficacité des réseaux de transport, on espère des techniques SLPSN une réduction forte de la consommation électrique de ces derniers. Cette réduction est justifiée par le fait qu'idéalement, les rafales de données sont aiguillés dans les réseaux SLPSN sans aucun traitement électronique, et que seul le traitement des paquets de contrôle y est éventuellement effectué.

De nombreuses variantes et déclinaisons dérivées de la notion originale OBS ont été proposées dans la littérature. Un critère pertinent pour classer ces différentes déclinaisons d'OBS est leur capacité à transmettre avec ou sans pertes de rafales.

Les solutions sans perte apparaissent cependant être les seules permettant d'atteindre des performances compatibles avec les exigences d'un réseau opérationnel.

Parmi les solutions les plus prometteuses, la solution basée sur du routage passif TWIN (Time-domain Wavelength Interleaved Networking) et étudiée dans [3], combine aiguillage en longueur d'onde et planification de l'accès à la longueur d'onde. L'aiguillage en longueur d'onde se base sur la pré-configuration d'arbres de couleur. L'aiguillage d'une rafale est réalisé par exemple par sa coloration à l'émission sur la longueur d'onde correspondant à l'arbre que l'on souhaite emprunter. La rafale est ainsi aiguillée vers la racine (ou destination) de l'arbre. Cette technique d'aiguillage permet d'éviter les dispositifs de commutation rapide dans les nœuds traversés (nœuds de cœur du réseau), tandis que la programmation des allocations des longueurs d'onde sur les arbres permet d'utiliser efficacement les ressources optiques (émetteurs, récepteurs, canaux de longueur d'onde) sans aucune perte de collision.

Les éléments technologiques (spécifiquement) nécessaires sont les lasers accordables rapidement et la synchronisation en temps.

La technologie super-channel

Une autre solution pour accéder à la granularité sous-longueur d'onde est d'utiliser le concept super-channel qui est constitué de différentes bandes de fréquence indépendantes que l'on peut router dans un réseau maillé séparément. On a ainsi accès optiquement à un canal de transmission de capacité plus faible sans avoir besoin de recourir aux conversions O-E-O augmentant par voie de conséquence l'étendue géographique de la zone de transparence optique.

Il y a deux formats de modulation permettant de construire super-channel : Orthogonal Frequency Division Multiplexing multi-bandes (MB-OFDM) et Nyquist Wavelength Division Multiplexing (Nyquist-WDM). Tous les deux technologies sont des technologies multi-bandes, et ont atteint une haute efficacité spectrale, plus de 5 bits/s/Hz, en utilisant de haute commande quadrature amplitude modulation (QAM) format. Dans [4], les auteurs ont démontré expérimentalement que Nyquist-WDM et MB-OFDM ont des performances similaires en termes de débit binaire, de portée de distance, de tolérance aux effets non linéaires des fibres, de granularité sous-bande et de bande de garde. Cependant, ils ont toujours 2 différences principales. Premièrement, OFDM se déploie toujours avec la technologie d'estimation de canal assistée par données tandis que Nyquist-WDM est souvent implémenté avec la technologie d'estimation de canal aveugle, qui indique que le temps de traitement d'estimation de canal d'OFDM est beaucoup plus court que le temps de Nyquist-WDM. Deuxièmement, OFDM offre la possibilité d'implémenter la technologie de bit&power loading, qui a été démontré de pouvoir atteindre un débit binaire plus élevé, atteindre une distance plus longue et montrer plus de tolérance de désaccord de fréquence que la solution Nyquist-WDM dans la transmission en mode rafale optique. En conclusion, la solution OFDM multi-bandes est plus adaptée à la transmission en mode rafale optique que Nyquist-WDM

La technologie OFDM multi-bandes consiste à juxtaposer les bandes spectrales correspondant à plusieurs signaux OFDM indépendants de façon à transporter des débits plus élevés que ce que permettrait une technologie mono-bande. Chaque signal OFDM est constitué de plusieurs centaines de sous-porteuses (128, 256, 512, …).

La largeur de bande des signaux OFDM est limitée par la performance des convertisseurs numérique-analogique (DAC) qui ont aujourd'hui typiquement une bande passante de 15 GHz. On peut imaginer générer des signaux OFDM qui auront dans le domaine optique une largeur de bande allant de 10 GHz à 30 GHz. Dans cette largeur de bande, on peut faire passer des débits allant de 10 Gbit/s à 100 Gbit/s. L'exemple ci-dessous fournit un cas de figure typique de gestion du spectre optique grâce à la technologie OFDM multi-bandes.

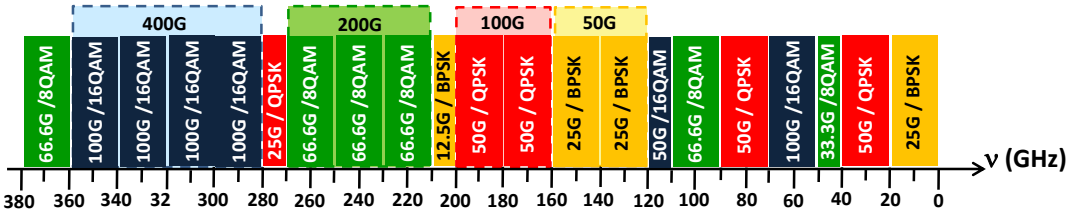

Figure 1 : Gestion du spectre de la fibre avec la technologie MB-OFDM.

Dans cet exemple, chaque bande est indépendante et est générée par son propre émetteur. On peut regrouper ensemble des bandes dans un super-canal, car elles partent d'une même origine pour aller vers une même destination. La largeur du signal OFDM et la modulation portée par les sous-porteuses constitutives du signal OFDM peuvent être choisies en fonction de la capacité et de la portée visée (comme dans l'exemple de la Figure 1). Par exemple, la modulation BPSK a une portée en transmission très grande mais une efficacité spectrale faible, alors qu'à l'inverse la modulation 16-QAM a une portée limitée mais une très bonne efficacité spectrale.

Avec la technologie Nyquist WDM, l'efficacité spectrale la plus élevée est obtenue avec la modulation 16-QAM qui permet de transporter 200 Gbit/s dans une bande passante de 37.5 GHz. Cette efficacité spectrale résulte d'un compromis entre capacité transportée et robustesse à l'accumulation de bruit d'émission spontanée amplifiée (ASE) et des effets non-linéaires de propagation dans la fibre (effet Kerr qui engendre SPM, XPM, et FWM). Avec la technologie OFDM, comme illustré sur Figure 1, on peut imaginer faire passer 100 Gbit/s dans 20 GHz de bande passante avec la modulation 16-QAM, ce qui génère peu ou prou la même efficacité spectrale maximale que la technologie Nyquist-WDM.

Limitations de chacune des solutions

Les solutions SLPSN

Il existe quantité de solutions SLPSN dans la littérature, cependant toutes n'offrent pas le même niveau de qualité de transport. Les plus prometteuses sont à notre avis celles qui interdisent la perte de rafales. Nous nous intéressons spécifiquement aux solutions qui utilisent l'aiguillage par la longueur d'onde, telle que décrit plus haut, car elles reposent sur des briques technologiques (lasers accordables) réalisables aujourd'hui. Il y a cependant deux manières d'implémenter ces solutions :

- *accord à la source :* dans ce cas on associe une longueur d'onde à une destination et la source émet son SLPSU à la longueur d'onde de la destination avec laquelle elle veut communiquer,
- *accord à la réception* : dans ce cas la source émet toujours ses SLPSU à la même longueur d'onde, c'est chaque récepteur qui s'accorde à la longueur d'onde des SLPSUs qui lui sont destinés.

En général chaque nœud source est aussi un nœud destination donc la taille du réseau (nombre de sources/destinations) est limitée par le nombre de longueurs d'onde transitant dans le réseau. Les systèmes de transmission WDM (Wavelength Division Multiplexing) actuellement déployés dans les réseaux transportent environ 80 longueurs d'onde. Il est possible d'augmenter un peu ce nombre en utilisant les bandes de transmission C+L ou en réduisant l'espacement entre canaux mais pour cette 2ème solution on est limité par le fait que le débit augmentant, la bande passante des canaux possède une valeur minimale incompressible.

D'autre part, la durée minimale, et donc le quantum de données transmises dans une rafale optique, est de l'ordre de plusieurs microsecondes compte tenu du temps de reconfiguration des différents éléments nécessaires à l'envoi de la rafale (laser accordable, récepteur mode rafale, …). Actuellement, pour un débit de 10 Gbit/s par exemple, le nombre de bits dans une rafale de 4.5 µs [3] est de 45000 (soit 5625 octets) ce qui représente plusieurs trames Ethernet. Il est donc nécessaire de construire la rafale en mettant dans des files d'attente, les paquets ou trames devant constituer la rafale. Selon la manière dont sont assemblés les rafales (prise en compte de la qualité de service, fragmentation ou non, taille de rafales fixe ou variable, …) la construction de la rafale conduit à une latence des paquets/trames ce qui a un impact négatif sur les services offerts et notamment les services temps réel. Il serait donc intéressant de pouvoir envoyer par exemple une seule trame Ethernet (ou un seul paquet de données) par rafale avec une adaptation du format de la rafale au format de la trame Ethernet (ou du paquet de données) ce qui pourrait permettre de remplir plus efficacement la rafale (éviter les signal intervalles lors de la constitution de la rafale avec des trames Ethernet) ou alors éviter la fragmentation (solution utilisée pour remplir complètement les rafales mais qui nécessite des mécanismes complexes pour étiqueter les morceaux de trames/paquets et les reconstituer).

L'augmentation des débits des interfaces à 100 Gbit/s voire plus (requis par les besoins d'augmentation de la capacité par fibre) vont rendre ce conteneur beaucoup plus grand (> 56000 octets, accentuant encore ces questions de latence et de remplissage des rafales.

Une technique permettant d'accéder à des granularités plus petites que les rafales pourrait donc être avantageuse.

La technologie OFDM multi-bandes dans le concept super-channel

Chaque bande du signal OFDM multi-bandes peut être extraite du signal global (multi-bandes) à l'aide de filtres optiques très sélectifs. Toutefois, ces filtres ont une granularité en bande passante de l'ordre de 10 GHz. Cette valeur de 10 GHz représente une limite de ce que l'on peut espérer réalisable dans les dix années à venir. Comme illustré sur Figure 1, un slot spectral de 10 GHz peut typiquement transporter de 12.5 Gbit/s à 50 Gbit/s, ce qui peut être encore trop grand pour effectuer un remplissage efficace de cette bande. Par conséquent, accéder à une granularité plus fine apporterait plus de flexibilité dans l'attribution des ressources de transport.

D'autre part, la technologie MB-OFDM n'est pas pour le moment mise en œuvre par les industriels, car elle nécessite l'utilisation de convertisseurs numérique-analogique (DAC) et d'ASIC pour faire du traitement de signal numérique (DSP : Digital Signal Processing) dans le transmetteur. Mais avec le développement de la solution mono-porteuse Nyquist-WDM et l'utilisation de la modulation 16-QAM pour les débits supérieurs à 100 Gbit/s, la mise en œuvre de DAC et de DSP à l'émission devient indispensable. L'OFDM n'a donc plus ce désavantage vis-à-vis des techniques mono-porteuses.

La solution TISA

Nous avons souligné les avantages et les inconvénients des solutions de commutation de sous-longueurs d'onde temporelles et spectrales dans les paragraphes précédents. Ici, une nouvelle approche est proposée: la solution TIme and Spectral Optical Aggregation (TISA) [5]. TISA combine la solution TWIN et la technologie multi-bandes dans le concept super-channel permettant une agrégation et une désagrégation optique pure dans les domaines temporels et spectraux avec la granularité de sous-longueur d'onde la plus fine possible. TISA permet de construire un réseau de topologie maillée et réalise un routage de base de longueur d'onde.

Combinant la solution TWIN et la technologie multi-bandes, TISA bénéficie des avantages de chaque solution. Dans TISA, chaque source envoie des données sous forme de rafales qui n'occupent qu'une sous-bande. Les données sont modulées dans le format OFDM. Chaque sous-bande est associée à une destination, et chaque nœud source est capable de générer des données dans

différentes sous-bandes. La destination est fixe, ce qui signifie qu'elle reçoit les rafales à une seule longueur d'onde. Ainsi, le routage est également fait sur une base de longueur d'onde, comme dans la solution TWIN. L'agrégation de données, le routage et la désagrégation des données sont réalisés de manière purement optique. Pour la même raison que dans le réseau TWIN, TISA présente un risque potentiel de collision en rafale aux nœuds principaux. Afin de garantir le routage sans perte, un contrôleur centralisé est implémenté pour gérer soigneusement le signal de rafales en termes de temps d'émission et de sous-bande allouée. La solution TISA est composée d'un plan de commande et d'un plan de transfert. Le pan de commande exécute tous les processus liés à l'allocation des ressources réseau, à la configuration des équipements, à la synchronisation du réseau. Le plan de transfert réalise physiquement la transmission de données d'un nœud à l'autre. Il est composé des nœuds de bord, des combinateurs, des séparateurs et des nœuds principaux.

L'objectif de cette thèse est de construire un Proof of Concept (PoC) de TISA pour démontrer expérimentalement sa faisabilité. Ensuite, la performance TISA sera évaluée pour voir si l'opération en mode rafale apporte une pénalité, et si TISA permet d'allouer une ressource réseau avec une granularité fine. Dans les paragraphes suivants de ce chapitre, nous présenterons le concept TISA en détail (d'abord le plan de transfert, puis le plan de commande) et ses blocs de construction.

Plan de transfert

Le plan de transfert fait référence à la couche physique (c.-à-d. La couche 1 du modèle de réseau OSI) dans le réseau: elle assure toutes les fonctions et les processus liés au transfert de données d'un nœud à l'autre (d'une source à une destination). Figure 2 présente un exemple simple de plan de transfert pour le réseau TISA. Dans cet exemple, il existe cinq groupes de nœuds de périphérie et deux nœuds de noyau: les groupes de nœuds de périphérie Am et Bj (m, j de 1 à 4) sont des nœuds source et les groupes de nœuds de périphérie Ci, Dn et Ek (i, n, k de 1 à 4) sont des nœuds de destination. Une seule direction de transmission est représentée dans cet exemple. Les rectangles gris avec différents types de motifs représentent les rafales de données envoyées vers les groupes de nœuds C et E, tandis que chaque type de motif représente une sous-bande. Les rectangles colorés représentent les rafales de données envoyées vers le groupe de nœuds D, et chaque couleur représente une sous-bande associée à un nœud Dn. Chaque rectangle représente une rafale de données et tous les rectangles simples, qui ont seulement une couleur ou un motif, ont des dimensions uniformes (c'est-à-dire la durée et la bande passante occupée). Les rafales multicolores ou les rafales multi-motifs représentent les rafales multi-bandes qui occupent une plus grande bande passante.

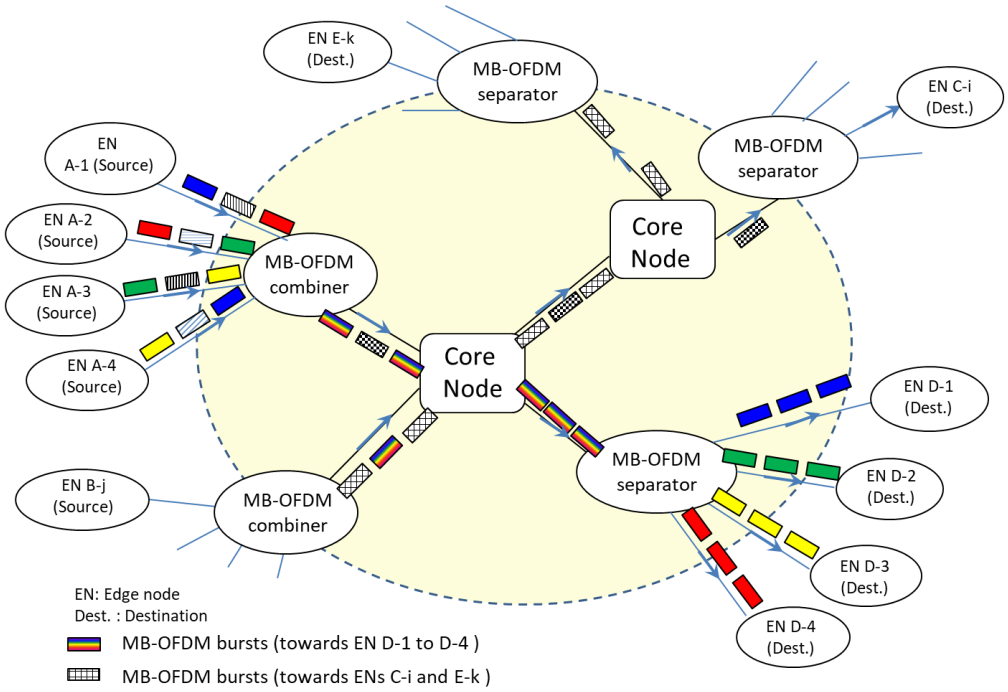

Figure 2 : Un exemple de plan de transfert pour le réseau TISA.

Dans cet exemple, le cercle jaune central représente la même fonction de routage que dans le réseau TWIN. Le routage est basé sur la longueur d'onde (c'est-à-dire la grille de 50 GHz) et est réalisé purement optiquement. Chaque nœud de périphérie source du réseau TWIN est remplacé par un combinateur MB-OFDM associé à 4 nœuds sources. Ces nœuds sources peuvent être placés à différentes distances du combineur. Chaque source est capable d'envoyer les données au format OFDM sous la forme de rafales à différentes longueurs d'onde. Chaque rafale occupe une seule sous-bande et chaque sous-bande est associée à une destination. Après l'émission des rafales, les rafales provenant de différents nœuds sources entrent d'abord dans le combineur MB-OFDM. Le combineur collecte passivement et de manière transparente les données de rafales et les aligne en une rafale composée de plusieurs bandes occupant toute une largeur de bande de 50 GHz (qui est une structure similaire au super-canal mais en mode rafale). Une rafale multi-bande est envoyée vers le nœud central à la place de 4 rafales. Ce schéma permet de réutiliser la structure de réseau SLPSN. Cependant, l'alignement des rafales au niveau du combineur augmentera la complexité du contrôle, mais comme TISA est une solution à créneaux temporels, l'absence d'alignement des rafales entraînera une perte d'efficacité d'utilisation du canal. En conséquence, l'alignement est nécessaire. Après l'alignement des rafales, la rafale multi-bande entre dans le nœud central.

Viennent ensuite les nœuds de routage de rafales multi-bandes OFDM ; il s'agit des mêmes nœuds que ceux utilisés dans la solution TWIN. Ils peuvent être constitués de démultiplexeurs avec une grille spectrale fixe ou alors de WSS de façon à permettre une reconfiguration (lente) du réseau notamment dans le cas de la protection.

Concernant les séparateurs de bandes, ils sont constitués de filtres très sélectifs en longueurs d'onde (granularité minimale de 10 GHz) utilisés dans les solutions multi-bandes OFDM. Les filtres développés sont basés sur l'utilisation de technologie « optique en espace libre » (avec réseau de diffraction et monochromateur) et bientôt sur les technologies LCOS (Liquid Crystal on Silicon) largement utilisées par les industriels aujourd'hui.

Chaque nœud de périphérie est équipé d'un émetteur et d'un récepteur, c'est donc un nœud source ainsi qu'un nœud de destination. La transmission de données dans le réseau est bidirectionnelle dans une paire de fibres optiques. Un nœud de périphérie est associé simultanément au combinateur et au séparateur MB-OFDM. La commutation optique est réalisée à deux niveaux: le niveau de bande entier (50 GHz) aux nœuds de base et le niveau de sous-bande aux combinateurs et séparateurs MB-OFDM. Ce schéma permet de réutiliser l'architecture TWIN et le réseau TISA alloue la ressource réseau avec une granularité plus fine pour chaque nœud source en même temps. Dans TISA, le nombre de nœuds périphériques est lié au nombre de sous-bandes au lieu du nombre de longueurs d'onde dans la bande C avec la norme de réseau fixe ITU-T 50 GHz, ce qui permet d'avoir plus de nœuds périphériques dans le réseau à une approche purement TWIN.

Plan de commande

Au-dessus du plan de transfert, un plan de commande est construit pour gérer le plan de transfert et tous les périphériques associés. Le plan de commande assure toutes les fonctionnalités et les processus concernant la synchronisation du réseau, l'allocation des ressources réseau, la configuration des équipements.

Comme TISA est un réseau synchronisé, la première tâche du plan de commande dans TISA est de garantir la synchronisation de l'ensemble du réseau. Nous choisissons une solution largement utilisée pour réaliser la synchronisation du réseau réel à grande échelle: nous implémentons une horloge à chaque nœud de périphérie et toutes les horloges sont synchronisées, elles ont donc le même rythme et le même temps. Nous pouvons également distribuer une horloge commune à chaque nœud. Mais il y a toujours une incertitude temporelle entre chaque nœud. Comme toutes les rafales doivent être envoyées à un moment précis dans le réseau TISA, cette incertitude de temps peut conduire à une mauvaise heure d'envoi en rafale et induire ainsi un chevauchement des différentes rafales. Afin de surmonter ce problème, il est proposé d'insérer un intervalle de temps entre deux rafales successives, appelé temps de garde. Le temps de garde est plus grand que l'incertitude temporelle de l'horloge du nœud, de sorte qu'il n'y a pas de chevauchement même si le temps d'envoi de la rafale n'est pas aussi précis que nous le souhaitons. La valeur de l'incertitude de synchronisation est un paramètre important pour la conception du temps de garde. Afin de donner une référence pour la conception du temps de garde, nous avons choisi le Global Positioning System

(GPS) [6, 7] comme source d'horloge avec une haute précision à implémenter dans chaque nœud source. La mise en œuvre du GPS dans chaque nœud source peut offrir une horloge avec une incertitude de seulement ± 100 ns, ce qui peut être un choix disponible à réaliser dans les réseaux métropolitains ou long-courriers. En conséquence, le temps de garde ci-après devrait être au moins supérieur à 200 ns.

Ensuite, la deuxième tâche du plan de commande est l'allocation des ressources et est utilisé pour assurer qu'il n'y a pas de collisions de rafales au sein du réseau ni dans les destinations. Comme dans le réseau TWIN, une entité de contrôle central (CCE : Central Control Entity) est implémentée pour calculer les motifs d'envoi (que l'on appelle les grants) qui contiennent les instants d'envoi et les longueurs d'onde utilisées pour chacun des rafales émis. Les grants sont une sorte d'autorisation distribuée du CCE aux nœuds sources afin de contrôler le temps d'émission et la longueur d'onde des sous-bandes d'une rafale. Grâce aux grants, CCE peut contrôler l'allocation des ressources. Dans TISA, les délais de propagation sont différents selon la distance entre les sources et les destinations. Différentes rafales émises par différentes sources à la même longueur d'onde peuvent arriver en même temps à une destination. Il y a donc une collision par rafales potentielles et cela pourrait entraîner une perte de rafale du fait que le récepteur ne peut pas lire simultanément deux rafales de même longueur d'onde et qu'il n'y a pas de solution (mémoire optique) pour stocker la rafale optique au récepteur. Dans le processus d'allocation de longueur d'onde, le plan de commande devrait être chargé d'éviter de telles collisions en rafale afin de garantir le routage sans perte dans le réseau TISA. Dans TISA, une sous-bande est associée à une seule destination. Par conséquent, la destination de la rafale est unique et le chemin de transmission est donc prévisible. Les nœuds de base sont transparents et les combinateurs et les séparateurs sont également transparents; il n'y a pas de conversion OEO dans la transmission par rafales et donc pas de variation de délai de processus de routage associée. Par conséquent, une fois qu'une rafale est émise, l'heure de réception au nœud de destination est prévisible. Par conséquent, une émission de rafale programmée minutieuse du côté de l'émetteur est suffisante pour contrôler les heures d'arrivée des rafales au niveau des nœuds centrales et du nœud de destination.

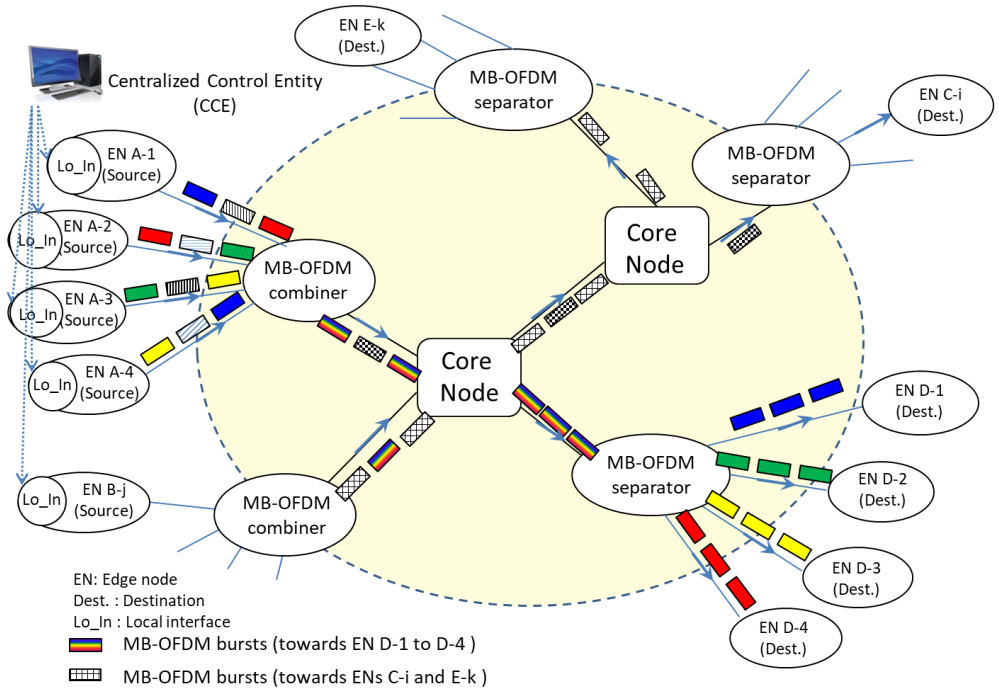

Figure 3: Un exemple de plan de commande au-dessus du plan de transfert pour le réseau TISA.

TISA est une solution temporelle. La rafale présentée dans l'exemple de la Figure 2 et la Figure 3 ont une dimension uniforme temporelle et spectrale. Pour la tâche concernant la configuration des appareils, les appareils et leurs états de fonctionnement seront collectés et envoyés au CCE ou à un contrôleur de niveau supérieur dans un réseau réel. Comme ce n'est pas la fonctionnalité nécessaire pour un prototype, nous n'implantons pas ces fonctions dans notre banc d'essai.

Flexibilité de la solution TISA

La solution proposée consiste à associer les deux domaines, temporel et spectral pour accéder à la granularité sous la longueur d'onde.

La Figure 4 (a) montre un exemple de représentation d'un canal de transmission découpé selon le mode proposé : une découpe temporelle par rafale (de 4.5 µs pour une durée de slots de 5 µs par exemple) et une découpe spectrale par bande (de 12.5 GHz, 5 bandes pour un canal de 50 GHz).

Les couleurs correspondent à une bande spectrale (du signal multi-bandes OFDM) différente. Dans l'exemple dessiné, le quantum de données est constitué d'un signal occupant une bande spectrale de 12.5 GHz et une durée de 4.5 µs.

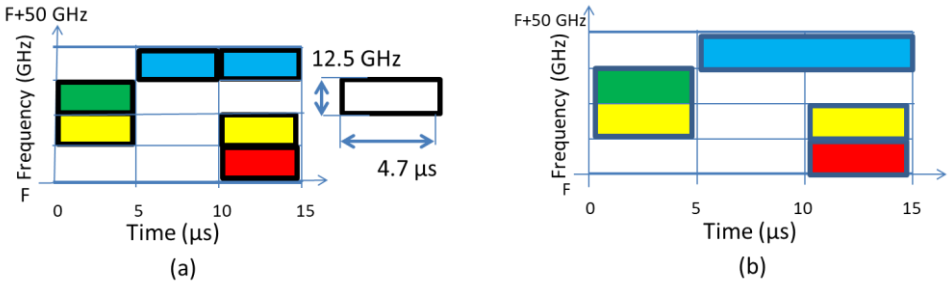

Figure 4: Exemples de granularité de base dans les domaines temporels et spectraux.

Ainsi, dans le temps, le canal « multi-bandes OFDM » est découpé en slots temporels (rafales) qui peuvent être de durée variable (entre quelques microsecondes et quelques centaines de microsecondes) et dans le domaine fréquentiel, la rafale, qui occupait une bande spectrale de 50 GHz, voit sa bande spectrale et par conséquent sa capacité de transmission, réduite d'un facteur égal au nombre de bandes constituant le canal multi-bandes OFDM. On divise ainsi le quantum de capacité mentionné à l'état de l'art de l'OFDM par le nombre de bandes constituant le canal spectral.

Le quantum de capacité est alors équivalent à celui que pourrait avoir un paquet optique d'une durée plusieurs fois plus petite que la rafale (4 dans l'exemple de la Figure 2) mais en gardant les mêmes composants que ceux actuellement utilisés dans la technologie rafale optique.

Il est important de noter ici, que la modulation OFDM appliquée à l'optique apporte non seulement une finesse de gestion du spectre dans sa version multi-bandes, mais également la possibilité de s'adapter finement au canal de transmission (très utilisé dans le domaine de la radio). En effet la flexibilité en termes de choix de modulation (débit et format) pour chaque bande OFDM et à l'intérieur du signal OFDM lui-même, offre une multiplicité de combinaisons permettant d'adapter parfaitement la quantité de ressources utilisées à la quantité de données à transporter et aux objectifs de portées (en distance).

On voit donc que la combinaison de ces deux solutions (temporelle et spectrale) d'accès à la granularité sous la longueur d'onde permet ainsi de démultiplier la capacité des réseaux en offrant une granularité la plus fine possible tout en permettant une augmentation des débits par canal jusqu'au Térabit/s voire au-delà et offre une flexibilité accrue. La Figure 4 (b) montre un exemple de répartition possible des données dans les slots et les bandes lorsqu'on utilise TISA. On peut occuper plusieurs slots temporels (rafales) dans une bande (en bleu), on peut avoir une rafale sur plusieurs bandes OFDM (bande verte, jaune) par exemple pour la diffusion d'un même contenu à plusieurs destinataires. On peut utiliser un quantum de données ou une combinaison selon l'axe temporel et/ou spectral. D'autre part, il est possible d'ajuster le débit à l'intérieur du quantum de données (entourage rouge pour 50 Gbit/s, vert pour 25 Gbit/s et noir pour 10 Gbit/s).

En résumé, chaque solution apporte de la flexibilité en termes de gestion de la bande passante mais la combinaison des 2 domaines permet :

- d'avoir des quanta de données plus petits (comme ceux de l'OPS sans les contraintes au niveau des composants),
- la très grande capacité du réseau (très grands débits avec OFDM) avec un accès à une granularité très fine (rafales) et très grande flexibilité dans la gestion de la ressource (débits et formats de modulation variables, plus possibilité de rafales de durée variable)
- l'utilisation possible des architectures utilisées pour les solutions SLPSN sans pertes (solutions basées sur le routage en longueur d'onde) avec des nœuds de cœur passifs (sans conversion optique/électrique/optique) et donc économes en consommation énergétique. Il suffit de rajouter un étage de filtrage/combinaison des signaux à la solution TWIN [3],
- la réalisation d'architectures pour des réseaux couvrant à la fois le métro-accès jusqu'au cœur de réseau,
- un plus grand nombre de sources/destination (on multiplie par le nombre de bandes possibles) pour les solutions SLPSN, chaque bande pouvant être une destination. Mais une destination peut aussi avoir accès à plusieurs bandes si elle a besoin de beaucoup de débit. Les étages de filtrage des nœuds cœur peuvent être reconfigurés (lentement) si besoin.

L'objectif de ma thèse était de fabriquer une preuve de concept de TISA. Nous avons réalisé une preuve de concept avec 6 nœuds d'extrémité (deux nœuds sources, et 4 nœuds destination) et un nœud cœur. Nous avons seulement réalisé un sens de transmission mais dans un réseau réel bidirectionnel chaque nœud d'extrémité serait équipé d'un émetteur et d'un récepteur. La preuve de concept TISA est composée de deux parties : le plan de transfert et le plan de commande. Pour le plan de transfert, on a réalisé le transmetteur en mode rafale, le récepteur cohérent et les fonctions de combinaison/séparation et de routage du réseau TISA. Dans les paragraphes suivants, la mise en œuvre de la preuve du concept TISA et les résultats expérimentaux seront présentées en détail. D'abord, on va présenter la mise en œuvre de transmetteur et récepteur. Et puis, on va présenter la mise en œuvre du banc TISA.

Transmetteur et récepteur

Dans le concept TISA, comme une source est capable de générer des rafales à différentes sous-bandes de longueurs d'onde, un émetteur en mode rafale à accord rapide doit être implémenté sur le nœud source. Ensuite, du côté de la destination, chaque destination ne reçoit qu'une seule sous-bande, de sorte qu'un récepteur cohérent recevant une sous-bande fixe sera réalisé conformément au concept TISA.

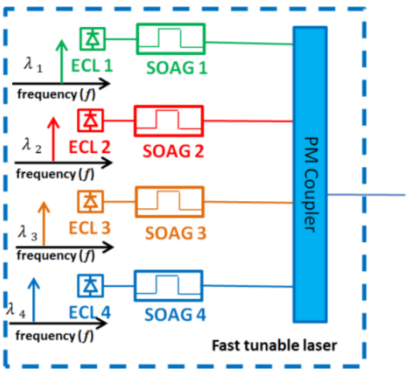

Figure 5: Architecture laser accordable rapide basée sur les SOAGs.

Pour la réalisation d'émetteur en mode rafale à accord rapide, un laser accordable rapidement est donc nécessaire. La largeur de raie doit inférieur à 100 KHz et le temps de commutation est inférieur à 100 ns. Comme il n'y a pas de laser commercial ayant ces 2 caractéristiques, on a fabriqué un laser en utilisant des lasers à cavité externe (ECLs : External Cavity Lasers) et des portes optiques (SOAGs : Semiconductor Optical Amplifier Gates). Nous avons réalisé deux lasers accordables à 4 longueurs d'onde chacun donc utilisant chacun 4 lasers à cavité externe et 4 SOAGs (voir Figure 5). Les 4 lasers à cavité externe restent allumés en permanence et les SOAGs permettent d'allumer ou éteindre les signaux venant des lasers à cavité externe de façon à émettre un signal optique de la durée d'une rafale à la longueur d'onde du signal à émettre (qui correspond à la longueur d'onde du nœud de destination de la rafale). Ensuite, le signal émis par le laser accordable est envoyé au modulateur qui reçoit les signaux analogiques venant de l'AWG de façon à générer les rafales OFDM à la longueur d'onde de la destination.

Tout d'abord, le SOAG est allumé et éteint alternativement avec la même durée d'activation et de désactivation. Lorsque la durée "on" et "off" varie de 5 µs à 100 µs, les temps de montée et de descente restent les mêmes pour chacun des quatre SOAG étudiés (voir Figure 6). Ça montre que le temps de commutation qui est la somme du temps de montant et descendant est inférieur à 100 ns.

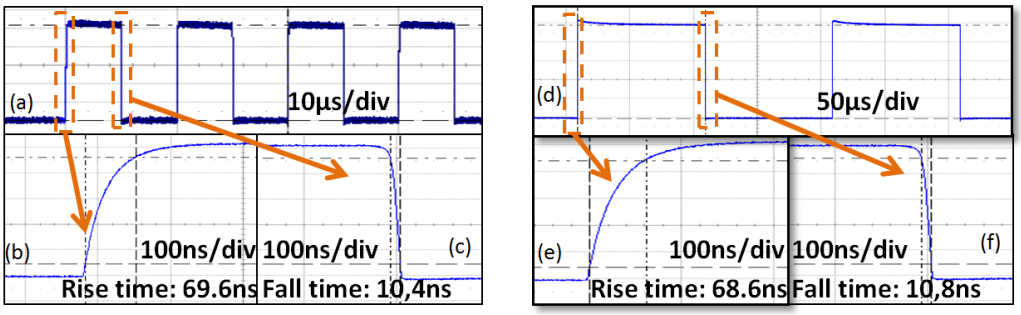

Figure 6: Le signal de sortie optique de SOAG1 pour (a) 5 µs "on" - 5 µs "off", 10 %-90% temps de montant (b) et descendant (c) pour la durée 5 µs "on" et "off", (d) 100 µs "on" - 100 µs "off", 10 %-90% temps de montant (e) et descendant (f) pour la durée 100 µs "on" et "off".

Et puis, quatre longueurs d'onde différentes sont configurées: 192,682 THz, 192,694 THz, 192,706 THz et 192,718 THz. Les quatre longueurs d'onde différentes sont allumées et éteintes alternativement et périodiquement. Le spectre à la sortie de la source laser accordable rapide, mesuré avec un analyseur de spectre optique (OSA) à haute résolution (20 MHz) Apex, est présenté à la Figure 7.

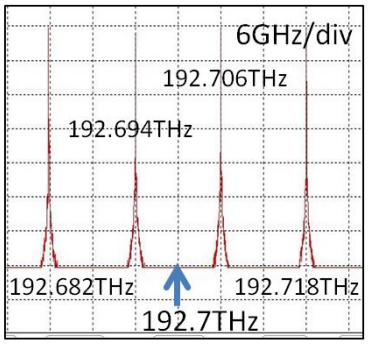

Figure 7: Spectre à la sortie du laser accordable

Après la validation du laser accordable rapidement, on a réalisé un banc expérimental pour tester la performance du transmetteur et récepteur. La configuration du banc expérimental est présentée dans Figure 8. Un récepteur cohérent a été réalisé. On peut utiliser l'oscillateur local pour sélectionner la sous-bande reçue. Un plan de commande a été réalisé en technologie FPGA, contrôlé à moyen d'un ordinateur déporté. L'ordinateur joue le rôle d'entité centrale de contrôle (CCE). L'horloge externe génère l'horloge commune pour tous les composants afin de synchroniser le banc expérimental. Les grants sont préprogrammées par CCE. Et puis les grants sont envoyées au FPGA, selon les grants reçus, FPGA générera les signaux de contrôle électrique pour contrôler tous les SOAGs. Dans l'émetteur, la synchronisation entre les portes optiques et l'AWG est importante pour mettre les données sur la sous-bande correspondante en fonction des grants reçues. Lorsque le FPGA génère les signaux de contrôle pour les SOAGs, il génère également un déclencheur pour activer l'AWG. Tous les temps de réponse et de transmission du signal sont pris en compte lors de la génération du déclencheur pour AWG. Nous pouvons donc mettre des données correctes sur la sous-bande correspondante.

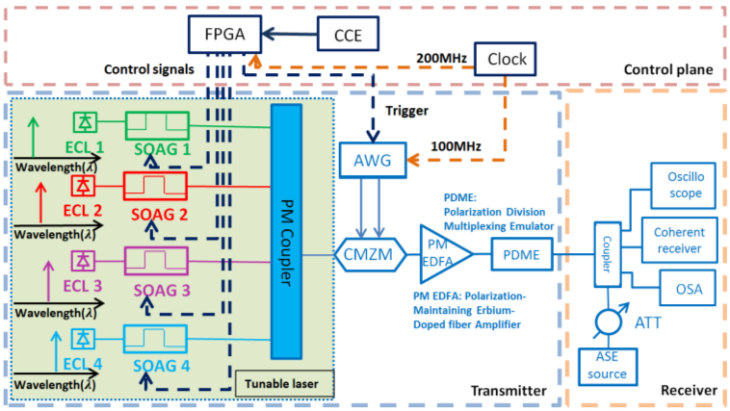

Figure 8: Configuration expérimentale pour l'évaluation back-to-back de l'émetteur et du récepteur.

Pendant le test, quatre rafales aux quatre longueurs d'onde différentes sont générées périodiquement et successivement (par exemple lambda 1, lambda 2 lambda 3 et lambda 4, et ainsi de suite. voir Figure 9). Cette configuration peut assurer une puissance constante à l'entrée d'EDFA qui fonctionne en mode continu. Chaque time slot est de 5 µs, le temps de guard est réglé à 350 ns et trois trames OFDM sont insérées afin d'évaluer l'impact des fronts montants et descendants de la source laser (voir Figure 9). Pour une trame OFDM, il est composé de 1 symbole de synchronisation, 8 symboles d'apprentissage et 46 symbole de données. La taille du FFT est 256 et la largeur de la bande optique est 6.6 GHz. Le débit brut au format Dual-Polarisation QPSK est 26.6 Gbps.

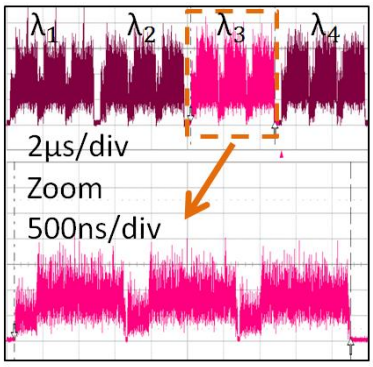

Figure 9: Signaux à la sortie du transmetteur.

Les courbes BER et OSNR mesurées lors de l'utilisation de SOAG1 sont présentés à la Figure 10. La courbe en pointillés montre les performances du signal CO-OFDM en mode continu avec ECL1; la ligne continue affiche le BER en mode continu avec SOAG1 dans l'état "on" entre l'ECL1 et le CMZM. Nous observons que le SOAG en état "on" n'apporte aucune pénalité au BER 10^{-5}. Les 3 courbes avec cercles, triangles et carrés correspondent respectivement aux 1er, 2ème et 3ème trames OFDM émises à travers SOAG1 à la longueur d'onde 1 (en une durée de rafale), selon le schéma représenté sur Figure 9. Nous pouvons voir que les trois trames OFDM ont les mêmes performances, ce qui indique que la synchronisation entre l'émission de données et la commutation de longueur d'onde est correcte et aucune pénalité n'est liée aux fronts montants et descendants de la source laser car aucune pénalité ne survient sur les trames 1 et 3 par rapport à la trame 2.

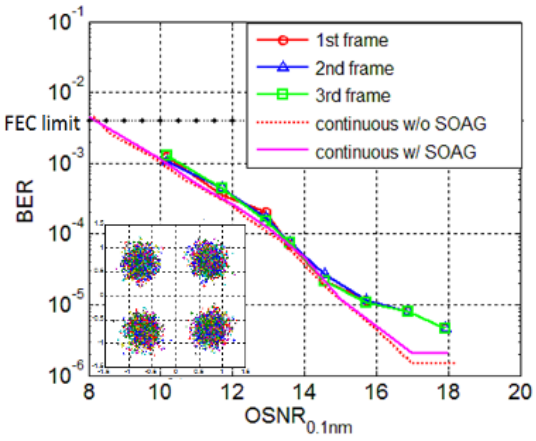

Figure 10: Les courbes BER-OSNR (0.1nm) pour trois trames OFDM lorsqu'on utilise SOAG1.

Les courbes BER et OSNR de la Figure 11 montrent les résultats pour les 4 SOAG commutés périodiquement. Comme le récepteur cohérent ne détecte qu'une seule sous-bande OFDM, nous l'ajustons pour mesurer le BER de SOAG1 à SOAG4 respectivement. Le BER mesuré pour chaque longueur d'onde est une moyenne des trois trames OFDM sur 30 mesures. Les performances des SOAG (de 1 à 4) sont respectivement représentées par des cercles, des triangles, des carrés et des diamants. Nous n'observons aucune différence significative entre les quatre courbes montrant que les performances sont les mêmes pour les quatre longueurs d'onde. Nous pouvons également voir sur la Figure 11 qu'il n'y a pas de pénalité OSNR au BER 10^{-4} et qu'il y a moins de 1 dB de pénalité au BER 10^{-5}.

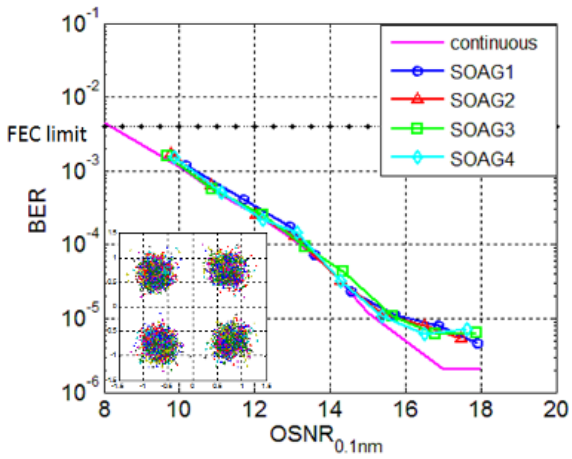

Figure 11: Les courbes BER-OSNR (0.1nm) pour les quatre SOAGs.

TISA network

Après la validation de l'émetteur et du récepteur cohérent, le réseau TISA est construit. Figure 12 montre l'architecture ciblée : 6 nœuds d'extrémité (deux nœuds sources, et 4 nœuds destination) et un nœud cœur. Nous avons seulement réalisé un sens de transmission.

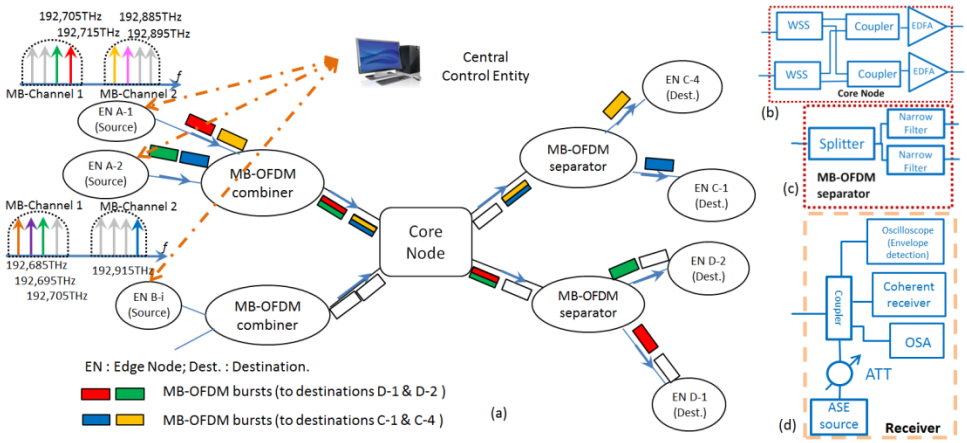

Figure 12: (a) Architecture TISA (une direction de transmission), (b) Mise en place expérimentale du nœud central, (c) Mise en place expérimentale du séparateur MB-OFDM, (d) Mise en place expérimentale du récepteur cohérent.

Les rafales sont générées au transmetteur et alors transmis dans le réseau et restent dans le domaine optique jusqu'à leur détection par le récepteur qui est dans le nœud de destination. D'abord, les rafales venant de différentes sources sont assemblés dans le combineur. Ensuite, les rafales arrivent au nœud cœur où le routage des rafales est fait en fonction de la longueur d'onde d'une bande de 50 GHz (qui regroupe 4 sous-bandes de 10 GHz). Puis, les rafales sont transmises au séparateur de sous-bandes. Le séparateur est composé d'un coupleur optique qui duplique le signal entrant en 2 signaux et de filtres de 10 GHz pour sélectionner chaque sous-bande qui est ensuite envoyée vers la destination associée. Pendant le test, chaque émetteur est programmé pour générer successivement un flux de données périodique composé de quatre slots à différentes longueurs d'onde. Tx-1 génère des données à λ5, λ3, λ6, λ4, tandis que Tx-2 génère des données à λ1, λ6, λ1, λ7.

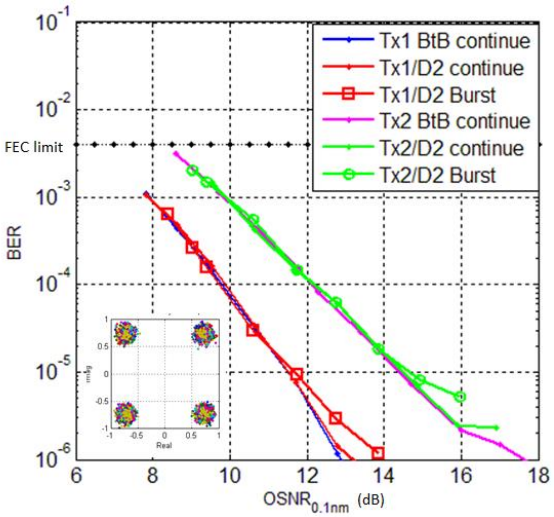

Figure 13 : Les courbes BER-OSNR (0,1 nm) pour Tx-1 et Tx-2 / Rx au nœud D-2 en utilisant une modulation format QPSK.

Les courbes BER et OSNR mesurées pour le Tx-1 / Rx au nœud D-2 en utilisant DP-QPSK sont représentées sur la Figure 13. Chaque trame OFDM est composée de 1 symbole de synchronisation, 14 symboles d'apprentissage et 156 symboles de données. La courbe rose représente la performance Tx-2 / Rx dans une configuration back-to-back lorsque le Tx-2 génère un signal continu à λ6. La courbe pointillée verte correspond au même signal après transmission à travers le réseau TISA. La courbe verte avec cercles montre la performance en mode rafale (avec 1 trame OFDM dans la rafale de 4,7 µs) lorsque le Rx est au nœud D-2 recevant des données de Tx-2. La courbe bleue représente la performance Tx-1 / Rx dans une configuration back-to-back lorsque le Tx-1 génère un signal continu à λ6. La courbe pointillée rouge correspond au même signal après transmission à travers le réseau TISA. La courbe rouge avec les carrés montre les performances en mode rafale lorsque le Rx

est au nœud D-2 recevant des données de Tx-1. Comme on peut le constater, les performances globales de Tx-1 sont bien meilleures que celles de Tx-2 (même que sur paper1) du fait de la linéarité optimisée des RF drivers qui alimentent le Complex Mach-Zehnder Modulator (qui a un meilleur taux d'extinction). Pour les deux Tx, nous pouvons voir que les composants passifs comme le WSS, les coupleurs et le séparateur OFDM n'introduisent aucune pénalité. Lorsque nous transmettons des salves, il n'y a pas de pénalité au BER 10^{-4} et environ 0,3 dB de pénalité au BER 10^{-5} par rapport aux configurations continues. Les performances de Tx-1 / Rx au nœud D-1 et Tx-1 / Rx au nœud C-4, à l'aide de signaux QPSK, sont similaires à celles de D-2.

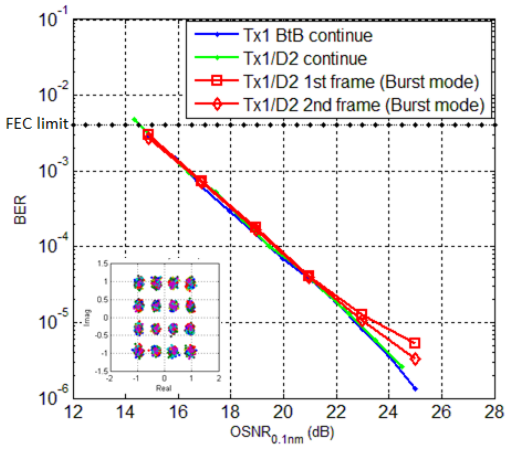

Figure 14 : Les courbes BER-OSNR (0,1 nm) pour Tx-1 / Rx au nœud D-2 en utilisant une modulation format 16QAM.

Les courbes BER et OSNR mesurées pour le couple Tx-1 / Rx au nœud D-2 en utilisant le format de modulation DP-16QAM sont représentées sur la Figure 14. Tx-2 ne permet pas d'effectuer des mesures de 16QAM; ainsi nous gardons le format QPSK pour Tx-2. Ainsi, les signaux QPSK et 16QAM se propagent en même temps à travers le réseau TISA. Afin d'améliorer les performances du signal DP-16QAM de Tx-1, nous avons placé deux trames dans chaque rafale, chaque trame contenant 1 symbole de synchronisation, 14 symboles d'apprentissage et 70 symboles de données. La ligne bleue montre la performance en configuration back-to-back lorsque le Tx-1 génère un signal continu à λ6; la courbe pointillée verte présente la performance du même signal après transmission à travers le réseau TISA; comme deux cadres sont insérés dans une rafale, la performance de la première trame est représentée par la courbe rouge avec des carrés et la performance de la deuxième trame est représentée par la courbe rouge avec des diamants. Nous n'observons pas de différence significative (seulement une pénalité de 0,3 dB au BER 10^{-5}) entre la seconde trame et les données en mode continue. Mais la première trame a une pénalité de ~ 0,8 dB au BER 10^{-5} par rapport à la configuration continue. Parce que Le format 16QAM est plus sensible aux distorsions de signal que le format QPSK, le DSP compense moins efficacement les distorsions du signal. En effet, la nature en rafale des signaux nécessite de récupérer la fréquence et la phase pour chaque rafale. L'amélioration du DSP pour les trames OFDM avec plus haut ordre QAM modulation format a besoin

d'une étudiée en détail plus tard. Les performances de Tx-1 / Rx aux nœuds D-1 et C-4 sont similaires à celles du nœud D-2. Ces résultats confirment que la transmission transparente des signaux QPSK et 16QAM, via le réseau TISA, est possible avec des pénalités très faibles.

Amélioration de la performance du récepteur

Dans TISA, étant donné que le trafic est sous forme de rafales, le récepteur n'est pas assuré de recevoir un flux de symboles en continu. Quand le récepteur ne reçoit pas de données, il n'y a que les bruits à l'entrée du récepteur, on appelle cette partie du signal de «signal intervalle». Dans TISA, il y a des «signal intervalles» de temps en temps à l'entrée du récepteur et la durée des «signal intervalles» est variable, et on peut les classifier par la durée du signal intervalle : le petit signal intervalle de 0 µs à 5 µs, le moyen signal intervalle de 5 µs à 15 µs, le grand signal intervalle supérieur à 15 µs. Comme le récepteur est conçu pour recevoir un flux OFDM continu, il a des difficultés à gérer l'absence de signal ce qui génère une pénalité. Si une rafale OFDM arrive dans le récepteur après un «signal intervalle» de grande longueur, les premières centaines de nanoseconde de trame signal (en particulier les symboles d'apprentissage) subissent une distorsion à cause de phénomènes de réponse transitoire des composants embarqués dans le récepteur. Il y a alors une inadéquation entre les coefficients calculés de l'égaliseur et les coefficients à appliquer réellement sur le signal pour l'égaliser correctement.

Afin d'identifier l'influence de la distorsion, on a évalué les performances de la trame OFDM avec différentes durées de «signal intervalle». Dans la figure 15, les courbes de taux d'erreur binaire (BER) en fonction du rapport signal sur bruit optique (OSNR) mesurées dans différentes configurations sont présentées. Pour chaque configuration, une trame OFDM a 1 symbole de synchronisation, 14 symboles d'apprentissage et 156 symboles de données, occupant en tout une durée de 4.7 µs est générée. La courbe rouge en marqueur point représente le résultat mesuré en mode continu. Les courbes en marqueurs carré, diamant, hexagone, triangle, cercle représentent respectivement les résultats mesurés en mode rafale avec un «signal intervalle» de 0.3 µs, 5.3 µs, 10.3 µs, 15.3 µs et 50.3 µs. On voit que la pénalité pour un BER égal à $2x10^{-5}$ augmente quand la durée du «signal intervalle» augmente.

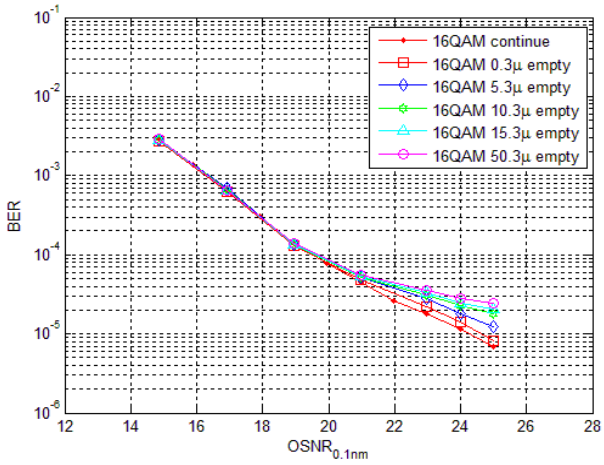

Figure 15 : Les courbes BER en fonction de l'OSNR (0.1 nm) sur différentes signal intervalles configurations

Il y a des solutions dans la littérature pour résoudre ce type de problème. Dans [8], les auteurs ont proposé d'ajouter des rafales de « bourrage » à l'entrée du récepteur quand il y a des «signal intervalles» pour créer un flux signal quasi continu, et ainsi garder toujours le récepteur dans l'état de fonctionnement continu. La méthode utilisée dans [8] utilise le plan de commande (signal de grant) pour identifier la présence de signal intervalles au niveau du récepteur, ainsi qu'un émetteur pour générer les rafales de bourrage, au prix donc d'une augmentation de la complexité de l'ensemble. Une autre méthode est de changer les composants du récepteur afin qu'il présente une fréquence de coupure basse de quelques centaines de Hz. De la sorte, le récepteur conserve le même comportement en présence ou en l'absence de signal. Mais fabriquer des composants large bande ayant en même temps une fréquence de coupure basse très petite (i.e. quelques centaines de Hz) n'est pas chose aisée : il est très difficile de réaliser des composants opto-électroniques, par exemple les amplificateurs RF linéaires, ayant une réponse spectrale plate des fréquences basses (les enveloppes de rafales) aux fréquences hautes (signal OFDM lui-même). En conséquence, une solution moins chère, plus flexible, est encore attendue.

La solution proposée consiste à insérer plus de symboles d'apprentissage dans la trame OFDM et ensuite à calculer la moyenne des coefficients de l'égaliseur non plus sur tous les symboles de la séquence d'apprentissage mais sur une partie seulement de cette séquence. Comme on sait que le début de la trame a subi une distorsion en raison des phénomènes transitoires (inhérents à la présence de «signal intervalles ») du récepteur, l'idée est d'utiliser les coefficients de l'égaliseur sur une partie de la séquence d'apprentissage qui ne subit peu ou plus la distorsion. Pour ce faire, une fenêtre glissante englobant plusieurs symboles d'apprentissage (sur laquelle le moyennage des coefficients de l'égaliseur s'opérera) est mise en place. Lorsque les coefficients de l'égaliseur se stabilisent, c'est le signe que les transitoires n'affectent plus le processus d'égalisation.

Afin de réaliser cette méthode, il est nécessaire de savoir d'abord comment déterminer la position dans une trame à partir de laquelle la distorsion se termine. Dans le transmetteur, on construit des trames OFDM composées de 1 symbole de synchronisation, 50 symboles d'apprentissage et 120 symboles de données, pour garder la même durée de rafale (4.7 µs) que dans le mode de fonctionnement initial. Dans le récepteur, le DSP est identique à celui mis en œuvre dans un Rx classique à flux continu. Seul le processus d'égalisation diffère. Nous allons maintenant le décrire. . Concernant l'égaliseur, on calcule les coefficients moyennés en se basant sur un groupe de 12 symboles d'apprentissage successifs, par exemple du 3ème au 14ème symbole d'apprentissage. Et puis, on calcule le taux d'erreur binaire en utilisant cet égaliseur. Le nombre de 12 symboles pour le moyennage des coefficients est choisi pour augmenter la robustesse au bruit de l'égaliseur. Une autre valeur paire (i.e. 8, 10,14 …) pour le moyennage peut bien sûr être sélectionnée. Dans la figure 16, un exemple pour poser la fenêtre dans les symboles d'apprentissage est donné. Les colonnes représentent les symboles et les lignes représentent les sous-porteuses. La colonne verte représente le symbole de synchronisation, les colonnes bleues représentent les symboles d'apprentissage où un carré représente 5 symboles et les colonnes jaunes représentent les symboles de données où un carré représente 12 symboles. Les rectangles rouges représentent différentes fenêtres glissantes : une fenêtre a une taille de 12 symboles et la position du premier symbole de la fenêtre est nommée « position de commencement » (starting position). Le premier rectangle à gauche représente la fenêtre du 3ème au 14ème symbole d'apprentissage, et le deuxième rectangle représente la fenêtre du 7ème au 18ème symbole d'apprentissage et ainsi de suite. Entre deux fenêtres adjacentes, il y a 4 symboles de décalage dans cet exemple. Il pourrait y en avoir plus ou moins dans une autre implémentation.

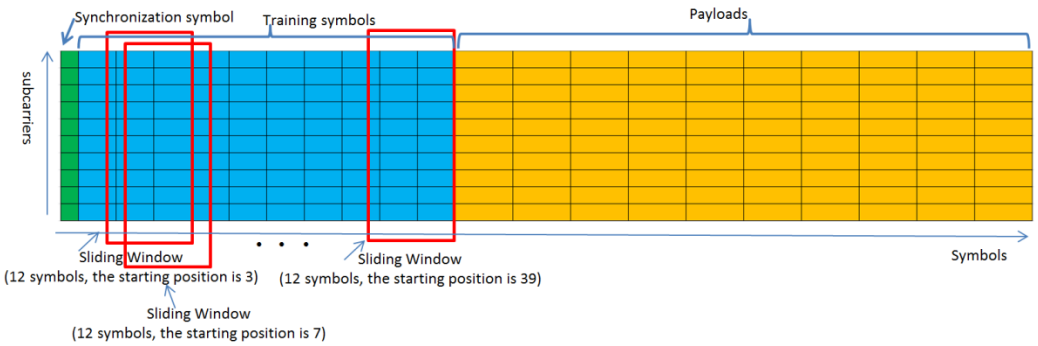

Figure 16 : Le schéma de la position de la fenêtre glissante.

Ensuite l'étape 2 : pour la même trame, on utilise un autre groupe de 12 symboles d'apprentissage successifs ayant 4 symboles de décalage avec les premiers (par exemple du 7ème au 18ème symbole d'apprentissage (voir la figure 16)), pour calculer les coefficients de l'égaliseur et ainsi le taux d'erreur binaire des données. Et ainsi de suite, on répète l'étape 2 afin d'utiliser différents groupes de 12 symboles d'apprentissage jusqu'à la fin de la séquences des symboles d'apprentissage.

Les taux d'erreur binaires sont notés à chaque fois, et les résultats de différentes configurations sont présentés dans la figure 17.

Dans la figure 17, la courbe verte représente le résultat mesuré en mode continu. On voit que les taux d'erreur binaires restent constants quand on utilise différents groupe de 12 symboles d'apprentissage. Ça montre que la trame ne subit pas de distorsion en mode continu. Les courbes rouge, bleu, cyan et violette représentent respectivement les résultats mesurés en mode rafale avec un signal intervalle de 0.3 µs 5.3 µs, 15.3 µs et 50.3 µs. En comparant les résultats, on voit que la distorsion introduite par le récepteur se termine de plus en plus tard au fur et à mesure que la durée du «signal intervalle» augmente. Mais à partir d'une position, le taux d'erreur binaire reste constant et a la même valeur que celui obtenu en mode continu. Donc, pour améliorer la performance, au lieu d'utiliser tous les symboles d'apprentissage pour calculer les coefficients de l'égaliseur, on n'utilise que le groupe de 12 symboles qui donne un taux d'erreur binaire le plus faible possible.

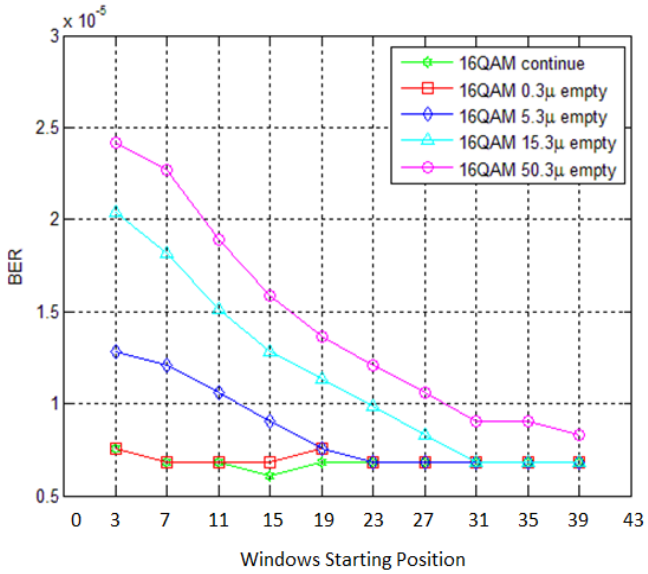

Figure 17 : Les courbes BER en fonction de la position de la fenêtre (le début de la fenêtre) à OSNR fixé (25 dB dans 0.1 nm) pour différentes durées de signal intervalle.

Pour vérifier la performance de cette méthode, les courbes de BER en fonction de l'OSNR sont mesurées présentées dans la figure 18. La courbe rouge en marqueur point représente le résultat mesuré en mode continu. Les courbes rouge, bleu, cyan et violette représentent les résultats mesurés en mode rafale avec un signal intervalle de 0.3 µs 5.3 µs, 15.3 µs et 50.3 µs et en utilisant la fenêtre glissante qui commence à la position 7, 23, 31, et 39, respectivement. En comparant avec le résultat en mode continu, on voit que la performance est quasi-identique, en particulier dans le bas de la courbe (à forts OSNRs) où les imperfections de la chaine de mesure sont les plus significatifs : la performance entre le mode continu et le mode rafale pour un taux d'erreur binaire de $2x10^{-5}$ est quasiment identique. La comparaison par rapport à la figure 15 montre que la solution proposée est

efficace pour gérer le problème de l'absence de signal ou «signal intervalles» au niveau du récepteur dans le cas de transmission avec réception cohérente en mode rafale.

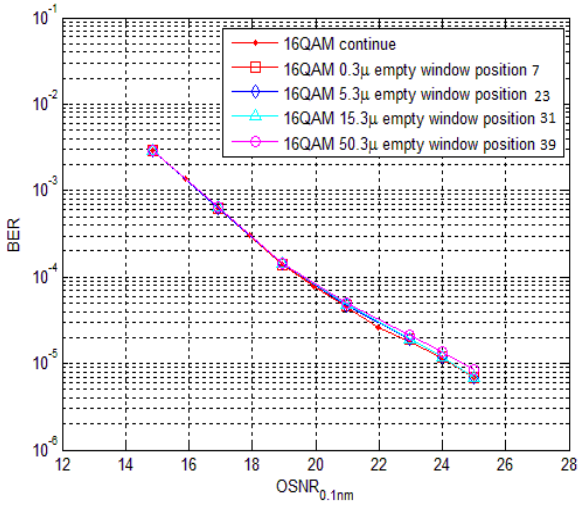

Figure 18 : Les courbes BER en fonction de l'OSNR (0.1 nm) sur différentes signal intervalle configurations en utilisant la méthode fenêtre glissant.

Cette solution permet de faire fonctionner le récepteur OFDM à la fois en mode continu et en mode rafale au prix simplement d'une augmentation modérée de l'overhead (pour allonger la séquence d'apprentissage). Cette solution nous permet surtout d'économiser les coûts de développement d'un récepteur spécifique « mode burst » avec des composants opto-électroniques optimisés ou bien encore les coûts associés avec la génération d'un signal de bourrage comme décrit plus haut.

Conclusion

La solution TISA a été proposée afin d'améliorer la flexibilité et d'affiner la granularité de l'allocation des ressources dans le domaine optique. Dans cet article, nous démontrons expérimentalement la faisabilité du concept TISA pour la première fois en utilisant à la fois les signaux de salves DP-QPSK et DP-16QAM CO-OFDM. Pour le signal DP-QPSK, seule une pénalité de 0,3 dB au BER 10^{-5} est introduite. Pour le signal DP-16QAM, une pénalité maximale de ~ 0,8 dB au BER 10^{-5} par rapport à la configuration continue apparaît. La pénalité est différente pour les deux trames de la rafale qui montre qu'une amélioration du DSP pour les rafales OFDM est toujours attendue. Ces bons résultats valident la solution TISA (agrégation / désagrégation optique et routage transparent des données quel que soit leur format de modulation et leur débit binaire) et leur capacité à effectuer une allocation de ressources dans le domaine optique, ce qui correspond aux besoins des clients.

Bibliographie

[1] “Terms and definitions for Sub-Lambda Photonically Switched Networks”, ITU, COM15-C2322 Rev.-E, Geneva, August 2012.

[2] E. Pincemin, M. Song, J. Karaki, A. Poudoulec, N. Nicolas, M. Van der Keur, Y. Jaouen, P. Gravey, M. Morvan and G. Froc, "Multi-band OFDM Transmission with Sub-band Optical Switching,", Proc. ECOC 2013, invited paper Th.2.A.1 (2013).

[3] A. Triki, P. Gavignet, B. Arzur,·E. Le Rouzic,·A. Gravey., “Efficient control plane for passive optical burst switching network”, ICOIN 2013, pp. 535-540.

[4] M. Song, "WDM transmission of 400 Gbps and beyond using multi-band OFDM & Nyquist-WDM", thesis manuscript, Télecom ParisTech, 2016

[5] P. Gavignet, E. Le Rouzic, E. Pincemin, B. Han, M. Song, L. Sadeghioon “Time and Spectral optical Aggregation for Seamless Flexible Networks”, Photonics in Switching, 2015.

[6] Official U.S. government information about the Global Positioning System (GPS) and related topics, [available online], http://www.gps.gov/systems/gps/performance/accuracy/

[7] W. Lewandowski, J. Azoubib and W. J. Klepczynski, "GPS: primary tool for time transfer", in *Proceedings of the IEEE*, vol. 87, no. 1, pp. 163-172, Jan 1999.

[8] L. Sadeghioon, P. Gavignet, V. Alaiwan, L. Bramerie, E. Le Rouzic, JL. Barbey, T. Guillossou, E. Borgne, S. Lobo, "Software-based burst mode reception implementation for time-domain wavelength interleaved networks," 2015 European Conference on Optical Communication (ECOC), Valencia, 2015.

Table of Contents

List of abbreviations

A

ADC	Analog to Digital Converter
ASE	Amplified Spontaneous Emission
AWG	Arbitrary Waveform Generator
AWGs	Arrayed Waveguide Gratings

B

BER	Bit Error Rate

C

CAPEX	CApital EXPenditure
CCE	Central Control Entity
CD	Chromatic Dispersion
CFO	Carrier Frequency Offset
CMZM	Complex Mach-Zehnder Modulator
CP	Cyclic Prefix

D

DAC	Digital to Analog Converter
DP-16QAM	Dual-Polarization -16 Quadrature Amplitude Modulation
DP-QPSK	Dual-Polarization Quadrature Phase-Shift Keying
DSP	Digital Signal Processing

E

ECL	External Cavity Laser
EDFA	Erbium Doped Fiber Amplifier

F

FFT	Fast Fourier Transform
FIFO	First In First Out
FPGA	Field Programmable Gate Array

I

ICI	Inter-Carrier Interference
ITU-T	International Telecommunication Union – Telecommunication
IP	Internet Protocol

ISI	Inter-Symbol Interference

M

MB-OFDM	Multi-Band - Orthogonal Frequency Division Multiplexing
MZM	Mach-Zehnder Modulator

O

OBS	Optical Burst Switching
OCS	Optical Circuit Switching
O/E/O	Optical/Electrical/Optical
OFDM	Orthogonal Frequency Division Multiplexing
OPEX	OPerational EXpenditure
OPS	Optical Packet Switching
OSA	Optical Spectrum Analyzer
OSI	Open System Interconnection
OSNR	Optical Signal to Noise Ratio

P

PAPR	Peak to Average Power Ratio
PMD	Polarization Mode Dispersion
PM	Polarization Maintaining
PoC	Proof of Concept

R

ROADM	Reconfigurable Optical Add-Drop Multiplexer

S

SLPSN	Sub-lambda Photonic Switched Networks
SOA	Semiconductor Optical Amplifier
SOAGs	Semiconductor Optical Amplifier Gates

T

TISA	TIme and Spectral optical Aggregation
TWIN	Time-domain Wavelength Interleaved Network

W

WDM	Wavelength-Division Multiplexing
WSS	Wavelength Selective Switch

Introduction

In a context where the optical transport networks are under the pressure of an exponential traffic growth (~ 40% per year), there is a big challenge to increase the network capacity while lowering CAPEX and OPEX costs. Two principal directions are under study to solve this problem for content and service providers: adding new capacity and corresponding equipment (i.e. transceivers, fibers) and better using the already deployed network resources. Sub-wavelength switching technologies applied directly at the optical layer level have ever demonstrated their interest and relevance to improve the flexibility in the resource allocation in the optical transport network and constitute interesting candidates to better manage the existing network resources.

The current Wavelength-Division Multiplexing (WDM) network respects to the 50 GHz fixed grid standard channel spacing network which is normalized by the International Telecommunication Union – Telecommunication (ITU-T). A wavelength in WDM network refers to a data flow occupying 50 GHz bandwidth. Sub-wavelength switching consists in breaking up the wavelength into smaller sub-wavelength parts. For example, the bit rate of a wavelength is 100 Gbps using Dual-Polarization QPSK modulation format. In the sub-wavelength switching, the 100 Gbps data flow can be divided into several smaller flows (i.e. 10 flows at 10 Gbps). The services between end-users now are built up on small data flows with a granularity as fine as 10 Gbps. Through the flexible sub-wavelength grooming directly at the optical transport network, services are provided with the sub-wavelength connections and thus would be better adapt to customers' requirements. Moreover, sub-wavelength switching solution improves the IP traffic forwarding efficiency, ensures fast reconfiguration and reduces the capacity requirements at the IP layer and the total cost of ownership of the entire network. Furthermore, sub-wavelength switching in the optical layer has the potential to reduce the cost and power consumption of the overall transport networks.

There are two principal kinds of solutions that permit accessing to the sub-wavelength granularity at the optical layer level: the multi-band (MB) or super-channel technology with sub-bands of low bandwidth and Sub-lambda Photonic Switched Networks (SLPSN) technology in the time domain.

A super-channel is a large optical spectrum structure that is larger than an optical channel with a single carrier. The entire structure can cover a bandwidth of several hundreds of GHz and transport huge data rates. A super-channel is composed of multiple optical sub-bands inside the super-channel structure with minimal or even no guard-band, which allows saving spectral bandwidth. Inside the super-channel, the sub-band allocation is governed by the G.694.1 flex-grid ITU-T standard. The super-channel is considered as a single spectral entity by the optical switching devices inside the network. Recently, a new generation of elastic switching solutions based on high spectral resolution optical filters and Wavelength Selective Switches (WSSs) has been developed.

These solutions offer dynamic all-optical traffic aggregation/grooming at the sub-band level inside the super-channel. Thus, super-channel technology with the filtering and switching elements permits the sub-wavelength switching. Two modulation technologies are candidates to build super-channels: Multi-Band Orthogonal Frequency Division Multiplexing (MB-OFDM) and Nyquist-WDM. Both of them have high spectral efficiency and their sub-wavelength switching feasibilities have been demonstrated in the literature and the European projects like FOX-C (Flexible Optical Cross-Connects).

The SLPSN is normalized by the ITU-T to describe the whole sub-wavelength switching solutions in the time domain. The SLPSN solutions divide a wavelength into time entities, called time slots, which contain several packets that have the same destination. The time slots, as network resource units, are distributed to different end-users to build up the services between nodes pairs. The allocation of the time slots between end-users is fast reconfigurable in the time domain, which improves the flexibility of resources allocation. Different end-users can access the same wavelength while using the wavelength for only a fraction of time (several time slots), which permit to realize a temporal statistic multiplexing of the wavelength resource in the network. This scheme improves the channel filling efficiency and thus better uses the already deployed network resources. In SLPSN, according to the size of the optical burst or optical packet, the sub-wavelength switching solution in the time domain is called Optical Packet Switching (OPS) or Optical Burst Switching (OBS). The OPS manages the time entities with data duration lower than 1 µs, while the OBS manages time entities in the range of 1 µs to 10 ms. Therefore, the OBS releases the constraints that OPS will meet on the switching components, such as big size optical memory and commercial fast optical switch. Among the OBS solutions, the lossless solutions are preferred in the optical transport network since they can ensure no bursts contention in the network. Time-domain Wavelength Interleaved Network (TWIN) solution is an interesting lossless OBS solution. TWIN allows constructing a mesh topology optical network. In TWIN, each source node sends the data at various wavelengths and a wavelength is associated to one destination. Each destination node receives the bursts at its associated wavelength. The routing is realized on a wavelength basis without burst loss thanks to the careful scheduling of the control plane.

With the purpose of further improving the flexibility of the resources allocation at the optical layer level, TIme and Spectral optical Aggregation (TISA) solution has been proposed recently by combining the MB-OFDM and TWIN concept. It offers the best in terms of flexibility thanks to the as fine as possible granularity at the optical layer level in both time and spectral domains. Each source sends data in the form of bursts that occupy only one spectral sub-band of low bandwidth. Each sub-band is associated with a single destination. The source nodes are able to generate the bursts data at various wavelengths as they are rapidly tunable and the destination is fixed (which means that it receives the bursts at only one wavelength). Thus, the aggregation, routing, and separation of the data are performed passively on a wavelength basis.

The objective of this thesis was to implement an experimental Proof of Concept (PoC) of the TISA solution. For the PoC, we have built six edge nodes (two source nodes and 4 destination nodes)

and one core node. Only one transmission direction has been realized in our test-bed, but in a real TISA network, each node would be equipped with transmitters and receivers. Then, using both Dual-Polarization Quadrature Phase-Shift Keying (DP-QPSK) and Dual-Polarization-16 Quadrature Amplitude Modulation (DP-16QAM), the performance of the TISA network has been evaluated extensively through Bit Error Rate (BER) measurements.

The present manuscript is organized as follows:

Chapter 1 gives an overview of sub-wavelength switching solutions in both spectral and time domains. We introduce the evolution of the transmission system. We detail the state of the art of sub-wavelength switching solutions in the spectral domain and different time domain sub-wavelength switching solutions are presented and discussed.

Chapter 2 gives a detailed introduction to the TISA concept. We present the network structure and all the possible functionalities offered by the TISA solution. After that, the necessary building blocks necessary for the implementation of the proof of concept are presented, including fast tunable burst mode transmitters, coherent receivers, routing devices and control plane. Then, we compare TISA with TWIN solutions and present the new flexibilities and main innovations of the TISA technology.

Chapter 3 presents the implementation of our fast tunable burst mode transmitters and coherent receivers. In order to realize the burst mode transmitter, a fast tunable laser source with narrow linewidth has been proposed and realized. Then we evaluate the performance of our pair of transmitter and receiver using both DP-QPSK and DP-16QAM modulation formats.

Chapter 4 presents the specific and advanced control plane that has been designed and built for the TISA network. The control plane is used to guarantee the absence of collision at the destinations and in the network. Field Programmable Gate Array (FPGA) and real-time controller are used to achieve the control plane. The control signals are generated in real-time to control the burst emission. In order to synchronize the whole experimental test-bed, a common clock has been implemented and the technical solution is described.

Chapter 5 describes the whole TISA network. The TISA PoC contains six edge nodes (two source nodes and 4 destination nodes) and one core node. Then we evaluate the performance of the TISA network by using both DP-QPSK and DP-16QAM modulation formats. We find that the coherent receiver optimized for continuous OFDM data flows is not perfectly adapted to receive the OFDM burst traffic and introduces some penalties. So, a new signal processing method at the receiver side is proposed in order to deal with the introduced penalties.

At last, we conclude the PhD manuscript by summarizing our main and emblematic results before giving perspectives and insights over the possible next developments of the TISA technology.

CHAPTER 1

State of the art: Sub-wavelength switching solutions

Optical fiber systems are the cornerstone of the modern communication networks. Compared to the internet over coaxial cables, the fiber-optic internet offers more bandwidth, much higher bit rate and is more eco-friendly. Therefore, fiber-optic internet becomes the suitable transmission media for high bit rate communications. The combination of low loss high bandwidth optical fibers and Erbium Doped Fiber Amplifiers (EDFAs) enables long-haul transmission with high bit rates. The most used bands are the C- and L-band, where EDFA exhibits its gain and telecom optical fibers show their lowest attenuation in the entire optical telecommunication wavelength bands (from 1260 nm to 1675 nm) (see Figure 1-1). The invention of EDFA enables the deployment of Wavelength Division Multiplexing (WDM) technology, which is proposed in order to increase the capacity of the optical fibers. More than 80 channels can be simultaneously transmitted over the C-band, and single wavelength can be separated from each other using simple optical filters. Since 2012, the 100 Gbps coherent DP-QPSK systems have been deployed on a 50-GHz grid WDM infrastructure with ~2000 km maximum transmission reach. However, the capacity and the distance reach of optical signals have an upper limit due to the presence of physical impairments when optical signals propagate along the fiber. These physical impairments can be classified into linear effects and nonlinear effects. The linear effects consist of fiber attenuation, Chromatic Dispersion (CD) and Polarization Mode Dispersion (PMD). The nonlinear phenomenon is the Kerr effect: Self-Phase Modulation (SPM), Cross-Phase Modulation (XPM) and Four Wave Mixing (FWM) [1]. Note that the linear impairments can be compensated by advanced Digital Signal Processing (DSP) in the electrical domain. The nonlinear impairments are more difficult to be compensated through DSP, so these nonlinear impairments are the more important factors in the current long-haul transmission.

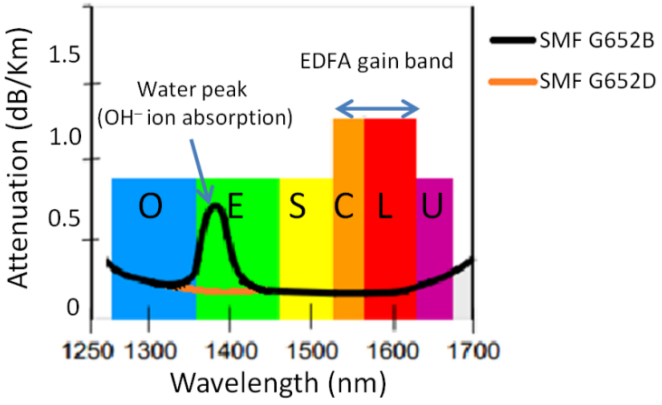

Figure 1-1: Attenuation spectrum of single mode optical fiber G652B and G652D.

Currently, long-haul optical transport is entered in the 400 Gpbs or beyond era. The ever-increasing traffic volume in the network still forces operators to increase their network capacity to meet capacity needs at different network levels (access, metropolitan and core) while lowering CAPital EXpenditure (CAPEX) and OPerational EXpenditure (OPEX) costs. There are a lot of

approaches to achieve this objective. Adding new network capacity is one of the most studied research directions: such as opening new optical amplification windows O, E, S, C, L; using parallel single mode fiber WDM network; deploying new multi-modes and/or multi-cores fiber network. Better using the already deployed network resources is another promising research direction which offers the potential ability to lower the CAPEX and OPEX compared to the approaches of adding new capacity. The optimization of the bandwidth utilization is one of the available approaches in the frame of better using the deployed network resources. We can reduce the spectral gap between sub-bands inside the super-channel and thus improves the spectral efficiency with the help of flex-grid and super-channel technology. We can also reduce the guard band between channels with the emerging technology shown in the literature and the European projects like FOX-C [2]. As current network bandwidth is over dimensioned to support the peak traffic, the channel filling ratio is relatively poor when we consider the average traffic (~55% of average filling ratio). Improving the channel filling efficiency is thus another option to optimize the use of existing network resources and thus to reduce the network costs.

The WDM network was first based on high bit rate point-to-point connections. The whole WDM channels should pass the multiplexer/demultiplexer when we want to extract only one wavelength, which constitutes a lack of the flexibility for the resources allocation and introduces the waste of energy consumption. In order to easily add (or drop) one or more new wavelength channels to (or from) an existing multi-wavelength WDM, the Optical Add-Drop Multiplexer (OADM) was proposed. Based on the OADM structure, Reconfigurable OADM (ROADM) architectures [3, 4] have been proposed later, with remotely reconfigurable switches implemented in the middle stage, in order to improve the flexibility of the resources allocation and reduces the waste of network resources. ROADM is an all-optical subsystem that enables remote wavelengths configuration at any node, so that network operator can choose remotely whether a wavelength is added, dropped, or passed through at the node. It offers the flexibility at optical layer for metro/regional or long-haul WDM networks. In order to still further improve the flexibility of the optical layer, the ROADMs have evolved to support the G.694.1 flex-grid ITU-T standard [5]. The flex-grid concept has been proposed by the ITU-T, it aims as adapting the bandwidth allocation to the super-channel concept through the reduction of the granularity of the WDM network to a nominal central frequency granularity of 6.25 GHz and a slot width granularity of 12.5 GHz. This scheme provides the possibility to allocate more flexibly network resource. Even though the flex-grid concept constitutes a big step towards more agility for optical transport networks, further steps need to be done to go towards an effective full-flexibility of WDM networks, in particular sub-wavelength or sub-band disaggregation and add/drop functionality inside the super-channel which for the moment has been only performed in the research labs. The flexibility offered by the super-channel and flex-grid techniques does not entirely satisfy for the moment the operators' need for a full agility of optical transport networks.

In this context, sub-wavelength switching has been proposed in order to increase further the flexibility of resource allocation while accessing to the sub-wavelength or sub-band granularity at the optical layer level. Sub-wavelength switching consists in breaking up the wavelength into smaller sub-wavelength parts. Through the flexible sub-wavelength grooming directly at the optical transport network level, services are provided thanks to sub-wavelength connections and thus are better adapted to customers' requirements. In current WDM network, a wavelength has traditionally a 50 GHz bandwidth. The bit rate of a wavelength is currently fixed to 100 Gbps using dual-polarization (DP) QPSK modulation format. The source allocation granularity is 100 Gbps. But some kinds of flows require a bandwidth lower than 100 Gbps, which introduces a waste of capacity. With sub-wavelength switching, a flow of 100 Gbps can be for instance divided into 10 flows of 10 Gbps that are distributed to end-users independently. This scheme improves the flexibility of the resource allocation, and thus can lead to a better filling ratio of the network resources resulting in significant CAPEX cost reduction. The sub-wavelength switching could be performed in the optical layer level either in the spectral domain or in the time domain or in both domains. In the spectral domain, a wavelength is divided into several sub-bands that are managed by the optical nodes of the networks exactly in the same way than currently used 100 Gbps DP-QPSK channels today. In the time domain, a wavelength is divided into several time entities, called time slots, which occupies an entire spectral bandwidth of 50 GHz, the same bandwidth as a non-bursty or continuous channel. So, the time slots are considered as the basic network resource units and are distributed to different nodes pairs of the network. Each node pair uses the entire bandwidth not permanently, only for the duration of one (or several) time slot(s). In the following paragraph, we use "sub-band" as the sub-wavelength granularity in the spectral domain and the "time slot" as the sub-wavelength granularity in the time domain.

In this chapter, the sub-wavelength switching solutions in the spectral domain will be discussed first, and the sub-wavelength switching solutions in the time domain will be discussed afterwards. A lot of researches have been carried out (for passive optical networks, data center networks, metro/regional WDM or long-haul DWDM system), we focus only on the potential candidates for the metro / long-haul WDM network solutions.

1.1 Sub-wavelength switching solutions in the spectral domain

1.1.1 Super-channel concept

In WDM transport networks, a technology to increase the channel capacity carried by a wavelength is to increase the bandwidth it occupies. But this solution is limited by a lot of hardware constraints: the bandwidth of Digital to Analog Converters (DACs) and Analog to Digital Converters (ADCs), the speed of DSP, the nonlinear impairments, and so on. In order to improve the capacity of

the WDM network, the super-channel solution has been proposed. A super-channel is a large optical spectrum structure that is larger than a single wavelength optical channel. In this structure, multiple optical bands are assembled together with minimal or even no guard-band, which allows saving spectral bandwidth. Moreover, this scheme releases the constraints, such as DAC, ADC, and DSP speed, at transmitters and receivers side, since it is easier to deal with a data flow with less bandwidth and smaller bit rate compared to the previous solution. The entire structure of a super-channel can cover a bandwidth of several hundreds GHz and transport huge bit rates. Inside the super-channel, the sub-band allocation is governed by the G.694.1 flex-grid ITU-T standard [5]. The super-channel technology now is always deployed in the network based on the Optical Circuit Switching (OCS) technology. In OCS, the network is configured to establish circuits, from one node to another node, by adjusting the optical cross-connect circuits in the core routers. The super-channel is considered as a single spectral entity by optical switching devices at the network and is distributed to a node pair will be kept for a long duration. Recently, a new generation of elastic switching solutions based on high spectral resolution optical filters and Wavelength Selective Switches (WSSs) [6][7] has been developed. These solutions offer dynamic all-optical traffic aggregation/grooming at the sub-band level inside the super-channel. Thus, super-channel technology with the filtering and switching elements permits the sub-wavelength switching.

1.1.2 Flex grid standard.

Flex-grid standard was normalized by the ITU-T [5][8] in the early 2010s to cope with the up-coming handling of super-channels. This standard offers a slot width granularity of 12.5 GHz with a nominal central frequency granularity of 6.25 GHz. Figure 1-2 shows a comparison example of the bandwidth allocation using fixed grid standard and flex-grid standard. For a 25 Gbps BPSK signal, it uses 15 GHz bandwidth; for a 50 Gbps BPSK signal, it uses 32 GHz bandwidth; for a 100 Gbps QPSK signal it uses 28 GHz bandwidth; for a 200 Gbps 16QAM signal, it uses 28 GHz bandwidth as well; for a 400 Gbps 16QAM signal composed of two 200 Gbps 16QAM signals, it uses 75 GHz bandwidth including the guard band between the two sub-bands. Using the allocated bandwidth, the signal transported at a raw bit rate that contains a certain percentage of overhead besides the effective bit rate. The raw bit rate is calculated by multiplying the bandwidth, the symbol rate and the number of polarizations. For example, for the 200 Gbps 16QAM signal previously introduced, the raw bit rate is 28 GHz*4 bits*2 polarizations that corresponds overall to 226 Gbps. Thus the net bit rate is about 200 Gbps. We can see that the application of the flex-grid allows using less bandwidth resource: in this example, 37.5 GHz bandwidth is saved. The application of super-channel and flex-grid brings a large flexibility in the channel/bandwidth allocation.

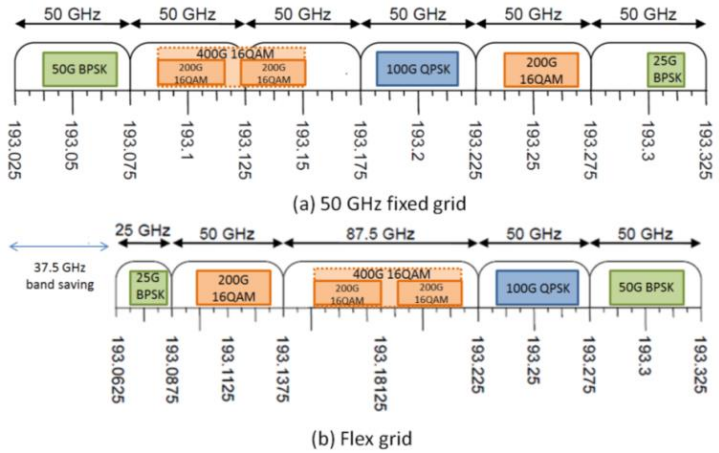

Figure 1-2: Examples of bandwidth allocation (a) using 50 GHz fixed grid and (b) using flex-grid.

1.1.3 Modulation formats adapted to sub-wavelength switching

In order to compose the super-channel, it is necessary to generate sub-bands signal having a rectangular profile, which allows reducing the guard band between two adjacent sub-bands. At the same time, the high spectral efficiency feature is also a key point to be considered. With these two criteria, there are two promising technologies that have been widely studied in the last decade: Nyquist-WDM [9][10] and Multi-Band Orthogonal Frequency Division Multiplexing (MB-OFDM) [11][12].

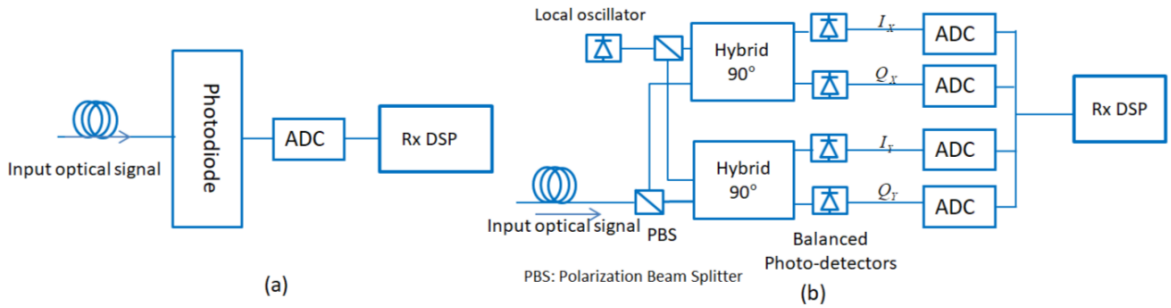

Figure 1-3: The architecture of (a) direct detection and (b) coherent detection technologies.

Both of these two candidates are compatible with direct detection and/or coherent detection technologies. The architectures of these two technologies are shown in Figure 1-3. The left architecture presents the direct detection technology. In direct detection, a photo-detector converts the optical signal in the electrical domain by producing a current proportional to the square of the received optical field amplitude. The right architecture presents the coherent detection technology. In coherent detection, it requires a Local Oscillator (LO), hybrid 90° and 4 balanced photo-detectors in order to detect the real part and imaginary part of the signal. When compared to direct detection, coherent detection is proportional to the optical field and allows recovering both amplitude and phase of the signal, opening the way to simple and efficient digital signal processing.

Direct detection is cheaper (requiring only one photodiode), having a lower power consumption and lower cost-per-bit than coherent detection. But the direct detection offers a lower

spectral efficiency [13][14]. With coherent detection, the linear impairments in transmission of the fiber, such as Chromatic Dispersion (CD) and Polarization Mode Dispersion (PMD), can be mitigated easily [15]. Coherent detection technology is thus more suitable for metro and long-haul transmission system applications than direct detection which is better suited for low spectral efficiency short-reach applications. Some experimental demonstrations using direct detection and coherent detection technologies are compared and shown in the table 1-1. As we can see that the direct detection technology is generally used in the short-reach transmission systems. Considering our specific specifications and requirements in this thesis, we chose coherent detection technology as the technology used in our test-bed.

Table 1-1: The comparison of the direct detection and coherent detection technologies.

Author (year)	Technology	Coherent Detection (CD) / Direct Detection (DD)	Modulation format	Bit rate (Gbps)	Transmission distance (Km)
Liu (2011) [16]	OFDM	CD	16QAM	485	4800
Zhang (2013) [17]	OFDM	CD	16QAM	117.6	10181
Huang (2012) [18]	OFDM	CD	32QAM	85.5	4242
Chaibi (2017) [19]	OFDM	DD	8QAM	14.69	100
Wang (2016) [20]	OFDM	DD	16QAM	128	320
Chagnon (2014) [21]	OFDM	DD	PAM8	112	10
Xia (2012) [22]	Nyquist	CD	8QAM/QPSK	1200/800	1503
Cai (2012) [23]	Nyquist	CD	RZ-QPSK	112	6860
Yu (2012) [24]	Nyquist	CD	CSRZ-QPSK	216.8	1750
Kikuchi (2016) [25]	Nyquist	DD	PAM4	74.67	20
Hirai (2014) [26]	Nyquist	DD	PAM4	100	2

Based on the frequency shift between the local oscillator and incoming optical signal [27], the coherent detection technology can be classified as: homodyne, intradyne and heterodyne. The intradyne technology is widely used in current systems since its phase lock loop is less complicated compared others solutions. In this sub-chapter, we are going to discuss and compare Nyquist-WDM and MB-OFDM when combined with intradyne coherent detection technology.

1.1.3.1 Nyquist-WDM

Nyquist-WDM (N-WDM) is a multi-band transmission technique. N-WDM bundles together multiple optical sub-bands which transport Quadrature Amplitude Modulation (QAM) signals at high symbol rates (for example, from 32 to 64 Gbaud) in order to create an ultra-high data-rate super-channel able to transport 400 Gbps, 1 Tbps or higher. Inside the super-channel, each single sub-band occupies a narrow bandwidth that satisfies the Nyquist criterion of zero Inter-Symbol Interference (ISI). Nyquist filters are used at the transmitter/receiver side to create a rectangular spectrum profile for each sub-band, which allows putting closer the adjacent individual sub-bands without introducing Inter-Carrier Interference (ICI), as shown in Figure 1-4 (a). Using the inverse Fourier transformation, the signals are transformed into time domain, and the signals of each sub-band are overlapped orthogonally without introducing ICI neither ISI.

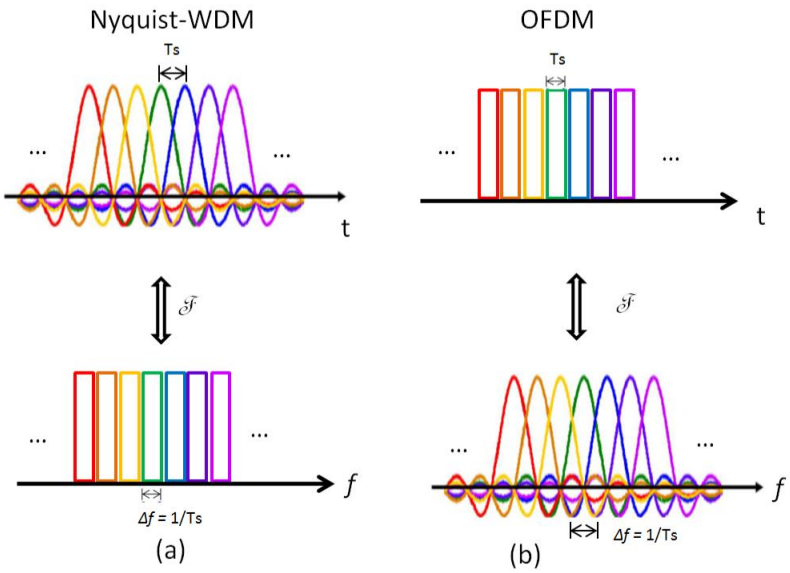

Figure 1-4: (a) Nyquist-WDM signal orthogonality; (b) OFDM signal orthogonality

Figure 1-5 shows a generic block diagram of a single sub-band coherent optical transmitter and coherent receiver. Both transmitter and receiver consist of three parts: the DSP part, analog-digital or digital-analog conversion in the electrical domain and the electrical/optical (E/O) or optical/electrical (O/E) conversion.

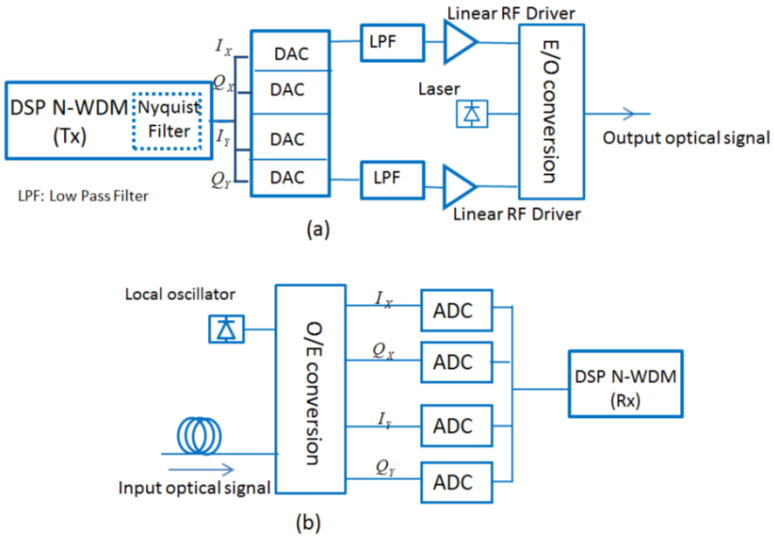

Figure 1-5: Nyquist-WDM (a) transmitter and (b) receiver block diagram.

At the transmitter side, N-WDM DSP is used to generate two complex signals for the X and Y polarizations. The Nyquist filtering function is usually realized inside the DSP. DSP begins with the symbol mapping and encoding. Afterwards, Nyquist pulse shaping is carried out. Signal distortion pre-compensation is then performed in order to compensate for the amplitude and phase distortions due to component imperfections. After the generation of two complex signals, the signals feed four DACs. The analog electric outputs of the DACs are sent to the Electric-Optic (E/O) conversion interface in order to be modulated on a continuous wave optical emission. The wavelength of the laser can be fixed or tunable based on the application configuration. The output optical data signal of the E/O conversion interface is then transmit to fiber lines.

At the receiver side, the received signal is converted to four baseband electrical tributaries at the Optic-Electric (O/E) conversion interface, which is usually composed of optical hybrid and balanced detectors. A fixed or tunable laser is used as local oscillator. The four analog electric signals are then converted to digital domain by four ADCs. Afterwards, the DSP is carried out to recover information. The DSP is often based on blind equalization even if data-aided equalization is also used in some proprietary and advanced DSP implementation. Blind equalization is often preferred for its simplicity and ability to avoid any additional overhead (training symbols) and therefore maximizes the spectral efficiency. During the equalization process, a Finite Impulse Response (FIR) filter is implemented to compensate for the linear fiber impairments such as CD and PMD [28] which are mitigated one after the other. The coefficients of the FIR filters are generally determined by the means of algorithms, such as the Constant Modulus Algorithm (CMA) [29] which is well-adapted to QPSK modulation, Radius-Directed Equalization (RDE) method [30] which works well with higher-order QAM, Decision-Directed Least Mean Square (DD-LMS) [31] and so on. For polarization recovery, a “butterfly” FIR filter bank is used to perform polarization demultiplexing/separation and PMD compensation. After that, a matched filter of the Nyquist pulse shaping filter used at transmitter side is implemented to filter signal while maximizing the signal to noise ratio. Then,

carrier frequency offset compensation is implemented. Afterwards, the phase compensation is realized using blind phase search method [32] at first and then the Maximum Likelihood Sequence Estimation (MLSE) technique [28] [33]. After carrier recovery, demodulation is carried out.

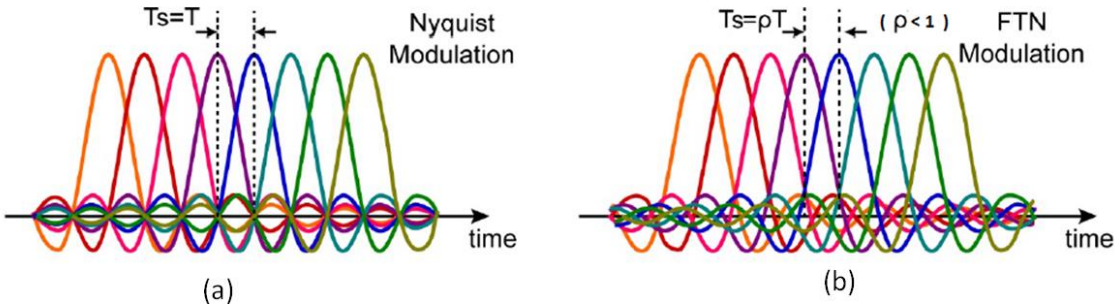

Figure 1-6: (a) Nyquist and (b) FTN signal time overlapping

In order to achieve a higher spectral efficiency while breaking the Nyquist limit, the Faster Than Nyquist (FTN) [34] [35] technique has been proposed. The principle of FTN pulse shaping technique is to reduce the employed optical bandwidth of each sub-band and put closer the adjacent sub-band by introducing a small and controlled ISI, as shown in Figure 1-6 (b). In return for that, a power-penalty is paid to recover the transmitted signal. In order to limit the introduced ISI without introducing so much power penalty, low-order QAM should be used in FTN approach. In [35], authors have shown that the power penalty increases dramatically when the order of modulation format increases. They also showed that FTN is able to provide a bandwidth reduction between 2.5% and 17.5% (depending on the different modulation formats) in comparison to a normal Nyquist modulation. Except the power penalty, the detection complexity of the FTN is considerably higher than normal Nyquist-WDM technology, since a trellis decoder is needed to decode the FTN data with the trellis-structured ISI. Even if FTN introduces power penalty and increases detection complexity, the benefit of spectral efficiency brought by FTN technology is still valuable for optical transmission system.

1.1.3.2 OFDM

OFDM is one of the most used multi-carrier transmission technologies. It comes from the radio communications domain. Its principle is to combine orthogonally a large number of subcarriers to generate a rectangular signal in the frequency domain. Each subcarrier has a sinc-function spectrum and occupies only a small bandwidth. The orthogonality between the sub-carriers is guaranteed by spacing the adjacent subcarriers of Δf that is the inverse of the symbol duration Ts, as shown in Figure 1-4 (b). The signal orthogonality permits to avoid any carrier interference from the other subcarriers while using Fast Fourier Transform (FFT) algorithm in the signal demodulation process. The combination of small subcarriers leads to a rectangular profile of the signal spectrum, which allows reducing guard bands between adjacent OFDM bands without inducing detrimental crosstalk.

The OFDM DSP block diagram is similar to the one of N-WDM shown in Figure 1-5, except the DSP which has to be adapted to OFDM. So here we will give a brief introduction of OFDM DSP. The OFDM DSP at the transmitter side, shown in Figure 1-7(a), begins with data encoding and symbol mapping. Then pilot tones are inserted into the data spectrum in order to estimate the phase noise after transmission. Afterwards, training symbols and synchronization symbol are added for channel equalization and time synchronization. Then the signal is transformed from frequency domain to time domain using inverse FFT. In order to improve the robustness against CD and PMD, cyclic prefix is inserted at the beginning or rear of each symbol. After parallel-to-serial conversion, clipping is carried out in order to reduce the Peak-to-Average Power Ratio (PAPR) of the OFDM signal. A lower PAPR can better take use of the Effective Number of Bits (ENOB) of DAC, and thus to reduce quantification noise.

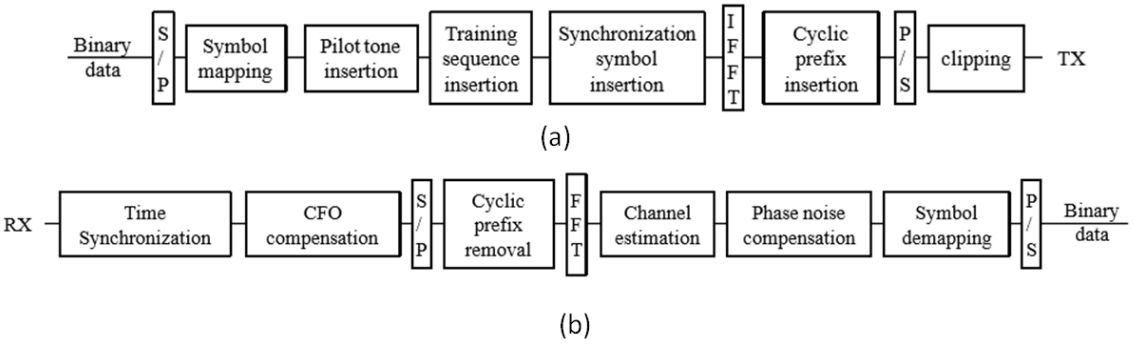

Figure 1-7: (a) The typical OFDM transmitter DSP process; (b) The typical OFDM receiver DSP process.

At the receiver side, as shown in Figure 1-7 (b), the DSP has almost the inverse process as the DSP process carried out at the transmitter side. The time synchronization is realized at first to recover the starting point of the OFDM frames. Then Carrier Frequency Offset (CFO) compensation is carried out. After serial-to-parallel conversion, the cyclic prefix is removed. Thanks to the cyclic prefix, the payload is protected from CD and PMD effects. Afterwards, FFT is applied to transform the signal from time domain to frequency domain. After that, a data-aided channel estimation using training symbols is performed and phase noise compensation using pilot tones is carried out. At last, the data demodulation and de-mapping are performed.

MB-OFDM is one of the OFDM variants: its principle is to divide the OFDM band into several OFDM sub-bands and then bundle them together to generate a super-channel. Each sub-band occupies a small bandwidth in the order of 10 GHz. This bandwidth is chosen to release the hardware constraints in the transmitter/receiver, such as DAC, ADC and linear RF-driver, TIA amplifiers, as it seems very challenging to realize a large bandwidth and high speed DAC, ADC and linear RF-driver with flat frequency response. As commercial ~10 GHz pass-band and stop-band optical filters are available, each OFDM sub-band can be added or dropped optically. Consequently, a two-level switching process (at the sub-band and super-channel levels) can be implemented with such MB-OFDM signal (note that it could be also implemented with Nyquist-WDM). In the literature, both

the transmission and the ability of sub-band add/drop have been demonstrated. In [12], an optical transmission system with 100 Gbps MB-OFDM on 1000 km of SSMF has been achieved. In [11], MB-OFDM transmission with sub-band add/drop functionality is demonstrated experimentally. In this experiment, each sub-band occupies only 8 GHz bandwidth and transports a 25 Gbps bit rate, while the 4 sub-bands carry 100 Gbps in a 50 GHz bandwidth. The guard band between two adjacent sub-bands is reduced to 2 GHz while the frequency spacing between two sub-bands is 10 GHz. This resource allocation is different from the 12.5 GHz ITU-T flex-grid standard, because the authors want to show the ability of MB-OFDM to reduce the guard band, but they cannot enlarging the bandwidth of signal due to the DAC constraint. All these results demonstrated that the high flexibility and high transmission capacity brought by the MB-OFDM technology.

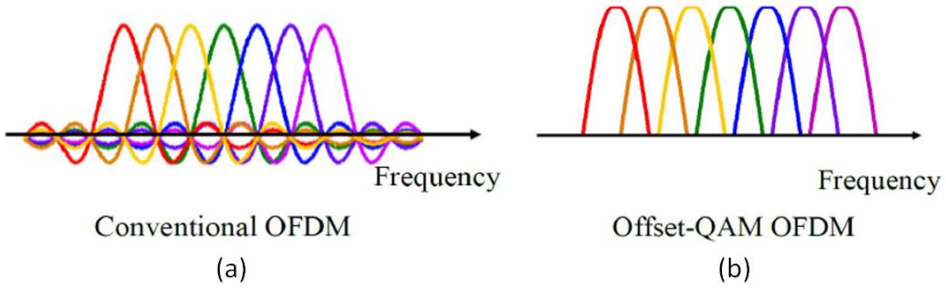

Figure 1-8: (a) Conventional OFDM and (b) Offset-QAM OFDM signal spectral overlapping.

Compared to N-WDM, the overheads of OFDM or MB-OFDM is higher due essentially to the insertion of a cyclic prefix (CP) required to avoid ICI and ISI. In order to reduce the overhead ratio, another variant of OFDM, called Offset-QAM OFDM [36, 37, 38], has been proposed. The principle of Offset-QAM OFDM is to delay the quadrature part of the signal by a half symbol period, compared to the in-phase part and set a $\pi/2$ phase difference between even and odd sub-carriers. After that, for each carrier, a pulse shaping filter is used to delete the side oscillation of the sinc-function spectrum of the conventional OFDM (as shown in Figure 1-8 (b)) and as a consequence to quasi-suppress the pedestals located from each side of the offset-QAM OFDM signal , which allows keeping sub-channel orthogonality and minimizing potential ISI. This scheme, the combination of $\pi/2$ phase shift and the pulse shaping filter, has been demonstrated to reduce greatly the CP length. On the other hand, due to the CP removal, the conventional channel equalization technology is no longer sufficient to perform the channel estimation when the CD and PMD are large [39]. As a result, a more complex DSP needs to be performed. Experimental results show that 111-Gbps PDM offset-QPSK OFDM achieves 23% increase in net capacity over conventional OFDM under the same transmission reach [37] thanks to the reduction of overheads. Compared to conventional OFDM, Offset-QAM OFDM has thus shown very attractive advantages in terms of spectral efficiency or potential resistance to sub-band switching (in a MB-offset-QAM OFDM implementation). It is precisely the two reasons why offset-QAM OFDM is seriously considered as the basic transmission technology for future 5G mobile networks.

1.1.1.3 Comparison between Nyquist-WDM and OFDM

MB-OFDM and N-WDM are two promising candidates to realize super-channel having similar performances. Generally, both of them can achieve a high spectral efficiency: spectral efficiency greater than 5 bits/s/Hz can be achieved with both MB-OFDM and N-WDM using high-order QAM [10][11][40][41]. For the tolerance to the fiber non-linear effects, authors in [42] [43] show that there is no significant differences between CO-OFDM and N-WDM.

In terms of digital signal processing technology, MB-OFDM uses data-aided channel equalization technology while N-WDM is often associated with blind channel equalization (even if data-aided equalization is also often used by equipment suppliers to refine further transmission performance). As a result, OFDM uses a heavier overhead due to the presence of training sequence. OFDM transport thus a slightly lower bit rate when using the same bandwidth and QAM format as N-WDM technology. However, data-aided channel equalization has a lower convergence time, making it particularly adapted to traffic bursts. In [44], authors have demonstrated that the blind channel estimation time is in order of 300 ns and the data aided channel estimation is based on the number of data used that is in the order of 100 ns in burst mode traffic. Moreover, OFDM offers the possibility to apply bit and power loading: it consists in using different orders of QAM and various powers at different OFDM sub-carriers in the same sub-band. For instance, the sub-carriers in the middle of the signal band carry high-order QAM while the side sub-carriers (affected by the filtering transfer function of ROADM) carry low-order QAM with higher power). This technology allows a better adaptation of the signal to the limitations/constraints of the transmission chain (i.e. transmitter, receiver, ROADM…).

Table 1-2: Comparison between N-WDM and MB-OFDM [45].

	Distance (Km)	Optimum span input power of a sub-channel (dBm)	Sub-band bandwidth (GHz)	Guard band bandwidth (GHz)	Optimum BER	SD-FEC limit
N-WDM	1000	~ -2.5	15	5	$6.5*10^{-3}$	$2*10^{-2}$
MB-OFDM	1000	~ -4.5	18	2	$1.2*10^{-2}$	$2*10^{-2}$

For the transmission and sub-band switching performance, authors in [45] have demonstrated experimentally the feasibility of sub-band switching using both N-WDM and MB-OFDM. In order to compare their performances, a transmission test with 1 Tbps super-channel, composed of 10 sub-channels, over 1000Km of G.652 fiber was carried out. DP-16QAM modulation format is implemented. The experimental results, about the optimum BER, optimum span input power are shown in the table 1-2. The results show that there is no significant difference between

these two technologies. N-WDM has about 2 dB higher optimal launch power and a slight lower BER level after 1000 Km transmission.

1.1.4 ROADM Principles

We have introduced the solutions that permit to generate super-channels signals. In order to perform sub-wavelength switching in the spectral domain, the optical network structure has to enable the add/drop functionality while having a fine switching granularity. With the combination of flex-grid WSS and ultra-selective or high-resolution optical filters, it becomes possible to add/drop sub-bands inside a super-channel. This kind of sub-wavelength switching network architecture provides a finer granularity and flexibility at the optical layer level in the spectral domain. In this section, we present a state of the art of modern ROADMs and functionalities they enable.

The role of a WDM transport network is to carry optical channels (wavelengths) corresponding to a specified traffic matrix. The network consists in nodes (also called sites) connected to each other through sections of optical fiber.

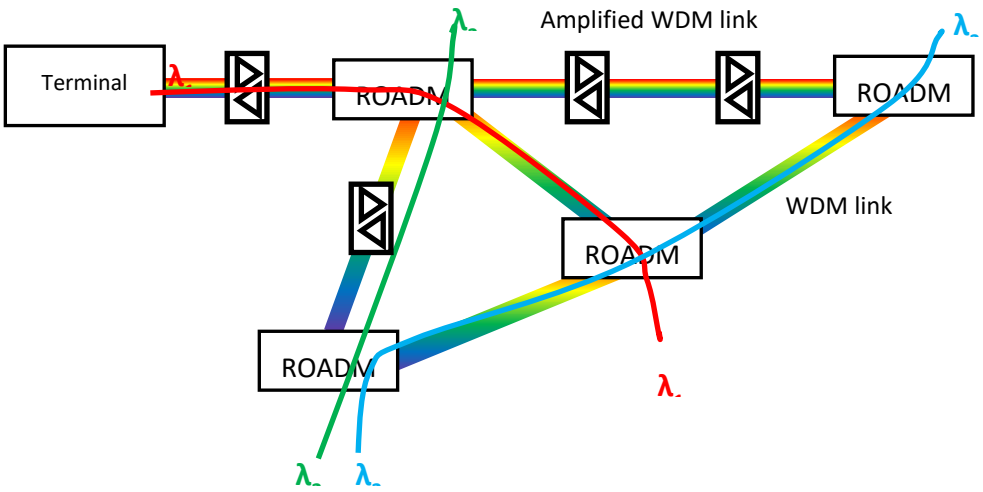

Figure 1-9: WDM network

The aim of OADM nodes is twofold. Firstly, these nodes allow the cross-connection of wavelengths across two or more pairs of fibers, also designated as directions or degrees. Secondly, they allow the addition and dropping of optical channels that are terminated locally. Figure 1-10 shows the schematics for such a 4-degree OADM node. In the early period of optical networks, such kind of nodes were commonly called “all optical cross-connect” or “photonic cross-connect”, while the word OADM was reserved for degree-two nodes, following the terminology introduced in the SDH layer. Fixed OADMs (FOADM) are the first generation of OADM nodes and are implemented using fixed optical filters. The set of wavelengths that are added and dropped locally at the FOADM,

and the set of wavelengths that are passed-through from one degree to another, cannot be modified. Therefore, the channel plan must be determined prior to the manufacturing.

Reconfigurable OADM (ROADM) [3, 4, 46, 47, 48] use more sophisticated structures and offer several levels of flexibility, depending on the chosen architecture. Based on ROADM technology, network operator can choose remotely whether a wavelength is added, dropped, or passed through at the node making full reconfigurability and automation at the optical layer level possible. This flexibility allows adapting to the resource allocation modification implied by network churn or new traffic demands.

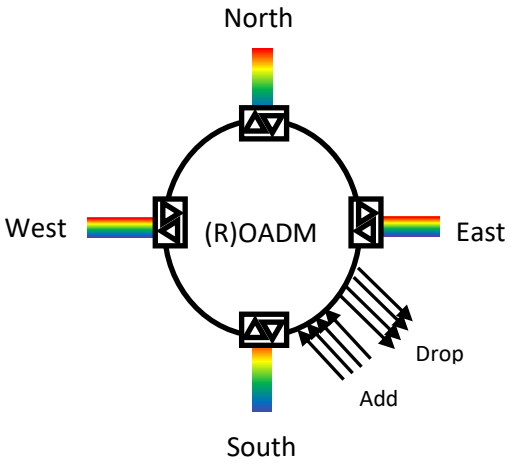

Figure 1-10: Architecture of 4 degrees basic ROADM functionality.

Because of the ever increasing traffic growth and the predominance of high-bandwidth data services over traditional voice services, it has become crucial for WDM network operators to be able to adapt quickly to a traffic matrix change. Their typical requirement is the ability to establish new connections across the network in just a few hours. Current trend in optical transport networks is to move towards a high level of automation, thanks to an intelligent control plane allowing the computation of routes across the network, and its associated management plane that can automatically configure the equipment to establish the resulting circuit. A fully automated network also implies to have no need for on-site (i.e. physical) intervention for cabling, once the node has been installed. In view of this trend, the data plane must be composed of highly reconfigurable nodes. ROADMs are the key part of these intelligent and automated networks. These nodes should be sized and pre-equipped with transceivers according to the planned add/drop capacity for each node.

The discussion hereafter is illustrated with a 4-degree ROADM as represented in Figure 1-10, but can be generalized to any N-degree ROADM ($N \geq 2$). ROADM nodes have two types of ports: degrees (or directions) which are connected to the WDM links and local Add/Drop which are connected to the local transceivers.

The main parameters of a ROADM node are:

- Number of degrees: It is the number of WDM links to which the node is connected considering the use of one pair of fibers per link.
- Number of add/drop ports: The number of add/drop ports sets the maximum capacity that can be added and dropped at the node.
- Colored/Colorless: An add/drop port of a colorless ROADM is not tied to a specific wavelength. When a tunable transceiver is connected to an add/drop port of a colorless ROADM, its wavelength can be reconfigured if needed, without physically disconnecting and reconnecting the interface to another port. In contrast, the wavelength of a transceiver connected to an add/drop port of a colored ROADM cannot be reconfigured without on-site intervention.
- Directed/Directionless: An add/drop port of a directionless ROADM is not tied to a specific degree. When a transceiver is connected to an add/drop port of a directionless ROADM, its traffic can be re-routed to any other direction if needed, without physically disconnecting and reconnecting the interface to another port. In contrast, the optical channel associated with a transceiver connected to an add/drop port of a directed ROADM cannot be re-routed to another degree without on-site intervention.
- Contentioned/Contentionless: Contentionless ROADMs allow several local transceivers to use the same wavelength over different degrees. In contrast, a contentioned ROADM does not allow the termination of two channels using the same wavelength over two different directions. Since a contentioned ROADM introduces a constraint on the add/drop wavelengths, the maximum capacity of the node is reduced. Moreover, in the context of a dynamic optical network, the end-to-end wavelength assignment algorithm used by the intelligent control plane is made more complex.

Colorless and Directionless (C/D) are the minimum ROADM attributes required to build a dynamic and automated WDM network. Indeed, these two attributes avoid the need for physical intervention at ROADM nodes during a network reconfiguration. C/D ROADMs are already commonly deployed in metro and regional WDM networks. As mentioned above, the wavelength contention problem in C/D ROADMs can lead to a significant reduction in the network capacity, and implies a more complex wavelength assignment algorithm to support highly loaded networks. Colorless/Directionless/Contentionless (C/D/C) ROADMs offer the ultimate flexibility to optimize the network capacity. C/D/C ROADMs are not yet widely deployed because of their high cost and complexity, but will become more and more common in the next few years with the growing need for flexibility and capacity. It is also worth noting that architectures offering a limited amount of contention may provide a suitable trade-off between node cost and wavelength assignment complexity.

In terms of flexible resource allocation, the flex grid WSS is proposed to replace the fix grid WSS and filters components in the conventional ROADM node, which enables the allocation of the bandwidth resource with a finer granularity of the spectral grid (12.5 GHz) and the variable bandwidth which is an integer multiples of 12.5 GHz granularity. Based on this more flexible concept, calculations and simulations have attempted to provide realistic benefits [49]. However, even though the ROADM has haven a great development, the technology based on WSS cannot achieve a sub-wavelength disaggregation at the optical layer. In consequence, the high spectral resolution optical filters should be implemented inside the ROADM node in order to separate the sub-band from the super-channel.

1.1.5 High spectral resolution filters

For the sub-wavelength switching in the spectral domain, the add/drop functionality should be realized with the help of narrowband optical filters. As a result, the optical narrowband filter that has a bandwidth from several GHz to dozens of GHz is the key component to determine the granularity in the spectral domain. In this section, we give a brief overview of some high spectral resolution filters.

An ideal pass-band filter should have a flat top and steep edges in order to realize a rectangular filter profile, which aims to keep high signal fidelity and suppress all the noise out of the signal bandwidth. Moreover, the filter wavelength and bandwidth tunability is also highly desired in order to reconfigure itself to cope with different requirements. Different solutions have been proposed in the literatures to realize such kind of filters: bulk-grating technique [50], Liquid-Crystal on Silicon (LCoS) [51], arrayed waveguide grating [6], Fiber Bragg Gratings (FBG) [52], cascaded micro-ring resonators [53] and Stimulated Brillouin Scattering (SBS) [54]. All of them have a promising development in the last years, but some limits restrict their wide application. In the following paragraphs, we will present the filters based on bulk-grating technique and arrayed waveguide grating, which can response best to our requirements.

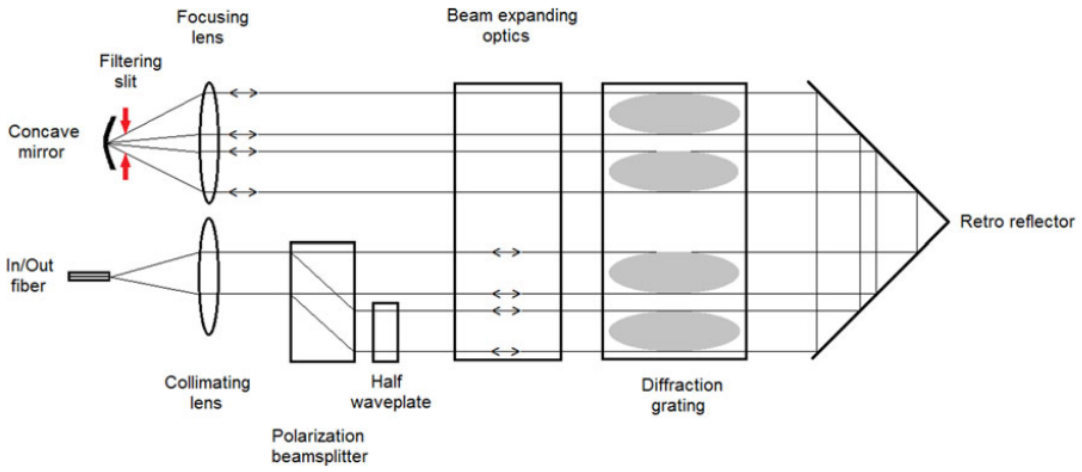

Figure 1-11: Typical FSO based filter architecture [50].

For the filters based on bulk-grating technique, a filter having a 10 GHz typical Full-Width-at-Half-Maximum (FWHM) and edge roll-off of 1000 dB/nm has been reported in [50]. This filter uses Free Space Optics (FSO) based technology, which is a combination of bulk diffraction grating and filtering slit. The filter architecture is shown in Figure 1-11. After the input collimating lens, a polarization-diversity configuration is used in order to separate the X and Y polarizations. The beam expanding optics is inserted before the diffraction grating to spread the beams thus illuminating the whole width of the following diffraction grating and refining the filter resolution. After a retro reflector, the beams are sent to a concave mirror. A reconfigurable slit is inserted before the concave mirror, which is used to filter the signal with the configured bandwidth. The filter central wavelength is chosen by the rotation of the retro-reflector, so that only the chosen wavelength can return back to the output fiber.

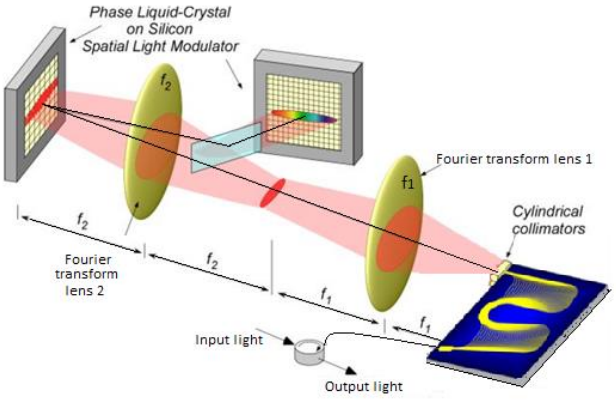

Figure 1-12: Typical LCoS based filter architecture [6].

For arrayed waveguide grating based filter, an additional phase LCoS SLM (Spatial Light Modulator) is used to modify each beam phase, so that the waveguide propagation inaccuracy is compensated and thus the high precision is achieved. In this implementation, as shown in Figure 1-12, the input optical signal passes through an arrayed waveguide grating at first, which is used to split and diffract the input signal into several beams. And then the diffracted signal is sent to pass through a 4-focus system which is composed by two Fourier lenses, in order to put the light signal on a 2D array of LCoS pixels. The first LCoS SLM is used to compensate the phase errors of the diffracted signal. After that, a pick-up mirror is placed between the first lens and the second lens in order to separate the input diffracted signal and the reflected phase corrected signal. The reflected phase corrected signal is passed to the second LCoS SLM. In the LCoS 2D array, each pixel is able to generate individually the phase retardation from 0 to 2π according to the control signal. After that, the phase-modified signal travel back in the same path as inputting, but as different wavelengths have different phases, after the conventional grating, different wavelength will be routed into different output ports. So the desired wavelength is selected. The authors in [6] record that 0.8 GHz optical resolution (the minimum passband bandwidth) and 200 GHz free spectral range is achieved.

The central wavelength can be modified with high precision, in a step as narrow as 200 MHz. This performance enables the cascade ability of a large number of WSS and realizes complex spectral filtering functions with extremely sharp features.

For the existing commercial productions, several providers are available for these kinds of filters: such as Finisar, Yenista, Teraxion and alnair Labs. The table 1-3 shows the available filters and the corresponding performance, which represent the commercial record. In order to implement our test-bed, the filter provided by Yenista and the WSS provided by Finisar are used.

Table 1-3: The current existing commercial high spectral resolution filters

Provider	FWHM	Tuning Resolution	Tuning Range
Finisar [55]	10 GHz to 100 GHz	1 GHz	1480 - 1620 nm
Yenista [56]	4 GHz to 625 GHz	0.125 GHz	1480 - 1620 nm
Teraxion [57]	50 MHz to 50 GHz	0.25 GHz	1525 - 1565 nm
Alnair Labs [58]	3.7 GHz to 370 GHz	0.5 GHz	1525 – 1610 nm

With the support of ROADM technology, high selective filters and super-channel technology, future WDM networks should permits to perform switching on a wavelength and sub-wavelength granularity basis. Thus, it will allow adapting the network resources to the dynamically varying traffic demands. This high flexibility switching functionality will also lead to a reduction of network cost compared to electronic-based alternatives [59]. However, with these sub-wavelength switching solutions in the spectral domain, switching is based on optical circuit switching technology, which is rather slow that limits the network flexibility. Therefore, it is particularly relevant to associate it to a fast optical switching technology, which relatively easy to achieve in the time domain.

1.2 Sub-wavelength switching solutions in the time domain

Besides the sub-wavelength switching in the spectral domain, the sub-wavelength switching can also be performed in the time domain. Indeed, time domain sub-wavelength switching solutions divide the wavelength into time entities, different end-users can access the same wavelength while using the wavelength for only a fraction of time (several time slots), which permit to share the same wavelength resource. Sub-Lambda Photonically Switched Networks (SLPSN) [60] has been normalized by the ITU-T in 2012 to describe the characteristics and common points of all time domain sub-wavelength switching solutions. In SLPSN, according to the length of the optical burst or optical packet, the sub-wavelength switching solution in the time domain is called Optical Packet Switching

(OPS) [61] or Optical Burst Switching (OBS) [62]. Due to the lack of key optical components, such as big size fast optical memories and commercial fast optical switches, the realization of OPS in the real scale network faces significant challenges. Thus, OBS has been introduced as an alternative to OPS. Indeed, in OBS, optical bursts are an assembly of several optical packets that are sent to the same destination. Therefore, OBS manages time entities in the range of 1 µs to 10 ms which releases the constraints on the switching components. Consequently, we will focus on discussion on OBS solutions in this subsection.

1.2.1 Principles and interests

Numerous OBS implementations have been proposed either by academics or by manufactories in order to perform optical burst switching. Most of these OBS solutions have a data plane and a control plane. The data plane is the physical layer that performs the burst transmission/reception, burst aggregation/disaggregation and burst switching. The control plane manages the burst transmission scheduling and configures all the network resources, including transmitters, receivers and optical switches.

Before we discuss about the OBS solutions, a brief introduction on the characteristics of the OBS solutions is given. As the performances of OBS solutions depend greatly on their nodes structures, network configurations and control strategies, these characteristics can be used to describe and classify the OBS solutions and are the main principal points used to evaluate an OBS solution. The characteristics are listed as lossy or lossless, transparent or opaque, centralized control or distributed control, synchronous or asynchronous:

- **Lossy/lossless**: Based on the point that whether the network can guarantee the successful data transmission, OBS solutions can be classified into lossy solutions or lossless solutions. The lossy solutions cannot guarantee the transmission/reception success of the bursts. When there is contention between two bursts which are going towards the same destination the node can decide to discard one burst, destroying the corresponding packets. By contrast, the lossless solutions guarantee the successful transmission, using certain technologies in the optical domain or in the electrical domain of all the bursts up to their destination.
- **Transparent/opaque:** Based on the core nodes architecture of the network, the OBS solutions can be classified into opaque or transparent solutions. The transparency refers to the ability of the core node to handle in the optical domain a broad range of heterogeneous signals regardless of protocol formats, bit rates, or modulation. In an opaque solution, the data can be converted in the electrical domain when they pass through a node. So the switching is realized in the electrical domain and the electrical components have a limit on the signal formats and bit rate. Afterwards, the data are converted back in the optical

domain and be sent to the next node. This process is referred as Optical-Electrical-Optical (OEO) conversion. In a transparent solution, there is no constraint on the signal that passes through the core node.

- **Centralized/distributed control:** Concerning the control plane architecture, the main control operations can be realized by one or a few control entities. This solution is referred as centralized control solution. In the distributed control solutions, each node has its own control entity that behaves independently from each other.
- **Synchronous/asynchronous:** In order to perform control protocol, the control entity of some OBS solutions requires a synchronization of the entire network. This synchronization can guarantee all the transmitters and/or receivers having an accurate time, which is necessary to define the time slots in a cyclic process or to time-stamp the data. This kind of solution is called a synchronous solution. By contrast, in the asynchronous solution, the nodes do not need any synchronization and work independently from the other nodes.

For each kind of solution, one of the key parameters for bursts design and management is the burst duration, which is from 1 µs to 10 ms as described in the ITU-T SLPSN standard. In the synchronous solution, a solution is called time slotted solution if the all the time slots have a fixed duration. In one time slot, one or several bursts are inserted in. Between two adjacent bursts, the guard times are inserted in order to cover system synchronization imprecision error due to clock jitter and devices tuning time. For a time slotted solution, the alignment refers to the synchronization between two bursts sequences. If the bursts of two sequences arrive at the destination node one by one with a synchronized arrival time (see Figure 1-13 (a)), the solution is called aligned slotted solution [63]. Otherwise, in the non aligned slotted solution, the arrival time between two time slots sequence is different at the destination (see Figure 1-13 (b)).

Figure 1-13: (a) aligned time slotted solution; (b) not-aligned time slotted solution

In order to share a wavelength between nodes pairs, the node should have the ability to process the burst data at various wavelengths, which means that the transmitter and/or the receiver shall be able to generate and/or receive the data at various wavelengths. As a result, three ways are possible to realize the OBS solutions: tunable transmitters with fixed receivers, fixed transmitters with tunable receivers and tunable transmitters with tunable receivers.

For tunable transmitters/receivers, there are lots of implementation methods. Different configurations are adapted to different use cases and lead to different performances. For the

transmitter, one of the solutions is to use fast tunable lasers in the transmitters. The tunable laser can change the wavelength of the generated carrier that will transport the burst data. An example of a fast tunable laser, with 50 ns switching time and a linewidth in the order of several MHz, is presented in reference [64]. It is used in the transmitter to generate the bursts at various wavelengths [65]. This kind of laser has a narrow linewidth for direct detection technology but not enough for coherent detection. At the receiver side, when we use coherent detection technology, local oscillator will be tuned to select the received wavelength. A fast tunable laser similar to the one used at transmitter side can also be used at the receiver. When we use direct detection technology, the fast switching devices such as filtering devices cascaded with optical gates, will be implemented before the input of each direct detection receiver to select the bursts at various wavelength. Note that if there is only one bursts data at each instant presented at the input of the direct detection receiver, the tunablility is not necessary since the broad band photodiode is usually implemented at the direct detection receiver, which is able to capture the burst data at various wavelengths. As a result, the fast switching devices are always implemented in the core node in place of destination node side in order to avoid implement a fast switching device at each destination node.

When we share the wavelength, different end-users can access the same wavelength at the same time or via the same port, so the contention arises. The contention can happens in the data plane, it can also be in the control plane. In order to avoid the contention, different optical burst switching strategies have been proposed. Optical burst switching strategy depends also strongly on the core node architecture and configuration. There are two typical node configurations: passive and active configurations. For the passive configuration, the core node is realized by passive filters and optical switches, such as demultiplexers/multiplexers and wavelength selective switches. The core node is configured to set up direct routes between sources and destinations, drawing a set of predefined paths for burst. One of the lossless routing solutions is to control the bursts emission time. Once the burst is generated at the transmitter side, the arrival time at each core node and destination node is predictable. So the accurate synchronization and careful scheduling of the burst emission can guarantee the lossless routing. For the active configuration, the core node can be realized by optical gates and wavelength converters. Based on these elements, the core node allows redirecting dynamically a wavelength to the desired output port (with fiber delay line or deflection route) or converting a wavelength to another one that is not occupied, which offers more possibilities for the control plane to realize the lossless routing. But this active architecture induces high cost and energy consumption.

The conventional OBS network has been introduced in [62] as an alternative solution combining the optical circuit switching and the fine grained optical packet switching. When the burst is sent, a corresponding control packet is generated optically and will be read electrically at every node. Then the node configures optical resource for the pure optical transmission of the payload.

Due to the lack of fast, scalable, and robust optical bit-level processing technologies, electronic processing is still necessary and thus OEO conversion is necessary. As the electronic processing is slower than the pure optical transmission, the control packet is generated before the optical bursts. Similar to conventional OBS, Labelled-OBS (L-OBS) [66] is also an OBS solution of the first generation. But in L-OBS solution, the header, called label here that contains the control information, is assembled together with the payload. These solutions reduce but not eliminate totally the challenge of energy consumption and processing speed related to the OEO conversion. Moreover, the contention can arise at the core node, when two packets from different input port/wavelength pairs must be switched to the same output port/wavelength pair at the same time.

In order to reduce the power consumption and the switching time at the node, a lot of researches have been carried out. NTT has achieved a success in the label processor in terms of reduction of the energy consumption and latency [67]. Through the combination of the label processor and 8 × 8 broadcast-and-select optical switch, they also have demonstrated 100 Gbps optical packet switching with low power consumption in [68]. The wavelength selector is considered as a key component in the node, it is interesting to build a fast switching and low OSNR degradation wavelength selector. In [69], authors reported an InP monolithically integrated wavelength selector based on a cascade of arrayed waveguide gratings and optical switches. They demonstrated that the proposed solution has the features of lossless and low OSNR degradation error-free wavelength selection of four modulated signals at distinct wavelengths. At the dynamic operation configuration, there are 2.6 dB power penalties and the switching time is in the order of 5 ns.

KDDI has applied the L-OBS technology into the data center network [70][71]. They break traditional centralized DCs down to small pieces (micro-DCs) spreading across metro areas while employing OBS over the micro-DCs. To holistically organize the distributed micro-DCs and network resources, a hierarchical Software-Defined Networking (SDN) control plane is adopted. Centralized control is used for each micro-DC and distributed control is used for the metro optical network.

Besides the data plane, a lot of researches have been carried out for the control plane layer. Generalized Multi-Protocol Label Switching (GMPLS) has been proposed in order to extend the protocol MPLS that is used in the electrical layer to control the resources allocation in the data plane, such as a wavelength for a DWDM system or a time slot for a SONET/SDH device. GMPLS enables the bypassing traffic router to optical layer, which can reduce the energy consumption. With the support of GMPLS control plane, a core architecture supporting time shared sub-wavelength switching was reported in [72][73]. In the core architecture, FPGA is implemented and performs as a node controller. The use of FPGA can easily combine with optical devices at the node, which enables various network functionalities such as aggregation, switch control. These remote reconfigurable

functions make the node support hardware virtualization and allow creating slices of the node associating them with arbitrary traffic types.

As we can see, OBS has raised interest in different laboratories and enterprises throughout the world. A lot of innovations, both industrial and academic, redesigned the network architecture top-down in the past years. Since we expect to eliminate the OEO interface in order to reduce the processing speed limit and the energy consumption as well as guarantee the successful data transmission in the network, we focus on the lossless solutions with transparent core nodes. We will only consider the industrial prototypes in the following paragraphs.

1.2.2 POADM solution

The Packet Optical Add/Drop Multiplexing (POADM) [74] [75] [76] has been proposed by Alcatel-Lucent Bell Labs (now Nokia). Even it is named as optical packet switching, as the packets duration is 10 µs, which is in the interval of 1 µs to 10 ms, we will consider it as an OBS solution. It is a time slotted synchronous solution. Both centralized and distributed controls can be implemented in POADM for the allocation of time slots. POADM is proposed to be implemented on a ring topology. The POADM node is transparent for signals with any bit rate, and the feasibility has been demonstrated in [77]. POADM was first proposed for metro network applications and recently some studies applied POADM on data center networks (DCN) [78][79] and mobile backhaul network [80].

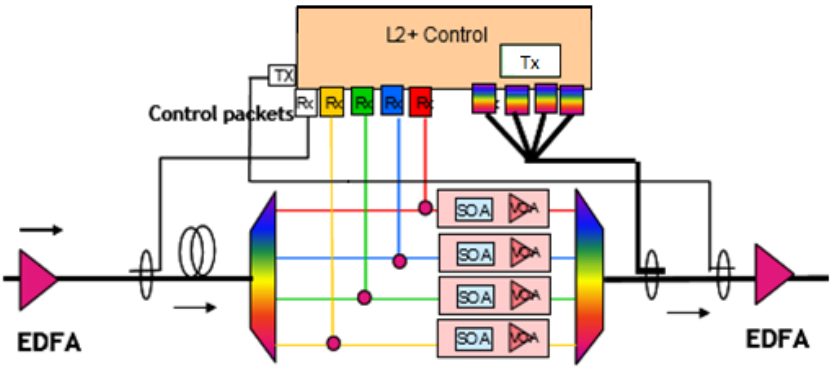

Figure 1-14: POADM node structure [74].

Figure 1-14 shows an example of POADM node structure. A POADM node is equipped several transmitters and several receivers, so that a node can send and receive several data bursts at different wavelengths at the same time. The fast tunable lasers (~ 50 ns switch time [64]) are used at transmitter side to generate the bursts at various wavelengths. Fixed wavelength receivers are implemented at the node, but the receivers can also be tunable with coherent technology. The burst switching and extraction is realized by the combination structure of a set of optical gates and demux / mux. If a burst is sent this node, the optical gate (i.e. SOA in Figure 1-14) will be closed to stop the burst to pass though this node. In addition, all the receivers listen continuously the network, but the

control plane will decide whether they detect or discard the data. Concerning the detection technology, both direct [81] and coherent [80] detection have been demonstrated.

In the POADM, a time slot lasts 10 µs containing only one optical burst. Each burst contains at least: one guard time, one preamble, one synchronization symbol and the payload. When no traffic is sent to the network, dummy bursts are generated to ensure the constant input power at the amplification stages [74].

In the control plane, the management optical devices, such as fixed wavelength receivers, optical gates and fast tunable laser in the transmitter, is ensured by a MAC protocol that can perform centralized or distributed resource allocation. In [76], a centralized MAC protocol, called virtual circuit allocation, was proposed. A centralized control entity is built to receive the request from all the edge nodes and then to allocate resources according to the requests. In [82], distributed MAC protocol called Tag-based Enhanced Access Mechanism (TEAM) is proposed. It manages network resources using a token game mechanism. A packet is sent only if a token corresponding to its destination is available at the source node.

Both simulation and experiment demonstrations have been carried out to demonstrate the reliable performances of POADM. Through simulation studies of POADM performance [83], the authors claim that without considering bandwidth loss due to guard time between optical packets, the average channel filling ratio of POADM is up to 80% using their control protocol, which can improve significantly the channel filling ratio. Some application cases have been experimentally demonstrated, like data center in [79] and mobile backhaul network in [80]. The good performance and wide applicability makes POADM as one of the promising sub-wavelength solutions.

1.2.3 OPST solution

Optical Packet Switch and Transport (OPST) [84] [85] [86] had been proposed by Intune Networks for deployment in the metropolitan network and DCN. It was proposed to be implemented in ring topology with transparent core nodes. It is an asynchronous network with a distributed control protocol, called Optical Media Access Control system (OMAC) that guarantees that there is no burst collision in the network. It employs Carrier Sense Media Access with a Collision Avoidance (CSMA-CA) mechanism. This solution is intended to be deployed in the metropolitan area network and the first industrial application for interconnection of data center was reported in [86]. The OPST solution was the only one solution that had been deployed in real network, even though it does not exist anymore, it is important to give a discussion on OPST solution.

In OPST, a dual-fiber ring configuration is used. All signals travel unidirectionally on one ring and in the opposite direction on the other ring. The transmitter has a fast tunable laser in order to send the data at various wavelengths. A wavelength is associated to one destination. At the receiver side, a fixed wavelength receiver is used to receive the data at the assigned wavelength.

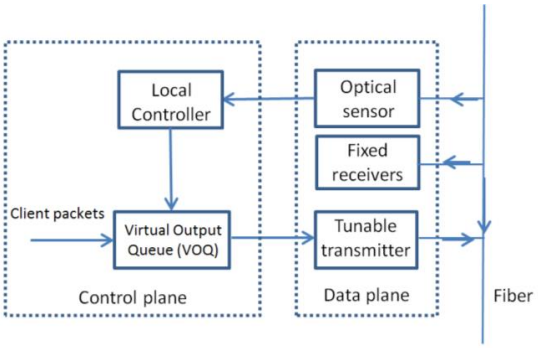

Figure 1-15: Functional blocks of an OPST node.

As the asynchronous access and distributed control OMAC is implemented, the system does not need a ring-wide synchronization. At each node, an optical channel state monitor is implemented acting as an optical sensor in order to detect whether the channel is free or not. When the channel is free, the upload burst data is inserted. Otherwise, when an upstream optical burst is detected, the local burst emission is stopped and reloaded when the channel returns free. The time slot is called OPST frame, it is composed of several client packets coming from the interface of the upper layer. After that, the OPST frames are queued in a Virtual Output Queue (VOQ) to wait for the availability of the required wavelength that is associated to the corresponding destination. The network resources allocation follows the service class basis: priority, best effort. Each control unit operates individually at the node, with only boundary conditions being given by the control system, such as bandwidth, latency and jitter. Therefore, the behavior of each control unit is completely autonomous and asynchronous. Figure 1-15 gives a simplified description of some functional blocks of an OPST node.

The evaluation of the OPST performance has been carried out experimentally. In [87], authors have compared OPST with IPoDWDM, and the results show that OPST enables 150%CAPEX savings in typical network scenarios compared to IPoROADM approach. The flexibility of the OPST also enables 100-300% reduction of power consumption and an average 150% savings on rack cabinets for typical configurations.

1.2.4 TWIN solution

Time-domain Wavelength Interleaved Networking (TWIN) was originally proposed by Bell Labs US [88] [89]. It is a time slotted synchronous solution with mesh topology architecture. Both centralized [90] and distributed controllers [91] [92] can be implemented to perform the lossless switching, but the centralized one has been demonstrated to be more efficient [63] [95]. Some experimental demonstrations have been carried out to demonstrate the feasibility of TWIN solution [93] [94].

In a TWIN network, the routing is based on wavelengths. There are several ways to realize TWIN network: tunable sources with fixed receptions and fixed sources with tunable receptions. Here we consider the first method which was implemented in the frame of the Safe and Secure

European Routing (SASER) European project. Using a fast tunable laser, each source is able to send optical bursts at different wavelengths. Each wavelength is associated to only one destination, so the wavelength is treated as destination address. Different bursts data are transmitted to core node where the bursts are routed optically towards the destinations on a wavelengths basis. At destination, bursts data coming from various sources will be received by a fixed wavelength burst mode receiver. In order to avoid potential collisions in the network, a control plane is implemented. A schedule pattern (called grant) is calculated by the control plane to be distributed to each node in order to control the burst emission. The grants contain the information of the burst emission time and wavelength. Since core node is totally transparent to formats and bit rate of the signals (no OEO conversion), TWIN architecture permits to increase the transparency of the network.

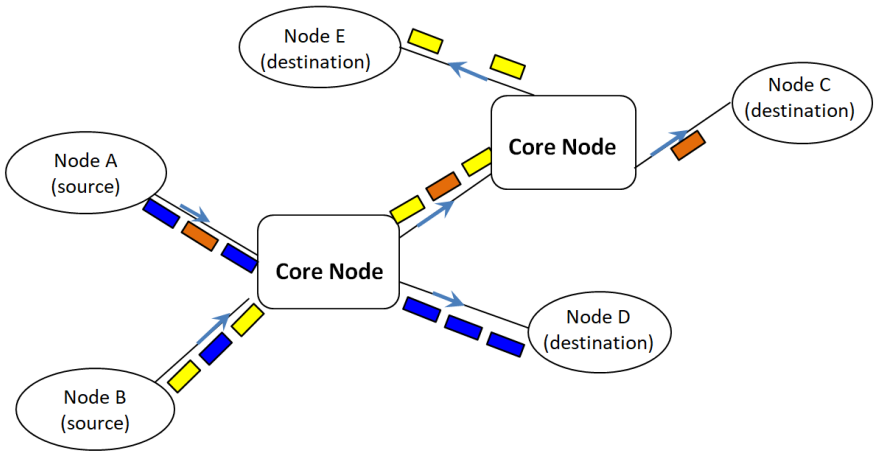

Figure 1-16: TWIN basic architecture

Figure 1-16 shows an example of TWIN network's data plane with five edge nodes (two sources, three destinations) and two transparent core nodes. The nodes A and B work as sources being able to transmit burst data colored in orange, blue and yellow, which are associated respectively to nodes C, D and E. In the first core node, coming bursts are separated on a wavelength basis, and then blue bursts are routed to node D while bursts orange and yellow are retransmitted to the second core node. In the second core node, burst orange and yellow are routed to node C and E respectively. In order to perform bidirectional transmission, each edge node is equipped with a transmitter and one receiver, but nodes can contain several transmitters and receivers according to the total traffic to transport. However, as the number of channels is limited in C-band, which means 80 channels with the ITU-T 50 GHz grids, the maximum number of edge nodes is 80.

For the control plane, TWIN can adopt both centralized controller [90] and distributed controller [91] [92] to perform the lossless switching. In [63] [95], the simulations results show that the centralized controller is more efficient than the distributed controller. And in some practical study cases, the centralized controller has a 15% gain compared to the distributed controller. In [95], both centralized and distributed schemes are investigated. Authors show that the centralized

solution with continuous slot allocation mechanism is the most efficient and it allows a throughput up to 7 Gbps for one wavelength while the capacity of the transmitter and receiver pair is 10 Gbps.

TWIN solution has been selected by Orange as a candidate for the metropolitan network, experimental demonstrations are presented in [93][96] transmitting 10 Gbps Non Return to Zero (NRZ) modulation format and using direct detection technology. In the demonstration, the time slot is set to 5 µs with 4.7 µs burst duration and 0.3 µs guard time that is used to cover synchronization inaccuracy (200 ns) and wavelength switching time (100 ns of a Modulated Grating Y laser). In front of each burst, a 200 ns preamble is inserted in order to recover the clock at the receiver side. The authors noted that there is a potential signal absence (called gaps) at the input of the receiver since the burst traffic cannot guarantee a continuous flow, which can destroy the clock recovery, especially when the gaps duration is larger than 1 µs. Therefore, a solution with inserting dummy burst at the gaps at the receiver side was proposed in order to keep a continuous data flow at receiver side. This solution has been proved efficient [93].

1.2.5 Comparison between the lossless solutions

In this section, three sub-wavelength switching solutions in the time domain have been discussed. In Table 1-4, we give a comparison of the solutions studied in this chapter according to the aforementioned criteria.

Table 1-4: Comparison of four time domain sub-wavelength switching network solutions

	Mesh / Ring (M,R)	Synchronous / Asynchronous (S,A)	Distributed / Centralized (D,C) controller
POADM	R	S	C
OPST	R	A	D
TWIN	M	S	C

For the data plane, both OPST and POADM permit to construct a ring topology while TWIN can realize a mesh topology. With combining several rings together, OPST and POADM can build up mesh connectivity. For TWIN solution, all core nodes can be connected one by one in order to realize also a ring topology. All these three solutions use tunable transmitters. In POADM, a source node is equipped several transmitter. For OPST and TWIN, a source node is equipped one transmitter, thus only one burst can be generated at each instant. At the receiver side, as destination node in OPST and TWIN solutions receives only one wavelength, the tunable receiver is not necessary. The demonstrations of OPST and TWIN use only fixed receiver. For POADM, both tunable receiver [78] and fixed receiver [74] have been implemented in the experimental demonstration. In the POADM, a

node is able to receive bursts at various wavelengths and it is able to receive several bursts with different wavelengths at the same time, which offers more flexibility compared to TWIN and OPST at the destination node. But in return for this flexibility, the POADM node is equipped a group of burst mode receivers (or fast tunable receiver) and a group of optical gates to stop the dropped wavelengths, which increases the construction complexity. Since the transmitters can generate only burst at each instant and the destination node receives only one wavelength, it is difficult to perform the multicast services. By contrary, POADM approach, the multicast service can be built up through sending the same burst at different wavelengths and/or receive a burst at the same wavelength by different destination nodes. For the control plane, TWIN and POADM use centralized control strategy while the OPST use distributed control strategy. In order to perform the resource allocation without contention, the control plane should accurately know the propagation time between the different nodes in mesh topology. As a result, TWIN must be realized as a synchronous solution. But for ring topology, both synchronous and asynchronous solutions are possible: POADM is realized as a synchronous solution and OPST is realized an asynchronous solution. In the mesh network (TWIN), studies have proved that the centralized controller has better performance than the distributed controller [95]. For ring topology, the performance varies between different configurations. It is difficult to judge the best time domain sub-wavelength solution among these three solutions, as the evaluation criteria are different based on different application backgrounds. Since TWIN allows building a mesh topology network and realizing the purely optical routing on a wavelength basis, which avoids the use of optical fast switches, it was selected by Orange as the candidate for the metro network.

1.3 Conclusion

For the purpose of better use of the already deployed network resource, sub-wavelength switching solutions have been proposed to improve the flexibility of network resource allocation at the optical layer level. The sub-wavelength switching can be performed in both spectral and time domain. In the spectral domain, the combination of super-channel, flex-grid, CDC-ROADM and high resolution filter offers the possibility to access to the sub-band granularity as fine as 12.5 GHz. In order to generate the super-channel signal, there are two promising candidates: Nyquist-WDM and MB-OFDM, which offer long distance reach and high bit rate with high spectral efficiency capabilities. Currently used flexible ROADMs even with functionalities such as colorless, directionless and contentionless suffers from lack of flexibility in the time domain, which does not fit well with the Internet philosophy of temporal packet switching. In the time domain, the TWIN solution has shown as a potential good candidate for up-coming metro/regional optical transport networks implementing optical burst switching. TWIN is a lossless synchronous centralized control network. Its routing is based on wavelength. Since each wavelength is associated to only one destination node,

the number of edge nodes are limited by the number of wavelength which is typically 80 (i.e. one wavelength per destination). Even if greatly improving flexibility of currently used optical transport networks, the TWIN solution suffers from a lack of flexibility in the spectral domain.

Since sub-wavelength switching solutions in either spectral or time domain has limitations in the other domain, the combination of both technologies in time and spectral domains has been proposed [97][98]. All of them choose to generate the optical burst using OFDM modulation format. But OFDM is not the only choice; we can also generate optical bursts using Nyquist-WDM. Nyquist-WDM and MB-OFDM constitutes both promising technologies to generate a super-channel signal. Nyquist-WDM and MB-OFDM have been demonstrated as having similar performance [45], in terms of bit-rate, distance reach, tolerance to fiber non-linear effects, sub-band granularity, and guard band. Here we only discuss the differences between them, and there are three main points of interest:

- MB-OFDM has a larger overhead compared to Nyquist-WDM
- MB-OFDM offers more flexibility thanks to bit and power loading
- MB-OFDM currently uses data-aided technology for channel estimation and equalization, which is faster than blind equalization usually implemented with Nyquist-WDM. As a consequence, it is particularly well-adapted to the context of optical burst switching.

As in the burst traffic, the receiver detects bursts coming from various sources nodes, thus the channel estimation/equalization is more challenging than with continuous data flows. As the duration of each burst is short (i.e. from 1 µs to 10 ms), the channel impairments has to be mitigated fast in order to optimize the use of time resources. MB-OFDM that naturally uses data-aided channel estimation/equalization is well-adapted to the OBS networks. Furthermore, MB-OFDM offers the possibility to implement bit and power loading technology. In [81], experimental results have shown that the transmission in optical burst mode using MB-OFDM technology with using bit and power loading technology can achieve a higher bit rate, longer distance reach and showing more tolerance to frequency detuning. The obtained results show that MB-OFDM has a higher adaptability for the burst traffic application.

For the solutions presented in [97][98], they aim to design respectively a network for the application between data centers and the application intra data center, so the targeted transmission distance is short and the direct detection technology is selected. Moreover, neither of the solutions introduces the concept of optical switching based on wavelength. TIme and Spectral Optical Aggregation (TISA) [99] solution is the first solution has been proposed for the optical transport network by combining sub-wavelength solutions in both time and spectral domains. The targeted transmission distance is long and the routing is realized purely optically based on wavelength, which are different from the previous solutions. TISA is a combination of TWIN and MB-OFDM that allows achieving our objectives to have an optimal filling of network resources and high degree of flexibility

and reconfigurability for the optical transport networks. We could imagine that the proposed solution works as an alternative to IP routers in several years (when further progresses will have been achieved): packet switching would not require any more optical-to-electrical conversions to be performed and would be supported entirely by the optical network layer. This idea constitutes a dream that could come true in a next future. In this thesis, we are going to demonstrate the feasibility of TISA solution. We will detail the experimental implementation of the TISA solution in a proof of concept.

References

[1] G. P. Agrawal, “Nonlinear Fiber Optics”, 4th ed. (Academic, 2007).

[2]. E. Pincemin, M. Song, B. Baeuerle, A. Josten, D. Hillerkuss, J. Leuthold, R. Rudnick, D. M. Marom, S. Ben-Ezra, J. F. Ferran, D. Klonidis, I. Tomkos, “Cascaded all-optical sub-channel add/drop multiplexing from a 1-Tb/s MB-OFDM or N-WDM super-channel with ultra-low guard-bands (Invited)”, *International Conference on Transparent Optical Networks (ICTON),* Tu.D1.3, 2017

[3] S. Tibuleac, “ROADM Network Design Issues,” *Optical Fiber Communications Conference and Exhibition (OFC)*, NMD1, 2009.

[4] S. Perrin, “the Need for Next-Generation ROADM Networks” white paper, http://www.calient.net/wp-content/uploads/downloads/2010/11/NG_ROADM_WP.pdf

[5] “Spectral grids for WDM applications: DWDM frequency grid”, ITU, Recommendation ITU-T G.694.1, 2012.

[6] R. Rudnick; A. Tolmachev; D. Sinefeld; O. Golani; S. Ben-Ezra; M. Nazarathy; D. M. Marom, "Sub-banded / single-sub-carrier drop-demux and flexible spectral shaping with a fine resolution photonic processor", *The European Conference on Optical Communication (ECOC)*, Cannes, 2014, pp. 1-3.

[7] R. Rudnick et al., D. Sinefeld, O. Golani, D.M. Marom, "One GHz Resolution Arrayed Waveguide Grating Filter with LCoS Phase Compensation," OFC 2014, San Francisco, USA, paper Th3F.7 (2014).

[8] O. Gerstel, M. Jinno, A. Lord and S. J. B. Yoo, "Elastic optical networking: a new dawn for the optical layer?," in *IEEE Communications Magazine*, vol. 50, no. 2, pp. s11-s20, February 2012.

[9] K. Toyoda, Y. Koizumi, T. Omiya, M. Yoshida, T. Hirooka, M. Nakazawa; “Marked performance improvement of 256 QAM transmission using a digital back-propagation method”. *Optics Express*, 2012.

[10] D. Qian, M. Huang; E. Ip; Y. Huang; Y. Shao; J. Hu; T. Wang, “High Capacity/Spectral Efficiency 101.7 Tb/s WDM Transmission Using PDM-128QAM-OFDM Over 165-km SSMF Within C- and L-Bands”. *Journal of Lightwave Technology*, 2012.

[11] E. Pincemin, M. Song, J. Karaki, O. Zia-Chahabi, T. Guillossou, D. Grot, G. Thouenon, C. Betoule, R. Clavier, A. Poudoulec, M. Van der Keur, Y. Jaouën, R. Le Bidan, T. Le Gall, P. Gravey, M. Morvan, B. Dumas-Feris, M. L. Moulinard, G. Froc, "Multi-Band OFDM Transmission at 100 Gbps With Sub-Band Optical Switching," in *Journal of Lightwave Technology*, 2014.

[12] E. Pincemin, M. Song, J. Karaki, A. Poudoullec, N. Nicolas, M. Van der Keur, Y. Jaouen, P. Gravey, M. Morvan, G. Froca; "Multi-band OFDM Transmission with Sub-band Optical Switching", *European Conference on Optical Communication (ECOC)*, invited paper Th.2.A.1, 2013.

[13] A. Lowery, "Amplified-spontaneous noise limit of optical OFDM lightwave systems," *Optics Express*, 16, 860-865 (2008).

[14] K. M. Feng, R. T. Shiu, Y. W. Huang and W. R. Peng, "Sensitivity improvement using amplified optical self-coherent detection in an optical OFDM system," *2009 IEEE LEOS Annual Meeting Conference Proceedings*, Belek-Antalya, 2009, pp. 41-43.

[15] J. M. Kahn and Keang-Po Ho, "Spectral efficiency limits and modulation/detection techniques for DWDM systems," in *IEEE Journal of Selected Topics in Quantum Electronics*, vol. 10, no. 2, pp. 259-272, March-April 2004.

[16]. X. Liu, S. Chandrasekhar, P. J. Winzer, B. Zhu, D. W. Peckham, S. Draving, J. Evangelista, N. Hoffman, C. J. Youn, Y. H. Kwon, E. S. Nam, "3x 485-Gb/s WDM transmission over 4800 km of ULAF and 12x 100-GHz WSSs using CO-OFDM and single coherent detection with 80-GS/s ADC*"s*. in *Optical Fiber Communication Conference*. 2011. Optical Society of America.

[17]. S. Zhang, Y. Zhang, Mi. Huang, F. Yaman, E. Mateo, D. Qian, L. Xu, Y. Shao, I. B. Djordjevic, "Transoceanic transmission of 40× 117.6 Gb/s PDM-OFDM-16QAM over hybrid large-core/ultralow-loss fiber*". Journal of Lightwave Technology*, 2013. 31(4): p. 498-505.

[18] M.-F. Huang, S. Zhang, E. Mateo, D. Qian, F. Yaman, T. Inoue, Y. Inada, T. Wang, "EDFA-only WDM 4200-km transmission of OFDM-16QAM and 32QAM". *Photonics Technology Letters*, IEEE, 2012. 24(17): p. 1466-1468.

[19] M. E. Chaibi, K. Hassan, L. Bramerie and C. Peucheret, "Directly-modulated IM/DD OFDM transmission over 100-km SSMF using SSB filtering with two silicon micro-ring resonators," *2017 Conference on Lasers and Electro-Optics (CLEO)*, San Jose, CA, 2017, pp. 1-2.

[20] Y. Wang, J. Yu and N. Chi, "Demonstration of 4 $\times$ 128-Gb/s DFT-S OFDM Signal Transmission over 320-km SMF With IM/DD," in *IEEE Photonics Journal*, vol. 8, no. 2, pp. 1-9, April 2016

[21] M. Chagnon, M. Osman, M. Poulin, C. Latrasse, J. Gagné, Y. Painchaud, C. Paquet, S. Lessard, and D. Plant, "Experimental study of 112 Gb/s short reach transmission employing PAM formats and SiP intensity modulator at 1.3 μm," *Optics Express* 22, 21018-21036 (2014).

[22] T. J. Xia and G. A. Wellbrock, Y-K. Huang, M-F. Huang, E. Ip, P.N. Ji, D. Qian, A. Tanaka, Y. Shao, T. Wang, Y. Aono, and T. Tajima, "21.7 Tb/s Field Trial with 22 DP-8QAM/QPSK Optical Superchannels Over 1503-km of Installed SSMF," *Optical Fiber Communications Conference and Exhibition* 2012, Postdeadline paper PDP5D.6 (2012).

[23] J-X. Cai, C.R. Davidson, A. Lucero, H. Zhang, D.G. Foursa, O.V. Sinkin, W.W. Patterson, A.N. Pilipetskii, G. Mohs, and N.S. Bergano, "20 Tbit/s Transmission Over 6860 km With Sub-Nyquist Channel Spacing," IEEE Photonics Technology Letters, 24, 1466-1468 (2012).

[24] J. Yu, Z. Dong, H-C Chien, Z. Jia, D. Huo, H. Yi, M. Li, Z. Ren, L. Xie, K. Liu, X. Zhang, Y. Xia, Y. Cai, M. Gunkel, P. Wagner, H. Mayer and A. Schippel, "Field Trial yquist-WDM Transmission of 8×216.4Gb/s PDM-CSRZ-QPSK Exceeding 4b/s/Hz Spectral Efficiency," *Optical Fiber Communications Conference and Exhibition (OFC)*, Postdeadline paper PDP5D.3 (2012)

[25] N. Kikuchi, R. Hirai and T. Fukui, "Quasi single-sideband (SSB) IM/DD Nyquist PAM signaling for high-spectral efficiency DWDM transmission," *Optical Fiber Communications Conference and Exhibition (OFC)*, Anaheim, CA, 2016.

[26] N. Kikuchi and R. Hirai, "Intensity-modulated / direct-detection (IM/DD) Nyquist pulse-amplitude modulation (PAM) signaling for 100-Gbit/s/λ optical short-reach transmission", *The European Conference on Optical Communication (ECOC)*, Cannes, 2014, pp. 1-3.

[27] F. Derr, "Coherent optical QPSK intradyne system: concept and digital receiver realization," in *Journal of Lightwave Technology*, vol. 10, no. 9, pp. 1290-1296, Sep 1992.

[28] S. Savory, "Digital filters for coherent optical receivers," *Optics Express*, 16, 804-817 (2008).

[29] D. Godard, "Self-recovering equalization and carrier tracking in two-dimensional data communication systems", *IEEE Transactions on Communications*, 28, 1867-1875 (1980).

[30]. P.J. Winzer and A.H. Gnauck. "111-Gb/s polarization-multiplexed 16-QAM on a 25GHz WDM grid". in *European Conference on Optical Communication*. 2008.

[31] D. Van den Borne, "Robust Optical Transmission Systems: Modulation and Equalization," Thesis Manuscript, Technical University of Eindhoven, 2008.

[32] T. Pfau, S. Hoffmann and R. Noe, "Hardware-Efficient Coherent Digital Receiver Concept With Feedforward Carrier Recovery for M -QAM Constellations," in *Journal of Lightwave Technology*, vol. 27, no. 8, pp. 989-999, April15, 2009.

[33]. X. Zhou, "Hardware efficient carrier recovery algorithms for single-carrier QAM systems". in *Signal Processing in Photonic Communications*. 2012. Optical Society of America.

[34] J. E. Mazo, "Faster-than-Nyquist signaling", *Bell System Technical Journal*, 54, 1451–1462 (1975).

[35] J. A. Altabas, P. Arribas, D. Izquierdo, F. Sotelo, A. Lerin, J. M. Fabrega, J. A. Lazaro, I. Garces, G. Junyent, "Survey of Faster-Than-Nyquist for Flexible Passive Optical Networks," *2015 17th International Conference on Transparent Optical Networks (ICTON)*, Budapest, 2015, pp. 1-5.

[36] Z. Zheng, D. Wang, X. Zhu, X. Lv, K. Zou, Y. Zhu, F. Zhang, Z. Chen, “Orthogonal-band-multiplexed offset-QAM optical super-channel generation and coherent detection”, Scientific Reports online, Article number: 17891, 2015.

[37] J. Zhao and A. D. Ellis, "Enhanced dispersion tolerance of coherent offset-QAM OFDM over conventional OFDM", *Optical Fiber Communications Conference and Exhibition (OFC)*, San Francisco, CA, 2014, pp. 1-3.

[38] J. Zhao, "DFT-based offset-QAM OFDM for optical communications", *Optics Express*, 2014.

[39] J. Zhao and P. Townsend, "Dispersion tolerance enhancement using an improved offset-QAM OFDM scheme", *Optics Express*, 17638-17652 (2015).

[40]X. Zhou, J. Yu, M. Huang, Y. Shao, T. Wang, L. Nelson, P. Magill, M. Birk, P. I. Borel, D. W. Peckham, R. Lingle, B. Zhu,, “64-Tb/s, 8b/s/Hz, PDM-36QAM transmission over 320km using both pre- and post-transmission digital signal processing”. *Journal of Lightwave Technology*, 2011.

[41] A. Pagano, E. Riccardi, M. Bertolini; V. Farelli, T. Van De Velde, “400G real-time trial using rate-adaptive transponders for next generation flexible-grid networks”, *Optical Fiber Communications(OFC)*, paper Tu2B4, 2014.

[42] J. Karaki, E. Pincemin, D. Grot, T.Guillossou, Y. Jaouen, R. le Bidan, T. le Gall, "Dual-Polarization Multi-Band OFDM versus Single-Carrier DP-QPSK for 100 Gbps Long-Haul WDM Transmission over Legacy Infrastructure," *The European Conference on Optical Communication (ECOC)*, Paper P4.17 (2012).

[43] M. Song, E. Pincemin, B. Baeuerle, A. Josten, D. Hillerkuss, J. Leuthold, I. Tomkos, "Fibre Nonlinearity Limitations of 1 Tbps (10x100 Gbps) Multi-Band e-OFDM Super-Channel," Advanced Photonics 2016 (SPPcom), paper SpW1G.2 (2016).

[44] J. M. Fabrega, Michela Svaluto Moreolo, F. J. Vflchez, B. R. Rofoee, Y. Ou, N. Amaya, G. Zervas, D. Simeonidou, Y. Yoshida, K. Kitayama, "Experimental demonstration of elastic optical networking utilizing time-sliceable bitrate variable OFDM transceiver," *OFC 2014*, San Francisco, CA, 2014.

[45] M. Song, "WDM transmission of 400 Gbps and beyond using multi-band OFDM & Nyquist-WDM", thesis manuscript, Télecom ParisTech, 2016

[46] P.N. Ji, Y. Aono, "Colorless and directionless multi-degree reconfigurable optical add/drop multiplexers", *Wireless and Optical Communications Conference*, 2010.

[47] *A.* Devarajan*,* K. Sandesha; R. Gowrishankar; B. Sai Kishore; G. Prasanna; R. Johnson; P. Voruganti*, "Colorless, Directionless and Contentionless Multi-degree ROADM Architecture for Mesh Optical Networks", Second International Conference on Communication Systems and Networks (COMSNETS), 2010.*

[48] S. Gringeri; B. Basch; V. Shukla; R. Egorov; T. J. Xia, "Flexible architectures for optical transport nodes and networks", *IEEE Communications Magazine*, July 2010.

[49] P. Wright, A. Lord and L. Velasco, "The network capacity benefits of Flexgrid," *2013 17th International Conference on Optical Networking Design and Modeling (ONDM)*, Brest, 2013, pp. 7-12.

[50] E. Pincemin, M. Song, J. Karaki, O. Zia-Chahabi, T. Guillossou, D. Grot, G. Thouenon, C. Betoule, R. Clavier, A. Poudoulec, M. Van der Keur, Y. Jaouën, R. Le Bidan, T. Le Gall, P. Gravey, M. Morvan, B. Dumas-Feris, M. L. Moulinard, G. Froc, "Multi-Band OFDM Transmission at 100 Gbps With Sub-Band Optical Switching," in *Journal of Lightwave Technology*, 2014.

[51] C. Pulikkaseril, L. Stewart, M. Roelens, G. Baxter, S. Poole, and S. Frisken, "Spectral modeling of channel band shapes in wavelength selective switches," *Optics Express*, 8458-8470 (2011).

[52] W. Li, M. Li and J. Yao, "A Narrow-Passband and Frequency-Tunable Microwave Photonic Filter Based on Phase-Modulation to Intensity-Modulation Conversion Using a Phase-Shifted Fiber Bragg Grating," in IEEE Transactions on Microwave Theory and Techniques, vol. 60, no. 5, pp.

[53] M. Ferrera, L. Razzari, D. Duchesne, R. Morandotti, Z. Yang. M. Liscidini, J. Sipe, B. Little, D. *J. Moss*, "Ultra-low power frequency conversion in high-index glass micro ring resonators," *2008 Conference on Lasers and Electro-Optics and 2008 Conference on Quantum Electronics and Laser Science*, San Jose, CA, 2008, pp. 1-2.

[54] L. Yi, W. Wei, Y. Jaouën, M. Shi, B. Han, M. Morvan, W. Hu, "Polarization-Independent Rectangular Microwave Photonic Filter Based on Stimulated Brillouin Scattering", in *Journal of Lightwave Technology*, vol. 34, no. 2, pp. 669-675, Jan.15, 15 2016.

[55] Finisar, "Wavelength Selective Switch (WSS)", [available online], https://www.finisar.com/roadms-wavelength-management/10wsaaxxfll

[56] Yenista, "Tunable Filter with Adjustable Bandwidth", [available online], https://yenista.com/IMG/pdf/XTA-50_DS_2-1v1-1.pdf

[57] Teraxion, "Unmatched narrowband filtering with bandwidth down to 50 MHz" [available online], http://www.teraxion.com/images/stories/pdf/MKT-FTECH-TFN_201312-3.2.pdf

[58] Alnair labs, "Ultra-Narrow Bandwidth-Variable Tunable Filter", [available online], http://www.alnair-labs.com/download/BVF-300.pdf

[59] G. Thouenon, C. Betoule, P. S. Khodashenas, J. M. Rivas-Moscoso, D. Klonidis, E. Le Rouzic, and E. Pincemin, "Electrical v/s optical aggregation in multi-layer optical transport networks," IEEE Photonics in Switching, Florence, Italy, paper WeIII1-2 (2015).

[60]. "Terms and definitions for Sub-Lambda Photonically Switched Networks", ITU, COM15-C2322 Rev.-E, Geneva, August 2012.

[61] M. J. O'Mahony, D. Simeonidou, D. K. Hunter and A. Tzanakaki, "The application of optical packet switching in future communication networks," in *IEEE Communications Magazine*, vol. 39, no. 3, pp. 128-135, Mar 2001.

[62] C Qiao , M Yoo, "Optical burst switching (OBS) - a new paradigm for an optical Internet", Journal of High Speed Networks, v.8 n.1, p.69-84, March 1999

[63] A. Triki, "Etude des techniques de transport de données par commutation de rafales optiques sans résolution spectrale de la contention" Thesis manuscript, Télecom Bretagne, 2014

[64] J. E. Simsarian and Liming Zhang, "Wavelength locking a fast-switching tunable laser," in *IEEE Photonics Technology Letters*, vol. 16, no. 7, pp. 1745-1747, July 2004.

[65] D. Chiaroni, "Optical packet add/drop multiplexers for packet ring networks", *34th European Conference on Optical Communication (ECOC)*, pp. 1-4, 2008.

[66] T. Legrand, H. Nakajima, P. Gavignet, B. Charbonnier and B. Cousin, "Etude numérique de la résolution spectro-temporelle de contention de burst et réalisation d'un noeud OBS", *Journées Nationales d'Optique Guidée*, 2008.

[67] S. Ibrahim, T. Nakahara, H. Ishikawa and R. Takahashi, "An ultralow-power optical label processor for 100-Gbps optical packet switching," *2015 International Conference on Photonics in Switching (PS)*, Florence, 2015, pp. 111-114.

[68] T. Segawa, S. Ibrahim, T. Nakahara, Y. Muranaka and R. Takahashi, "Low-Power Optical Packet Switching for 100-Gb/s Burst Optical Packets With a Label Processor and 8 × 8 Optical Switch," in *Journal of Lightwave Technology*, vol. 34, no. 8, pp. 1844-1850, April15, 15 2016.

[69] N. Calabretta, R. Stabile, E. Kleijn, T. de Vries, K. A. Williams and H. J. S. Dorren, "Lossless wavelength selector based on monolithically integrated flat-top cyclic AWG and optical switch chain," *The European Conference on Optical Communication (ECOC)*, Cannes, 2014, pp. 1-3.

[70] H. Guo, G. Chen, D. Zhang, X. Cao, J. Wu and T. Tsuritani, "Metro-embedded cloud platform with all-optical interconnections for virtual datacenter provisioning," *2016 21st OptoElectronics and Communications Conference (OECC) held jointly with 2016 International Conference on Photonics in Switching (PS)*, Niigata, 2016, pp. 1-3.

[71] G. Chen, H. Guo, D. Zhang, Y. Zhu, C. Wang,H. Yu, Y. Wang, J. Wang, J. Wu, X. Cao, N. Yoshikane, T. Tsuritani, I. Morita and M. Suzuki "First demonstration of holistically-organized metro-embedded cloud platform with all-optical interconnections for virtual datacenter provisioning," *2015 Opto-Electronics and Communications Conference (OECC)*, Shanghai, 2015, pp. 1-3.

[72] Y. Yan, G. Zervas, B. R. Rofoee and D. Simeonidou, "FPGA-based optical network function programmable node", *Optical Fiber Communications(OFC),* San Francisco, CA, 2014, pp. 1-3.

[73] G. S. Zervas, B. Rofoee, Y. Yan, D. Simeonidou, G. Bernini, G. Carrozzo, N. Ciulli, "Control and transport of Time Shared Optical Networks (TSON) in metro areas," *2012 Future Network & Mobile Summit (FutureNetw)*, Berlin, 2012, pp. 1-9.

[74] D. Chiaroni, "Optical packet add/drop multiplexers for packet ring networks", 34th European Conference on Optical Communication (ECOC), pp. 1-4, 2008.

[75] D. Chiaroni, G. Buforn, C. Simonneau, S. Etienne and J. Antona, "Optical packet add/drop systems", Optical Fiber Communication Conference (OFC), pp. 1-3, 2010.

[76] C. Cadere, N. Izri, D. Barth, J. Fourneau, D. Marinca and S. Vial, "Virtual circuit allocation with QoS guarantees in the ECOFRAME optical ring", 14th Conference on Optical Network Design and Modeling (ONDM), pp. 1-6, 2010.

[77] D. Chiaroni, C. Simonneau, M. Salsi, G. Buforn, S. Etienne, H. Mardoyan, J. Simsarian and J. Antona, "Optical packet ring network offering bit rate and modulation formats transparency", Optical Fiber Communication Conference (OFC), 2010.

[78] Y. Pointurier, B. Uščumlić, M. A. Mestre, P. Jennevé, H. Mardoyan, A. Dupas and S. Bigo "Green optical slot switching torus for mega-datacenters," *2015 European Conference on Optical Communication (ECOC)*, Valencia, 2015, pp. 1-3.

[79] M. A. Mestre, J. M. Estarán, P. Jennevé, H. Mardoyan, I. Tafur Monroy, D. Zibar and S. Bigo "Novel Coherent Optical OFDM-Based Transponder for Optical Slot Switched Networks," in Journal of Lightwave Technology, vol. 34, no. 8, pp. 1851-1858, April15, 15 2016.

[80] N. Benzaoui, Y. Pointurier, B. Uščumlić, T. Bonald, Q. Wei and S. Bigo, "Transport Mechanisms for Mobility Support in Optical Slot Switching-Based Next-Generation Mobile Backhaul Networks," in *Journal of Lightwave Technology*, vol. 34, no. 8, pp. 1946-1955, April15, 15 2016.

[81] N. Benzaoui, Y. Pointurier and S. Bigo, "Latency in a 2D torus burst optical slot switching data center," *Optical Fiber Communications Conference and Exhibition (OFC)*, Los Angeles, CA, USA, 2017, pp. 1-3

[82] T. Eido, F. Pekergin and T. Atmaca, “Performance analysis of an enhanced distributed access mechanism in a novel multiservice OPS architecture”, *Next Generation Internet Networks (NGI)*, pp. 1-7, 2009.

[83] B. Uscumlic, A. Gravey, I. Cerutti, P. Gravey and M. Morvan, “Stable optimal design of an optical packet ring with tunable transmitters and fixed receivers”, *Optical Network Design and Modeling (ONDM)*, 2013 17th International Conference on, pp. 81-87, 2013.

[84] J. P. Fernandez-Palacios, L. Perez, J. Rodriguez, J. Dunne and M. Basham, "IP offloading over multi-granular photonic switching technologies," *36th European Conference and Exhibition on Optical Communication*, Torino, 2010, pp. 1-3.

[85] J. Dunne, T. Farrell and J. Shields, "Optical Packet Switch and Transport: A new metro platform to reduce costs and power by 50% to 75% while simultaneously increasing deterministic performance levels," *2009 Sixth International Conference on Broadband Communications, Networks, and Systems*, Madrid, 2009, pp. 1-5.

[86] C. K. Kalló, M. Basham, J. Dunne and J. P. Fernández-Palacios, "Cost reduction of 80% in next-generation virtual personal computer service economics using a sub-wavelength metro network," *2011 16th European Conference on Networks and Optical Communications*, Newcastle-Upon-Tyne, 2011, pp. 224-227.

[87] C. Kiss Kalló, J. Shields, C. O'Malley, R. Carley, V. Lopez and J. P. Fernández-Palacios, "Cost-effective sub-wavelength solution for data centre location in scaled next-generation networks," *2012 16th International Conference on Optical Network Design and Modelling (ONDM)*, Colchester, 2012, pp. 1-6.

[88] I. Widjaja, I. Saniee, R. Giles and D. Mitra, “Light core and intelligent edge for a flexible, thin-layered, and cost-effective optical transport network”, *Communications Magazine, IEEE*, vol. 41, n° 5, pp. 30-36, 2003.

[89] I. Saniee and I. Widjaja, “A new optical network architecture that exploits joint time and wavelength interleaving”, *Optical Fiber Communication Conference (OFC)*, 2004.

[90] K. Ross, N. Bambos, K. Kumaran, I. Saniee and I. Widjaja, "Scheduling bursts in timedomain wavelength interleaved networks", Selected Areas in Communications, IEEE Journal on, vol. 21, n° 9, pp. 1441-1451, 2003.

[91] I. Widjaja and I. Saniee, “Simplified layering and flexible bandwidth with TWIN”, Proceedings of the ACM SIGCOMM workshop on future directions in network architecture, pp. 13-20, 2004.

[92] A. Brzezinski, I. Saniee, I. Widjaja and E. Modiano, "Flow control and congestion management for distributed scheduling of burst transmissions in time-domain wavelength interleaved networks", Optical Fiber Communication Conference (OFC), p. 3, 2005.

[93] L. Sadeghioon, P. Gavignet, V. Alaiwan, L. Bramerie, E. Le Rouzic, J.-L. Barbey, T. Guillossou, E. Borgne and S. Lobo, "Software-based burst mode reception implementation for time-domain wavelength interleaved networks," 2015 European Conference on Optical Communication (ECOC), Valencia, 2015, pp. 1-3.

[94] Y. Su, I. Widjaja, H. He, X. Xu, Y. Tian, J. Gao et T. Ye, “Demonstration of a Timedomain Wavelength Interleaved Network prototype without optical buffers and fast switches in the core nodes”, *Optical Fiber Communication Conference (OFC)*, pp. 1-3, 2007.

[95] A. Triki; P. Gavignet; B. Arzur; E. Le Rouzic; A. Gravey, “Efficient control plane for passive optical burst switching network”, *International Conference on Information Networking (ICOIN)*, pp. 535-540. 2013

[96] A. Triki, R. Aparicio-Pardo, P. Gavignet, E. Le Rouzic, B. Arzur and A. Gravey, "Is it worth adapting sub-wavelength switching control plane to traffic variations?," *International Conference on Optical Network Design and Modeling*, Stockholm, pp. 186-191, 2014.

[97] J.M. Delgado Mendinueta; S. Shinada; H. Furukawa; N. Wada, "Ultra-High-Capacity Optical Packet Switching Networks with Coherent Polarization Division Multiplexing QPSK/16QAM Modulation Formats". Photonics 2017, 4, 27.

[98] P. N. Ji, D. Qian, K. Sethuraman, J. Hu, Y, Aono, T. Tajima, W. Blakney, T. Wang, T. J. Xia and G. A. Wellbrock, "First demonstration of real-time all-optical software-defined intra-data center star network using OFDM and burst switching," OptoElectronics *and Communications Conference held jointly with 2013 International Conference on Photonics in Switching (OECC/PS)*, Kyoto, 2013.

[99] P. Gavignet, E. Le Rouzic, E. Pincemin, B. Han, M. Song, L. Sadeghioon “Time and Spectral optical Aggregation for Seamless Flexible Networks”, Photonics in Switching, 2015.

CHAPTER 2

Time and Spectral Optical Aggregation solution

Telecommunication networks are systems that connect a large group of end-users spread over a geographical area. The end-users transfer all types of traffic (voice, data) to each other. Internet Protocol (IP) is the most widely used protocol to ensure the communication in the network. In IP network, the transported data are in the form of IP packets. The current WDM networks using OCS are not flexible enough to transport packets traffic. Thus, the channel utilization efficiency is poor when the traffic volume does not consume a full wavelength bit rate, which results in a waste of network resources. Therefore, the introduction of sub-wavelength switching at the optical layer level is suggested in order to increase the flexibility in resource allocation. Through the flexible sub-wavelength grooming directly at the optical transport network, services are provided with the sub-wavelength connections and thus the channel is better filled. Furthermore, sub-wavelength switching at the optical layer level has the potential to reduce the cost and power consumption of the networks [1]. The sub-wavelength switching can be performed in the temporal or spectral domain or both domains. The temporal sub-wavelength switching solutions divide a flow in a communication channel into a number of data streams which are in the form of packets or bursts. Different emission/reception nodes can send/detect these bursts data at different time, which permits sharing the emission/reception interfaces. The sharing of the same wavelength resource permits to realize a statistical multiplexing in the time domain. Moreover, as most of these solutions remove the OEO conversions at the core nodes, the temporal sub-wavelength switching solutions have the potential to reduce the power consumption. For next generation optical transport systems, besides the time domain sub-wavelength switching solution, spectral domain sub-wavelength switching solution is another candidate to transport higher bit rate. The super-channels technology that are composed of different sub-bands, offers the possibility to perform sub-band switching and allows reducing the guard bands between sub-bands to improve the spectral efficiency. So, spectral sub-wavelength based granularity has been proposed to increase flexibility and network throughput [2]. We have pointed out the advantages and drawbacks of the temporal and spectral sub-wavelength switching solutions in chapter 1. Here a novel approach is proposed: the TIme and Spectral optical Aggregation (TISA) solution [3]. TISA combines the TWIN solution and MB-OFDM technology allowing a pure optical aggregation and disaggregation in both time and spectral domains with the finest possible sub-wavelength granularity. TISA allows building a mesh topology network and realizes a wavelength basis routing.

Combining TWIN solution and MB-OFDM technology, TISA benefits from the advantages of each solution. In TISA, each source sends data in form of bursts that occupies a sub-band only. The data are modulated in the OFDM format. Each sub-band is associated to one destination, and each source node is able to generate data at various sub-bands. The destination is fixed which means it receives the bursts at only one wavelength. Thus, the routing is also made on a wavelength basis, as

in TWIN solution. The data aggregation, routing and data disaggregation are realized purely optically. For the same reason as in TWIN network, TISA has a potential burst collision risk at the core nodes. In order to guarantee the lossless routing, a centralized controller is implemented to manage carefully the bursts signal in terms of sending time and allocated sub-band. TISA solution is composed of a control plane and a data plane. The control plane performs all the processes related to network resource allocation, devices configuration, network synchronization. The data plane realizes physically the data transmission from one node to another. It is composed of the edge nodes, combiners, separators and the core nodes.

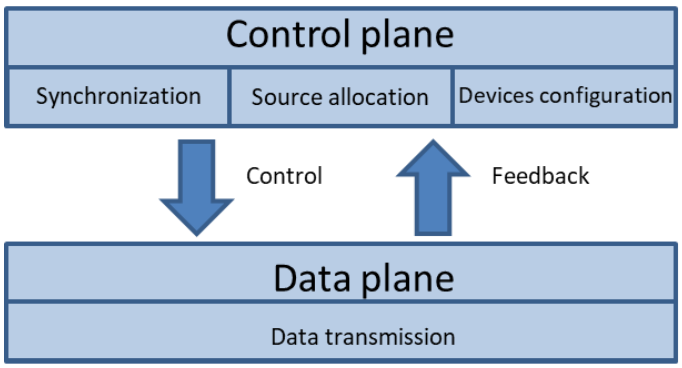

Figure 2-1: Control plane and data plane

The objective of this thesis is to build a Proof of Concept (PoC) of TISA to demonstrate experimentally its feasibility. Then the TISA performance will be evaluated to see if the operation in burst mode brings penalty, and if TISA permits to allocate network resource with a fine granularity. In the following paragraphs in this chapter, we will present the TISA concept in detail (first the data plane and then the control plane) and its building blocks.

2.1 Data plane

The data plane refers to the physical layer (i.e. the layer 1 of Open System Interconnection (OSI) network model) in the network: it ensures all the functions and processes that relates to the forwarding of data bursts from one node to another (from one source to one destination). Figure 2-2 presents a simple example of data plane for TISA network. In this example, there are five groups of edge nodes and two core nodes: the groups of edge nodes A-m and B-j (m, j from 1 to 4) are source nodes and the groups of edge nodes C-i, D-n and E-k (i, n, k from 1 to 4) are destination nodes. Only one transmission direction is represented in this example. The gray rectangles with different kinds of patterns represent the data bursts sent towards the groups of nodes C and E, while each kind of pattern represents one sub-band. The colored rectangles represent the data bursts sent towards the group of nodes D, and each color represents one sub-band that is associated to one node D-n. Each rectangle represents a data burst and all the simple rectangles, that have only one color or one

pattern, have uniform dimensions (i.e. the duration and the occupied bandwidth). The multi-colored bursts or multi-patterns bursts represent the multi-band bursts that occupy a larger bandwidth.

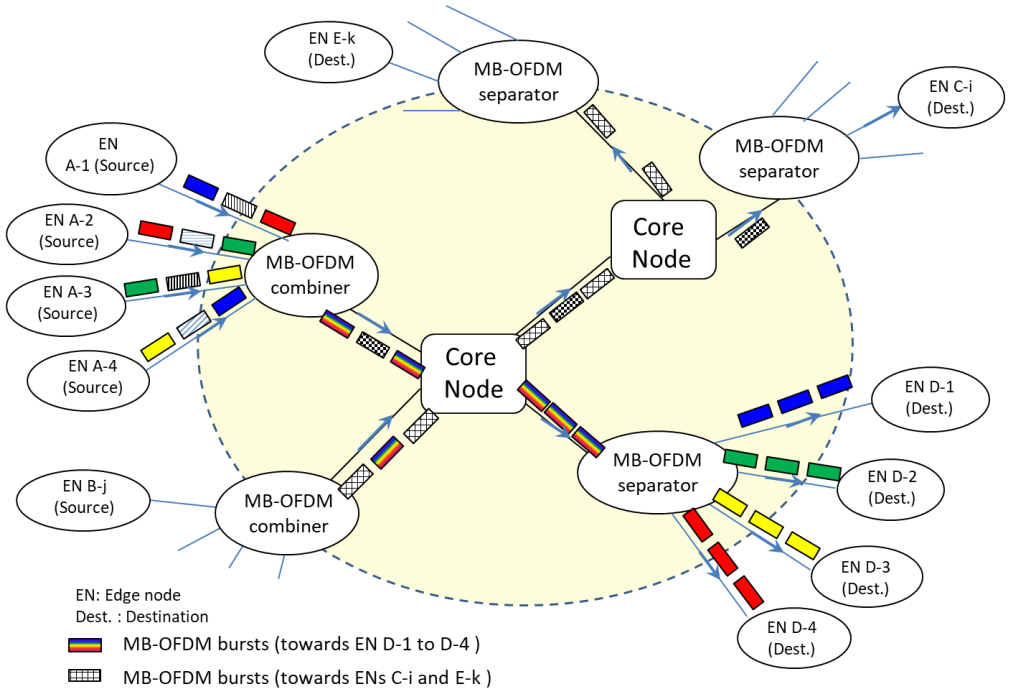

Figure 2-2: An example of data plane for TISA network.

In this example, the central yellow circle represents the same routing function as in TWIN network (see Figure 1-15). The routing is based on the wavelength (i.e. 50 GHz grid) and is realized purely optically. Each source edge node of TWIN network is replaced by a MB-OFDM combiner that is associated to 4 source nodes. These source nodes can be placed at various distances from the combiner. Each source is able to send the OFDM data in the form of bursts at various wavelengths. Each burst occupies only one sub-band and each sub-band is associated to one destination. After the bursts emission, the bursts coming from different source nodes enter the MB-OFDM combiner at first. The combiner collects passively and transparently the bursts data and aligns them together as a composed multi-band burst occupying an entire band width of 50 GHz (which is a structure similar to the super-channel but in burst mode). A multi-band burst is sent toward core node in place of 4 bursts. This scheme allows reusing the SLPSN network structure. However, the alignment of bursts at combiner will increase the control complexity, but since TISA is a time slotted solution, the no alignment of bursts will lead to a loss of channel utilization efficiency. As a result, the alignment is necessary. After the alignment of bursts, the multi-band burst enters the core node.

At the core node, the routing is on a wavelength basis. The bursts are redirected to the corresponding output port of the core node and then sent to MB-OFDM separator or to the next core node. The routing is realized pure optically without any OEO conversion. Therefore, there is any constraint related to the data processing speed of hardware to perform OEO conversion or the header process, and thus various data rate and formats signals can go through the core nodes.

At the destination side, each destination edge node in TWIN is replaced by a MB-OFDM separator that is associated to 4 destination nodes in this example. These destination nodes can be placed at various distances from the MB-OFDM separator. The MB-OFDM separator permits to separate the multi-band bursts data into different sub-bands passively and transparently in order to send a unique sub-band to each destination. At the destination side, a fixed wavelength receiver is implemented to receive the burst. As we use coherent detection technology, a local oscillator is implemented in the receiver and is tuned to the wavelength associated to this destination.

Each edge node is equipped with a transmitter and a receiver, thus it is a source node as well as a destination node. The data transmission in the network is bidirectional in a pair of optical fibers. An edge node is associated simultaneously to MB-OFDM combiner and separator. The optical switching is realized at two levels: the entire band (50 GHz) level at the core nodes and the sub-band level at the MB-OFDM combiners and separators. This scheme permits to reuse the TWIN architecture and TISA network allocates the network resource with a finer granularity for each source node at the same time. In TISA, as the number of edge nodes is related to the number of sub-bands instead of the number of wavelengths in the C-band with the ITU-T 50 GHz fixed grid standard, which allows having more edge nodes in the network compared to a purely TWIN approach.

In TISA, the physical topology is meshed, but the logical links inside the network allows creating various topologies. Suppose that one edge node is treated as source node and all other nodes as destination nodes, thus we have a logical tree topology: the root (source) sends the data bursts to every leaf (destination). The burst always transmit through a combiner, one or several core node(s) and a separator. There is no direct link from one edge node to another edge node without passing through a MB-OFDM combiner, a separator and core node(s), which is a difference with the TWIN solution.

2.2 Control plane

On top of the data plane, a control plane is built to manage the data plane and all the related devices. The control plane ensures all the functionalities and processes concerning network synchronization, network resource allocation, devices configuration.

As TISA is a synchronous network, the first task of control plane in TISA is to guarantee the synchronization of the whole network. We choose a widely used solution to realize the synchronization of full scale real network: we implement a clock at each edge node and all the clocks are synchronized, so they have the same rhythm and time. We can also distribute a common clock to each node. But there is always a time uncertainty between each node. Since all the bursts should be sent at a precise time in TISA network, this time uncertainty can lead to a wrong burst sending time and thus induce an overlap of different bursts. In order to overcome this problem, a time interval is

proposed to be inserted between two successive bursts, called guard time. The guard time is set larger than the time uncertainty of the node clock, so that there is no overlap even if the burst sending time is not as precise as we want. The value of synchronization uncertainty is an important parameter for the guard time design. In order to give a reference for the guard time design, we choose Global Positioning System (GPS) [4][5] as a clock source with high precision to be implemented in each source node. The implementation of GPS in each source node can offer a clock with only ±100 ns uncertainty, which can be an available choice to be realized in metro or long-haul networks. As a result, the guard time hereafter should be at least larger than 200 ns.

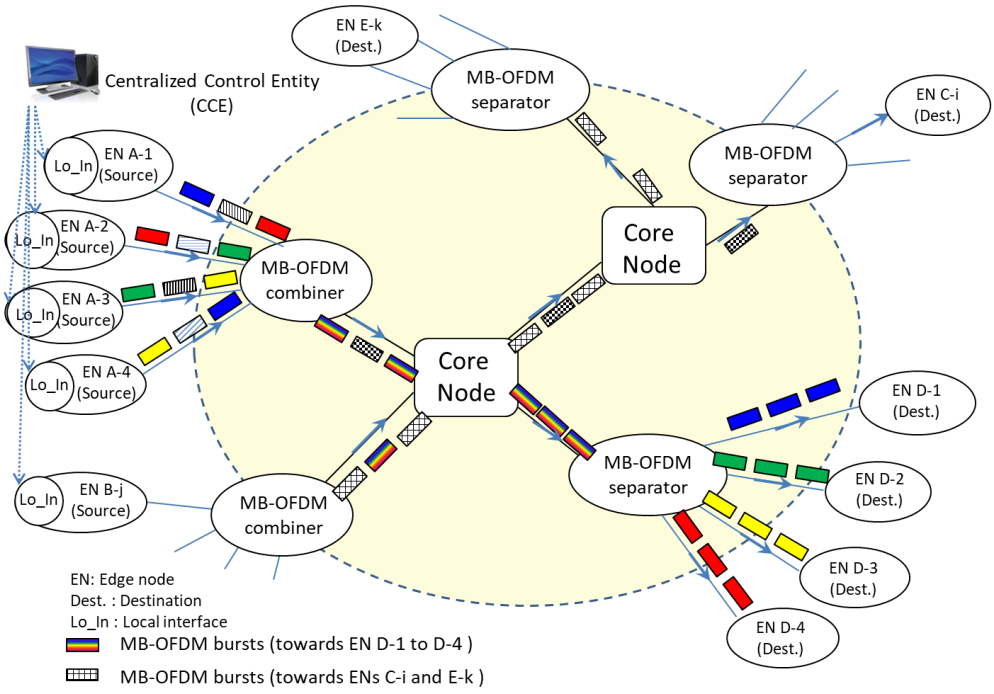

Figure 2-3: An example of control plane on the top of data plane for TISA network.

Then the second task of control plane is resource allocation. As in TWIN network, a Central Control Entity (CCE) is implemented to calculate the grants for each source node. The grants are a kind of authorization distributed from the CCE to the source nodes in order to control the sending time and the wavelength of sub-bands of a burst. Through the grants, CCE can control the resource allocation. In TISA, the propagation delay are various according to the distance between sources and destinations. Different bursts emitted by different sources at the same wavelength could arrive at the same time at a destination. So there is a potential burst collision and this could result in burst loss due to the fact that receiver cannot read simultaneously two bursts of at same wavelength and there is no solution (optical memory) to store the optical burst at receiver side. In the wavelength allocation process, the control plane should in charge of avoiding such burst collisions in order to guarantee the lossless routing in TISA network. In TISA, one sub-band is associated to only one destination. Therefore the burst destination is unique and thus the transmission path is predictable. The core nodes are transparent and the combiners and separators are also transparent; there is no any OEO conversion in the burst transmission and thus no related routing process delay variation. As

a result, once a burst is emitted, the reception time at the destination node is predictable. Therefore, a careful scheduled burst emission at the transmitter side is enough to control the times of arrival of the bursts at the core nodes and at the destination node.

Compared to TWIN, TISA has a new constraint in the source allocation: the bursts coming from different sources shall be aligned at the MB-OFDM combiner to build up a composed multi-band burst that occupies an entire band of 50 GHz. At first, the propagation distance from each source node to the associated combiner should be determined by the CCE. Since the distances from the edge nodes to the combiner are various and thus the corresponding propagation delays are different, a propagation delay table needs to be built at the CCE. As the transmission fibers suffer external phenomena, such as temperature or stresses, the reflective index of optical fiber and thus the propagation delays are variable at different times of a day. In order to follow the slow evolution of the propagation times, a ranging procedure, as in Passive Optical Network (PON) networks, has to be implemented. Therefore the propagation delay table will be updated periodically. Through the control of optical burst emission time, the difference of propagation delay between sources and MB-OFDM combiners can be compensated in the grants (i.e. in the electrical domain).

TISA is a time slotted solution. The burst presented in the example in Figure 2-2 and Figure 2-3 have a uniform dimension temporal and spectral. As we discussed in chapter 1, there are two kinds of technologies in the time slotted solutions: aligned and not-aligned. TISA can be realized with aligned time slot. The alignment of bursts can be realized in the electrical domain through the control of bursts emission time as discussed previous.

For the task concerning devices configuration, the devices and their working states will be collected and send to the CCE or a higher level controller in a real network. As it is not functionality necessary for a prototype, we do not implement these functions in our test-bed.

2.3 Flexibility of TISA solution

As TISA is a time slotted solution, the basic temporal granularity is the duration of the burst and the basic spectral granularity is a sub-band. Figure 2-4 (a) shows an example of basic granularity in the time and spectral domains. The rectangle represents a burst. Each color corresponds to a sub-band and in each time slot the data burst is different. Each burst occupies a sub-band (including the bandwidth of burst signal and the band guards), which is set to 12.5 GHz corresponding to the IUT-T flex grid standard. Each time slot contains a burst and a guard time. The guard time is designed to cover the synchronization errors and the wavelength switching time. The burst contains some overhead for the burst transmission (such as channel estimation, signal synchronization). The time slot is set to 5 µs in this example while the burst occupies 4.7 µs and the guard time is 0.3 µs. The time slot duration is variable, and here we have chosen the same time slot duration as in the

experimental demonstration of TWIN [6] carried out in Orange Labs. This duration is a compromise between the ratio of guard time and data filling ratio. If the burst duration is too long, data filling ratio is not optimal since burst data does not use a long duration. If the burst duration is too short, since the duration of the guard time is fixed, the ratio of effective data is poor. Once, the time slot duration is set, the duration has also an impact on the choice of DSP for the signal, for example, between Nyquist-WDM and MB-OFDM in terms of channel estimation solutions. As the burst duration is only 4.7 µs, we need fast channel estimation DSP to reduce the channel estimation time in order to increase the effective bit ratio. Therefore, the data aided channel estimation technology is preferred in the burst traffic. As MB-OFDM uses data aided channel estimation technology, it is preferred to Nyquist-WDM that use blind channel estimation in the burst traffic.

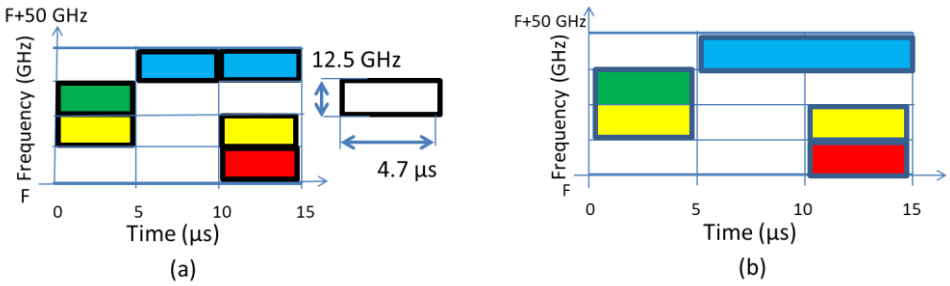

Figure 2-4: Examples of basic granularity in the time and spectral domains.

When the basic time slot is defined temporally and spectrally, there is another degree of flexibility without modifying the basic time slot configuration. We can combine the bursts in the time domain to generate a longer burst, as the blue burst shown in Figure 2-4 (b), or we can generate a burst occupying a larger bandwidth as the burst with green and yellow contents shown in Figure 2-4 (b). This burst will be generated by a transmitter even though the bandwidth is two times larger than before. Correspondingly, the transmitter at the source node should be able to generate such a burst, for example the transmitter has an enough large band DAC (to generate analog bursts signal occupying a large bandwidth).

We can also modify the bit rate of the bursts with different QAM orders. Furthermore, the use of MB-OFDM technology brings not only the flexibility to build a sub-band signal in the spectral domain, but also the possibility to modify the parameters of burst data. MB-OFDM technology offers the possibility to apply the bit and power loading, thus the QAM format order and transmission power used in each subcarrier can be adapted to resource need. This allows the data rate and the distance reach to be adapted flexibly and precisely to the demands.

Consequently, we can see that the TISA solution offers a fine granularity and has the flexibility in both time and spectral domains at the optical layer level.

2.4 Main building blocks of TISA

The realization of the TISA network requires building a data plane and a control plane in order to manage the data plane. For the data plane, there are three main building blocks: the transmitter/source node, the routing devices, and the receiver/destination node. For the control plane, there are two main building blocks: the CCE and the synchronization of network.

2.4.1 The data plane

In TISA, a source node has to be able to generate the burst data at various sub-bands, and each sub-band is associated to one destination. Therefore, a fast tunable source at transmitter side is necessary. There are two principal solutions to realize this kind of laser source: using a fast tunable laser or several fixed wavelength lasers associated to fast optical switches. In both solutions, the wavelength tuning time is an important parameter; it has direct impact on the guard time duration as discussed in the previous paragraph. It is set to be less than 100 ns in this thesis.

In TISA, the data can be generated for direct detection or coherent detection. Both of these two technologies require similar devices as discussed in chapter 1. But for the laser source, the requirement is different between direct detection and coherent detection. The coherent detection technology is sensible to the linewidth of the laser source. In order to realize the transmission of OFDM data in high order QAM modulation format, the phase noise should be taken into account during the DSP process [7] [8]. As an example, for the DP-16QAM in 7 Gbaud, the tunable laser source should process a narrow linewidth that is less than 100 KHz. For the direct detection technology, there is not a criterion on the linewidth. The fast tunable laser with a linewidth of several MHz has been proved feasible in different solution demonstrations [6][9]. In this thesis, coherent detection technology is selected as discussed in chapter 1 by considering the transmission distance and the spectral efficiency.

The routing devices include the MB-OFDM combiner, the core node routing structure, and the MB-OFDM separator. The MB-OFDM combiner is used to bundle together the burst data coming from different source nodes in order to generate a composed multi-band burst occupying an entire band. A simple coupler can be suitable.

The core node routing structure is used to route the multi-band bursts according to their wavelength on 50 GHz grid. This functionality can be realized by the combination of demultiplexers, multiplexers and couplers which offer a fixed routing strategy. Otherwise, the WSS can be used inside the core node, offering a reconfigurability of the routing strategy. WSS-based architectures became popular because they integrate part of the switching and de-multiplexing functions that performed in the core node. This integration allows overcoming the cascadability issue arising when the data cross successive multiplexers / demultiplexers pairs in conventional structures.

The MB-OFDM separator is used to disaggregate a composed multi-band burst into different bursts which occupy only one sub-band and to route each burst to the corresponding destination. Since a sub-band occupies only 12.5 GHz bandwidth, a filter having a rectangular spectrum with a fine bandwidth profile filter should be used. As we have shown in chapter 1, the filter [10] based on arrayed waveguide grating technology achieves as narrow as 10 GHz granularity meeting our requirements. As a result, the separator can be realized by cascading a power splitter and several high spectral resolution filters (for example, 4). It is necessary that the filters have the remote reconfigurability, because the reconfiguration of the TISA network needs to reconfigure the separators. The filter can delete all signals at other sub-bands and ensure only the bursts at the associated wavelength are sent to the destination, which can protect signal privacy that is important for clients. Furthermore, the implementation of the high spectral resolution filters helps to eliminate the interference coming from other sub-bands without advance DSP processing when using direct detection technology. As the composed multi-band burst is separated into several sub-band bursts, the bursts alignment is not necessary at the destination side.

In TISA, the destination node is fixed which means it receives the bursts at only one sub-band that is associated to itself. For the direct detection technology, a broadband photodiode is enough to receive the optical burst signal, as only a fixed sub-band signal is sent to the destination node thanks to the implementation of filters inside the separators. But the spectral efficiency of direct detection technology is poor than the spectral efficiency of coherent detection. For the coherent detection technology, we use a fixed wavelength laser as a local oscillator at the destination. After the beating of received signal and local oscillator, the optical signals are converted to four analog electrical signals (I and Q parts for polarization X and Y) by the four balanced photodiodes. The DSP is performed off-line or real-time to recover the information.

Due to the burst traffic nature, there is a time interval without data between two successive bursts, which is called signal gaps. Signal gaps can arise in both transmitter side (when the transmitters do not generate bursts) and receiver side (there is no signal arriving at the input of the receiver). It is possible that the signal gaps could degrade the performance of the system, so several solutions have been proposed. At the transmitter side, transmitter can be programmed to generate dummy burst when there is no signal to generate, as shown in POADM demonstration [9]. At the receive side, a dummy burst can generated to fill in the signal gaps in order to guarantee a constant power at the input of the receiver, as shown in TWIN demonstration [6]. However, these two solutions are applied in the system using the direct detection technology. The system performance in coherent detection of the transmitter and receiver in TISA need further study.

2.4.2 The control plane

The control plane is a building block necessary to realize the lossless routing and transport of the burst end-to-end through the network. The CCE takes over the calculation and the distribution of grants. The synchronization of the whole network is also an essential function of TISA.

For the CCE, grant calculation is one of the main tasks. A control algorithm will be implemented in real-time for an operator's network. The CCE should collect all the resource demands from each edge node, and then calculate the grants based on the demands. The grants should contain all the information concerning the bursts emission control. Based on different network configurations and the functionalities that network offers, the control information is different. The grant contains at least the information about sub-band that will be used and burst emission time. At each source node, a local interface of control plane is necessary. The local interface is in charge of the information exchange between CCE and source node. For the communication with CCE, it receives and stores the grants. For the communication with the source node, it translates the received grants to control signals for the source node. In order to enable more flexibility of the TISA solution as presented in section 2.3 (such as the combination of several time slots to generate a burst longer, the combination of several sub-bands to generate a burst occupying larger bandwidth and the signal structure and bit rate) the related control information should be integrated in the grants. In this thesis, as our work is to build a proof of concept to demonstrate experimentally the feasibility of TISA concept, the real-time grant calculation is not required. Therefore, the grants will be preprogrammed by the CCE in order to control the burst emission. And concerning the control information, each grant contains only burst emission time and sub-band. In our test-bed, the CCE will be realized by software and the local interface will be implemented using FPGA.

The realization of the synchronization of the whole network is another main task. There are two principal solutions: all edge nodes share a common clock or each edge node has a clock while all the clocks are synchronized. The synchronization is used to guarantee the same working rhythm of all edge nodes and to offer a precise time at each node. An uncertainty between clocks of each edge node is acceptable, but the uncertainty should be reduced as much as possible since it will degrade the system performance. In the previous paragraph 2.2, we said that the guard time is designed based on the clock uncertainty of the GPS system, which is ±100 ns, so the clock uncertainty implemented in the test-bed should be less than ±100 ns in order to respect the design criterion. In this thesis, as the core node is transparent and the DSP at receiver side is carried out in off-line that do not need the clock, the synchronization of the source nodes is enough to synchronize the whole network. Sharing a common clock source between source nodes is chosen as it is a cheaper solution requiring only one clock in our test-bed.

2.5 Conclusion

In summary, TISA allows constructing a synchronous network with a mesh topology with a centralized control plane (which has been proved more efficient than distributed control plane [11]). It offers a granularity as fine as possible in the optical layer and the flexibility in both time and spectral domains combining MB-OFDM and TWIN technologies. The aggregation and disaggregation of bursts are realized purely optically and transparently. The routing is realized based on the wavelength.

Table 2-1: TISA characteristic

TISA characteristic	Benefits/Reason
Synchronous network	A necessary condition for the control of burst sending time in order to realize lossless routing in mesh topology
Centralized control plane	More efficient than distributed control plane, which has been demonstrated in TWIN [11]
Wavelength basis routing	Remove OEO conversion and realize transparent routing
5 µs time slot duration	A choice (the same configuration as in TWIN experimental demonstration), which is a compromise between channel utilization efficiency and data filling ratio
0.3 µs guard time	0.2 µs for synchronization error and 0.1 µs for wavelength switching time
Coherent detection	To improve the spectral efficiency compared to direct detection
50 GHz switching bandwidth at core node	To adapt to 50 GHz fixed grid standard
Alignment of burst at MB-OFDM combiner	Avoid the loss of channel utilization efficiency
4 sub-bands of each wavelength	A choice corresponding to flex-grid standard

In this chapter, we give a description of TISA concept. We give also introduction of each characteristic of the TISA and explain the benefits of the characteristics. The TISA characteristics and the reasons are resumed in the table 2-1. A comparison of TISA and TWIN is presented in the table 2-2. Since the TISA is a concept combining MB-OFDM and TWIN, TISA and TWIN have many similar points. The main differences are in three points: the bandwidth granularity, the detection technology, the switching granularity. The differences on bandwidth and switching granularity show the better

flexibility in the spectral domain brought by TISA compared to TWIN, TISA can access to the sub-band granularity at the optical layer level thanks to the MB-OFDM technology. And thus, TISA can have much more destination nodes, it is a significant improvement brought by the new spectral flexibility. As TISA uses coherent detection technology, the signal has a better tolerance against the linear impairments in the transmission and can achieve a long distance reach. For TWIN solution, direct detection technology was implemented in the experimental demonstration. This solution is cheaper as it has fewer requirements on the transmitter components, such as fast tunable laser with narrow linewidth is not necessary and the modulator can be integrated with the laser. So TWIN solution can be deployed in Data Center (DC) network. Since DC networks are sensible to the component prices and the transmission distance are short. However, both direct and coherent detection technology can be implemented in TISA and TWIN solutions. Based on the application case of TISA or TWIN, we can choose to implement coherent or direct detection technology. Furthermore, as TISA has two switching levels while increasing the flexibility of the network resource allocation, the implementation of combiner and separator increases the deployment complexity.

Table 2-2: Comparison between TISA and TWIN solutions

		TWIN	TISA
Same characteristics	Transmitter	Tunable	Tunable
	Receiver	Fixed	Fixed
	Network Synchronization	Synchronous	Synchronous
	Topology	Mesh	Mesh
	Control plane	Centralized	Centralized
	Routing	Wavelength basis	Wavelength basis
	Burst duration	5 µs (variable based on configuration)	5 µs (variable based on configuration)
Difference characteristics	Bandwidth of bursts	Band (50 GHz)	Sub-band (~10 GHz)
	Detection technology	Direct detection	Coherent detection
	Switching granularity	wavelength (ex. 50 GHz)	Two levels: wavelength (ex. 50 GHz) at core node; sub-band (~10 GHz) at combiner and separator.

In this chapter, we give a description of TISA concept, and a brief introduction of each main building block. The implementation of the TISA experimental test bed will be presented in detail later. In chapter 3, the transmitter and the coherent receiver will be presented. The implementation of control plane is described in chapter 4. The experimental result of the core node and TISA network are described in chapter 5.

References

[1] C. Lange, D. Kosiankowski, C. Gerlach, F.-J. Westphal, A. Gladisch: Energy consumption of telecommunication networks, in Proc. ECOC 2009 - 35th European Conference on Optical Communication, Vienna, Austria, Paper 5.5.3, Sept. 2009.

[2] E. Pincemin, M. Song, J. Karaki, O. Zia-Chahabi, T. Guillossou, D. Grot, G. Thouenon, C. Betoule, R. Clavier, A. Poudoulec, M. Van der Keur, Y. Jaouën, R. Le Bidan, T. Le Gall, P. Gravey, M. Morvan, B. Dumas-Feris, M. L. Moulinard, G. Froc, "Multi-Band OFDM Transmission at 100 Gbps With Sub-Band Optical Switching," in *Journal of Lightwave Technology*, 2014.

[3] P. Gavignet, E. Le Rouzic, E. Pincemin, B. Han, M. Song, L. Sadeghioon "Time and Spectral optical Aggregation for Seamless Flexible Networks", Photonics in Switching, 2015.

[4] Official U.S. government information about the Global Positioning System (GPS) and related topics, [available online], http://www.gps.gov/systems/gps/performance/accuracy/

[5] W. Lewandowski, J. Azoubib and W. J. Klepczynski, "GPS: primary tool for time transfer", in *Proceedings of the IEEE*, vol. 87, no. 1, pp. 163-172, Jan 1999.

[6] L. Sadeghioon, P. Gavignet, V. Alaiwan, L. Bramerie, E. Le Rouzic, J.-L. Barbey, T. Guillossou, E. Borgne and S. Lobo, "Software-based burst mode reception implementation for time-domain wavelength interleaved networks," 2015 European Conference on Optical Communication (ECOC), Valencia, 2015, pp. 1-3.

[7] X. Yi, W. Shieh and Y. Ma, "Phase Noise Effects on High Spectral Efficiency Coherent Optical OFDM Transmission", in *Journal of Lightwave Technology*, vol. 26, no. 10, pp. 1309-1316, May15, 2008.

[8] S. Randel, S. Adhikari and S. L. Jansen, "Analysis of RF-Pilot-Based Phase Noise Compensation for Coherent Optical OFDM Systems", in *IEEE Photonics Technology Letters*, vol. 22, no. 17, pp. 1288-1290, Sept.1, 2010.

[9] D. Chiaroni, "Optical packet add/drop multiplexers for packet ring networks", *34th European Conference on Optical Communication (ECOC)*, pp. 1-4, 2008.

[10] R. Rudnick; A. Tolmachev; D. Sinefeld; O. Golani; S. Ben-Ezra; M. Nazarathy; D. M. Marom, "Sub-banded / single-sub-carrier drop-demux and flexible spectral shaping with a fine resolution photonic processor", *2014 The European Conference on Optical Communication (ECOC)*, Cannes, 2014, pp. 1-3.

[11] A. Triki, "Etude des techniques de transport de données par commutation de rafales optiques sans résolution spectrale de la contention" Thesis manuscript, Télecom Bretagne, 2014

CHAPTER 3

The burst mode CO-MB-OFDM transmitter/receiver

In the previous chapter, the TISA concept has been presented. In TISA concept, as a source is able to generate bursts at various wavelength sub-bands, a fast tunable burst mode transmitter should be implemented at the source node. Then at the destination side, each destination receives only one sub-band, so that a coherent receiver receiving a fixed sub-band will be realized according to TISA concept. In this chapter, we will present the choice among the available solutions for the realization of the burst mode transmitters and then we present the implementation of the transmitter and the coherent receiver. Afterwards, the performances of the pair of burst mode transmitter/receiver are evaluated in back to back configuration and the experimental results are presented and discussed.

3.1 Fast tunable laser with ultra-narrow linewidth

There are two main solutions to realize a fast tunable burst mode transmitter: using a fast tunable laser (as shown in Figure 3-(a)) or using several fixed wavelength transmitters and fast optical switches (as shown in Figure 3-1(b)). Here we have chosen the first method using a fast tunable laser inside the transmitter, since fewer modulators are required in this solution. As discussed in chapter 2, in order to implement the first solution for TISA concept, some requirements of the fast tunable laser should be met: less than 100 KHz linewidth and less than 100 ns wavelength tuning time. In the following section, we give a small state of art of the existing commercial fast tunable lasers.

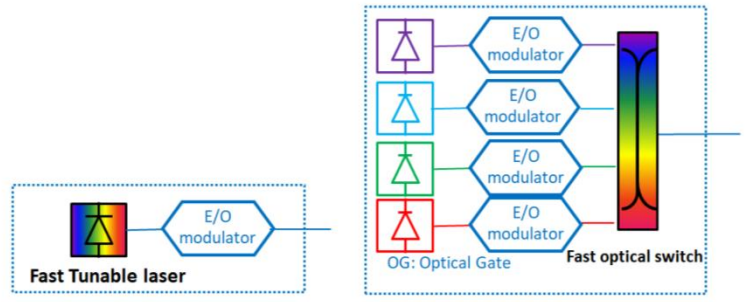

Figure 3-1: Fast tunable burst mode transmitter based on (a) fast tunable laser and (b) fixed transmitters and fast optical switch

3.1.1 Overview of tunable laser solutions

In the optical transport network, the semiconductor lasers are appreciated for their lower cost and compact volume. As the optical band used in the metro and long-haut network is the C-band (classically EDFA bandwidth from 1530 to 1565 nm), a brief overview of the lasers working in C-band is given. Several specifications are very important to be considered, such as the output frequency tunable range, the frequency stability, the wavelength tuning time and the phase noise, as

the tunable range and the frequency stability is not a big challenge nowadays [1][2], we discuss only the wavelength tuning time and the phase noise, these two characteristics when we present later the current solutions. We investigated 3 promising candidates: External Cavity Laser (ECL), Sampled Grating - Distributed Bragg Reflector (SG-DBR) laser, Modulated Grating-Y (MG-Y) laser.

3.1.1.1 External Cavity Laser

There are several approaches for implementing a tunable external cavity semiconductor laser [3], such as Littrow ECL configuration, Littman-Metcalf ECL configuration and so on. In Figure 3-2, an example of well-known ECL architecture using Littman-Metcalf configuration is shown. It uses diffraction grating as the wavelength selective feedback element. After the light emission, a lens is used to collimate the light and send the light to the diffraction grating. And then a mirror is placed at the diffracted signal direction to reflect the diffracted light to the diffraction grating. After that, the diffracted signal which goes the output port is the selected signal. The mirror and diffraction grating construct a double-pass wavelength selective element. Using this structure, an external cavity laser has efficient wavelength selectivity. Wavelength tuning is achieved by rotating the mirror. When the diffraction grating (grating constant), lens, and cavity length are well chosen so that only one longitudinal mode is selected within an acceptance angle of the waveguide, the external cavity laser will produce a single frequency laser emission. The output linewidth of the wavelength at the output of ECL is in the order of 50 KHz [4]. As the wavelength tuning is realized by a mechanical control technique, the wavelength switching time is in the order of several milliseconds.

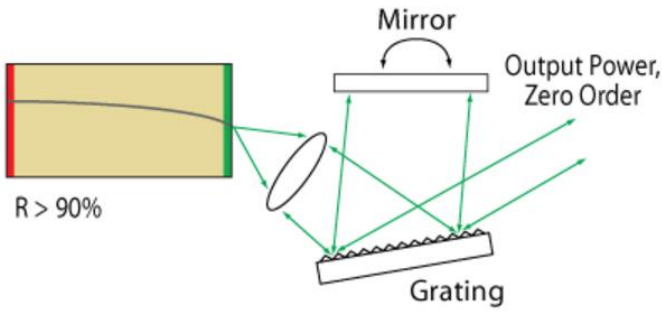

Figure 3-2: Example of ECL architecture using Littman-Metcalf configuration [5].

In Figure 3-3, another ECL architecture configuration is presented [6]. The optical cavity is formed by a gain chip and an external cavity with a high-reflection end-mirror. Two silicon etalon filters are placed inside the optical cavity with a slightly different Free-Spectral-Range (FSR) in order to create coupled cavities. The configurations of the two silicon etalon filters have a little difference, and then the dominant laser peak can be selected thanks to the Vernier effect. The wavelength tuning is realized by modifying the two etalon filters position through the heating of temperature controlled platform. And the position of the end mirror can be changed in order to modify the length of the external cavity and thus the modal resonance, which is supported by Piezo devices made of lead Zirconate Titanate (PZT) being capable to drive mechanical devices for precision positioning. So

the optical cavity can be modified with a high precision. And the gain control is performed by the In-P gain chip. This kind of ECL can achieve a linewidth as narrow as 10 KHz, but the wavelength switching is also in the order of several milliseconds.

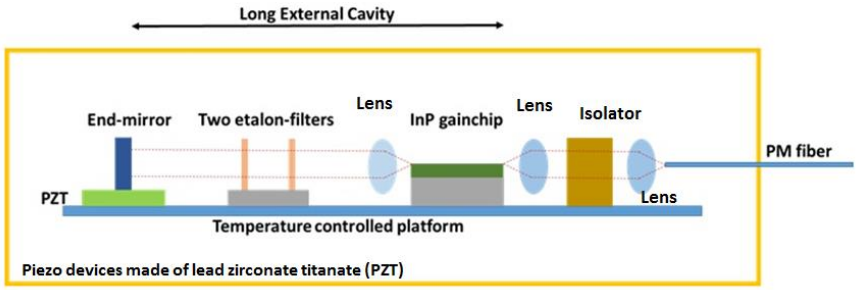

Figure 3-3: Example of ECL architecture [6].

3.1.1.2 Sampled Grating - Distributed Bragg Reflector laser

The conventional DBR laser architecture is shown in Figure 3-4. There are three parts in the DBR laser architecture: wavelength generation section, phase section and gain section. As the DFB laser, a diffraction grating structure is used to as the wavelength selective component to define the emission wavelength. Phase section and gain section is set to adjust the phase and gain of the output emission. But a DBR is only continuously tunable over approximately a 2 nm range, which cannot work in the whole C band.

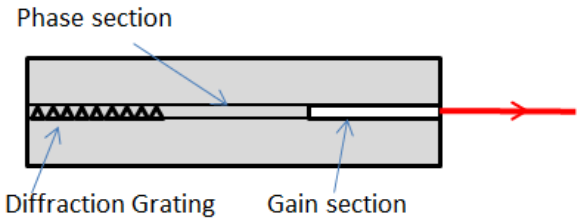

Figure 3-4: Example of DBR laser architecture.

Based on conventional DBR, the Sampled-grating DBR (SG-DBR) (as shown in Figure 3-5) has been proposed in [7] in order to improve the tunable range and the wavelength tuning time. There are four sections in the laser, two wavelength selective sections (the back DBR and the front DBR), the phase section and the gain section. Two DBR structures are implemented respectively at the rear and the front of the laser. These two structures have a little difference in the wavelength diffraction grating structure in order to selective different wavelength peaks for each diffraction grating. Then the selection of wavelength is selected through the Vernier effect. The wavelength tuning can be achieved by thermal tuning these two DBRs (the two diffraction grating structures). The wavelength tuning time is around 50 ns, but the linewidth is in the order of several MHz.

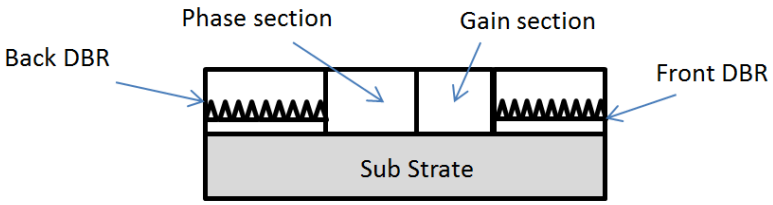

Figure 3-5: SG-DBR laser architecture

3.1.1.3 Modulated Grating-Y laser

MG-Y laser [8] is a kind of laser based on conventional DBR, with using multi-peak modulated reflector gratings structure in order to extend the tuning range. The schematic of MG-Y laser is shown in Figure 3-6. There are five sections: the gain section, the common phase section, the Multi-Mode Interferometer (MMI), the differential phase section and two multi-peak modulated reflectors. The two multi-peak modulated reflectors have slightly different grating structure in order to reflect different wavelength peaks, and only one pair of peaks can be overlapped at any time. The differential phase section is used to finely tune the phase of the light coming from the reflector-1. Then both the reflection lights coming from these two multi-peak modulated reflectors are combined at MMI. At MMI, one reflection peak for lasing is selected through the additive Vernier effect. Then the gain section and common phase section is used to adjust the output power and phase. The wavelength tuning is realized by tuning two reflectors and the differential phase section. MG-Y laser can achieve an output emission with a linewidth in the order of 2 MHz and the wavelength tuning time is in the order of 10 ns with using a suited electrical order driver.

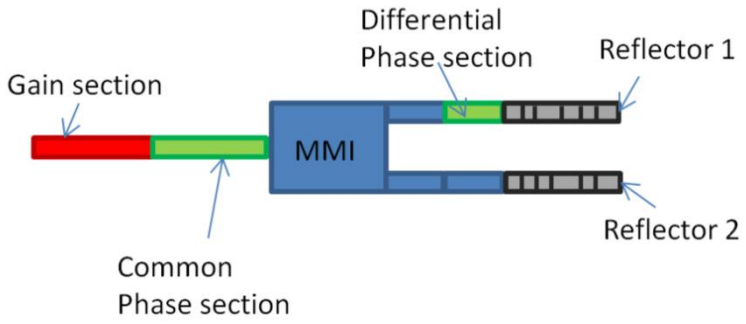

Figure 3-6: Example of MG-Y laser architecture

In conclusion, all the existing commercial lasers that can be tunable in the entire C-band do not meet these two criterions that we defined above that are a less than 100 KHz narrow linewidth and a less than 100 ns fast wavelength tuning time at the same time. As a result, the first step of the implementation of tunable burst mode transmitter for TISA network is to build the fast tunable laser with a narrow linewidth.

3.1.2 Fast tunable laser for TISA

In order to build a fast tunable laser with narrow linewidth for TISA, we have chosen to use a combination of fixed wavelength lasers with optical gates. There are two principals candidates to

realize the optical gates: Mach-Zehnder Modulator (MZM) or Semiconductor Optical Amplifier (SOA). The MZM, based on the electro-optics effect, can modulate a beam of light using electrical signal control with a switching time as low as tens picoseconds. However MZM solutions introduce a large insert loss. The SOA has a similar structure to Fabry–Pérot laser diodes using the semiconductor to provide the gain (i.e. low reflection of end facet of semiconductor waveguide). An electrical current drives the SOA in order to excite electrons, which can then fall back to the non-excited ground state and give out photons. The switching speed of SOA is based on the current command. The minimum switching time is related to the carrier lifetime which is the order of or even lower than 1 ns. In real application, the electric command can limit the switching time also, as the optical response cannot be faster than the electrical command. Moreover, the SOA can give a gain to the input signal, which is an advantage for the system implementation avoiding inserting an optical amplifier (ex. EDFA) at the output port. Since SOA has a small switching time, it is usually used as optical gate.

The proposed architecture is shown in Figure 3-7. It consists in 4 Purephotonics ECLs (model PPCL200) with ~100 kHz linewidth, 4 Thorlabs BOA1004PXS Semiconductor Optical Amplifier Gates (SOAGs) with small switching time (minimum 1 ns) and ~18 dBm output power and a 4:1 Polarization Maintaining (PM) coupler. Each ECL emits continuously at a unique wavelength, and the Semiconductor Optical Amplifier Gates (SOAGs) are in charge of switching “on” and “off” the continuous light. After the combination of each SOAG’s output together by a polarization maintaining coupler, the fast tunable laser source with 4 different wavelengths is implemented. Each wavelength here is corresponding to an OFDM sub-band in the TISA concept. We want to emphasize that in TISA, each source should be able to generate several sub-bands. So that the number of ECLs and SOAGs will be combined to build a fast tunable laser for a real TISA source will be extremely large, and thus the energy consumption and poser inserting loss are considerable. So this architecture is only for laboratory environment only at this moment. However, nowadays the photonic integrated circuits technology has a fast and great development, 16 channels transceivers has been successful integrated [9]. So this architecture can be integrated in photonic integrated circuits in near future.

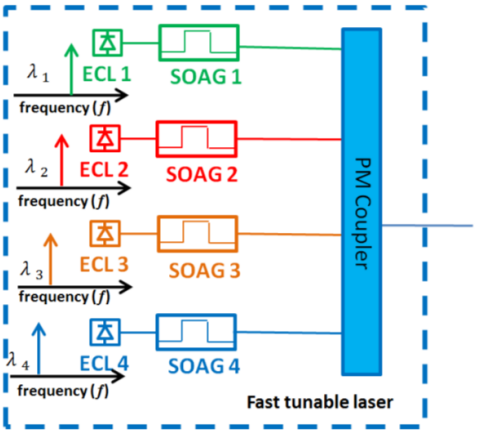

Figure 3-7: Fast tunable laser architecture based on SOAGs.

In the transmitter, a CMZM will be used to modulate the electrical signal at the optical carrier. A CMZM can introduce more than 15 dB optical power loss for the reasons such as insert loss. So that, the input optical power of the CMZM should be large enough to ensure the normal output optical signal power in order to output the signal with high Optical Signal to Noise Ratio (OSNR). As a result, the SOAGs should have a very high output power in order to avoid inserting an additional EDFA between the fast tunable laser source and the CMZM. The Thorlabs BOA1004PXS SOAG [10] is thus chosen as optical gate for its high output power ~18 dBm.

Figure 3-8: The SOAG driver.

As the SOAGs have a high output power, they require correspondingly a high driving current (~600 mA). This current value is much higher than the current for an ordinary SOAG working in ~150 mA (i.e. corresponding to a ~5 dBm output power), which is thus very challenging for the electrical SOAG driver. Moreover, as the response time of the SOAG is related to the electrical order, the rise and fall time of the driving current should be very small in order to guarantee the wavelength switching time of the SOAG lower than 100 ns. In order to drive the SOAG, a specific driver has been developed by the Vectrawave (in Figure 3-8), a specialist company in the electric driver component.

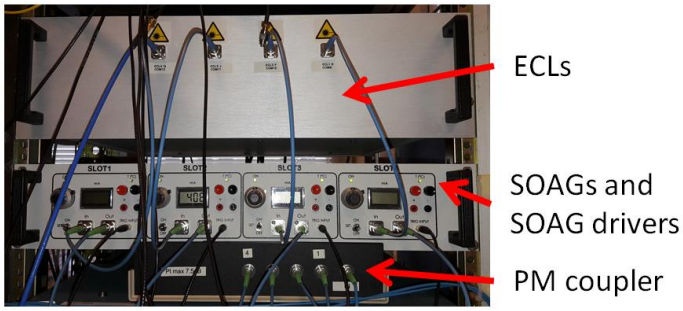

Figure 3-9: The rack of SOAG drivers and the rack of ECLs.

The driver can offer as high as 650 mA current variation. Each driver is used to driver one SOAG, which enables the independent control of each SOAG. So, each driver has its own trigger signal reconditioned by a Schmitt trigger gate, which transforms the input signal to two states: “on” or “off”. Current switching is assumed by a power Metal Oxide Semiconductor Field Effect Transistor (MOSFET). MOSFET is chosen for a tradeoff between high current drive and low rise and fall time (less than 10 ns). As 4 SOAGs are equipped in a fast tunable laser, a rack equipped with 4 SOAG independent drivers is built in order to create optical temporal windows. Figure 3-9 shows the SOAG

drivers rack and the rack with ECLs. The driver enables large and flexible range for the driving currents and no restriction on the duration of SOAG opening time except on switching time: the goal is to obtain an equivalent wavelength switching time (the sum of fall time of a SOAG and rise time of the following SOAG) lower than 100 ns.

First, the 10%-90% rise and fall times of the four SOAGs are measured in order to validate the wavelength switching time using a 600 MHz bandwidth oscilloscope. The control signals are generated by a FPGA card, which delivers a 3.3 V single ended signals with a rise and fall time lower than 2 ns. The generation of control signals will be detailed in chapter 4. The SOAG is switched "on" and "off" alternatively with the same "on" and "off" duration. When the "on" and "off" duration varies from 5 µs to 100 µs, the rise and fall times remain the same for each of the four SOAGs under study.

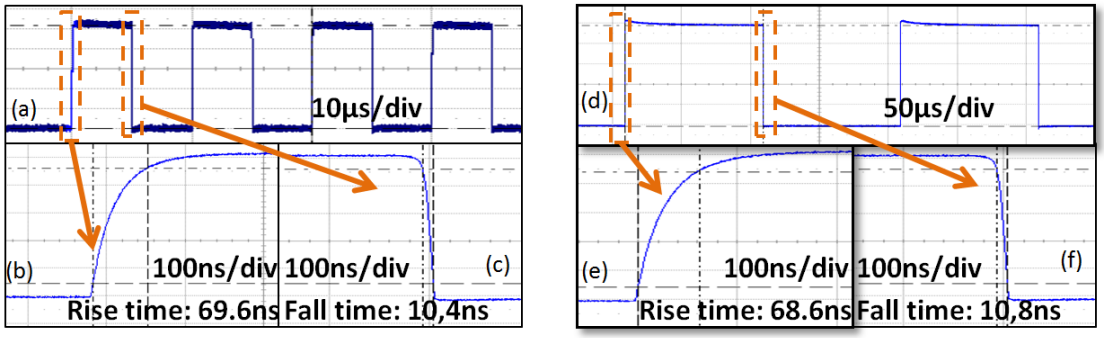

Figure 3-10: The optical output signal of SOAG1 for (a) 5 µs "on" - 5 µs "off" states, 10 %-90% rise (b) and fall (c) times for 5 µs "on" and "off" duration, (d) 100 µs "on" - 100 µs "off" states, 10 %-90% rise (e) and fall (f) times for 100 µs "on" and "off" duration.

Figure 3-10(a) represents the optical signal at the output of the SOAG1 with 5 µs "on" duration and 5 µs "off" duration. The rise and fall times of a 5 µs control patterns (Figure 3-10 (a)) are shown in Figure 3-10 (b) and Figure 3-10 (c) respectively. Figure 9(d) represents the optical signal at the output of the SOAG1 with 100 µs "on" duration and 100 µs "off" duration. The rise and fall times of a 100 µs "on" and "off" duration in the Figure 3-10 (d) are represented in Figure 3-10 (e) and Figure 3-10 (f) respectively. In two study cases (5 µs and 100 µs configurations), the rise time is ~70 ns and the fall time is ~11 ns. The explanation of the behavior of the SOAG with a rise time much longer than the fall time is that there is an inductor SOAG package contribution which influences more the process of switch "on". The results are similar with the other SOAGs, thus we are compliant with the TISA requirement on the switching time which has to be lower than 100 ns. Moreover, the extinction ratio is higher than 40 dB for the 4 SOAGs in dynamic mode. Then the 4 SOAGs are switched "on" and "off" alternatively in order to emit the 4 wavelengths successively, while each SOAG is switched "on" during 4.8 µs and is switched "off" during 15.2 µs.

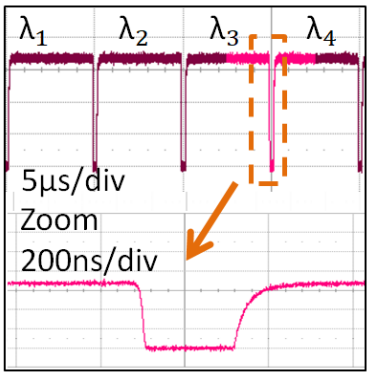

Figure 3-11: 4 SOAGs are switched “on” and “off” alternatively

The signal shown in Figure 3-11 demonstrates that no distortion appears which validates the proposed fast tunable laser. The spectrum at the output of the fast tunable laser source measured with an Apex high-resolution (20 MHz) Optical Spectrum Analyzer (OSA) is showed in Figure 3-12. Four different wavelengths are configured: 192.682 THz, 192.694 THz, 192.706 THz and 192.718 THz. We do not have an OSA with a resolution high enough to measure the linewidth of the output laser source; but the linewidth of the output laser source can be measured by performing the beating with a fixed wavelength ECL [11]. We do not carry out this experiment in this thesis.

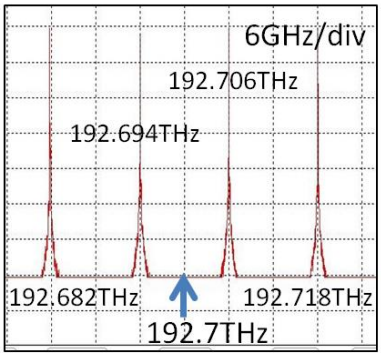

Figure 3-12: Spectrum at the output of the tunable laser

3.2 OFDM transmitter set up

After the validation of the fast tunable laser source, we begin to implement the transmitter using the proposed fast tunable laser source. The basic architecture is shown in Figure 3-1. The fast tunable laser is used to generate different optical carriers the transmitter.

3.2.1 Experimental transmitter set up

The architecture of the transmitter is shown in Figure 3-13. At the transmitter, the digital OFDM signals are generated in off-line using MATLAB. Then signals are separated into two parts: the real part (I) and the imaginary part (Q). After that two signals are downloaded into the Arbitrary Waveform Generator (AWG). The AWG converts the digital signals into analog electric signals. Then, Low Pass Filters (LPFs) are used to delete the aliasing signals. The aliasing signals are a periodical

unwanted signal around the sampling frequency, which are generated during the digital-analog conversion process [12]. Afterwards, two amplifiers working in their linear regime amplifies two analog signals and sent them to drive a CMZM in order to modulate the electrical signal on optical carrier. The laser source is the fast tunable laser we have implemented with four different wavelengths. As the CMZM introduces high power loss, the output power of CMZM is ~-12 dBm. So a PM EDFA is inserted at the output of CMZM in order to amplify the output power. Then a Polarization Division Multiplexing Emulator (PDME) is used to transform the single polarization signal into dual-polarization signals. The PDME divides the input signal polarization signal into two branches and then delays one branch by one OFDM symbol. After that the PDME rotates the delayed branch with 90° and then combines these two branches together. The output optical signal is transmit to the fiber transmission lines.

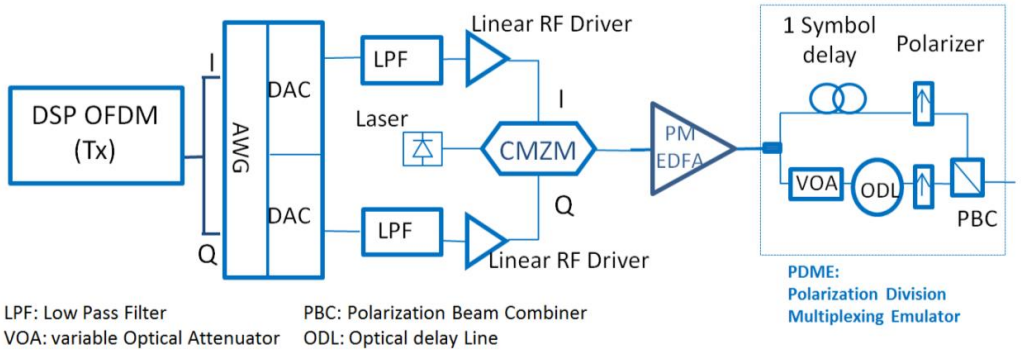

Figure 3-13: Transmitter experimental set-up.

One of the most complex steps of this experimental implementation is the fine adjustment of the CMZM bias. Figure 3-14 shows of the CMZM structure. The CMZM is constituted of a Mach-Zehnder super-structure comprising two MZMs in parallel, and a $\pi/2$ phase shifter which is inserted for instance in the lower arm of the CMZM super-structure. There are three bias voltages corresponding respectively to MZM1, MZM2 and phase shifter that allow us to adjust finely the CMZM working state. The optimal bias for MZM1 and MZM2 corresponds to the null transmission point while the optimal bias for MZM3 is to get $\pi/2$ shift.

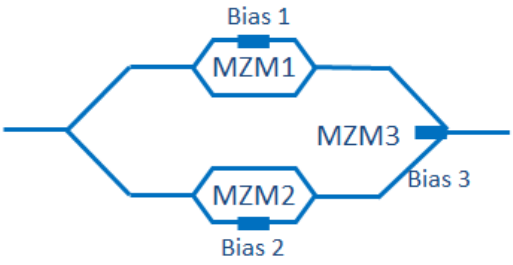

Figure 3-14: CMZM structure

The CMZM modulator adjustment method is given as follows:

1. Apply and adjust all the bias voltage to get maximum optical power without RF signal.
2. Adjust bias voltage 1 to get 25% of the maximum power at the super-structure output in order to find the null transmission point of the upper arm.
3. Adjust bias voltage 2 to get the minimum power at the super-structure output to find the null transmission point of the lower arm.
4. This step is used to set the optimal bias ($\pi/2$) for MZM3. Generate two same RF signal in I arm and Q arm. Then switch on the signal for the I arm while switch off the signal for the Q arm, and measure the output optical power by a power meter, the measured optical power is the I arm signal power, noted as P1. Then switch on the signal for the Q arm while switch off the signal for the I arm, and measure the output optical power again, the measured power is the Q arm signal power, noted as P2. In order to set a gain balance between I and Q arms, P1 should be equal to P2. Generally, there is a gain imbalance between I and Q arms, so we can correct the gain imbalance by modifying RF signal amplitude in AWG here. For example, P1 > P2, so we can reduce the voltage of the I arm electrical signal at AWG, in order to set the I arm signal power as P2 also. Afterwards, we switch on two arms, and adjust voltage 3 to ensure the output optical power (noted as P3) is exactly the sum of the I arm and Q arm signal power. Continue using the previous example, if we set both I arm and Q arm signal power at P2, the output power (P3) should be 3 dB more than P2, which means P3 = P2*2. The detailed explanation will be given later.
5. This step is used to fully suppress DC component by fining tuning Bias 1 and 2. If the step 2 and step 3 are well completed, this step is not necessary.

As CMZM is very sensitive to temperature variation, these optimal bias voltages should be repeated periodically, so daily tuning is necessary in the absence of automatic bias control circuit (that can introduce a slight penalty on the performance of the transmitter).

Concerning the detailed explanation for the step 4, assuming an ideal CMZM device (no insertion loss), the optical signal at output of CMZM [13] could be given by:

$$\mathrm{E_o(t)} = \mathrm{E_{o1}(t)} + E_{o2}(\mathrm{t})$$

$$\mathrm{E_{o1}(t)} = A\cos\left(\frac{\pi}{2}\frac{V_I+V_{Bias1}}{V_\pi}\right)\mathrm{e^{i\omega t}}$$

$$E_{o2}(\mathrm{t}) = A\cos\left(\frac{\pi}{2}\frac{V_Q+V_{Bias2}}{V_\pi}\right)\mathrm{e^{i\omega t+\theta}}$$

where $\mathrm{E_o(t)}$ is the output signal of CMZM, $\mathrm{E_{o1}(t)}$ presents output signal of MZM1 and $\mathrm{E_{o2}(t)}$ presents output signal of MZM2 while using $\mathrm{E_{in}(t)} = 2\mathrm{A\,e^{i\omega t}}$ to present input optical signal, V_I and V_Q stand for I and Q tributary voltages of input RF signal, V_{Bias1} and V_{Bias2} present bias voltage 1 and 2 respectively, V_π is the half wave switching voltage of each MZM, ω is the frequency of optical carrier and θ is phase shift obtained by phase shifter.

In order to get optimal configuration, we want to set V_{Bias1} and V_{Bias2} as V_π in order to set the null transmission point and set θ as $\pi/2$ for the $\pi/2$ phase shift. Since V_I and V_Q are much smaller than V_π, $E_{o1}(t)$ can be simplified by using the transformation $\cos\left(\frac{\pi}{2}\frac{V_I+V_{Bias1}}{V_\pi}\right) = -\sin\left(\frac{\pi}{2}\frac{V_I}{V_\pi}\right) = -\frac{\pi}{2}\frac{V_I}{V_\pi}$ and the same operation can be carried out for $E_{o2}(t)$ part. In result, we can write output signal as follow in the optimal configuration:

$$\mathrm{E_o(t)} = -\frac{\pi}{2}\frac{A}{V_\pi}(V_I + iV_Q)\,\mathrm{e^{i\omega t}}$$

The power of CMZM output signal could be written as:

$$P(E_o) = \left(\frac{\pi}{2}\frac{A}{V_\pi}\right)^2\left({V_I}^2 + {V_Q}^2\right) = P(E_{o1}) + P(E_{o2})$$

Note that

$$P(E_{o1}) = P1 \;\; and \; P(E_{o2}) = P2$$

$$P(E_o) = P3$$

So the output power of CMZM should be the sum of the output signal power of MZM1 and MZM2, P3 = P1+ P2 = P2*2 (if P1 = P2) as discussed in step 4 in the previous paragraph.

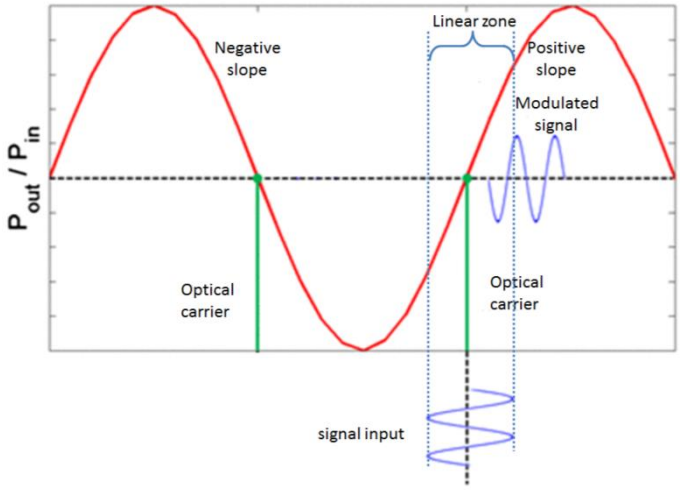

Figure 3-15: Transfer function of MZM

The performance of transmitter is related to various parameters of the components we used in the transmitter. The process to modulate OFDM signal, especially high order QAM signal, on an optical carrier require a high linearity. So the input signal of CMZM should work in the linear zone of each MZM transfer function, as shown in Figure 3-15. So the output of the linear RF driver should adapt its level to the linear zone of the CMZM transfer function. If the linear RF driver output power is larger than the CMZM input linear zone, the amplifier gain can be adjusted (provided that the

linearity of the amplifier is kept) and/or a fixed RF attenuator can be inserted between the RF driver and CMZM in order to optimize the CMZM performance. The linear driver has also a linear working zone which requires that the input signal power be lower than a certain threshold. The input signal power of the linear RF driver has to be precisely optimized (through the insertion of RF attenuator at the driver input) in order to ensure a linear operation for the RF driver. As the transfer function of the CMZM is fixed, the linear zone is the same for every CMZM. So the key component to guarantee the linear zone of the transmitter is the linear RF driver.

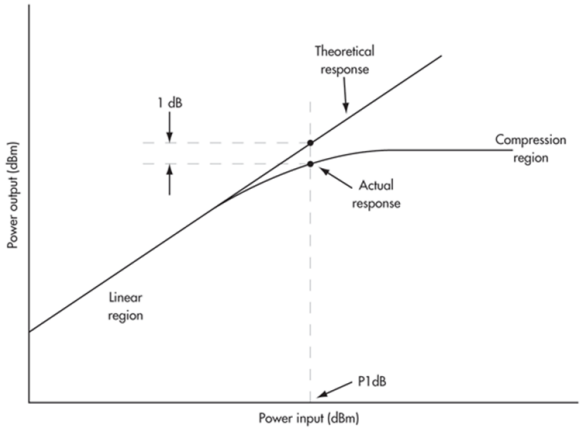

Figure 3-16: The comparison between the real response of a RF driver and its theoretical response.

For the choice of linear RF driver, two parameters should be carefully taken into account: gain and 1 dB compression point. The gain is the fixed power gain given by the amplifier, which can be used to estimate the output signal power from the input signal power. The 1 dB compression point, noted as P1dB, is a parameter used to evaluate the linear zone. As shown in Figure 3-16, the P1dB point is the input power that causes the gain to decrease 1 dB from the theoretical expected linear gain plot. So this point is important for us to know at what point the gain compression begins, so the input signal levels can be restricted to prevent distortion. The P1dB can also be given as an output signal power, as in the datasheet of the SHF 806E linear RF driver [14], the P1dB is given as “Output power at 1dB compression”. The larger P1dB it is, the larger the linear zone is. Except the linearity of the RF driver, the extinction ratio of CMZM is also important, which is used to evaluate the optical noise level of the output optical signal. This parameter can be measured by measuring the power of output signal of CMZM (that should be already in optimal working state) between switch on all data signals and switch off all data signals. In order to generate the 16QAM signal, it is better to have an extinction ratio larger than 23 dB in order to get a good performance from our experiences.

3.2.2 Transmitter DSP procedures

The Digital Signal Processing (DSP) of OFDM at the transmitter side is shown in Figure 3-17. We choose the data-aided signal processing technology. Compared to blind equalization largely used in the context of coherent optical communications (such as Constant Modulus Algorithm for polarization demultiplexing) the data-aided equalization is well-suited to the context of optical burst

switching because it can fast estimate the channel without previous knowledge. This feature is essential when burst traffic is considered, as the bursts arriving at the destination node come from different source nodes. The DSP begins with encoding and data mapping. Then pilot tones are inserted into the data spectrum in order to estimate the phase noise after fiber propagation. Afterwards, synchronization symbol and training symbols are added for time synchronization and channel equalization. Then inverse FFT transforms the signal from frequency domain to time domain. In order to improve the robustness to CD and PMD, Cyclic Prefix (CP) is inserted at the beginning or rear of each symbol. After parallel-to-serial conversion, clipping is carried out in order to reduce the Peak to Average Power Ratio (PAPR) of the OFDM signal and thus taking full use of the Effective Number of Bits (ENOB) of the DAC.

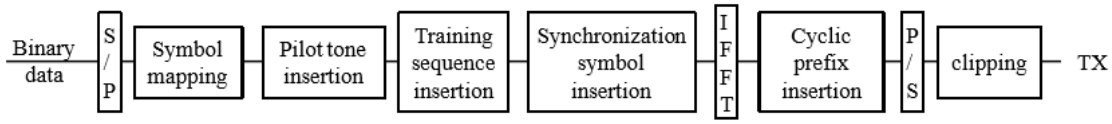

Figure 3-17: OFDM DSP procedure in the transmitter

Cyclic prefix is inserted in the OFDM symbol in order to prevent the ISI and ICI introduced by the PMD and CD. It copies a number of samples from the end of the OFDM symbol, and then appends them to the start of the symbol, as shown in Figure 3-18. During the signal transmission in optical fiber, CD and PMD cause a spreading of the symbols and thus lead ISI and ICI. With adding CP, we can careful selected a signal segment with all the transmitted signal avoiding the ISI and ICI in the receiver, as shown in Figure 3-18. The inserting of CP will introduce a phase shift after we perform the FFT transformation at the receiver side, but this phase shift can be compensated in the DSP thanks to the training symbol. Indeed, the CP protection can be replaced by an empty interval in the time domain in order to reduce the power consumption, but as the empty interval will introduce some constraints of the electric components, such as the low cut-off frequency, the CP is preferred.

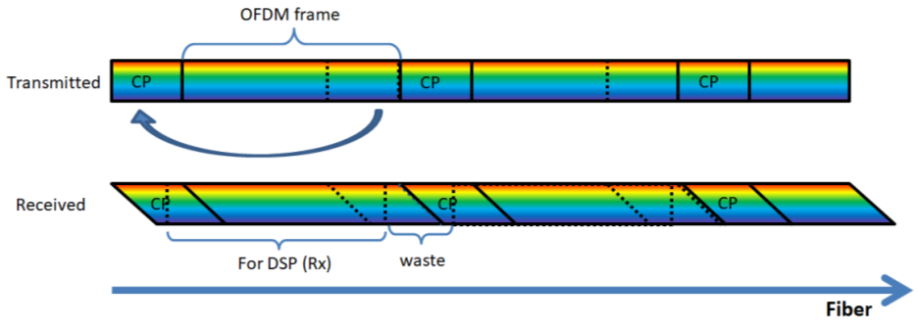

Figure 3-18: OFDM symbol with cyclic prefix in the time domain

In optical transmission, CP should be long enough to cover the spreading created by CD and PMD. However, since CP introduces a higher overhead ratio and reduces the overall bit rate, it should be as short as possible during the OFDM dimensioning. The relation between CP length, FFT size,

sampling frequency and CP overhead will be discussed in the following section of OFDM signal dimensioning.

Concerning the synchronization symbol, there are a lot of technologies to generate the synchronization symbol, such as Schmidl & Cox [15] and Minn & Bhargava [16]. Here we choose the methods Schmidl & Cox, since it has been proved as a simple, typical and reliable technology [12][17]. It consists in using one symbol which has two identical half parts in the time domain. We can generate a symbol with pseudo random signal and replace the second half part by copying the first half part signal. Accordingly, at the receiver side, the signal can be correlated with itself over a sliding window of half symbol length in order to find the repeated patterns and to locate the start of the synchronization symbol and thus the start of the training symbols. The start point of the synchronization symbol can be given at the maximum point of a time metric, as in Figure 3-19. As we can see, there is a plateau for the time metric, this is due to the inserting of CP, which repeating several samples of the rear of the synchronization symbol and the synchronization symbol has two identical parts. The length of the plateau equals to the CP length. Due to the polarization mixing in the fiber, there are two plateaus on the timing metric. The first plateau corresponds to the frame beginning point of the x polarization and the second one corresponds to that of the y polarization. The two plateaux are spaced by one symbol duration. In low OSNR, the accuracy of timing metric is affected by noise. One solution is to find the maximum, and then find the points at the left and right sides in the time domain that are more than 90% of the maximum, and average all these points to find the symbol timing estimate.

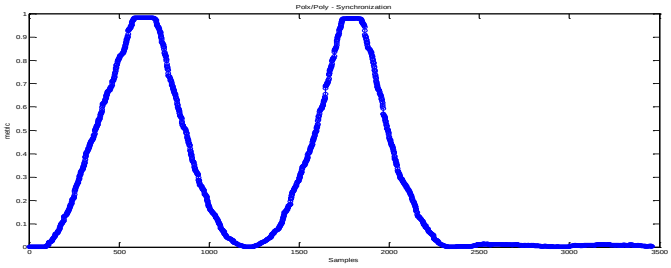

Figure 3-19: The timing metric of a back-to-back experimental DP-OFDM signal using Schmidl &Cox synchronization symbol.

3.2.3 Dimensioning

The OFDM signal is generated frame by frame; a frame is a completed OFDM data structure. The OFDM frame can be represented by a two dimensional structure, as shown in Figure 3-20. The horizontal and vertical axes represent respectively the symbols (time) and subcarriers (frequency) dimensions. So we can see that one OFDM frame is composed of a certain number of symbols in the time domain. On the other hand, one OFDM frame consists of a certain number of subcarriers in the frequency domain. In this section, we will explain the key parameters of OFDM signals and the

relationship between these parameters and the transmitted bit rate. Furthermore, the relation between raw bit rate (which indicates the bit rate transported by a data flow) and nominal bit rate (which indicates the effective bit rate transported by a data flow, usually excluding the overheads, correction bits, and so on), as well as the calculation of each overhead will be presented.

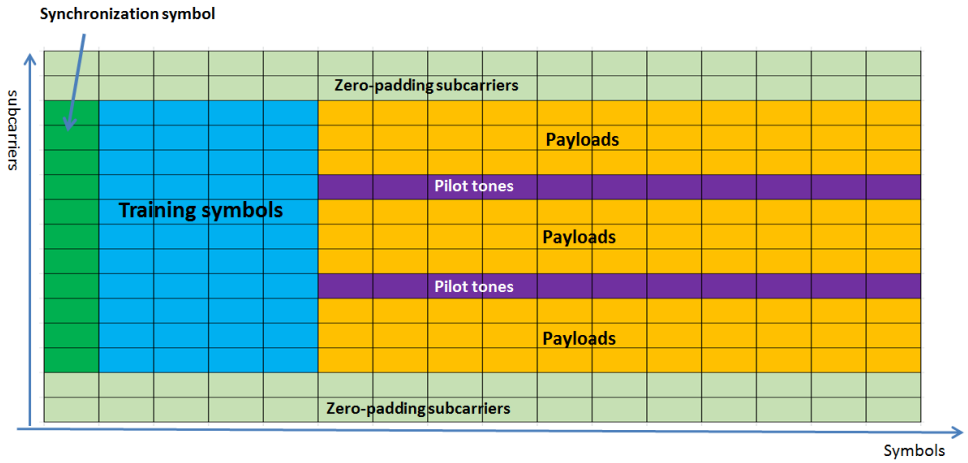

Figure 3-20: OFDM frame structure

At first, we define the symbols of each key parameter to describe the OFDM signal. The total number of symbols in an OFDM frame is noted as L_f; the number of synchronization symbol is noted as L_s; the number of training symbols is noted as L_{ts}; the number of data symbols is noted as L_{data}. These parameters should satisfy the relation: $L_f = L_s + L_{ts} + L_{data}$. The total number of subcarriers which is the FFT size is noted as N_{fft}; the number of pilot tones is noted as N_{pt}; the number of zero-padding subcarriers is noted as N_{zp}; the number of payload symbols is noted as N_{data}. These parameters should satisfy the relation: $N_{fft} = N_{zp} + N_{pt} + N_{data}$. Moreover, the number of CP is noted as N_{cp}.

The raw bit rate of an OFDM signal is expressed as

$$R_{raw} = f_s * \frac{N_{fft} - N_{zp}}{N_{fft}} * log_2 M * N_{pol} = B * log_2 M * N_{pol}$$

where f_s is the sampling frequency, B is the OFDM signal bandwidth, M is the number of points on the constellation and N_{pol} is the number of polarizations (1 for single polarization and 2 for dual-polarization). For the B, the OFDM signal bandwidth, the zero-padding subcarriers are not counted in the signal bandwidth as they are added on the left and right edges of the spectrum without transporting any information. Moreover, they are not considered as overhead either. The nominal bit rate after removing various overheads is expressed as

$$R_{nominal} = (1 - \varepsilon_{FEC})(1 - \varepsilon_P)(1 - \varepsilon_{TS})(1 - \varepsilon_{CP}) * R_{raw}$$

where ε_{FEC}, ε_P, ε_{TS}, ε_{CP} represent respectively the overhead ratios of FEC, pilot tones, training symbols and cyclic prefix. Here, the ratio of synchronization symbol is taken into account together with the training symbols, so ε_{TS} counts both the overhead of training symbols and synchronization symbol. The overhead ratios are calculated as follows:

$$\varepsilon_{FEC} = \frac{R}{1+R}\ ;\ \varepsilon_P = \frac{Npt}{Ndata + Npt}\ ;\ \varepsilon_{TS} = \frac{Ls + Lts}{Lf}\ ;\ \varepsilon_{CP} = \frac{Ncp}{Nfft + Ncp}$$

where *R* represents the code redundancy of FEC, which is ~7% for typical HD-FECs and ~20% for SD-FECs implemented in actual 100 Gbps transceivers. For the 7% HD-FECs redundancy, the FEC overhead ratio (ε_{FEC}) equals to 6.5%. For 20% SD-FECs redundancy, the FEC overhead ratio (ε_{FEC}) equals to 16.67%. The others overhead ratio in our test-bed are $\varepsilon_P = 2.94\%$ and $\varepsilon_{CP} = 5.88\%$ according the OFDM signal parameters we use during the thesis, which are shown in the next paragraph in Table 3-1.

For the pilot tones design, a certain number of pilot tones are inserted in order to estimate the phase noise. The number of pilot tones is related to the number of subcarriers and the transmission environment, the number of pilot tones increases when the number of subcarriers increases. Simulation results [12] have shown that 5 pilot tones subcarriers can achieve good performance for QPSK modulated OFDM signal with the 256 total subcarriers [12]. Here in order to ensure the good performance of phase noise correction, 6 pilot tones are inserted for all the experiment tests.

For the synchronization symbols, one synchronization symbol is enough to perform time synchronization process. For the training symbols, they are used to perform channel estimation. Since the number of training symbol is related to the transmission situation, during this thesis, the number is various and will be presented in each test specifications.

The cyclic prefix is related to the number of subcarriers, the transmission distance noted as L_{trans}, the coefficient of Differential Group Delay (DGD), the coefficient of CD (noted as *D*) and PMD (noted as *PMD*). The CP should be longer enough to cover the ISI and ICI. So the length of CP should satisfy this condition which is expressed as:

$$\frac{N_{cp}}{f_s} \geq T_{CD} + T_{DGD} = D * L_{trans} * B * \frac{c}{f_{Laser}^2} + 3.5 * PMD$$

where T_{DGD} is the time is the maximum DGD delay. It is usually equal to 3.5 times the PMD [18]. T_{CD} is the time of spreading caused by CD. The f_{Laser} is the frequency of the optical carrier. The c is the light speed. For the calculation of the CP length in our test-bed, we consider a target reach L_{trans} = 1000 Km, with D = 17 ps/(nm*Km), PMD = 12 ps, f_{Laser} = 193.41 THz, f_S = 10 GHz, B = 6.67 GHz. The 1000 Km transmission distance is chosen as a reference example, even though we did not perform experimentally a transmission in the thesis. Considering the given parameters, the N_{cp} should satisfy:

$$N_{cp} \geq (908 + 42)\ ps * fs = 9.5$$

So the samples of CP should be more than 9.5. In the following, we choose $N_{cp} = 16$ for all the experimental tests during the thesis. Table 3-1 below summarizes the main parameters of the proposed OFDM signal.

Table 3-1 Main parameters of the OFDM signal

Optical bandwidth	6.67 GHz
Base bandwidth	3.33 GHz
Sampling frequency f_s	10 GHz
Coefficient of CD	17 ps/(nm*Km)
Coefficient of PMD	12 ps
Length of CP	16
Length of synchronization symbol	1
Length of training symbol	Various based on different test situations
Length of payload symbol	Various based on different test situations
FFT size	256 points
Number of pilot tones	5
Number of zero-padding	86
Symbol duration without CP	25.6 ns
Symbol duration with CP	27.2 ns

3.3 OFDM receiver set up

For the receiver, a dual-polarization receiver based on coherent detection technology is implemented. A tunable wavelength laser is used as Local Oscillator (LO) in the receiver. The coherent detector detects only one sub-band in TISA concept. Since we are using intradyne coherent detection technology as we discussed in chapter 1, the wavelength of the LO should be tuned carefully to receive the designed sub-band. In this section, the implementation of receiver and the DSP procedure will be presented, and then the specific DSP procedure for the burst mode traffic will be presented.

3.3.1 Experimental receiver set up

The experimental set-up of a coherent receiver is shown in Figure 3-21. As the coherent detection technology is sensible to phase noise, the linewidth of the local oscillator should also be less than 100 KHz. The received signal and the LO are split into orthogonal polarization components using two Polarization Beam Splitters (PBSs). After that, each polarization enter into a 90° hybrid, the received signal will beat with the LO. After the beating, the real and imaginary parts of polarization X and Y are converted to four baseband electrical signals through four balanced detectors. The four analog electric signals are then converted to digital domain by four ADCs operating at 50 GSamples/s and embedded into a real-time fast sampling oscilloscope. Afterwards, the off-line DSP is carried out to recover information.

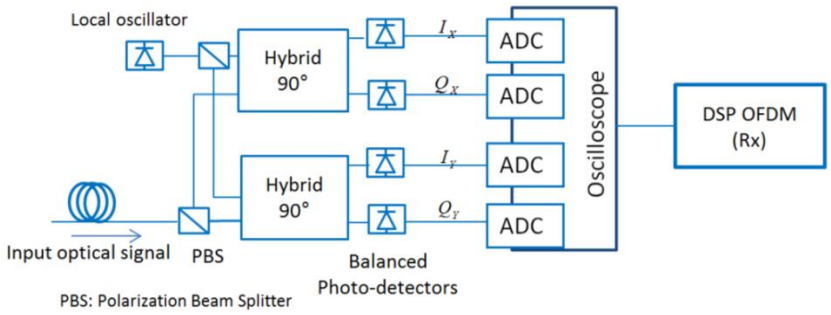

Figure 3-21: Receiver experimental set-up.

3.3.2 Receiver DSP procedures

At the receiver side, the DSP implemented is roughly based on the reverse process than the one implemented in the transmitter, as shown in Figure 3-22.

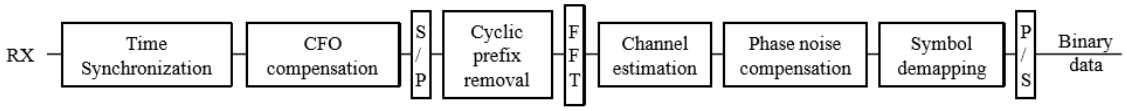

Figure 3-22: OFDM DSP procedure in the receiver

The time synchronization is performed at first to find the maximum point as discussed in the previous paragraph and thus to find the start point of the OFDM frame. After that, Carrier Frequency Offset (CFO) compensation is performed. In the Schmidl & Cox synchronization approach [15], we can estimate a phase rotation (the CFO) by calculating the phase difference between the *i*th samples of two identical sub-symbols.

$$\Delta_{CFO} = \frac{\phi f_s}{2\pi L} \quad \text{for} \quad 0 \leq \phi < 2\pi$$

where f_s is the sampling frequency, ϕ is the phase difference and L is the distance (the number of sub-carriers) in terms of number of samples between the two samples calculated. But this solution can only estimate the CFO between 0 and 2π. In thesis of Julie Karaki [12], a method has been proposed to estimate large CFO. CFO is proposed to be written as:

$$\Delta_{CFO} = (2\pi * n + \varepsilon_{CFO}) * \frac{f_s}{2\pi L}, \quad 0 \leq \varepsilon_{CFO} < 2\pi$$

where n is an integer, 2π*n is the integer part and the ε_{CFO} is the fractional part. The integer part can be estimated by comparing the spectrum of the training symbol of the received signal and the spectrum of the designed training symbol. If there is no CFO, these two spectrums should be in the same place in the frequency domain. So, the difference of the edges of these two spectrums represents the CFO. This method can fast estimate the CFO, but it is lack of precision, so the evaluated CFO can be used to compensate the integer part. In the case that the CFO is larger than sampling frequency (f_s), we compensate the fractional part CFO at first while performing the

synchronization, and then we perform the compensation of the integer part CFO using the training symbols.

After CFO compensation, serial-to-parallel conversion is performed and then the cyclic prefix is removed. Thanks to the cyclic prefix, the payload is protected from the CD and PMD effects. Then FFT is applied to transform the signal from time domain to frequency domain. After that, channel estimation of dual-polarization using training symbols is performed. The training symbols are generated with a typical structure suggested by Jansen [17] as following form:

$$\begin{bmatrix} s^{pol-x}(i) & 0 \\ 0 & s^{pol-y}(i+1) \end{bmatrix}$$

Each training sequence period consists of two OFDM training symbols of two polarizations. For a training symbol, only one of the two polarizations is filled with designed data. And we cannot fill the data in the same polarization in two successive training symbols. At the receiver side, by comparing the received training symbols and the designed training symbol as depicted in Figure 3-23, we can obtain the transfer function of the channel. Then the zero forcing technology is applied to eliminate the distortion (gain/phase) experienced by the subcarriers and to recover the received signals.

Figure 3-23: Particular structure of the training symbols used for channel estimation and equalization, in the case of a dual-polarization OFDM system [19].

Afterwards, for each payload symbol, phase noise compensation using pilot tones is carried out. The phase noise is estimated by comparing the difference between the received pilot tones and the designed pilot tones. At last, the data demodulation and de-mapping are performed. More OFDM DSP details can be found in [19].

3.3.3 Specific DSP for burst mode

In the burst traffic, the received signal is not a continuous flow. There is a time interval without data signal before the burst signal and the duration of the time interval is various (from 100 ns to tens of microseconds). In the conventional OFDM DSP, the time synchronization is realized by performing the correlation between two successive half symbols over the received signal [15], as discussed in the paragraph 3.2.2. This method can give a precise point to indicate the start point of the OFDM frame, but the processing time is very long since we must perform the correlation calculation from the first received symbol. Here in order to reduce the processing time, we proposed a simple method. This method is composed by two steps: the first step is to find coarsely the start

position of the OFDM frame by finding the position of the guard time interval; then the second step is to perform the Schmidl & Cox on the reduced window for precise time synchronization in order to find precisely the start point of the OFDM frame.

For the step to find coarsely the start position of the OFDM frame, it operates in three steps, as follows:

1. Detect the signal envelope of the received signal. In order to reduce the impact of noise, we will average the received signal power by half symbol. A threshold is set to transfer the averaged power signal to signal envelope containing only 0 and 1: if the power is larger than the threshold it will noted as 1, otherwise noted as 0. Figure 3-24 (a) shows an example of the received signal from the oscilloscope and (b) shows the obtained signal envelope. Here we set the threshold to a third of the maximum symbol power.

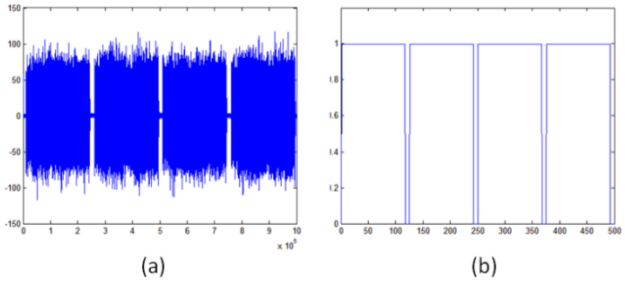

Figure 3-24 (a): An example of the received signal. (b) The corresponding signal envelope.

2. Detect the rise edge. Cross-correlate the signal envelope with a step mask is carried out to detect the edge. The step mask has a length of $2p$, where p is an integer less than quarter of the symbol length. In our experiments, the parameter p was set to 11 while the symbol length at the receiver side is 1360. After the cross-correlation, we search the peaks from left to right and note the first peak position n. Then the edge location d can be expressed as $d = n + p - 1$ and the coarse symbol start position is $(n + p - 1)*L_{HalfSymbol}$, where $L_{HalfSymbol}$ is the half symbol length.
3. Using this coarse symbol start position, verify whether the received signal contains a complete burst. Since the time interval between two bursts can be very long and the samples length we receive from the coherent receiver is limited, we can sometimes get only a part of OFDM frame. So if the received signal length is not correct, we will re-execute a turn to get a new data and begins the same process from the step 1.

As the signal power is calculated on the samples with half symbol length, so the found coarse time synchronization point has a precision of half symbol. After that, the Schmidl & Cox method can be performed over one and a half symbols to find the fine time synchronization point. Compared to the conventional Schmidl & Cox method, which we should perform correlation over the received signal from the beginning, this proposed solution can reduce considerably signal processing time.

3.4 Experimental back-to-back validation

In this thesis, two transmitters and two coherent receivers have been built in order to simulate the multi users in the TISA network. For the transmitter 1 (noted as Tx-1 hereafter), it uses the SHF 806E as linear RF driver and Fujitsu FTM7977HQA as CMZM. For the transmitter 2 (noted as Tx-2 hereafter), it uses Inphi 2811DZ as RF driver and Fujitsu FTM7960EX as CMZM. All these two transmitters have been optimized at the optimal working state. Their performance will be tested in this paragraph and the difference between their performances is related to the components used in the transmitter. Concerning the coherent receiver, the receiver 1 (noted as Rx-1 hereafter) is built by using the discrete components, such as balanced photodiodes, RF amplifiers. The receiver 2 (noted as Rx-2 hereafter) is built using the U^2T CPRV1010A integrated chip. This chip integrates the two hybrids and four balanced photodiodes together.

After the implementation of the transmitter and the receiver, the experimental back-to-back evaluation of the transmitter and receiver is carried out through Bit Error Rate (BER) measurements. The experimental set-up is presented in Figure 3-25: it is composed of the transmitter, the receiver and the control plane. The transmitter and receiver are implemented as described in the previous sections (section 3.2 and 3.3). For the control plane, the main module is the CCE, which is realized with a National Instrument (NI) real-time controller. The CCE preprograms the grants, each grants contains the 100 time slots configuration. In the TISA concept, the grants can be updated every control cycle that has the duration with 20 grants. A FPGA card is used as the local interface to generate the electrical control signals according to the received grants. The electrical control signals will control the SOAGs for switching “on” and “off”, so as to realize the wavelength emission at various wavelengths. When a new grant is set-up, a trigger is generated by the FPGA card and sent to the AWG. The AWG is configured to work in sequence mode, so after receiving the trigger signal, it starts to send OFDM data to the CMZM. In this way, at the input of the CMZM, electrical OFDM data are synchronized with the optical signal coming from the tunable laser, and thus the data flow is generated at the wavelength corresponding to the scheduling pattern. The implementation and the functions of the control plane will be presented in detail in chapter 4.

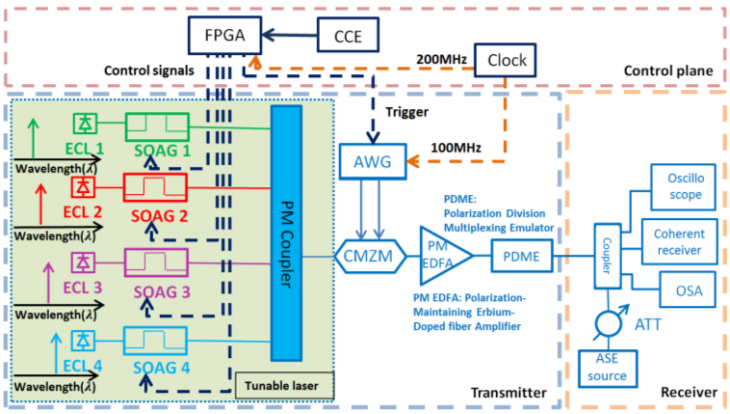

Figure 3-25: Experimental set-up for the back-to-back evaluation of the transmitter and receiver

At the receiver side, the received sub-band wavelength is selected by properly adjusting the wavelength of the LO. In TISA concept, the sub-band selection is realized by the sub-band separator. In order to plot the BER versus the Optical Signal to Noise Ratio (OSNR) curves, an Amplified Spontaneous Emission (ASE) source is inserted just before the receiver. An attenuator is inserted between the ASE source and the receiver to tune the OSNR level. A 600 MHz oscilloscope is used at the receiver side in order to monitor the signal envelope.

3.4.1 Settings of the transmitter and the receiver

The test-bed is configured to generate a periodic data composed of four slots at the four different wavelengths. For each of the four SOAGs, it represents a periodic sequence of 4.75 μs "on" followed by 15.25 μs "off" for the test using Dual Polarization (DP)-QPSK modulation format. The 4.75 μs is chosen to cover 4.65 μs OFDM burst signal (as shown in Figure 3-26) and 100 ns switching time. For the test using DP-16QAM modulation format, the control patterns are a periodic sequence of 4.8 μs "on" followed by 15.2 μs "off". The 4.8 μs is chosen to cover 4.7 μs OFDM burst signal and 100 ns switching time. Concerning the OFDM burst duration, a calculation example is shown in Figure 3-26. We inserted 3 OFDM frames in one burst. Each OFDM frame contains 1 synchronization symbol, 8 training symbols and 46 payload symbols. So there are 55 symbols in one OFDM frame. Note that there is one symbol delay between polarization X and Y, so the total OFDM duration has one symbol longer. In addition, in order to fast distinguish the OFDM frame from the successive OFDM, we insert one empty symbol before each OFDM frame, so the total longer of each OFDM frame is 57 symbols duration which is obtained by sum 55 and 1 symbol delay and 1 symbol empty. As each symbol duration is 27.2 ns, so the burst duration is 4.65 μs, which is obtained by (55+1+1)*3*27.2 ns. Furthermore, note that the OFDM frame durations for DP-QPPSK and DP-16QAM are different, so the "on" durations of SOAGs are correspondingly different. The reason for setting different OFDM frame duration will be given in section 3.4.3. As the OFDM burst signal duration varies a little in different tests, the exact OFDM burst signal duration will be presented at each test in the following sections and the switch "on" of SOAGs duration is set in order to cover the burst signal and the 100 ns switching time. The spectrum at the output of the tunable laser source is showed in Figure 3-12 in the previous paragraph. Four different wavelengths are configured: 192.682 THz, 192.694 THz, 192.706 THz, and 192.718 THz. Each peak represents a wavelength that will be used to carry an OFDM sub-band, while four sub-bands occupy a 50 GHz band with central frequency of 192.7 THz. At the receiver side, the wavelength of the LO is tuned to receive a sub-band. The wavelength is various in different study case.

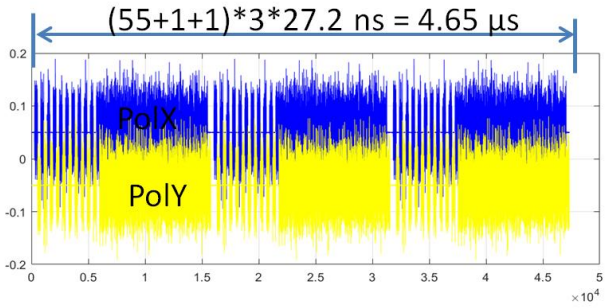

Figure 3-26: An example of dual-polarization signal duration generated by the transmitter.

3.4.2 Experimental validation using DP-QPSK format (in burst mode)

For the back to back evaluation, the first task is to evaluate the influence of the rising and falling edge of the tunable laser. So in one burst, three MB-OFDM frames are inserted. Figure 3-27 shows the three successive MB-OFDM frames signal at the output of the transmitter at the four wavelengths. Each OFDM frame is composed of 1 synchronization symbol, 8 training symbols and 46 payload symbols in order to ensure that the duration of three OFDM is about 4.7 µs. The OFDM burst duration is 4.65 µs. The others parameters, such as CP, base bandwidth and FFT size, are designed with the OFDM parameters shown in Table 3-1. So using DP-QPSK modulation format, the raw bit rate is 26.6 Gbps (integrating all overheads) in continuous operation.

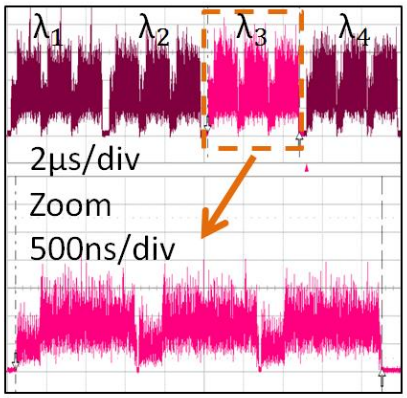

Figure 3-27: Signal at the output of the transmitter.

As presented in section 3.3.1, the performance of the Tx-2 with the Rx-2 is carried out at first. The BER versus OSNR curves measured when using SOAG1 are presented in Figure 3-28. The dotted line curve shows the performance of the CO-OFDM signal in continuous mode with ECL1; the solid line shows the BER in continuous mode with SOAG1 in “on” state between the ECL1 and the CMZM. We observe that the SOAG in “on” state does not bring any penalty at BER 10^{-5}. The 3 curves with circles, triangles and squares correspond respectively to the 1st, 2nd and 3rd OFDM frames emitted through SOAG1 at wavelength 1 (in one burst duration), according to the pattern represented in Figure 3-27. We can see that the three OFDM frames have the same performance, which indicates

that synchronization between data emission and wavelength switching is correct as no penalty arises on frames 1 and 3 compared to frame 2.

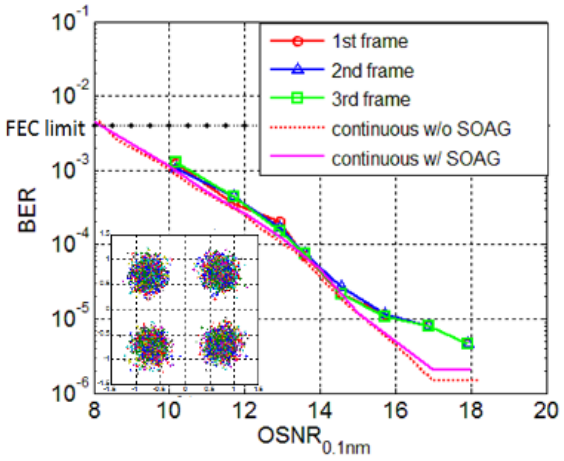

Figure 3-28: BER-OSNR (0.1nm) curves for three OFDM frames of SOAG1 with Tx-2 and Rx-2.

The BER versus OSNR curves in Figure 3-29 show the results for the 4 SOAGs switched periodically according to the pattern of Figure 3-27. As the coherent receiver detects only one OFDM sub-band, we tune it to measure the BER of SOAG1 to SOAG4 respectively. The BER measured for each wavelength is an average of the three OFDM frames over 30 runs. The performances of SOAGs (from 1 to 4) are respectively represented by circles, triangles, squares and diamonds. We observe no significant difference between the four curves showing that the performances are the same for the four wavelengths. As in Figure 3-28, we can also see in Figure 3-29 that there is no OSNR penalty at BER 10^{-4} and there is less than 1 dB penalty at BER 10^{-5} induced by the switching compared to the continuous mode with SOAG1.

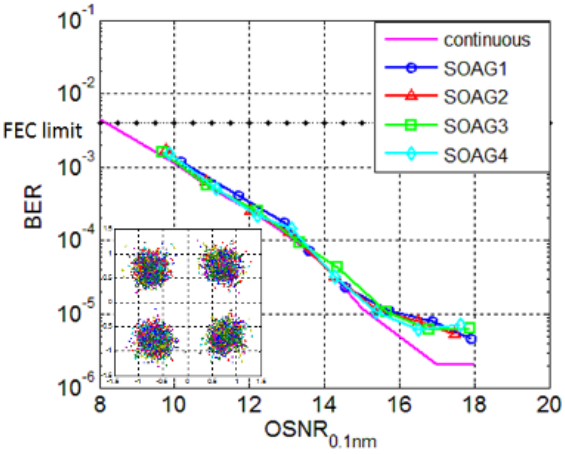

Figure 3-29: BER-OSNR (0.1nm) curves for four SOAGs.

After the validation of the Tx-2 / Rx-2 pair, the evaluation of the Tx-2 / Rx-1 pair and the Tx-1 / Rx-1 pair are carried out. As we know that the rising and falling edge do not have an influence on OFDM signal performances, we insert only one OFDM frame in a burst. One OFDM frame is composed of 1 synchronization symbol, 14 training symbols and 156 payload symbols. The OFDM

burst duration is 4.7 µs. The others parameters keep the same as the parameters we used in the evaluation of the Tx-2 / Rx-2 pair. The raw bit rate is still 26.6 Gbps (integrating all the overheads) in continuous operation using DP-QPSK modulation format.

The BER versus OSNR curves in Figure 3-30 show the results of SOAG1 when the 4 SOAGs are switched periodically according to the pattern of Figure 3-27. The coherent receiver is tuned to detect the OFDM sub-band SOAG1. The BER measured for each wavelength is an average over 40 runs. The performances in continuous mode of SOAG1 for the three pairs of transmitters and receivers, Tx-2/Rx-2, Tx-2/Rx-1, Tx-1/Rx-1, are respectively represented by red, blue, and green dotted curves. We observe that there is ~1 dB difference between the red and blue dotted line, which demonstrated that the Rx-1 has a better performance than Rx-2. Because that the Rx-2 introduces a signal distortion, which comes from the resonance between the integrated receiver chip and its evaluation board. We observe that there is ~2.5 dB difference between the green and blue dotted curves, which demonstrates that the Tx-1 has a better performance than Tx-2. Since, in the Tx-1, we use a better linear RF drivers and a better CMZM which has furthermore a better extinction ratio. For two transmitters and coherent receivers, Tx-1 works better than Tx-2, and Rx-1 works better than Rx-2. In order to simulate multi users in the TISA network, the two transmitters are necessary for the source nodes. As Tx-2 has a worse performance than Tx-1, it does not permit to perform DP-16QAM measurements. So we will use only Tx-1 to transmit DP-16QAM signals. But at the destination node side, we can place the same coherent receiver at different destination nodes while tuning the local oscillator in order to receive the OFDM burst data at different sub-bands. As a result, we will use only the Rx-1 to do the following experiment.

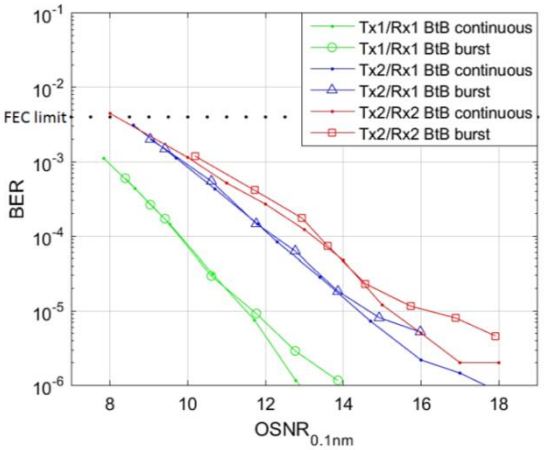

Figure 3-30: BER-OSNR (0.1nm) curves for SOAG1.

The performances in burst mode of SOAG1 for the three pairs of transmitters and receivers, Tx-2/Rx-2, Tx-2/Rx-1, Tx-1/Rx-1, are respectively represented by red curve with squares, blue curve with triangles and green curve with circles. For the performance of the pair of Tx-1/Rx-1, there is no penalty at BER 10^{-4} and about 0.3 dB penalty at BER 10^{-5} compared to the continuous mode configuration. The other 3 SOAGS have the similar performance.

3.4.3 Experimental validation using DP-16QAM format (in burst mode)

The BER versus OSNR curves measured for the pair of Tx-1/Rx-1 using DP-16QAM modulation format are represented in Figure 3-31. During the evaluation, the 4 SOAGs are switched periodically according to the pattern of Figure 3-27. Two study cases have been carried out. For the case 1, only one OFDM frame is inserted in one burst. Each OFDM frame is composed of 1 synchronization symbol, 14 training symbols and 156 payload symbols. The OFDM burst duration is 4.7 µs. For the case 2, two OFDM frames are inserted in one burst. Each OFDM frame is composed of 1 synchronization symbol, 14 training symbols and 70 payload symbols. The OFDM burst duration is 4.7 µs.

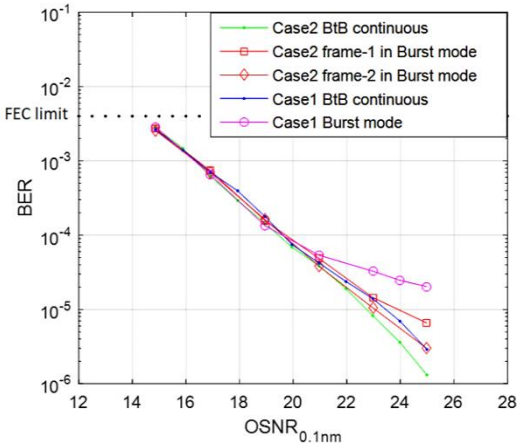

Figure 3-31: BER-OSNR (0.1nm) curves for SOAG1.

The blue dotted curve and green dotted curve represented respectively the performance of the study case 1 and 2 measured in continuous mode. For the study case 1, the performance in burst mode is represented by the pink curve with circles. For the study case 2, the performance of the first frame is represented by the red curve with squares and the performance of the second frame is shown by the red curve with diamonds. We observe that there is 0.5 dB difference between blue dotted curve and green dotted curve. Since there is always a light dis-synchronization of clock between AWG (DAC) and oscilloscope (ADC) [20], when the OFDM frame is short (shorter than 3 µs by our observation), this impairment is negligible. In order to avoid this impairment, two frames are inserted in a burst. As DP-16QAM is more sensible than DP-QPSK, there is a visible penalty only for DP-16QAM OFDM burst data. After the comparison between the performances in the continuous mode, we compare the performances in the burst mode. For the study case 2, we observe no significant difference (only 0.3 dB penalty at BER 10^{-5}) between the second frame and the continuous data. But the first frame has ~0.8 dB penalty at BER 10^{-5} compared to the continuous mode configuration. For the study case 1, we observe that there is about 1.5 dB penalty at BER 10^{-5}. Since DP-16QAM format is more sensitive to signal distortions than DP-QPSK, it is more challenging for the DSP. In TISA, due to the nature of burst traffic, the coherent receivers are regularly exposed to variable absence of signal (i.e. from several µs to several tens of µs), which introduces a low frequency (i.e. 1 MHz for 1 µs signal absence and 20 KHz for 50 µs signal absence) signal that is

related to the envelope of the burst signal. This introduced low frequency signal stress the optoelectronic components used in our coherent receiver, such as Trans-Impedance Amplifiers (TIA) which has 3-dB low cut-off frequency as ~50 KHz. Thus these optoelectronic components generate transients that impact the system performance. This phenomenon will be further studied and presented in section 5.4.

3.5 Conclusion

We have implemented two burst mode transmitters and two coherent receivers. The BER versus OSNR measurements have been carried out in order to evaluate the performance of the Tx / Rx pair. These works have been published in papers [21] [22]. The experiment results show that the Tx-1 / Rx-1 pair has the best performance thanks to the components used in the Tx-1 and the Rx-1, which shows that the components performances are the bottleneck of the performance of the Tx / Rx pair. For the transmitter, the fast tunable laser, the linear RF driver and the CMZM are the components that should be carefully selected. For the fast tunable laser, 3 criteria are most important: linewidth (less than 100 KHz), wavelength switching time (less than 100 ns) and tunable bandwidth (all the C-band); for the linear RF driver, 3 criteria should be met: gain bandwidth (from tens of KHz to 10 GHz), high gain flatness, linearity; for the CMZM, a high extinction ratio of the output power and low insert loss are required. At the receiver side, due to nature of the burst traffic, the variable signal absence at the input of the coherent receivers pose a challenge to the optoelectronic components inside the receiver, which are required to have a low cut-off frequency (less than 10 KHz) in order to avoid the transients state. Since the Rx-1 has a better performance than Rx-2, and we can use Rx-1 at different destination nodes to receive the bursts at different sub-bands by tuning the local oscillator, we use only Rx-1 in the following tests. Tx-2 can only be used to generate the OFDM bursts in DP-QPSK modulation format while the Tx-1 can generate the OFDM bursts in both DP-QPSK and DP-16QAM modulation formats.

References

[1] C. Clivati, A. Mura, D. Calonico, F. Levi, G. A. Costanzo, C. E. Calosso and A. Godone "Planar-waveguide external cavity laser stabilization for an optical link with 10^{-19} frequency stability," in *IEEE Transactions on Ultrasonics, Ferroelectrics, and Frequency Control*, vol. 58, no. 12, pp. 2582-2587, December 2011.

[2] B.Bobbs and A. Montalvo "Tunable DFB semiconductor lasers with active feedback for frequency stability", *Proceedings of SPIE - The International Society for Optical Engineering*, 2008.

[3] P. Zorabedian, "Tunable External Cavity Semiconductor Lasers." Tunable Lasers Handbood, Ed. F. J. Duarte. New York, Academic, 1995. Chapter 8.

[4] F.S. Ujager; S.M.H. Zaidi; U. Younis, "A review of semiconductor lasers for optical communications," *High-Capacity Optical Networks and Enabling Technologies (HONET)*, 2010 , vol., no., pp.107,111, 19-21 Dec. 2010

[5] Thorlabs, "ECL Tutorial", [Available online], https://www.thorlabs.com/tutorials.cfm?tabID=f7dfa931-5afa-441b-8176-292d8735b143

[6] Tunable External Cavity Laser (ECL) technology of Pure Photonics [Available online] http://www.pure-photonics.com/technology/

[7] A. Bhardwaj, J. Gripp, J. E. Simsarian and M. Zirngibl, "Demonstration of stable wavelength switching on a fast tunable laser transmitter," *in IEEE Photonics Technology Letters*, vol. 15, no. 7, pp. 1014-1016, July 2003.

[8] J.-O. Wesström, G. Sarlet; S. Hammerfeldt; L. Lundqvist; P. Szabo; P. -J. Rigole , "State-of-the-art performance of widely tunable modulated grating Y-branch lasers" *in Proceedings of Optical Fiber Communication Conference and Exhibition (OFC)*, 2004, paper TuE2.

[9] T. Aoki , S. Sekiguchi; T. Simoyama; S. Tanaka; M. Nishizawa; N. Hatori; Y. Sobu; A. Sugama; T. Akiyama; A. Hayakawa; H. Muranaka; T. Mori; Y. Chen; S. -H. Jeong; Y. Tanaka and K. Morito, "Low-Crosstalk Simultaneous 16-Channel × 25 Gb/s Operation of High-Density Silicon Photonics Optical Transceiver," in *Journal of Lightwave Technology*, vol. 36, no. 5, pp. 1262-1267, March1, 1 2018.

[10] Thorlabs SOA data sheet, [Available Online], https://www.thorlabs.de/drawings/e7902e53e1f4a643-E34DEF8B-A57A-4345-EA978F6B031EBFD7/BOA1004PXS-SpecSheet.pdf

[11] K. Kikuchi, "Characterization of semiconductor-laser phase noise and estimation of bit-error rate performance with low-speed offline digital coherent receivers," *Optics Express* 20, 5291-5302 (2012)

[12] J. Karaki, "100 Gbps Coherent MB-OFDM for Long-Haul Optical Transmission", thesis manuscript, Télécom ParisTech, 2013

[13] W. Shieh and I. Djordjevic, "OFDM for optical communications". Elsevier, 2010

[14] SHF, "Driver Datasheet", https://www.shf.de/wp-content/uploads/datasheets/datasheet_shf_806e.pdf

[15] T.M. Schmidl and D.C. Cox, “Robust frequency and timing synchronization for OFDM”. *Communications, IEEE Transactions on*, 1997. **45**(12): p. 1613-1621.

[16] H. Minn, V.K. Bhargava, and K. Letaief, “A robust timing and frequency synchronization for OFDM systems”. *Wireless Communications, IEEE Transactions on*, 2003. **2**(4): p. 822-839.

[17] S.L. Jansen, "Long-haul transmission of 16× 52.5 Gbits/s polarization-division-multiplexed OFDM enabled by MIMO processing," *Journal of Optical Networking*, **7**, 173-182 (2008).

[18] S. Ten and M. Edwards, "An introduction to the fundamentals of PMD in fibers," *White paper*, no. Corning Incorporated, 2006

[19] M. Song, "WDM transmission of 400 Gbps and beyond using multi-band OFDM & Nyquist-WDM", thesis manuscript, Télecom ParisTech, 2016

[20] B. Ai, Z. Yang, C. Pan, J. Ge, Y. Wang and Z. Lu, "On the synchronization techniques for wireless OFDM systems," in *IEEE Transactions on Broadcasting*, vol. 52, no. 2, pp. 236-244, 2006.

[21] B. Han; P. Gavignet; E. Pincemin; T. Guillossou; M. Cresseaux; D. Le Brouster; B. Haentjens; Y. Jaouen, "Low phase noise CO-MB-OFDM optical burst transmitter for time and spectral optical aggregation," *2017 Optical Fiber Communications Conference and Exhibition (OFC)*, Los Angeles, CA, 2017, pp. 1-3

[22] B. Han, P. Gavignet and E. Pincemin, "Low phase noise optical burst transmitter for TIme and Spectral optical Aggregation solution," *2017 19th International Conference on Transparent Optical Networks (ICTON)*, Girona, 2017, pp. 1-6.

CHAPTER 4

Control plane for TISA solution

As discussed before, TISA has a control plane and a data plane. The data plane realizes physically the data transmission from one node to another. The control plane is on top of the data plane. It performs all the processes related to network resource allocation, devices configuration and network synchronization. The control plane performs the lossless routing of the bursts through the network. It calculates and distributes the grants which contain the sending time and the (sub-band) wavelength for each burst. As all the propagation times of the bursts (occupying a given wavelength from a source node to a destination node) is predictable, the control of the bursts sending times is enough to guarantee the avoidance of burst collision at the destination side and through the network. In order to follow the slow evolution of the propagation times due to temperature, a ranging procedure, as in PON networks, has to be implemented. In order to control correctly and precisely the bursts sending times at all source nodes, the control of the network shall be implemented in real-time. As TISA is a synchronous network, the synchronization of the whole network is also an essential function of the control plane. In this thesis, we have chosen to share a common clock between the various source nodes to perform the network synchronization. Compared to the TWIN solution [1], TISA has a new time constraint at the MB-OFDM combiner: the bursts coming from different sources should be aligned at the combiner in order to be regrouped as a multi-band burst occupying 50 GHz bandwidth considering the grants calculation complexity and the reusing of the SLPSN architecture. The multi-band burst is similar to the super-channel but it is in the burst mode. This new requirement is taken into account when calculating the grants. In this chapter, the implementation of the control plane will be presented in detail.

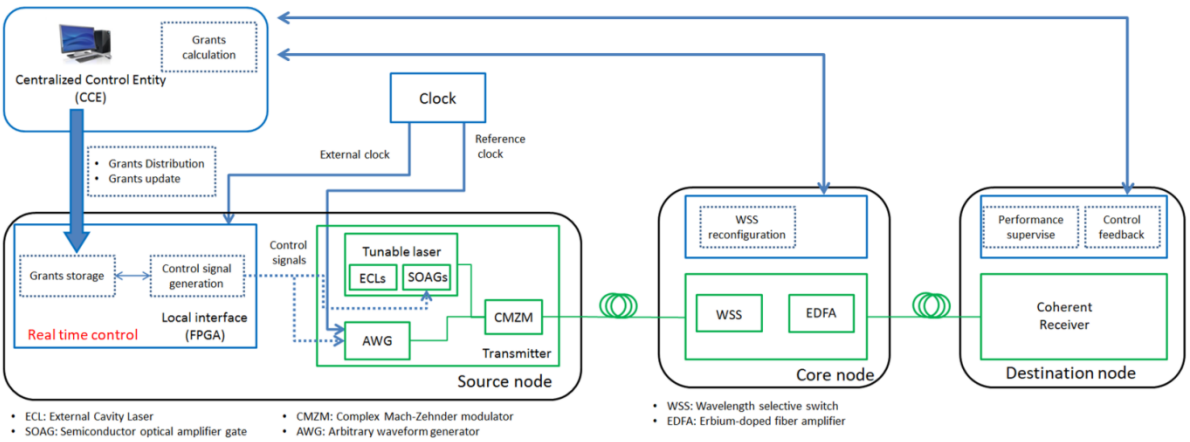

Figure 4-1: Control plane architecture (blue parts) for TISA network (only a source node, a core node and a destination node).

4.1 Control plane architecture

The main part of the control plane is the Centralized Control Entity (CCE). The CCE is in charge of the grants calculation. The grants are a kind of authorization for source nodes to send

bursts at a given time and at a specific wavelength (the one associated to the destination) for each burst. After the calculation of the grants, the CCE distributes the grants to all the source nodes. At the source node side, a local interface, which is realized by a FPGA in our experimental test-bed (see Figure 4-1), is implemented to receive and store the grants and then convert the grants into control signals which control the transmitters and bursts emission in a real-time way. In general, the control plane should communicate with both source nodes and destination nodes in order to control and know the working state of the network. As we discussed in chapter 2, the control of the sending time and the sub-band wavelength for each burst at transmitter side is enough to guarantee the lossless routing in the TISA network. So only the control of transmitters is realized in our test-bed and is realized in a real-time way. However, in a real network, the control plane would be also in charge of the configuration and the monitoring of the various elements of the network not only inside the edge nodes but also inside the core nodes (as shown in Figure 4-1). For example, inside the core node, it could be possible to reconfigure the wavelength selection strategy through the filters and WSSs and it is possible to supervise the evolution of the performances of the bursts. Inside the edge, it is possible for the control plane to reconfigure the modulation format used at the bursts. Moreover, the control plane is in charge of supervising the performance of the received bursts at the receiver side, such as OSNR, BER. These functions have been implemented in our test-bed, but not in a real-time way.

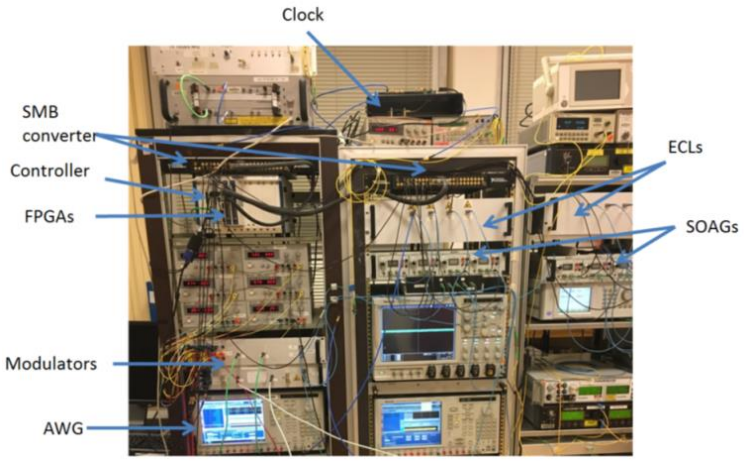

Figure 4-2: Experimental test-bed.

As discussed in chapter 2, a real-time device should be implemented in the source node to perform real-time controlling, FPGA is selected thank to its programmable, preferment, and real-time characteristics. Figure 4-2 shows the control plane part of our experimental test-bed. In this experimental test-bed, we have chosen National Instrument (NI) devices to build the control plane: FPGA 7975R for the local interface and the NI-PXIe8840 real-time controller for the CCE. The controller is used to code the FPGA program. The FPGA is guaranteed to work in real-time using single cycle control loops technology [2]. The controller works in the Windows environment, which is not a real-time operating system. In order to perform real-time control, a file containing several

grants (for example 100) is sent to and then is saved at the FPGA at first. Afterwards, FPGA reads the grants from the first to the last and repeats this process in a loop until a new grants file arrives. When the FPGA reads grants, the transformation from the grants to electrical control signals is realized in real-time in the FPGAs. In Figure 4-2, there are two transmitters that have been implemented as described in chapter 3. In the transmitter, a fast tunable laser is implemented using ECLs and SOAGs. The control signals are used to control the SOAGs in order to switch “on” and “off” the light of the various wavelengths. The burst emission control is in real-time and is guaranteed by FPGAs.

As FPGA requires robust coding and configuration tools to ensure the interconnection between the different elements, the corresponding LabVIEW FPGA module has been chosen. The LabVIEW FPGA module can reduce program developing time by providing a powerful and graphical programming environment, which simplifies the coding difficulty. The other peripheral devices are also chosen from NI, including FPGA digital I/O adapter NI6583, the SMB 2163 terminal block and the chassis NI-PXIe1082 where the real-time controller and FPGAs are installed in. The I/O adapter and terminal block are used to convert the FPGA output signal from the FPGA pins format to single ended SMB format. And the FPGA output signals are amplified to standard 3.3 V at the same time.

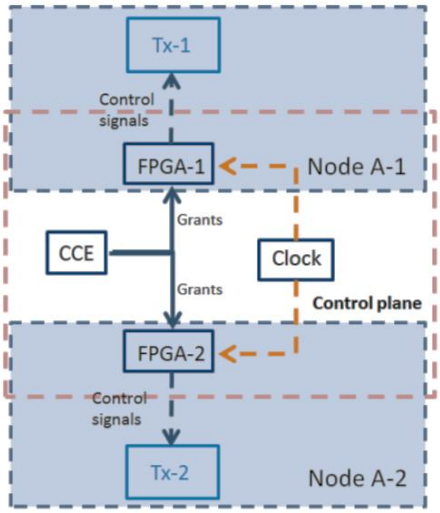

Figure 4-3: Experimental set-up of control plane for two source nodes in real-time control.

In this thesis, as we have built two transmitters, a control plane for two source nodes is realized. The experimental set-up of the control plane is represented in Figure 4-3. The gray dotted rectangles represent the nodes A-1 and A-2. The transmitters Tx-1 and Tx-2 are implemented respectively in the nodes A-1 and A-2. The dark claret dotted rectangle represents the control plane. Two FPGAs are implemented as local interfaces in each source node: FPGA-1 and FPGA-2 are respectively in source node A-1 and A-2. In order to synchronize these two FPGAs, a common clock is built and shared between these two FPGAs. The implementation of the clock is described in section 4.3.2.

4.2 Grants calculation and distribution

The calculation of the grants can be regularly refreshed in order to follow the evolution of the resource demands of each source. However, the study [3] concerns the TWIN solution has shown that the performance of the network is not always improved by a change of grants according to the traffic evolution. In paper [4] which concerns the TWIN solution, the control plane is organized by repetitive short period cycles called control cycles. The duration of a control cycle is common to all nodes and is in the order of several milliseconds based on the size of the network. The duration of a control cycle should be equal to, or larger than, the time which is necessary to exchange control information between the edge nodes and the CCE; it is called RTT for Round Trip Time. Each control cycle is composed of several (i.e. 20 in our test-bed) data cycles containing a number of slots (i.e. 100 in our test-bed). This organization of several data cycles inside a control cycle simplifies the grant calculation: indeed the pattern of grants is calculated on 100 slots and is repeated 20 times which is easier than calculating a pattern with 2000 slots.

The grants are calculated according to the traffic variation observed during one or several control cycles. During all the data cycles of the control cycles, the source nodes use the same resources allocation configuration and send the bursts according to the received grants. Therefore, the time scale of resource allocation is different between the control plane (i.e. the control cycle duration) and the data plane (i.e. the time slot duration). This feature can have a dynamic resource allocation at the data plane while keep a relative slow configuration mechanism at the control plane since it is difficult and not necessary to build a fast configurable control plane [3].

In our experimental test-bed, as our work is to build a PoC to demonstrate experimentally the feasibility of the TISA concept, the real-time grant calculation is not necessary. The grants are preprogrammed at the controller and then are distributed to FPGAs. Each grants file contains the grants for a data cycle. In the FPGA, the program will repeat this grants for 20 times during a control cycle (20 data cycles in a control cycle). All these processes are performed in LabVIEW using LabVIEW FPGA module.

4.2.1 Grants calculation and generation

The grants are used to control the burst emission and to guarantee the lossless routing in the network. The grants should contains all the control information: the sub-bands used for bursts, the time slot duration, the emission time of bursts, the modulation format of data, the structure of the OFDM frame in the bursts etc. As the bursts emission control is realized in real-time, all related hardware is implemented to support the control process and different control information has correspondingly different properties. Here we use three properties to describe the control information: reconfigurable, static and off-line. In our test-bed, if the control information can be updated when the control plane is running, this control information is reconfigurable. For the not reconfigurable control information, if the information can be defined by the controller (obviously

before the control plane runs), this control information is static. If the control information cannot be defined by the controller, but we can modify it manually in some ways, this control information is offline. The grants should contain all the control information. But as the grants are reconfigurable in order to allocate dynamically network resources, only the reconfigurable control information is contained in the grants in our test-bed. Static and off-line control information can be upgraded to be reconfigurable control information with further improvement on both hardware and control program. Anyway, in our test-bed, all the parameters for the burst emission control are modifiable. The control information and its property are listed in the table 4-1. In this section, we will present how we generate these 5 kinds of control information.

Table 4-1: Control information and the property

Control information	Property	In grants or not
Sub-bands of bursts	reconfigurable	Yes
Bursts emission time	reconfigurable	Yes
Duration of time slot	static	No
Modulation format of data	off-line	No
OFDM frame structure in bursts	off-line	No

The duration of time slot is defined at the controller. As TISA is a time slotted solution, we only need to define once for all time slots in the controller during a test. So this parameter is described in a static way that we cannot update this parameter when the control plane is running. In the experiment, one time slot is set to 5 μs. In order to perform the tests with different time slot durations for the evaluation of the flexibility of the TISA solution in the time domain, the time slot duration should be modified before a run of test. The evaluation with different time slot durations will be described in detail in chapter 5.

The control information about the sub-bands is used to control the sub-band of each burst according to the destination of the burst. In order to generate the control information about the sub-bands, there are three steps: configure of lasers wavelengths, configure the wavelength of transmitters at the control plane, and generate the grants file containing the name of each sub-band. At first, we should configure the wavelengths of each transmitter. We have built two transmitters, and each transmitter is able to generate 4 different wavelengths. Each wavelength corresponds to a sub-band. We name each wavelength at the controller with a unique number: the number “1” to “8” for the wavelengths λ_1 to λ_8. Then, we can configure the wavelengths of the transmitters at the controller through a program and the program interface is shown in Figure 4-4. The parameters shown in Figure 4-4 are an example of wavelengths configuration. The lasers 1 to 4 are used in the

Tx-1 which is called master 1 to 4 and the lasers 5 to 8 are used in the Tx-2 which is called slave 1 to 4. The figures in the input windows indicate the configured wavelengths. So the Tx-1 is configured to generate λ_3, λ_4, λ_5 and λ_6 while the Tx-2 is configured to generate λ_1, λ_6, λ_7 and λ_8. The number of the Digital Input/Output (DIO) shown in the interface of each laser is the number of the SMB converter output ports used to send the control signal for the optical gate associated to the corresponding laser. The use of these DIOs will be presented in section 4.3.1. After the configuration of the wavelengths generated by each transmitter, in the grants, we will only indicate the number of the wavelength that we want to generate for each transmitter at a time slot. We also reserve the number "0" in order to generate a time slot without any optical signal. As a wavelength number is used for one time slot, and there are 100 time slots in one data cycle, so a grants file contains 100 wavelength numbers.

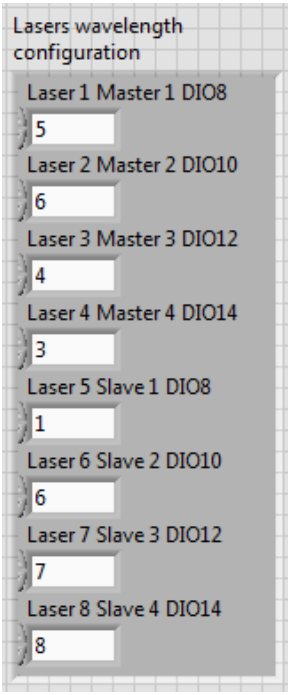

Figure 4-4: Interface for the wavelength configuration.

For the control information about the bursts sending time, the order of the 100 wavelength numbers defines the order of the wavelength that the transmitter will generate, which means that the burst emission time of each burst is also defined by the grants. The burst sending time used in the test-bed is not an absolute time indicating the hour, minute, second, microsecond but a reference time which indicates the sending order. The reference time is designed for the control of bursts emission time at each transmitter, but the synchronization between different transmitters is necessary in order to avoid the time shift between different transmitters. As we discussed in chapter 2, the control plane realizes a synchronization of the source nodes by sharing a common clock in our test-bed. So, two transmitters are synchronized and use a common clock. As we can only input one wavelength number at each instant, the transmitter can only generate one sub-band at each instant in this scheme.

In the test-bed, the fiber lengths from the transmitters to the receivers (and from the transmitters to the MB-combiner) are carefully measured, so that the propagation time from the transmitters to receivers are known. In a full-scale real network, the distance will be calculated using the time of flight method [14] by measuring the propagation time from the source node to the combiner with a control plane interface at the combiner. When we preprogram the grants to define the burst emission time and the sub-band wavelength for each burst, the propagation time of each burst from the transmitter to the receiver is taken into account, in order to guarantee the absence of collision in the network.

In this test-bed the grants do not define the OFDM frames that will be inserted in each burst. As presented in chapter 3, the OFDM frames are generated off-line. Then the OFDM frames are downloaded to the AWGs where the digital signals are transformed into electrical analog signals, which is not a real-time process. As a result, according to the preprogrammed grants, the OFDM frames are pre-generated and then are downloaded to the AWG. Therefore, the grants used in our test-bed do not need to contain the OFDM design parameters. In a real network, it would be different as the bursts would be built once the data arrival (so in real-time) and could follow some recommendations included in the grants like the burst duration (using several time slots for example), the modulation format or other parameters.

4.2.2 Grants distribution

The grants are distributed from the CCE (controller) to the local interface (FPGA) at each node. As discussed previously, the CCE works in Windows Operating System, which is not a real-time operating system. But the FPGA works in real-time, so the communication between them cannot be realized in a real-time process. The communication between the FPGA and the controller is implemented based on Direct Memory Access (DMA) First In First Out (FIFO) queues technology (see in Figure 4-5). The DMA communication consists of two DMA FIFOs: one FIFO on the controller (called FIFO-C) and another FIFO on the FPGA (called FIFO-F). When the CCE distributes the grants, the grants are written in the FIFO-C at first, and then are assembled together as a bigger data. Then the data will be transferred to the FIFO-F in FPGA. In the FIFO-F, the data packet will be separated into several discrete data as the original grants. The FPGA program will read the grants from the FIFO-F one by one in the original order. The signal processing of FIFO at FPGA and controller is isolated from each other in DMA communication technology, so FPGA and controller can read and write the data with its own rate, and there is no interference between them. Furthermore, since the data is assembled together at the FIFO-C and then transferred to FPGA, FPGA receives a data packet in place of several. DMA communication can reduce the resources consumption in the FPGA when transferring arrays of data. In addition, the data transmission is automatically synchronized between the FPGAs and the controller.

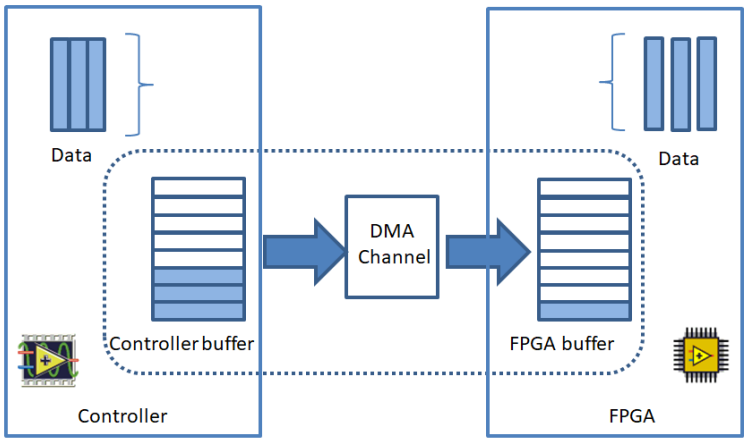

Figure 4-5: DMA communication from controller to FPGA.

4.2.3 Grants storage and update

After the distribution of the grants, each FPGA receives the corresponding grants. Since we do not need to modify too often the resources allocation, the grants are not updated every control cycle. For the burst emission control, we need to read the grants to generate the control signal every time slot which is much shorter than the control cycle and data cycle (20 data cycles in a control cycle and 100 time slots in a data cycle). So, in this experiment, the received grants are stored in a block memory at FPGA. The FPGA program can re-read the grants whenever it wants.

In our test-bed, the grants can be modified during a run of test. For the grants updating, the CCE will distribute new grants to each source node to update the allocation configuration. As discussed previous, the grants will be transferred by DMA FIFO and then are stored in a block memory in the FPGA. However, a block memory offers only one interface to the FPGA program to read or write data. When the FPGA program read the data in the memory, we cannot write new data in. So a second block memory is used to store the new grants. When a control cycle is finished, the FPGA will turn to read the grants in the second memory, and the first memory block is used to store next updating grants. There three states for the memory: when the FPGA program reads the grants from a memory, the memory is on working state; when the FPGA program uses the memory to store or to wait for the new grants, the memory is on free state; when the memory is stored the new grants but it is waiting the current control cycle finished, the memory is on ready state. The program diagram is shown in Figure 4-6. The FPGA program is divided into two parts that keep running. The upper part in Figure 4-6 is used to receive the new grants from the CCE. The lower part in Figure 4-6 is used to generate the control signals according to the grants. The CCE is in charge of sending the order to start or stop this FPGA program.

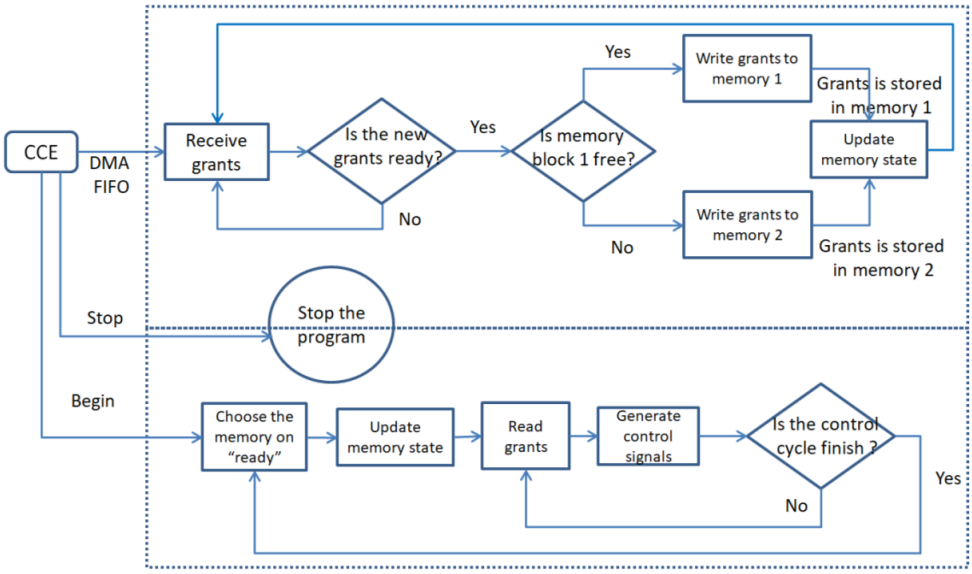

Figure 4-6: Program diagram for grants updating

4.3 Burst generation according to Grants

In the FPGA, the program will read the grants and generate the corresponding control signals. The control signals can be divided into two parts: the control signals to control the sub-bands of each burst and the control signals to control the electrical burst data emission. The control signals used to control the sub-bands are sent to the SOAGs of the fast tunable laser in order to switch "on" and "off" the continuous light, in order to generate an optical signal at a wavelength corresponding to the one of the destination with the duration corresponding to a burst. At the same time, FPGA also generates a control signal to AWG in order to active the electric burst data emission. The burst data should be put in the correct sub-band, so these two types of signals and related hardware should be synchronized. In order to realize the synchronization, a common clock is implemented. In this section, the control signals for sub-bands are presented at first. Then the implementation of clock is presented. At last, we will talk about the generation of control signal for electric burst data emission and the synchronization between the sub-bands and burst data.

4.3.1 SOAG control signal

As already detailed in paragraph 3.1.2, the fast tunable laser is composed of 4 ECLs and 4 SOAGs. The ECLs emit a continuous signal at a single wavelength and the SOAGs are in charge of switching "on" and "off" the continuous light. In order to control the SOAGs, a specific SOAG driver has been built in order to switch the continuous light "on" and "off". The "off" state is set by a 0 V signal, and the "on" state by a 3.3 V signal: if we want to switch "on" a SOAG, the FPGA will generate a 3.3 V control signal, on the contrary, the FPGA do not generate any signal to switch "off" a SOAG. In our test-bed, the output SMB adapter of the FPGA has 32 outputs. An output is enough to control a SOAG. So, 4 outputs of each FPGA are used in total to control the SOAGs. The numbers of the output pins used for each SOAG are indicated in the interface (see Figure 4-4). The two FPGAs (one FPGA per

transmitter) use DIO8, DIO10, DIO12 and DIO14 to control the 4 SOAGs. When the program read the wavelength number of a wavelength in the grant, it will generate the 3.3 V control signal at the corresponding output port (DIO) during a correct duration (the burst duration + the SOAG switching time). For example, we can generate 3.3 V at DIO8 of master FPGA in order to switch "on" the λ_5 when we read the number "5" on the grant.

4.3.2 External clock realization

TISA is a synchronous network solution, so the synchronization of the whole network is also an essential function of the control plane. In this thesis, we have chosen to share a common clock source between the two source nodes as discussed in chapter 2. The clock is implemented by using a common oscillator and a clock multiplier. The architecture of the common clock is presented in Figure 4-7. The common oscillator is a Vectron VT-804-EAW-5080-40M oscillator [5]. The VT-804 is a Temperature Compensated Crystal Oscillator (TCXO) which can offer a quartz stabilized 40 MHz oscillation with $\pm$ 50 ppb frequency stability. The output signal is a 3.3 V single ended Complementary Metal Oxide Semiconductor (CMOS) signal with 3.3 V voltage supply. The clock multiplier is a Silicon Labs Si5347A [6] which can offer 8 outputs combining fourth-generation DSPLL and MultiSynth [6] technologies to enable any-frequency clock generation and jitter attenuation. So it can be applied in the applications requiring the highest level of jitter performance which is very interesting for the TISA network application. The frequency output range is from 100 Hz to 720 MHz. Here we choose 100 MHz output frequency for both FPGAs and AWGs.

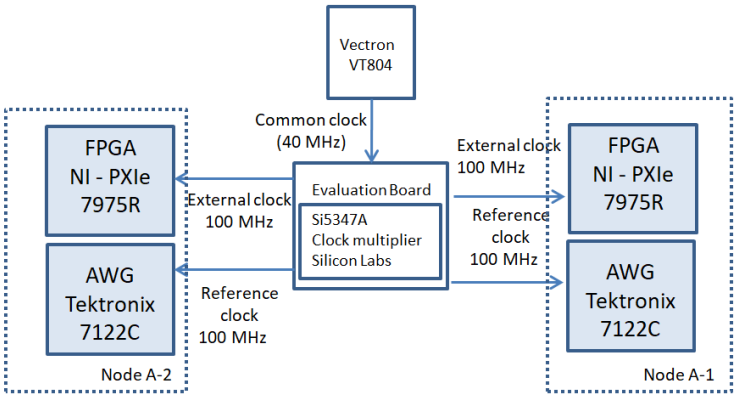

Figure 4-7: Common clock architecture.

The FPGAs use this 100 MHz external input clock as the working clock for their internal operations. The 100 MHz frequency allows a good trade-off between the FPGA operations duration and the program time precision requirements. Indeed, in order to guarantee the FPGA working in real-time, the Single Cycle Timed Loop (SCTL) [7] technology is used in FPGA program. Using SCTL technology, all the designed program operations (shown in Figure 4-6) in a loop should be finished in single loop duration. The signal loop duration is related to the clock used in FPGA program: loop duration equals to the inverse of the clock frequency. As the FPGA uses an external clock, the frequency of the external clock should be enough small in order to have a long loop duration for all

FPGA program operations. On the other hand, small loop duration can improve the program control precision, since we can modify the output signal every loop. In order to gain the time precision of the program, we must reduce the operation time of a loop. There are some methods to optimize the program operations time such as pipeline [8] and parallelizing operations [9], data type optimization. With using these technologies, the program operations can be finished in 10 ns. Therefore, the external clock is set to 100 MHz and the time precision is ±5 ns.

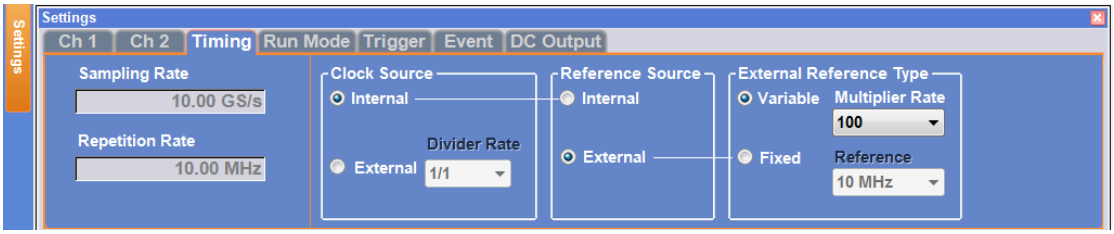

Figure 4-8: AWG timing setting interface.

Concerning the AWG, the 100 MHz clock is only used as a reference clock, which means that the AWG works with its own internal clock but from time to time, it compares the internal clock with the reference clock in order to synchronize the internal clock with the reference clock. In the AWG, the sampling rate is the internal clock frequency that we use. The input reference clock can take various frequency values, and then we need to modify the parameter "variable multiplier rate" (as shown in Figure 4-8) to indicate the ratio between the required sampling rate and the reference clock following the formula:

*Sampling rate = Variable multiplier rate * Reference clock frequency*

But as the multiplier is realized in hardware using Phase Locked Loop (PLL), the basic multiplier factor is 2. So it is better to choose a multiplier rate that avoids having the odd factors [10][11] in order to avoid accumulated jitter and stability problems. The ratio between the final required frequency (sampling rate in AWG) and the original frequency (the frequency of the oscillator in the common clock) is 250 (10 GHz/40 MHz) which has the multiplier factors 5, 5, 5 and 2. So we cannot avoid the odd factor, but we can choose a frequency of the reference clock without introducing a new odd factor. As a result, the reference clock frequency is chosen equal to 100 MHz, while the ratio between 40 MHz and the reference clock is 5/2 (note that the 5 is the multiplier factor and the 2 is the divider factor), and the variable multiplier rate is 100 in order to get 10 GHz sampling rate.

4.3.3 Synchronization

The synchronization of the whole test-bed is classified into two tasks: the synchronization of the working rhythm of the devices that have a clock inside, such as FPGAs and AWGs at the transmitter side and the oscilloscope at the receiver side; the synchronization of the SOAGs and AWGs in order to modulate the correct optical signal with the correct OFDM data.

Concerning the synchronization of the working rhythm, the oscilloscope at the receiver side do not need to be synchronized, as we use off-line technology to perform the OFDM DSP, the synchronization error can be mitigated in the electric domain. The synchronization of the working rhythm of FPGAs and AWGs is guaranteed by sharing a common clock that is described in paragraph 4.3.2. As AWGs and FPGAs, use or refer to a unique oscillator that is in the clock multiplier, their working rhythms are synchronized.

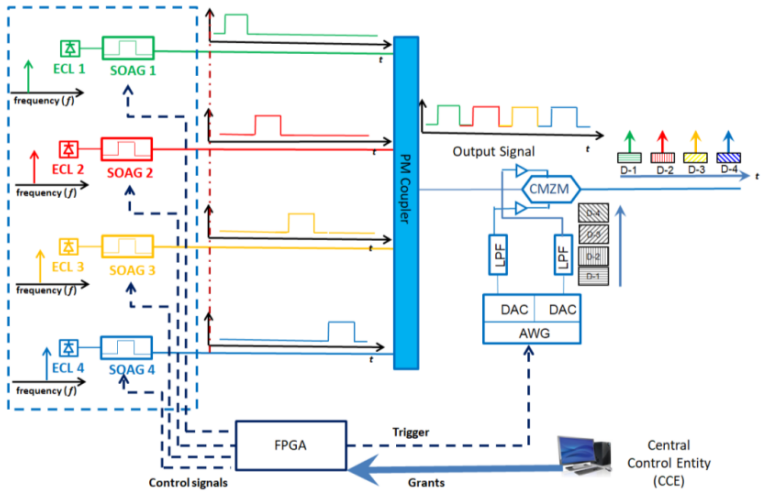

Figure 4-9: Synchronization mechanism between SOAGs and AWG.

Figure4-9 shows the synchronization mechanism of the SOAGs and the AWG in order to modulate the correct optical signal with the correct OFDM data. The 4 SOAGs, 4 ECLs and the PM coupler are used to realize the fast tunable laser that is detailed in paragraph 3.1.2. The fast tunable laser, CMZM, AWG and the RF drivers build up the transmitter. The FPGA is the local interface of control plane at the source node. When the FPGAs generate the control signals for the SOAGs, they generate also a trigger to activate the OFDM data emission. The trigger is either generated earlier or later than the control signals, in order to take into account all the response and signal propagation delays. Two parameters: the delay of SOAG control signals and the delay of AWG trigger,are used to adjust the control signal precise generation time for the SOAGs and the trigger for the AWGs. Figure 4-10 shows an example of the relation between the delay of SOAG control signals and the delay of AWG trigger. In the example, the burst signal (the power of training sequences is lower than the payload, since the training sequence follows the Jansen structure [13]) is not totally inside the optical carrier, so we can reduce the delay of AWG trigger or increase the delay of SOAG control signals to adjust the synchronization of burst signal and optical carrier. In the FPGA program, the delay of SOAG control signals is represented by “DIO Nb of delay tickets” (in red circles in Figure 4-11) and the delay of AWG trigger is represented by “AWG Nb of delay tickets” (in blue circle in Figure 4-11). The “ticket” is the time unity that we can control through the FPGA program. As we use 100 MHz external clock in FPGA, a ticket equals to 10 ns and the best precision that can be obtained between the SOAGs and the AWGs synchronization is $\pm$5 ns.

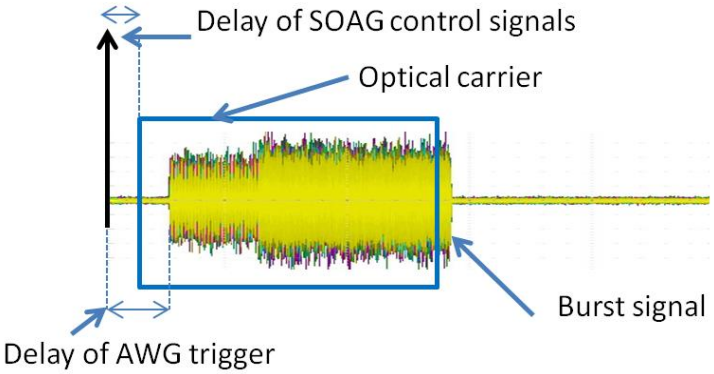

Figure 4-10: The relation between signal and optical carrier

In the FPGA program, besides the two delays parameters, there are other parameters to control the burst emission with a high time precision. The program interface is shown in Figure 4-11. The parameter “DIO Nb of time slot tickets” is used to define the duration of time slot: as a ticket equals to 10 ns, the time slot is set to 5 µs. The parameter “DIO Nb of time slot tickets” is used to define the opening duration of SOAG: 488 tickets equals to 4.88 µs in order to cover ~4.7 µs burst signal and 0.1 µs wavelength switching time. And concerning the AWG parameter, the parameter “AWG Nb enable tickets” is used to define the duration of AWG trigger which should be longer than 30 ns [12]. The parameter “AWG Nb time slot tickets” is used to define the time interval to repeat the AWG trigger, this parameter is used inside of the FPGA program.

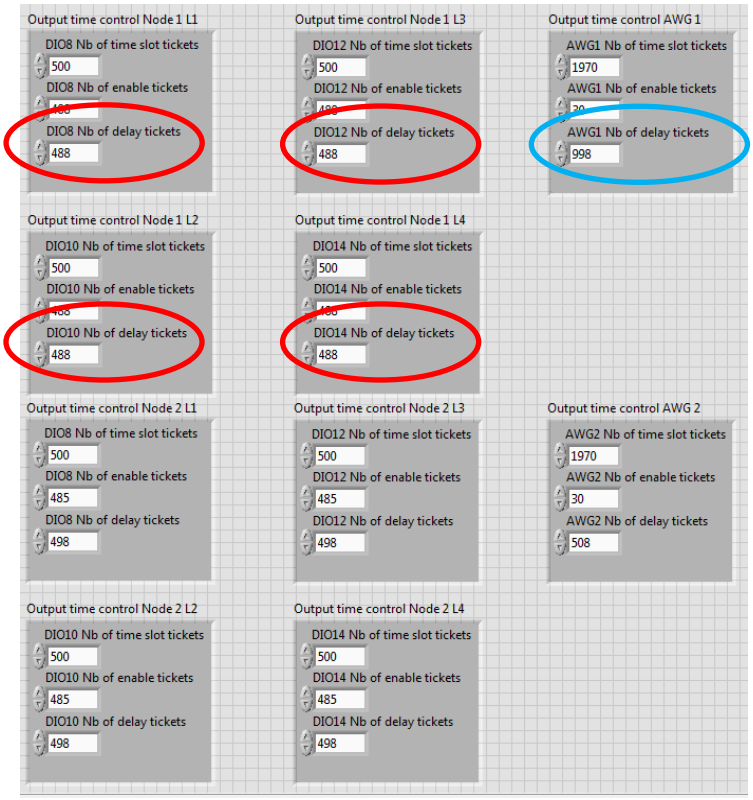

Figure 4-11: Program interface for the wavelength emission control.

4.4 Bursts alignment at the Multi-Band OFDM combiners

Compared to the TWIN solution, TISA has a new constraint: the bursts coming from different sources should be aligned at the MB-OFDM combiner in order to be regrouped as a multi-band burst occupying a 50 GHz bandwidth in order to reduce the grants calculation complexity as discussed in chapter 2. In order to align the bursts coming from different sources, we can also use the "delay ticket" parameter presented in Figure 4-11 to adjust the burst generation time of each transmitter. In this section, the burst alignment experiment will be presented in detail.

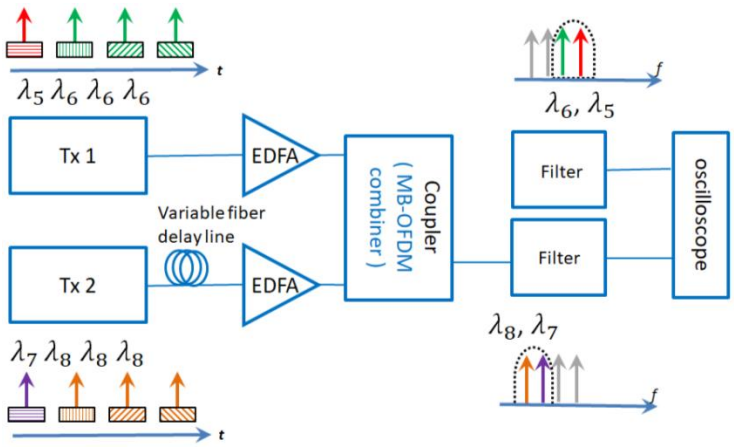

Figure 4-12: Experimental set-up for burst alignment.

Figure 4-12 shows the experimental set-up that is used to make this alignment. Two transmitters Tx-1 and Tx-2 are implemented representing two edge nodes. A fiber delay line is inserted between Tx-2 and the MB-OFDM combiner (realized with a coupler) in order to configure different transmission distances between the MB-OFDM combiner and Tx-2. In this experiment, various distance difference configurations between the two transmitters and the combiner (400 m, 1 Km, 2 Km and 10 Km) have been tested. In this experiment, we have configured the 4 different wavelengths at 192.715 THz (λ_5), 192.705 THz (λ_6), 192.695 THz (λ_7), 192.685 THz (λ_8), which are in the same 50 GHz channel. The transmitter Tx-1 is configured to generate periodically and successively bursts at λ_5, λ_6, λ_6, λ_6 and Tx-2 generates periodically and successively bursts at λ_7, λ_8, λ_8, λ_8 (as shown in Figure 4-12). The order of wavelengths generation is also defined as shown in Figure 4-12. So the bursts generated by the two transmitters will be synchronized as indicated: burst at λ_5 (Tx-1) is aligned with burst at λ_7 (Tx-2), then 3 successive bursts at λ_6 (Tx-1) are aligned with 3 successive bursts at λ_8 (Tx-2). At the 50/50 combiner, the bursts will be aligned. As we have only two transmitters, we can only simulate the alignment of two bursts, but the alignment of more bursts would be realized with the same mechanism. Then the two coupler output signals are filtered by two 20 GHz passband filters. One filter selects the burst signals at λ_5 and λ_6, and another filter selects the burst signals at λ_7 and λ_8. After that, the signals are detected by photo-detectors and are observed with an oscilloscope. The bursts generation configuration and the filters configuration can ensure a constant power at the input of the photodiodes. The propagation distances from the combiner to the oscilloscope for the two channels are equal. The bursts at

different wavelengths carry the same OFDM data. In order to better distinguish the data and then to observe them easily on the oscilloscope, the optical signal power levels of the bursts are set different. The optical signal powers of the bursts at λ_6 generated by Tx-1 and the bursts λ_8 generated by Tx-2 are set at a level of $P_{\lambda 6 \lambda 8}$. The optical signal powers of the bursts at λ_5 generated by Tx-1 are reduced: the level is called $P_{\lambda 5}$. And the optical powers of bursts λ_7 generated by Tx-2 are increased: the level is called $P_{\lambda 7}$. The power levels follow the relation as $P_{\lambda 7}<P_{\lambda 6 \lambda 8}<P_{\lambda 5}$.

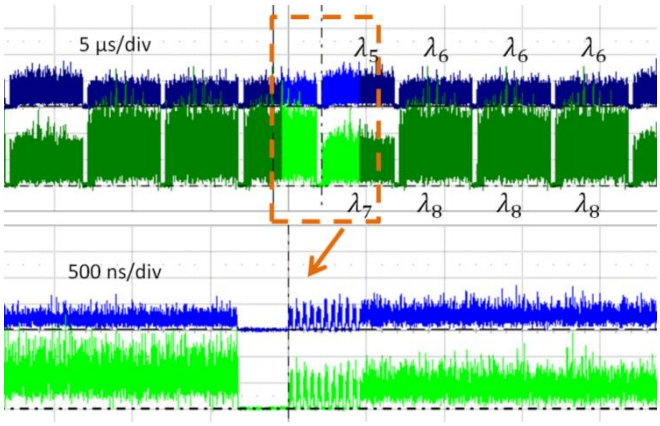

Figure 4-13: The observed burst signals on the oscilloscope before inserting any fiber delay line.

Figure 4-13 shows the observed burst signals on the oscilloscope before inserting any fiber delay line. The blue burst, which has a power higher than the average power, is the burst at λ_7 generated by Tx-2. The green burst, which has a power lower than the average power, is the burst at λ_5 generated by Tx-1. We can see that the bursts are well aligned at the combiner.

In order to simulate a difference in the propagation times between the two transmitters and the combiner, we insert a 400 m fiber delay line between Tx-2 and the combiner. Figure 4-14 shows the observed burst signals on the oscilloscope. The 400 m fiber delay line introduces about 2 µs delay between these two channels.

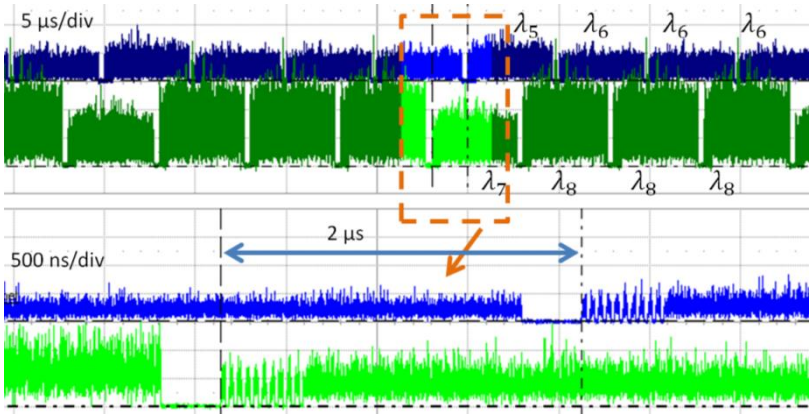

Figure 4-14: The received burst signals on the oscilloscope with a 400 m fiber delay line without alignment control.

Then we can modify the parameters “delay tickets” of both SOAG control signals and AWG trigger to compensate for the 2 µs time shift. As each ticket is equal to 10 ns, we have to increase the delay ticket value of the two SOAG control signals of Tx-1 and the AWG trigger of Tx-1 of 200 in order to compensate the time shift introduced by the fiber delay line at Tx-2. Afterwards, we observe the received signals on the oscilloscope as shown in Figure 4-15. We can see that the burst signals are well aligned. We can align the bursts coming from two sources by inserting different lengths of fiber: 1 Km, 2 Km and 10 Km fiber delay lines have been tested and the alignments have been achieved successfully. Note that each ticket being equal to 10 ns, we can only compensate the time shift with a granularity of 10 ns leading to a bursts alignment precision of ± 5 ns.

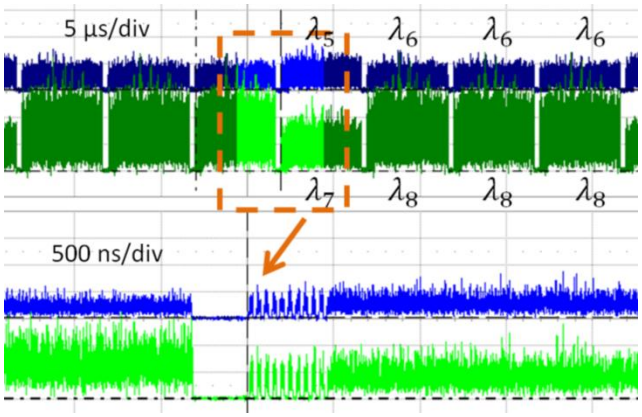

Figure 4-15: The received burst signals on the oscilloscope with a 400 m fiber delay line with alignment control.

4.5 Conclusion

In this chapter we have presented the TISA control plane which is used to manage the data plane and guarantee the absence of collision at the destinations and in the network. It is composed of two FPGAs and a controller. The controller is used to preprogram the grants which contain the sending time and the sub-band wavelength for each burst. The grants are distributed to the sources to control the bursts emissions. Each source has a FPGA, which is used to receive, store the grants and then convert the grants into control signals which control the SOAGs. Moreover, the FPGAs generate a trigger signal to the AWGs in order to synchronize the data emission with the optical signal arrival. For the synchronization of the whole experimental test-bed, a common clock has been implemented. The common clock offers four 100 MHz clock signals to FPGAs and AWGs in order to guarantee that all the devices work at the same rhythm. Compared to the TWIN solution, the bursts coming from different sources should be aligned at the MB-OFDM combiner. This new constraint has been taken into account and the specific alignment has been achieved by carefully modifying the bursts sending times.

Reference

[1] L. Sadeghioon, P. Gavignet, V. Alaiwan, L. Bramerie, E. Le Rouzic, J.-L. Barbey, T. Guillossou, E. Borgne and S. Lobo,, "Software-based burst mode reception implementation for time-domain wavelength interleaved networks," 2015 European Conference on Optical Communication (ECOC), Valencia, 2015, pp. 1-3.

[2] National Instrument, “Single Cycle Timed Loop”, [available online], http://zone.ni.com/reference/en-XX/help/371599G-01/lvfpga/fpga_timed_loop/

[3] A. Triki, R. Aparicio-Pardo, P. Gavignet, E. Le Rouzic, B. Arzur and A. Gravey, "Is it worth adapting sub-wavelength switching control plane to traffic variations?," 2014 International Conference on Optical Network Design and Modeling, Stockholm, 2014, pp. 186-191.

[4] A. Triki, P. Gavignet, B. Arzur, E. Le Rouzic et A. Gravey, “Efficient control plane for passive optical burst switching network”, *International Conference on Information Networking (ICOIN),* pp. 535-540, 2013.

[5] Vectron, “VT-804 TCXO data sheet” [available online], https://www.vectron.com/products/pl_detail.aspx?rid=96

[6] Silicon Labs “Si5347/46 Rev D Data Sheet” [available online] https://www.silabs.com/documents/.../Si5347-46-D-DataSheet.pdf .

[7] National Instrument, “Single-Cycle Timed Loop FAQ for the LabVIEW FPGA Module”, [available online], https://knowledge.ni.com/KnowledgeArticleDetails?id=kA00Z000000P8sWSAS

[8] National Instrument, “Pipelining to Optimize FPGA VIs (FPGA Module)”, [available online], http://zone.ni.com/reference/en-XX/help/371599G-01/lvfpgaconcepts/fpga_pipelining/.

[9] National Instrument, “Optimizing your LabVIEW FPGA VIs: Parallel Execution and Pipelining”, [available online], http://www.ni.com/white-paper/3749/en/

[10] Analog Devices, “Fundamentals of Phase Locked Loops (PLLs)”, [available online], http://www.analog.com/media/en/training-seminars/tutorials/MT-086.pdf

[11] Texas Intruments, “Fractional/Integer-N PLL Basics”, [available online], http://www.ti.com/lit/an/swra029/swra029.pdf

[12] Tektronix “AWG7000 Series Arbitrary Waveform Generator Manual”, [available online], http://download.tek.com/manual/077006105web.pdf

[13] S.L. Jansen, "Long-haul transmission of 16× 52.5 Gbits/s polarization-division-multiplexed OFDM enabled by MIMO processing," *Journal of Optical Networking*, **7**, 173-182 (2008).

[14] R. Noé, B. Koch, D. Sandel, "Optical time-of-flight measurement based on data transmission in a ring oscillator". *Optics Express*. 2009 Dec 7;17(25):22925-36.

CHAPTER 5

TISA network realization and evaluation

As presented in chapter 2, the TISA network is composed of a data plane and a control plane. The implementation of the control plane has been described in chapter 4, which offers all the necessary management functions for the data plane configuration of the proof of concept of TISA. For the data plane, there are three main building blocks: the transmitter/source nodes, the routing devices (core nodes, MB-OFDM combiner and separator), and the receiver/destination nodes.

In this chapter, we first describe the implementation of the routing devices in order to build the whole TISA network. Then the evaluation of the whole TISA network performance and the filter detuning effect are presented. The flexibility in terms of burst composition and burst duration of the TISA solution is also investigated. Finally we propose a novel method to improve the TISA performances at the receiver side: the evaluation and the experimental results of this new method are presented in the last section.

5.1 Burst routing through the TISA network

Figure 5-1 represents the targeted TISA architecture for the experimental test-bed implemented in this thesis. There is only one core node and several edge nodes containing the emission and the reception parts (only one transmission direction is represented and evaluated). The group nodes A-i and B-i are source nodes, the group nodes C-i and D-i are destination nodes. The arrows presented beside source node A-1 and A-2 are the wavelength of sub-bands will be configured in the test-bed: the colored ones are the wavelength used and the gray ones are the wavelength that we do not use during the tests. Each rectangle presents a time slot, which has a uniform dimension in TISA concept.

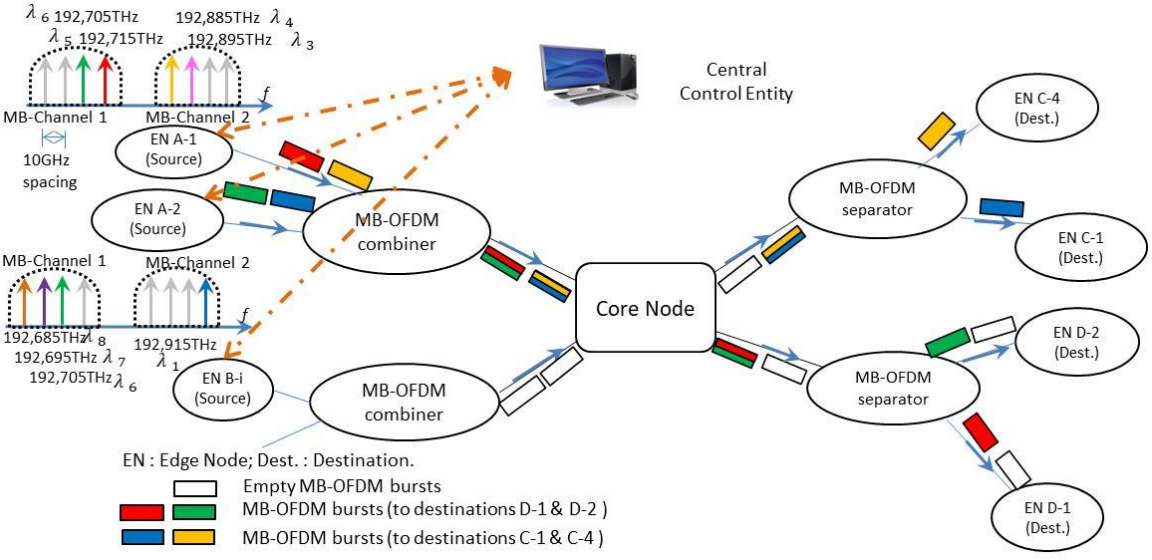

Figure 5-1: TISA architecture (one transmission direction is presented)

The two independent transmitters (Tx-1 and Tx-2) that we have implemented in chapter 3 are used here. Each transmitter is able to generate OFDM bursts data at 4 different wavelengths each corresponding to one sub-band in the TISA architecture. The transmitter Tx-1 is in node A-1 and the transmitter Tx-2 is in node A-2. In this experiment, we have configured the 8 different wavelengths at 192.915 THz (λ_1), 192.905 THz (λ_2), 192.895 THz (λ_3), 192.885 THz (λ_4), 192.715 THz (λ_5), 192.705 THz (λ_6), 192.695 THz (λ_7), 192.685 THz (λ_8), which are attached respectively to Nodes C-1 to C-4 and Nodes D-1 to D-4. Thus, Multi-Band (MB)-channel 1 is composed of λ_5 to λ_8 channels and MB-channel 2 is composed of λ_1 to λ_4 channels. The spacing between two sub-bands a MB-channel is 10 GHz, which is set in order to keep a 5 GHz margin at each side of the MB-channel avoiding the penalty related to the transfer function of the routing devices. The spectral bandwidth of MB-channels 1 and 2 is 50 GHz and they are 200 GHz spaced. The transmitter Tx-1 is configured to generate λ_3, λ_4, λ_5, λ_6 and Tx-2 generates λ_1, λ_6, λ_7, λ_8 (see colored arrows in Figure 5-1).

In the destination nodes (D-1, D-2, C-1 and C-4), the coherent receiver (Rx-1, see Figure 5-2) as described in chapter 3 is placed at these nodes to receive bursts data and perform the BER measurements. Note that each destination is associated to a unique sub-band in TISA network, so we will tune the Rx-1 to the corresponding sub-band at different destination node. The received sub-band wavelength is selected by properly adjusting the wavelength of the LO. An ASE source is inserted just before the Rx-1 to modify the OSNR level for the BER versus OSNR measurements. OFDM digital signal processing is performed in off-line.

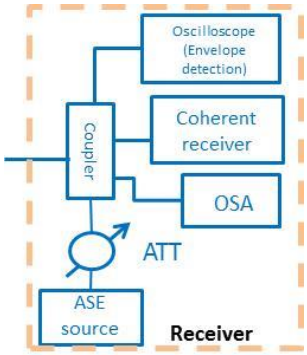

Figure 5-2: Experimental set-up of the coherent receiver.

5.1.1 MB-OFDM combiner

The MB-OFDM combiner is used to bundle together the burst data coming from different source nodes in order to generate a multi-band burst occupying an entire band (MB-channel), which is a structure similar to a super-channel but in burst mode. A simple coupler can be suitable as the number of sources connected to a multiband combiner is limited. Otherwise a multiplexer is also a possible solution that would introduce lower insertion losses. The requirement on the bursts alignment at the combiner is achieved thanks to control plane implemented in section 4.4.

5.1.2 Core Node

The core node routing structure is used to route the multi-band bursts according to the MB-channel wavelength. This functionality is realized in our test-bed by the WSS, which is a commercial product purchased from Finisar [1]. The architecture of a two inputs and two outputs core node is represented in Figure 5-3 (a). In the experiment, two central frequencies of the MB-channels are around 192.7 THz and 192.9 THz. Correspondingly, the WSS is configured on a 50 GHz fixed grid, and only two output ports are used: 192.7 THz and 192.9 THz. The transfer function of the WSS is shown in Figure 5-3 (b), as the 3-dB passband is about 45 GHz, we put 4 sub-bands in a MB-channel with 10 GHz spacing in order to give a 5 GHz for each side of the MB-channel. The bursts coming from the multiband combiners (from group nodes Ai and Bi) enter the WSS, and then the bursts exit different ports based on MB-channel wavelength. After that, the bursts at the same MB-channel wavelength are combined together by a coupler. In order to ensure an adequate output signal power, an EDFA is inserted at the output ports of the core node. The MB-channels can be transmitted to their corresponding MB-OFDM separators.

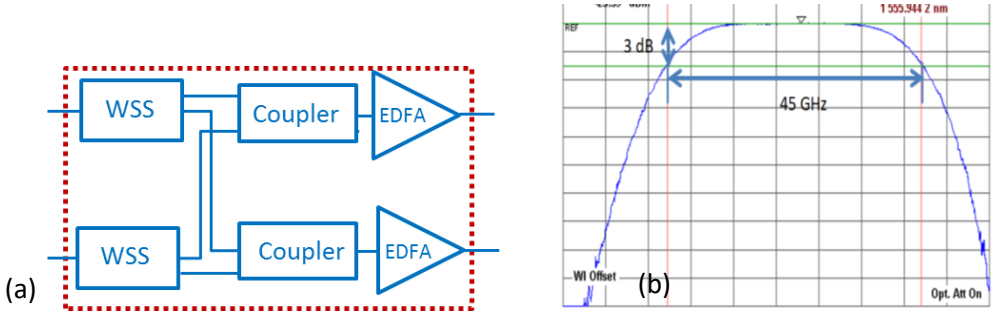

Figure 5-3: (a) Experimental set-up of the core node; (b) transfer function of 50 GHz fixed grid WSS.

This core node architecture can support transparent routing, so that we don't need to implement signal-dependent interfaces for extremely high input/output bandwidth. As it's easy to enlarge the number of input/output port of WSS by cascading and combining several WSSs, couplers and EDFAs, this architecture helps to flatten the network topology, and thus it permit avoiding bandwidth bottleneck and large latency due to the conventional hierarchical structures. Excited by this motivation, some novel optical flat network architectures have been proposed [2][3]. All of them permit increasing the scalability of the network and reducing energy consumption.

5.1.3 MB-OFDM separator

The MB-OFDM separator, called also sub-bands separator, is built with a splitter followed by 10 GHz pass-band filters used to perform the sub-band separation as discussed in chapter 2. The filter is a commercial product built by Yenista [4]. In this experiment, a separator with two output ports is implemented as shown in Figure 5-4 (a). In our test-bed, each destination nodes group has only two destination nodes. Therefore, the separator in our test-bed should have two output ports. We can increase the number of filters in order to increase the number of output ports if necessary.

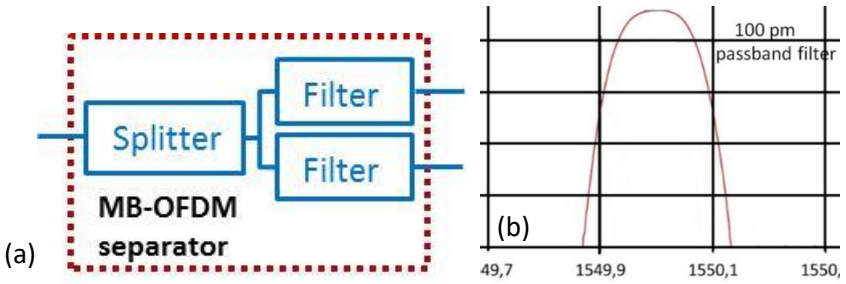

Figure 5-4: (a) Experimental set-up of separator; (b) transfer function of filter (100 pm passband) [4].

Even if the filter in the MB-OFDM separator is not mandatory in the TISA concept when using coherent reception, it protects the customers from snooping, as each destination receives only its corresponding data. This feature is also important for the operator who wants to protect its customers' privacy offering secured network solutions. Furthermore, as we discussed in chapter 2, the TISA network is also compatible with direct detection technology. In this case, the MB-separator with 10 GHz filtering is mandatory, which can prevent the crosstalk coming from the adjacent sub-bands. Concerning the filters, the bandwidth of the passband filter is tunable and we can thus modify it according to the different configurations under study.

5.1.4 Performance of bursts through the TISA network

We first measure spectra at some key points of the TISA network with an Apex high-resolution (20 MHz) Optical Spectrum Analyzer (OSA). We switch on all the 8 wavelengths (from λ_1 to λ_8) that constitute the two 50 GHz MB-channels (192.7 THz and 192.9 THz). As described in chapter 4, the control plane can switch "on" only one wavelength at once; a special control order is generated exceptional and sent directly to SOAG drivers from the FPGAs in order to switch "on" all the 8 wavelengths. Figure 5-5 (a) shows the spectrum of the signal at the input of the core node when we switch on permanently all the 8 wavelengths, Figure 5-5 (b) shows the spectrum at the output of the core node for nodes D-i (MB-channel 1) and Figure 5-5 (c) is the spectrum of the selected signal at the input of node D-2 (λ_6). We can see that the wavelength at 192.7 THz and its corresponding sub-band are routed correctly through the network up to node D-2. Figure 5-5 (d) presents the dimension of a MB-channel and the 4 sub-bands inside.

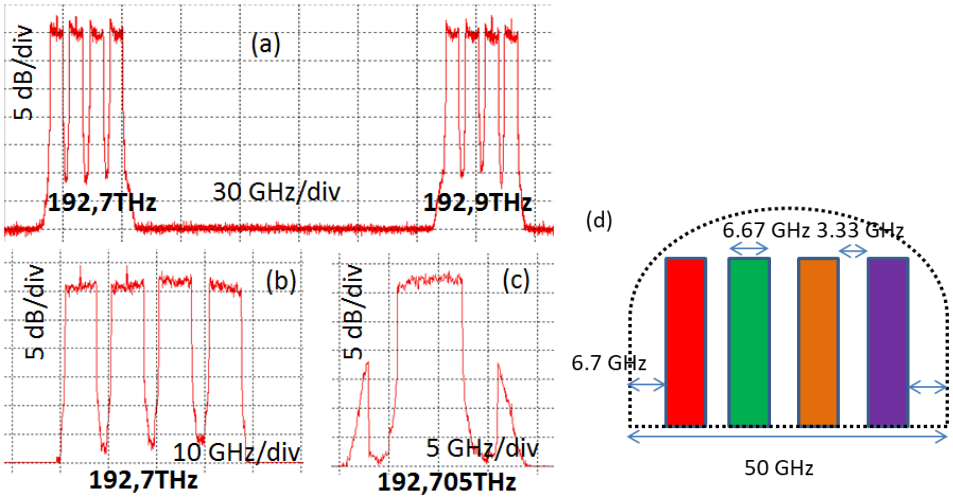

Figure 5-5: The spectrum of the signal (a) at the input of the core node, (b) at the output of the core node (MB-channel 1), (c) at the input of the node D-2 (λ_6), (d) the dimension of 4 sub-bands in a MB-channel.

Then, each transmitter is programmed to generate successively a periodic data flow composed of four slots at different wavelengths. In order to ensure a continuous flow at the input of the EDFAs of the core node, Tx-1 generates bursts successively and periodically at λ_5, λ_3, λ_6 and λ_4, while Tx-2 generates bursts successively and periodically at λ_1, λ_6, λ_1 and λ_7.

The BER versus OSNR curves measured for the Tx-1/Rx-1 at node D-2 using DP-QPSK are represented in Figure 5-6. Each OFDM frame is composed of 1 synchronization symbol, 14 training symbols and 156 payload symbols. So using DP-QPSK modulation format, the raw data rate is 26.6 Gbps (integrating all overheads) in continuous mode operation. The burst signal duration is 4.7 µs. The pink curve represents the Tx-2/Rx-1 performance in back-to-back configuration when the Tx-2 generates a continuous signal at λ_6. The green curve with dots corresponds to the same signal after transmission through the TISA network. The green curve with circles shows the performance in burst mode (with 1 OFDM frame per burst of 4.7 µs) when the Rx-1 is at node D-2 receiving data from Tx-2. The blue curve represents the Tx-1/Rx-1 performance in back-to-back configuration when the Tx-1 generates a continuous signal at λ_6. The red curve with dots corresponds to the same signal after transmission through the TISA network. The red curve with squares shows the performance in burst mode when the Rx-1 is at node D-2 receiving data from Tx-1. As we have discussed in chapter 3, the global performances of Tx-1 are much better than those of Tx-2 due to the optimized linearity of the RF drivers which feed the CMZM (that has furthermore a better extinction ratio). For both Txs, we can see that the passive components like WSS, couplers, and OFDM separator do not introduce any penalty at BER 10^{-5}. There is no penalty at BER 10^{-4} and about 0.3 dB penalty at BER 10^{-5} compared to the continuous mode configurations performing bursts transmission. The performance of Tx-1/Rx-1 at node D-1 and Tx-1/Rx-1 at node C-4, using DP-QPSK signals, are similar to those at D-2.

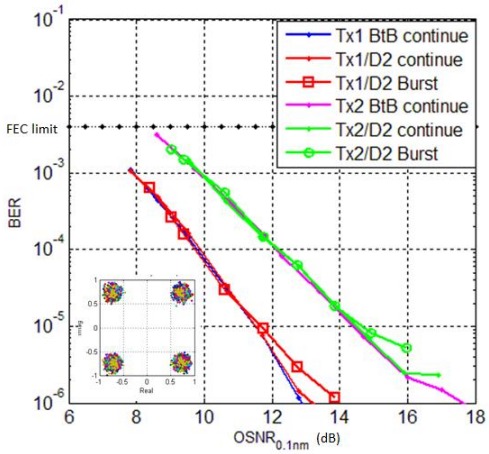

Figure 5-6: BER versus OSNR (0.1nm) curves for Tx-1 and Tx-2/Rx-1 at node D-2 using DP-QPSK modulation format.

The BER versus OSNR curves measured for the couple Tx-1/Rx-1 at node D-2 using DP-16QAM modulation format are presented in Figure 5-7(a). The raw data rate is 53.2 Gbps (integrating all overheads) in continuous mode operation. The burst signal duration is 4.7 µs. Tx-2 does not permit to perform DP-16QAM measurements (due to its poor quality: the linearity of RF drivers is not sufficiently good); thus we keep DP-QPSK format for this Tx. Thus, both DP-QPSK and DP-16QAM signals propagate at the same time through the TISA network showing the transparency of TISA to the modulation format and bit rate. In order to improve the performances of the DP-16QAM signal from Tx-1, we have built two frames in each burst, each frame containing 1 synchronization symbol, 14 training symbols and 70 payload symbols. The blue line shows the performance in back-to-back configuration when the Tx-1 generates a continuous signal at λ_6; the green curve with dots represents the performance of the same signal after transmission through the TISA network. As two frames are inserted into one burst, the performance of the first frame is represented by the red curve with squares and the performance of the second frame is shown by the red curve with diamonds. We observe no significant difference (only 0.3 dB penalty at BER 10^{-5}) between the second frame and the continuous mode operation. But the first frame has ~0.8 dB penalty at BER 10^{-5} compared to the continuous mode configuration. In this experiment, there is a time interval without signal between two successive bursts at the input of the coherent receiver (Figure 5-7 (b)), note that the signal absence duration impacts the measured bursts (generated by Tx-1) is only 0.3 µs. The signal absence duration stresses the optoelectronic components such as Trans-Impedance Amplifiers (TIA) and thus generates transitions distortions. As the DP-16QAM format is more sensitive to signal distortions than DP-QPSK, the DP-16QAM format stresses more DSP than the DP-QPSK format. An improvement of the DSP for DP-16QAM OFDM bursts is proposed in this thesis and the results will be presented in section 5.4. The performances of Tx-1/Rx-1 at nodes D-1 and C-4 are similar to the ones at node D-2. These results confirm that the transparent transmission of both DP-QPSK and DP-16QAM signals, through the TISA network, is possible with very low penalties.

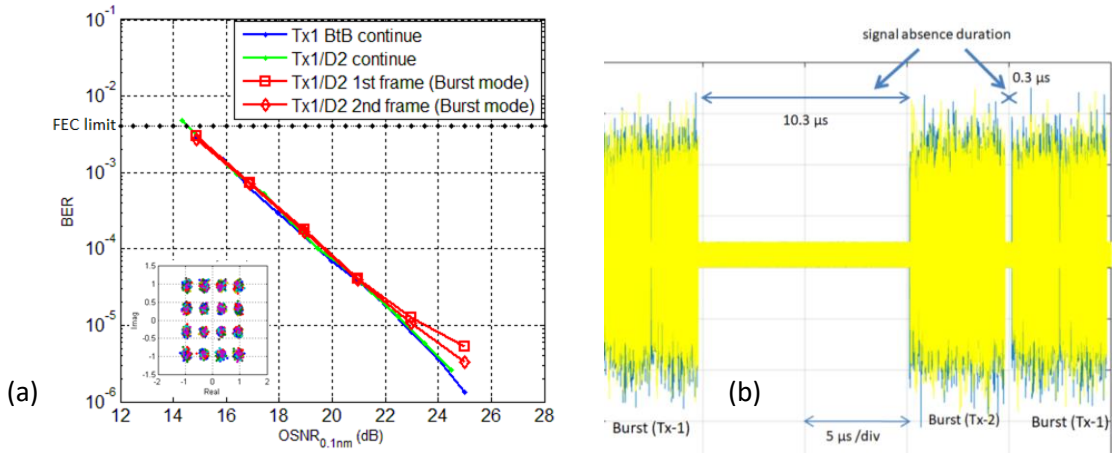

Figure 5-7: (a)BER versus OSNR (0.1nm) curves for Tx-1/Rx-1 at node D-2 using DP-16QAM modulation format (left); (b) Signals received at node D-2(right).

5.2 Sensitivity to high resolution filter detuning

It is well known that commercially available high performance lasers and optical filters components, such as DMUX and MUX, specify frequency uncertainties of ~1.5 GHz [5]. Such uncertainties leads to a frequency mismatch between the lasers frequencies and the central frequencies of the core nodes and MB-separators. This frequency mismatch causes filtering distortions which are a reason for performance degradation in optical burst switching network. In this section, we suppose that the lasers frequencies are stable while the central frequency of high resolution filters can be shifted in the sub-band separator. We evaluate the burst performance through BER measurements at a fixed OSNR in order to characterize the filter detuning tolerance.

In this experiment, the Tx-1 is configured to generate a periodical bursts sequence successively at λ_1, λ_3, λ_6, λ_4. And the Tx-2 is configured to generate bursts simultaneous at λ_5 and λ_7 by switching "on" continuously the corresponding optical gates of the fast tunable laser as described in chapter 3. The coherent receiver is placed at node D-2 and is configured to receive the bursts at λ_6. This configuration generates burst traffic while generating adjacent sub-bands (λ_5 and λ_7): one at the left hand side and another one at the right hand side of the measured sub-band (λ_6). As the spacing between two adjacent sub-bands is supposed to have an impact on the bursts performance, two spacing configurations, 10 GHz and 8 GHz, are evaluated. Knowing that the optical bandwidth of our OFDM signal is 6.67 GHz, the guard band between two adjacent sub-bands is correspondingly 3.33 GHz and 1.33 GHz. Note that the wavelength λ_6, in the 8 GHz spacing configuration, is not modified and thus the λ_5 and λ_7 are correspondingly configured at 192.713 THz (λ_5) and 192.697 THz (λ_7). The configurations of the wavelengths at MB-channel 2 (λ_1, λ_3 λ_4 in this test) are kept the same as before. Both DP-QPSK and DP-16QAM modulation formats are evaluated. For the burst with DP-QPSK modulation format, only 1 OFDM frame is inserted into the burst, while each OFDM frame is composed of 1 synchronization symbol, 14 training symbols and 156

payload symbols. With DP-16QAM modulation format, each burst contains 2 OFDM frames, while each OFDM frame is composed of 1 synchronization symbol, 14 training symbols and 70 payload symbols. The burst durations for the DP-QPSK and DP-16QAM format are the same, 4.7 µs. During the test, the OSNR for the DP-QPSK format is set to 10 dB and the OSNR for the DP-16QAM format is set to 20 dB in order to set the BER around the 10^{-4} when no filter detuning is applied.

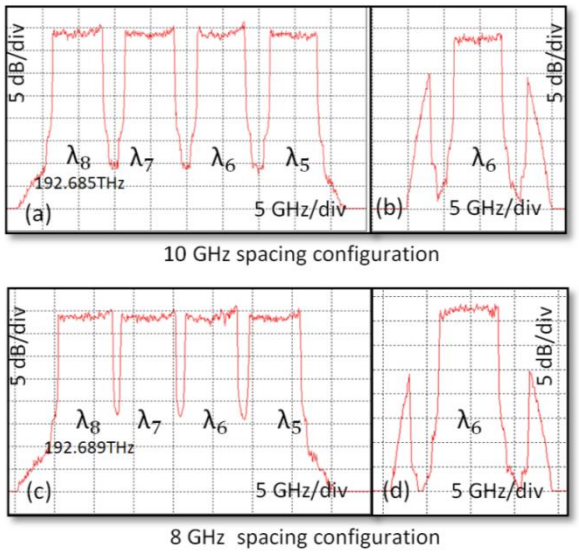

Figure 5-8: The spectra of the signal (a) at the separator (10 GHz spacing); (b) at the node D-2 (10 GHz bandwidth of filter); (c) at the separator (8 GHz spacing); (d) at the node D-2 (8 GHz bandwidth of filter).

We first measure spectra at the separator associated to the group nodes D-i at the node D-2. Figure 5-8 (a) shows the spectrum of the signal at the separator associated to the group nodes D-i in the 10 GHz spacing configuration. Figure 5-8 (b) shows the spectrum of signal at the node D-2 with the 10 GHz bandwidth filter. For the 8 GHz spacing configuration while using 8 GHz bandwidth filter, the spectrum of signal at the separator and node D-2 are represented respectively in Figure 5-8 (c) and (d).

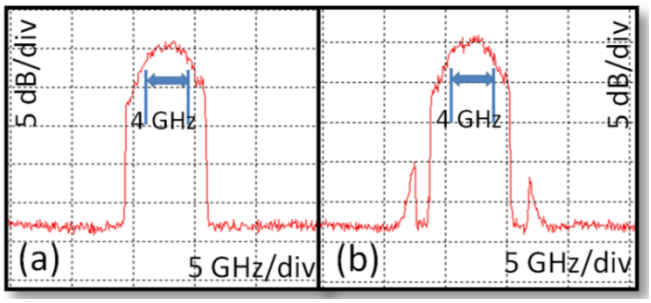

Figure 5-9: The spectra of the signal at node D-2 using 4 GHz bandwidth of filter in (a) 10 GHz spacing configuration and (b) 8 GHz spacing configuration.

At first, we evaluate the influence of the optical filter bandwidth that is integrated in the MB-separator on the burst performance. The bandwidth of the filter used is tuned from 10 GHz to

4 GHz. The spectra of the signal at node D-2 are shown respectively in Figure 5-9 (a) and (b), when the bandwidth of the passband filter is 4 GHz in the configurations where the sub-band spacing is 10 GHz and 8 GHz. The spectra of the signal at node D-2 when the bandwidth of the passband filter is 10 GHz in the configurations where the sub-band spacing is 10 GHz and 8 GHz are shown respectively in Figure 5-8 (b) and (d). We measure the BER versus the optical filter bandwidth curves (see Figure 5-10). For the 10 GHz spacing configuration, the red curves with squares and diamonds represent respectively the BER of the first and second DP-16QAM OFDM frame. The blue curve with dots represents the BER of the DP-QPSK OFDM frame. For the 8 GHz spacing configuration, the pink curves with circles and triangles represent respectively the BER of the first and the second DP-16QAM OFDM frame. The green curve with dots represents the BER of the DP-QPSK OFDM frame. We compare the performances obtained with the 10 GHz and 8 GHz sub-band spacing configurations: we can see that there is no significant difference in terms of performance between the two configurations under study. Because we choose the coherent detection technology here, we use advantageously the digital filtering functionality of our real-time oscilloscope to reduce the crosstalk coming from the adjacent sub-bands. As the optical bandwidth of the burst signal is 6.67 GHz, the signal has a significant penalty in BER since the filter bandwidth is much lower than 6 GHz (ex. 4 GHz filter with 1.5 $*10^{-3}$ BER shown in Figure 5-10). Our results demonstrate that MB-OFDM using coherent detection permits to reduce the guard band between two consecutive sub-bands and thus improve the spectral efficiency of the network.

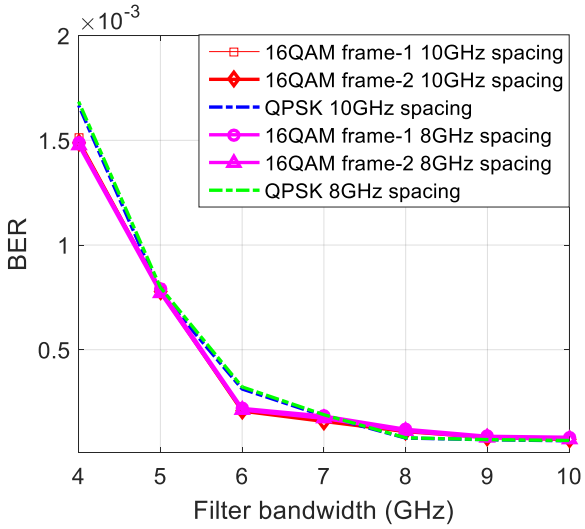

Figure 5-10: BER versus the filter passband bandwidth (GHz) curves.

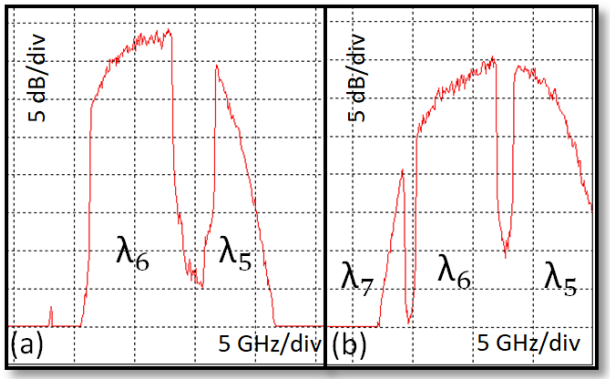

Figure 5-11: The spectra of the signal at node D-2 (a) with 2.5 GHz filter detuning in 10 GHz spacing configuration and (b) with 2 GHz filter detuning in 8 GHz spacing configuration.

After that, we study the burst performance tolerance against the frequency detuning between the laser and high resolution filter frequencies. Suppose that the filter transfer function is symmetrical, we only detune the filter to the higher frequency (right side observed over the OSA). The spectra of the signal at node D-2, when the filter frequency detuning is 2.5 GHz with the 10 GHz sub-band spacing and 2 GHz with the 8 GHz sub-band spacing configurations are shown respectively in Figure 5-11 (a) and (b). The spectra of the signal at node D-2 without detuning is shown in Figure 5-8 (b) and (d). The BER versus filter frequency detuning curves are represented in Figure 5-12. For the 10 GHz sub-band spacing configuration, the red curves with squares and diamonds represent respectively the BER of the first and the second DP-16QAM OFDM frames. The blue curve with dots represents the BER of the DP-QPSK OFDM frame. For the 8 GHz sub-band spacing configuration, the pink curves with circles and triangles represent respectively the BER of the first and the second DP-16QAM OFDM frame. The green curve with dots represents the BER of the DP-QPSK OFDM frame. The bursts performances are very similar for the DP-QPSK and DP-16QAM modulation format. We can see that the tolerance of the filter detuning is almost the same for both 10 GHz and 8 GHz sub-band spacing configurations, the tolerance is ~ 1 GHz respecting to the criterion of a lower than $2*10^{-4}$ BER level.

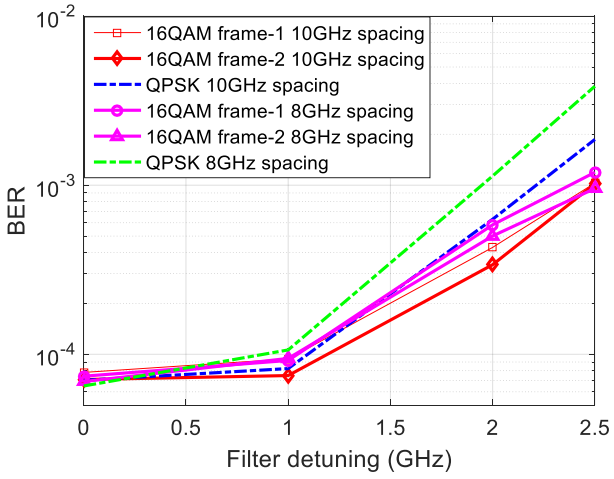

Figure 5-12: BER versus filter detuning (GHz) curves.

5.3 Flexibility evaluation

As we have discussed in chapter 2, the flexibility of the TISA solution is in both time and spectral domains. We can flexibly design the dimension of the time slot: the duration of the time slot and the bandwidth of one sub-band. During this thesis, the dimension of the time slot is fixed and we do not carry out any evaluation on the flexibility of the time slot dimension. However, we can combine the bursts in the time domain to generate a longer burst. Note that we have not the possibility to play on the burst bandwidth, as we have not in the laboratory an AWG that has an output bandwidth as large as two sub-bands. We thus evaluate the performance of bursts of 9.7 µs with 0.3 µs guard time.

The test-bed is configured identically to the configuration presented in section 5.1.4. Each transmitter is programmed to generate successively a periodic data flow composed of four time slots at different wavelengths. The coherent receiver is tuned to receive the corresponding sub-band at each node destination. In order to ensure a continuous signal flow at the input of the EDFAs of the core node, Tx-1 generates successively and periodically bursts at λ_5, λ_3, λ_6, λ_4, while Tx-2 generates successively and periodically bursts at λ_1, λ_6, λ_1, λ_7. Each burst has a length of 9.7 µs, and the raw bit rate (including all the overhead, such as training symbols and CP) in the continuous mode configuration is 26.6 Gbps for DP-QPSK format and 53.2 Gbps for DP-16QAM format. The receiver is placed at node D-2 to receive the bursts at λ_6. So the receiver will receive periodically a data sequence of empty, bursts (generated by Tx-2) at λ_6, bursts (generated by Tx-1) at λ_6, empty. Only the bursts generated by Tx-1 are taken into account for BER calculation.

The BER versus OSNR curves measured for the Tx-1/Rx-1 at node D-2 (λ_6) using the DP-QPSK format are represented in Figure 5-13. Three OFDM frames are inserted into one burst in order to avoid inserting a too long OFDM frame that could be difficult to equalize from the DSP perspective. Each OFDM frame is composed of 1 synchronization symbol, 12 training symbols and 104 payload symbols. The red curve with dots represents the Tx-1/Rx-1 performance after transmission through the TISA network when the Tx-1 generates a continuous signal at λ_6. The cyan curve with triangles, blue curve with diamonds and red curve with squares show the performances of the first OFDM frame, the second OFDM frame and the third OFDM frame respectively in burst mode. We can see that there is no significant difference among these three curves. There is only ~0.4 dB penalty at BER 10^{-5} for all these three curves. The pink curve with crosses represents the burst performance with 4.7 µs duration (shown in Figure 5-6). The pink curve is stick together with the red curve and blue curve, there is not significant difference. Compared to the performance carried out with bursts of 4.7 µs, the bursts of 9.7 µs keep the same performance as before. The results demonstrate the flexibility of the TISA network in the time domain: TISA can generate longer burst without introducing significant penalty with the DP-QPSK format.

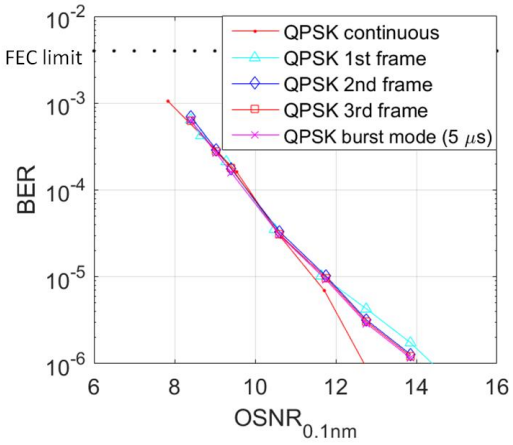

Figure 5-13: BER versus OSNR (0.1 nm) for 10 µs time slot using DP-QPSK format.

The BER versus OSNR curves measured for the Tx-1/Rx-1 at node D-2 (λ_6) using DP-16QAM are represented in Figure 5-14. Three OFDM frames are inserted into each burst, and each OFDM frame structure is kept the same as that used in the evaluation with DP-QPSK. The red curve with dots represents the Tx-1/Rx-1 performance after transmission through the TISA network when the Tx-1 generates a continuous signal at λ_6. The red curve with squares, blue curve with diamonds and cyan curve with triangles show the performances of the first, the second and the third OFDM frame respectively in burst mode. We observe no significant difference (only 0.3 dB penalty at BER 10^{-5}) between the second frame, third frame and performance of the continuous mode configuration. There is ~0.9 dB penalty at BER 10^{-5} for the first OFDM frame compared to the continuous mode configuration performance. The penalty of the first OFDM frame is slightly larger than the second and third OFDM frame due to the same reason (signal absence duration) as discussed in section 5.1.4. The pink curve with crosses and circles represents respectively the performance of the first and second OFDM frames in the bursts of 4.7 µs duration (shown in Figure 5-7). We can see that there is no significant between the second OFDM frame in the bursts of 4.7 µs and the second and third OFDM frame in the burst of 9.7 µs. And there is no significant penalty between the first OFDM frame in the bursts of 4.7 µs and 9.7 µs. These results prove that the bursts of 9.7 µs keep the same performance as the bursts of 4.7 µs. There is difference between the performance of the first and second, third OFDM frame of the 9.7 µs bursts due to the signal absence duration, the same reason as discussed in section 5.1.4. The signal absence duration will be studied in section 5.4.

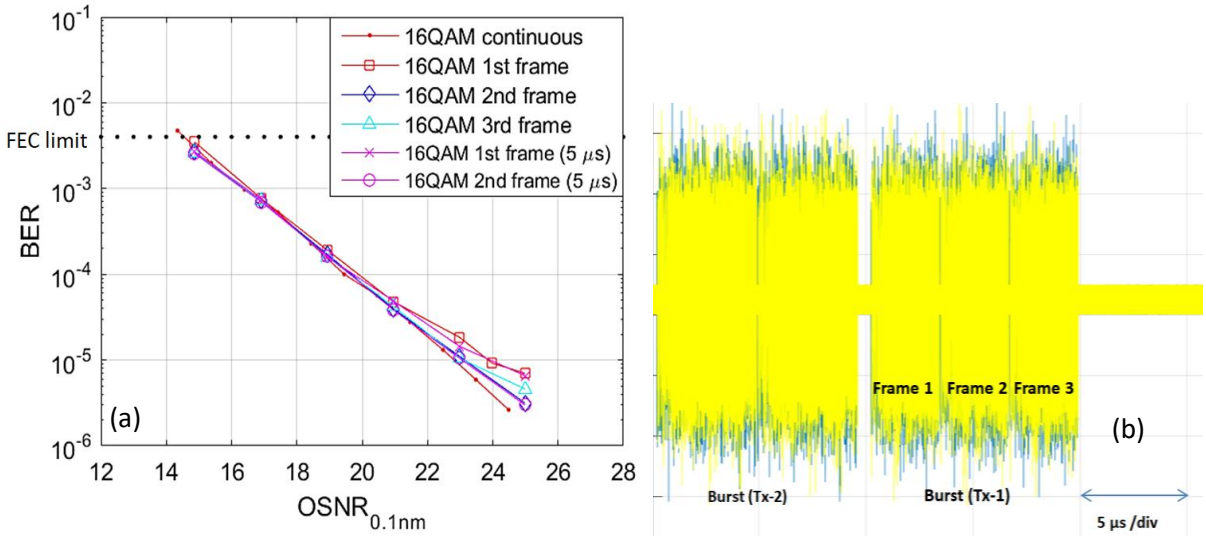

Figure 5-14: (a) BER versus OSNR (0.1 nm) for 10 µs time slot using DP-16QAM format; (b) Received signal at node D-2.

5.4 Novel training sequence strategy

In TISA, due to the nature of burst traffic, the coherent receivers are regularly exposed to variable absence of signal (i.e. from several µs to several tens of µs), stressing the optoelectronic components such as Trans-Impedance Amplifiers (TIA) and generating transients that impact the system performance. This can be very challenging for the receivers that have been originally designed to receive continuous OFDM flows. In the previous study in sections 3.4 and 5.1, the results showed that transient phenomena affect particularly bursts using DP-16QAM OFDM format, generating error floors. Based on this observation, it appeared particularly relevant to evaluate the impact of the presence of time intervals without signal (we called “gaps” here) on the BER performance and to propose solutions to mitigate these effects.

In this section, after having evaluated the performance degradation involved by the presence in the burst traffic at the receiver side of signal gaps of various durations, a novel OFDM training sequence strategy based on the implementation of a channel estimator using a sliding window is presented. Its positive impact on the system overall performance is shown and suppression of error floors is demonstrated.

5.4.1. Experimental setup and system characterization

During this experimental test, the targeted TISA network architecture is shown in Figure 5-15. It has the same architecture as the network presented in Figure 5-1 in section 5.1, with only one core node and several edge nodes containing the emission and reception parts (note that only one transmission direction is represented here). But the wavelengths configured at each source node are different from the previously described configuration.

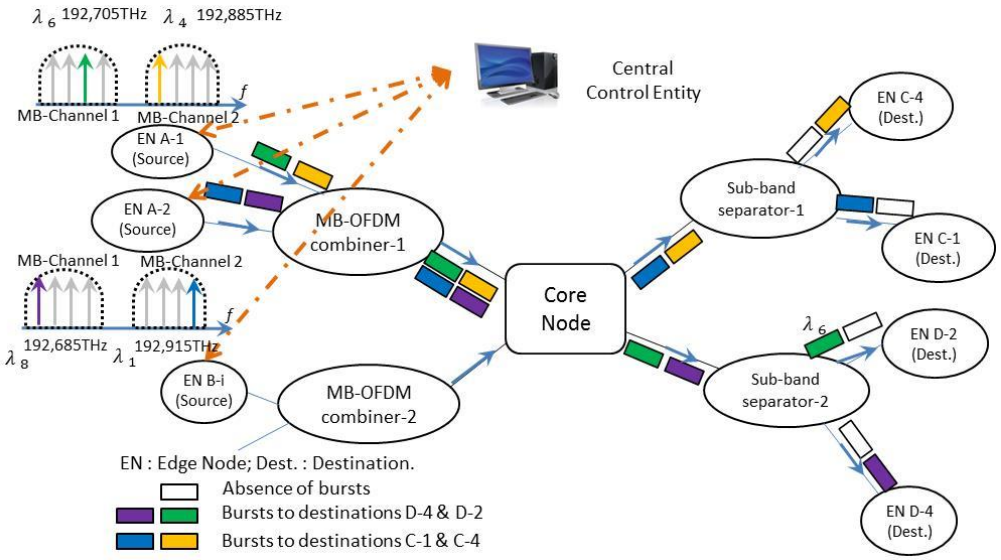

Figure 5-15: TISA network architecture with the wavelength configuration for gaps evaluation.

The experimental set-up is largely identical to what has been described in the performance evaluation of the bursts routing through the TISA network: time slots are set to 5 µs and are constituted of signal bursts of 4.7 µs and guard intervals of 0.3 µs. The node A-1 is configured to generate periodically and successively OFDM bursts at λ_4 (192.885 THz) and λ_6 (192.705 THz), while the node A-2 generates periodically and successively bursts at λ_8 (192.685 THz) and λ_1 (192.915 THz). The bursts at λ_4 and λ_8 (resp. λ_6 and λ_1) coming from the nodes A-1 and A-2 respectively are generated simultaneously with the same length. These various bursts are multiplexed and time-interleaved at the combiner level (Figure 5-15). Then, the core node spectrally separates the bursts at λ_1 and λ_4 (MB-channel 1) from the bursts at λ_6 and λ_8 (MB-channel 2). Note that there is still no signal gap (except the guard intervals of 0.3 µs between bursts) after this wavelength separation process, ensuring the absence of transients in the EDFAs that are inserted at the output of the core node. This is important to separate the various transient problems that can occur in burst-based networks: the goal of this section being to evaluate what occurs in the coherent receiver. We are now focusing on the bursts at λ_8 and λ_6. They are spectrally demultiplexed through the sub-band separator-2 and routed towards the edge nodes D-4 (λ_8) and D-2 (λ_6), respectively. Due to sub-band separation, gaps appear on λ_6 between signal bursts (Figure 5-16). The duration of gaps is equal to the sum of guard intervals and one or several signal bursts (generated here at λ_8). As the number of bursts at λ_8 generated between two consecutive bursts at λ_6 is variable, the gap duration can be adjusted. At the destination side, in the edge node D-2 which receives only the bursts at λ_6, a coherent receiver is implemented. Each burst occupies a 6.67 GHz optical bandwidth. The OFDM signal parameters are identical to what has been presented in chapter 3. As DP-QPSK is not so sensitive to the impact of gaps, DP-16QAM is selected as the modulation format used in the test. In the continuous mode operation (i.e. without bursts), each OFDM frame has one synchronization symbol, 14 training symbols and 156 payload symbols. The bursts duration is 4.7 µs with 0.3 µs guard time between two successive bursts while the raw data-rate is 53.2 Gbps.

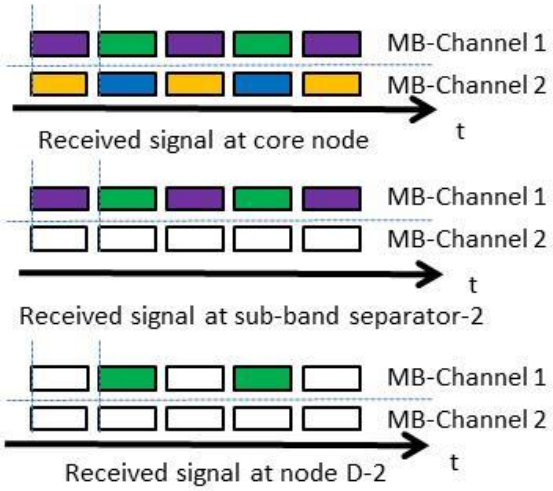

Figure 5-16: Timing diagram at the core node input (top), at the sub-band separator-2 input (middle), at the edge node D-2 (bottom).

The BER versus Optical Signal-to-Noise Ratio (OSNR) curves are measured and plotted in Figure 5-17 for various durations of gaps. Only one OFDM frame is inserted in the burst. The red curve with dots represents the performance of the continuous mode. The curves with red squares, blue diamonds, cyan triangles and violet circles correspond to gaps durations of 0.3 µs, 5.3 µs, 15.3 µs and 50.3 µs respectively. We can see that the presence of gaps (or equivalently the absence of signal) introduces penalties that are all the larger the gaps are. Furthermore, at high OSNRs, error floors appear for the greatest gap durations (≥ 10.3 µs). The presence of gaps of several tens of microseconds in the burst traffic imposes to the coherent receiver to have a very low cut-off frequency (~ 10 kHz), which is not the case (the low cut-off frequencies of our coherent receiver is rather ~ 30-50 kHz).

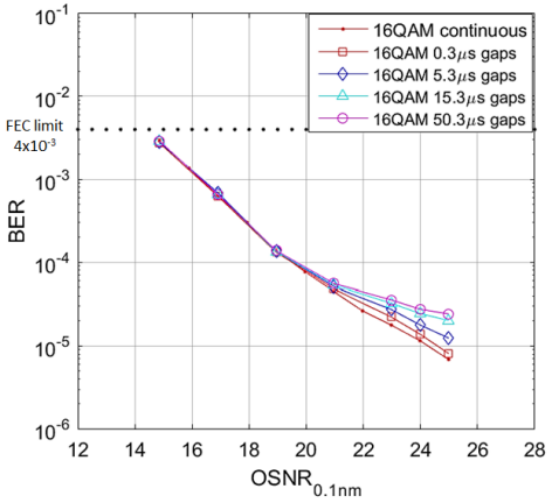

Figure 5-17: BER versus OSNR (in 0.1nm) curves for various gap durations.

In the Digital Signal Processing (DSP) algorithms related to optical OFDM, training symbols which are usually inserted at the beginning of OFDM frames are used to estimate the channel and

calculate the corresponding equalizer coefficients. In burst mode, due to transients affecting the receiver operation, the beginning of OFDM frames (where are located the training symbols) suffers from distortions, that severely affect the channel estimation. As a consequence, equalizer coefficients are no longer adapted to the equalization of the data inside the payload.

5.4.2. Proposed solution and results

The proposed solution consists in (i) inserting more training symbols in the OFDM frame, (ii) introducing a sliding window of a pre-determined size, (iii) moving this sliding window along the training sequence, (iv) calculating the equalizer coefficients for the various positions of the sliding window and corresponding BER, (v) finding the window position where the BER is minimized, (vi) using this optimal window position to equalize the data of the payload. Thanks to this process, channel estimation is performed over a part of the training sequence that is clean and not polluted by the receiver transients. The size of the sliding window is of course a parameter that can be optimized. The sliding window size corresponds to the number of training symbols that are used to average the equalizer coefficients during the channel estimation. Nonetheless, we have decided here to reuse a window length which gives satisfying performance in continuous mode, i.e. corresponding to 12 symbols here. Note that the window size is always an even number, since we use dual-polarization modulation format.

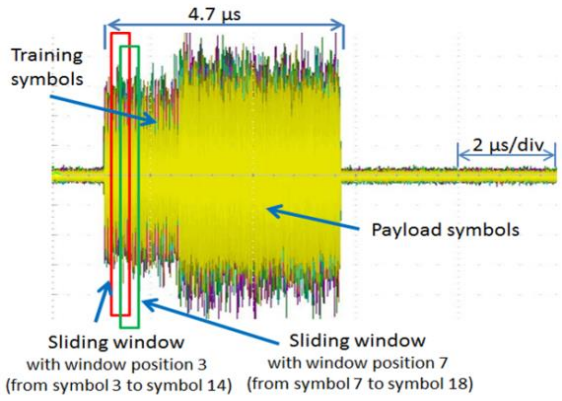

Figure 5-18: Received burst signal and sliding window for two different positions.

To implement the channel estimation/equalization described above while keeping the length of the signal burst at 4.7 µs, we have modified the OFDM frame as follows: 50 training symbols (instead of 14 training symbols previously) are inserted just behind the synchronization symbol while only 120 symbols constitute the payload. Figure 5-18 shows one OFDM frame with its synchronization symbol, 50 training symbols and 120 payload symbols. Since the generation of the training sequence follows the structure suggested by Jansen [6], the data are filled alternatively in the training sequence; the power of training symbols is lower than the payload as shown in Figure 5-18. Note that each burst of signal comprises one OFDM frame. The position of the sliding window in the training sequence is identified by the location of its first symbol, named in Figure 5-19 "window position". In Figure 5-18, two positions of the sliding window are represented. As shown in

Figure 5-19, the channel estimation/equalization is carried out all along the training sequence with a sliding step corresponding here to four symbols. The corresponding BER is calculated over an average of 50 runs and reported along the Y-axis. Measurements are performed for an OSNR of 25 dB in 0.1 nm.

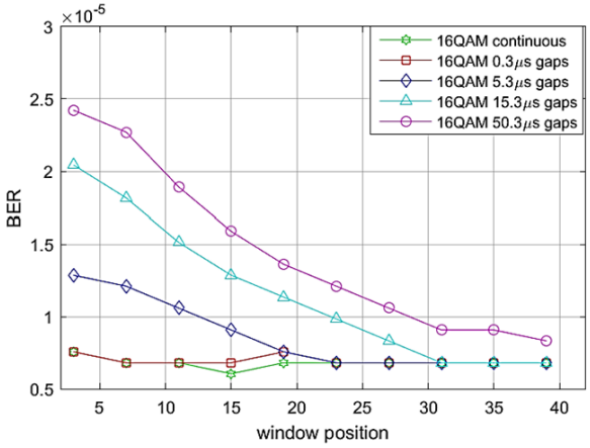

Figure 5-19: BER versus window position for various gap durations @ OSNR = 25 dB with 12-symbols window size.

The green curve represents the system performance in the continuous mode. As expected in this reference case, BER is constant whatever the sliding window position showing the continuous mode does not suffer from any transient. For the other configurations (corresponding to burst mode with various gaps durations), the BER is gradually improved as the window is shifted towards the end of the training sequence. We observe then that longer the gaps are, later the optimal BER is obtained. That means transients affecting the receiver become more and more important along with the gap increase. For each configuration, we choose the first position (from left side as shown in Figure 5-19) of the sliding window as the location where the BER reaches the performance of the continuous mode, i.e. window position 3 for gaps of 0.3 µs, window position 23 for gaps of 5.3 µs, window position 31 for gaps of 15.3 µs, and window position 39 for gaps of 50.3 µs. Note that a small residual BER penalty remains in the worst 50.3 µs configuration. Even we increase the number of training symbols to 70 and then move the sliding window to the end of training sequence; we cannot compensate the BER penalty. For the windows size, we have evaluated the 8-symbols and 4-symbols window size, the results show that the 8-symbols window can achieve the same performance as 12-symbols window while the 4-symbols window does not satisfy the channel equalization performance requirement since the window size is too short. When we perform the sliding window strategy using 8-symbols window, the optimal window position is not changed. The modification of the windows size does not have an impact on the optimal window position, since the optimal window position is only related to the transients generated by the optoelectronic components.

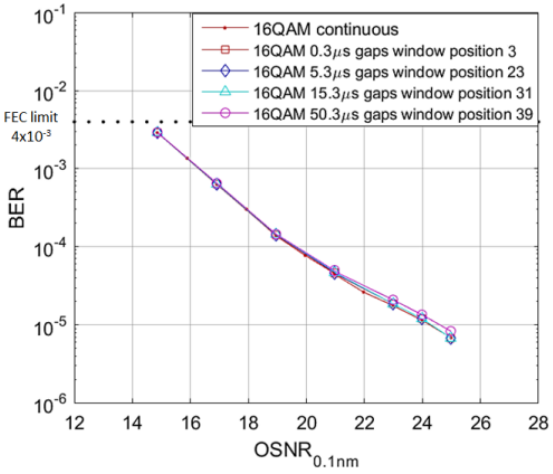

Figure 5-20: BER versus OSNR (in 0.1nm) for various gap durations at the optimal position of the sliding window.

At last, Figure 5-20 presents the BER versus OSNR sensitivity curves for the various configurations under study (continuous and burst modes) when the channel estimator is calculated with the optimal sliding window position determined previously. It can be observed that penalties are removed, and error floors of Figure 5-17 have disappeared. These results clearly demonstrate the efficiency of the new channel estimator based on a sliding window, as proposed here. The new channel estimator solution improves significantly the system performance suppressing in particular the error floor and allowing the use of standard coherent receivers for burst mode applications.

As we have discussed in chapter 2, TISA has a control plane. The control plane can manage the sending and receiving bursts and distribute the network resources. The control plane sends the grants to the source nodes to control the emissions of bursts. In grants, there is the information about the wavelength, the burst duration, the emission time of bursts, the modulation format, and the structure of the OFDM frame in the burst. It is known that the burst emission time, the propagation duration through the TISA network and the arrival time of burst at each destination are predictable in TISA as discussed in chapter 2, and thus the gaps durations at receiver side are also predictable. In addition, the receiver can give feedback to the control plane about the performance of each received burst. Therefore, the control plane can precisely control the transmission of each burst and can get the performance of each burst.

Experimental results show that the 50 training symbols are not always necessary. The window can be placed in the middle of the sequence of training symbols in certain situations (ex. the sliding window starts at position 31 when the gaps size is 15.3 µs) to obtain optimal performance. So we can reduce the number of inserted training symbols and thus improve the usable rate through the control plane.

A possible process is described in the following. First, the control plane has to be able to collect all information about the number of training symbols. Once the grants are defined, the

duration of a gap at the receiver is predictable. Then, the performance of the received burst is returned by the receiver to the control plane. Thus, the number of training symbols required for each link from a source to a destination is known by the control plane. And then, the control plane is able to update the grants to control the structure of the OFDM frame inserted into a burst. The grants are sent to source nodes to change the number of training symbols inserted for different point-to-point links (from sources to destinations). After that, the bursts have only the necessary number of training symbols. This solution allows modifying the size of the training sequence inserted using the control plane. Thus TISA can adapt the burst to the transmission conditions (the busy links and the less busy ones) to achieve optimal performance and make better use of network resources.

5.5 Conclusion

In this chapter, the feasibility of the TISA network has been demonstrated. Both DP-QPSK and DP-16QAM modulation formats have been evaluated. For the DP-QPSK format, only 0.3 dB penalty at BER 10^{-5} is measured. For the DP-16QAM signal, a maximum ~0.8 dB penalty at BER 10^{-5} compared to the continuous mode appears. This work has been published in paper [7].

The impact of the optical filter bandwidth, frequency detuning as well as the size of the guard band between two consecutive sub-bands have been evaluated. We have also evaluated the flexibility in the time domain of TISA: bursts of 9.7 µs (instead of 4.7 µs originally) with 0.3 µs guard time have been evaluated. The results show that the longer bursts with DP-QPSK format have the same performance as the bursts of 4.7 µs. For the longer bursts with DP-16QAM format, the first frames have a worse performance than the two other frames due to the signal gaps before the received signal (which generate transients at the receiver level). Then in order to mitigate the penalties related to the transients occurring in the receiver working in the burst mode, a novel OFDM training sequence strategy based on a sliding window has been proposed and evaluated experimentally with the DP-16QAM OFDM format. The new channel estimator solution improves significantly the system performance suppressing in particular the error floor and allowing the use of standard coherent receivers for burst mode applications. Moreover, with the help of control plane, this new channel estimator allows dynamically modifying the number of training symbols. Thus we can adapt the burst architecture to the transmission condition and optimize their filling. This investigation has been published in reference [8]. All these good results validate the TISA solution (optical aggregation/disaggregation and transparent routing of data regardless of their modulation format and bit rate) and its ability to perform a flexible allocation of resources in the optical domain.

This first experimental demonstration validates the TISA solution, but the performance could be improved if the TISA network parameters were perfectly optimized. Based on the experimental validation of the TISA solution, a qualitative discussion of performance improvement through the

network parameters modification is given here. As TISA has the flexibility in both temporal and spectral domains, the parameters modifications have to be considered in both domains.

In the spectral domain, we can modify: the guard band between two adjacent sub-bands, the optical bandwidth of the burst signal and the sub-band spacing. The sub-band spacing is the distance between the central frequencies of two consecutive sub-bands, and thus it equals to the sum of guard band and optical bandwidth of the burst signal. The guard band is used to avoid crosstalk between two adjacent sub-bands. Two guard band configurations - 3.33 GHz and 1.33 GHz - have been evaluated in section 5.2. No significant difference between these two configurations has been noticed. So, we could reduce further the bandwidth of the guard band in order to improve the spectral efficiency. Concerning the optical bandwidth of the burst signal, only one configuration (6.67 GHz) has been evaluated in our test-bed. The performance of the DACs embedded into the Arbitrary Waveform Generator (9 GHz 3-dB bandwidth and 12 GSa/s) explains why we have not been able to play further with the OFDM signal bandwidth. Generating sub-bands of ~4 GHz bandwidth represented a good trade-off. Aliasing phenomena prevented us to use signal more than ~5-6 GHz. However, this signal bandwidth limit is a particular case in our laboratory, which does not adapt to the real network. In TISA solution, the bursts coming from different source nodes is assembled in the MB-OFDM combiner, resulting in a multi-band burst occupying 50 GHz. In our test-bed, 4 source nodes are connected to one MB-OFDM combiner, thus the sub-band spacing should be less than 12.5 GHz. Besides this configuration, it would have been possible to insert 5 sub-bands in the 50 GHz spectral slot authorized by the core node. The high resolution optical filter used in the sub-band separator would have been compatible with this configuration using 5 sub-bands of 8 GHz separated by 1 GHz guard-band.

The increasing need for flexibility can motivate to play with the burst duration in the TISA network, as it is currently done in the IP router (Note that the dream of opticians would be to have an all-optical IP network, and OBS network constitute a first step towards this objective). With small time slot durations, it is possible to change the signal gaps at the receiver side from large gaps into several smaller ones with the careful control of the control plane and the sacrifice of the corresponding latency. As the TISA performance penalty is related to the gaps duration (as shown in the section 5.4), small time slot duration configuration has the potential to improve the TISA performance. However, there are also some constraints that force to lengthen the time slot duration. As discussed in chapter 2, 0.3 μs guard time between two successive bursts is necessary to cover the synchronization error and wavelength switching time. Therefore, long time slot durations will improve the channel filling. The 5 μs time slot configuration as chosen in this thesis is a good choice. We can set the TISA solution to a no-time slotted solution (which means source node can generate a burst with various durations) using what is called time stamp. This solution will increase largely the complexity of grants calculation at the control plane level, since a new variable parameter (burst

duration) should be taken into account during the grants calculation. Since it is potentially difficult for the control plane to optimize the network resource allocation with this configuration, we suggest keeping the TISA network as a time slotted solution.

Besides the parameters in the spectral and time domains, we can also improve the performance through the optimization of the OFDM frame structure. At first, we can reduce the CP length. The CP was designed for 1000 Km transmission distance as discussed in chapter 3, which is very long for a metro/regional European transport network. Consequently, it would have an interest to better optimize the CP with respect to the transmission reach in order to reduce OFDM overheads. Concerning the training sequence, as the sliding window strategy can be applied in TISA, the training sequence length could be adjusted automatically with the control plane, as explained before in this chapter 5.

Concerning the application of the TISA approach to a full-scale optical transport network, further improvements could be expected from the hardware implemented. For instance, the fast tunable lasers with low phase noise constitute critical devices. In our test-bed, a fast tunable laser is able to generate 4 different wavelengths. In a full-scale network, the fast tunable laser should be able to generate 320 different wavelengths (80 channels in C-band, and 4 sub-bands in each channel). As a result, the cost and power consumption of fast tunable lasers could be very important. TISA would gain a lot from a photonic integration of fast tunable lasers with low phase noise, in terms of performance, cost and power consumption. The core nodes constitute also critical devices: each port is equipped with WSSs/demultiplexers, couplers/multiplexers and EDFAs. The scaling-up (with the increase of the port number) could results in prohibitive cost and strong increase of energy consumption. Finally, the availability of low-cost high spectral resolution optical filters is not today ensured as their industrialization is not today effective.

Reference

[1] Finisar, “Wavelength Selective Switch (WSS)”, [available online], https://www.finisar.com/roadms-wavelength-management/10wsaaxxfll

[2] F. Yan, W. Miao, O. Raz and N. Calabretta, "Opsquare: A flat DCN architecture based on flow-controlled optical packet switches," in *IEEE/OSA Journal of Optical Communications and Networking*, vol. 9, no. 4, pp. 291-303, April 2017.

[3] C. Raack, R. Wessälly, D. Payne and M. Ruffini, "Hierarchical versus flat optical metro/core networks: A systematic cost and migration study," *2016 International Conference on Optical Network Design and Modeling (ONDM)*, Cartagena, 2016, pp. 1-6.

[4] Yenista, “Tunable Filter with Adjustable Bandwidth”, [available online], https://yenista.com/IMG/pdf/XTA-50_DS_2-1v1-1.pdf

[5] Enablence, “100GHz WAVELENGTH DIVISION MULTIPLEXER/DEMULTIPLEXER”, [available online], http://www.enablence.com/media/mediamanager/pdf/18-enablence-datasheet-ocsd-awg-standard-100ghzmultidemulti.pdf

[6] S.L. Jansen, "Long-haul transmission of 16× 52.5 Gbits/s polarization-division-multiplexed OFDM enabled by MIMO processing," *Journal of Optical Networking*, **7**, 173-182 (2008).

[7] B. Han, P. Gavignet and E. Pincemin, "First Experimental Demonstration of the Time and Spectral Optical Aggregation Solution, " *European Conference on Optical Communication (ECOC),* 2017.

[8] B. Han, P. Gavignet and E. Pincemin, "A Novel OFDM Training Sequence Strategy Based on a Sliding Window for Optical Burst Traffic, " *Optical Fiber Communications Conference and Exhibition (OFC), 2018*.

Conclusion and perspectives

Conclusion

The TISA solution has been proposed in order to improve the filling ratio of the optical network resources, to increase the flexibility/agility of existing optical transport networks in particular in terms of resource allocation while optimizing the CAPEX and OPEX costs. In this thesis, we have built a proof of concept and demonstrate for the first time experimentally the feasibility of the TISA approach.

At first, we have implemented a CO-MB-OFDM optical burst transmitter adapted to the TISA solution. Since the transmitter that generates the optical bursts in TISA has to operate at various wavelengths, a fast tunable laser with narrow linewidth is necessary. The laser shall have a linewidth of ~100 kHz to satisfy the coherent detection requirements; the switching time has to be shorter than 100 ns with the purpose of changing rapidly the wavelength from one burst to another. However, current existing commercial lasers cannot meet these two criteria at the same time: lasers with a sufficient narrow linewidth do not have a fast switching time and vice versa. In order to implement the burst mode transmitter, we have proposed a solution combining SOAGs and ECLs to realize a fast tunable (less than 100 ns) laser source with narrow linewidth (~100 kHz) ensuring low phase noise. Then, two burst mode transmitters and two coherent receivers have been implemented. The Tx/Rx pairs have been validated through BER versus OSNR measurements when performing both DP-QPSK and DP-16QAM OFDM bursts signals in the back-to-back configuration. Through the comparison of the performance among the Tx/Rx pairs, an investigation on the quality and compliance with the burst mode of the various opto-electronic components used in the experimental proof of concept have been carried out: it concerns linear RF-drivers in the transmitter, or TIAs in the receiver. Compared to the continuous flow configuration, only 0.3 dB penalty at BER 10^{-5} is introduced with the DP-QPSK MB-OFDM burst signal; 0.3 dB at BER 10^{-5} is introduced for the second frame and ~0.8 dB penalty at BER 10^{-5} is introduced for the first frame preforming DP-16QAM MB-OFDM burst signal. These results validate the proposed transmitters and coherent receivers and suggest the best choice of opto-electronic components for the burst mode operation.

After that, we have realized a centralized control plane for the TISA network on FPGAs with real-time controller. The control plane is in charge of calculating the scheduling patterns, called grants, which are used to control the burst emission times and sub-band allocation for each source node. Through the careful scheduling of grants, a lossless routing is performed making the TISA solution still more attractive. In our test-bed, the grants are pre-programmed and the control of the

burst emission at source nodes is implemented in real-time. Compared to the TWIN approach, a specific control process on the burst emission times is implemented in the control plane in order to align the bursts coming from different source nodes at the MB-OFDM combiner.

Thereafter, we have extended our experimental test-bed by introducing the routing devices such as MB-OFDM combiner, core node and sub-band separator. The TISA network performance has also been evaluated using both DP-QPSK and DP-16QAM CO-OFDM signal bursts. Only 0.3 dB penalty at BER 10^{-5} is introduced with the DP-QPSK modulation format operating at 26.6 Gbps compared to the continuous flow configuration. For the DP-16QAM signal bursts two OFDM frames have been generated in a burst: this stratagem allows us to evaluate the potential impact of the operation in burst mode of our transceivers. Only 0.3 dB penalty at BER 10^{-5} is measured for the second DP-16QAM frame operating at 53.2 Gbps and a maximum ~0.8 dB penalty at BER 10^{-5} is measured for the first frame compared to the continuous flow configuration. Compared to the experimental results carried out in the back-to-back configuration, the insertion of the routing devices does not introduce significant penalty. These good results validate the TISA solution (optical aggregation/disaggregation and transparent routing of data regardless of their modulation format and bit rate) and its ability to perform an optimal allocation of the network resources on the basis of optical burst, which fits well with our initial objectives and requirements.

Furthermore, we have observed that there is a difference of the performance between the two DP-16QAM frames that constitutes each data burst. Due to the burst traffic nature, the coherent receivers detect regularly variable signal gaps (i.e. from several µs to several tens of µs). As the coherent receivers have been originally designed to receive continuous OFDM flows, the presence of variable signal gaps stresses the optoelectronic components inside the receiver (e.g. Trans-Impedance Amplifiers (TIAs)): these gaps give birth to temporal transients that impact the receiver performance with DP-16QAM. Note that we did not observe performance degradation due to transients with DP-QPSK modulation format. In order to mitigate the penalties in the electrical domain without modifying the optoelectronic components, we have proposed a novel OFDM training sequence strategy based on a sliding window. We have evaluated experimentally this novel strategy using DP-16QAM format. The experimental results show that the proposed channel estimator solution improves significantly the system performance suppressing the error floor and allowing the use of standard coherent receivers with burst mode application. This proposed training sequence strategy is expected to achieve similar improvement on higher order QAM (32, 64…) formats. In addition, this strategy can be integrated with the control plane: thanks to the control plane, the length of the training sequence in the OFDM frame can be dynamically adapted to the link conditions (i.e. traffic saturation or not involving the absence or the presence of signal gaps).

Perspectives

Based on the obtained experimental results, observations, and achievements, the future research work can be oriented towards new items.

At first, some experimental tests could be carried out to complete the evaluation of the TISA solution. Transmission fibers could be added between the various nodes of the TISA network, and we could thus better evaluate the maximum transmission distance allowed by such OBS networks. Due to limited experimental means, we have associated together in the TISA network only few core and edge nodes. We could in the future investigate more deeply the impact of a higher number of nodes over the performance of signals propagating in the network. To do that in the absence of new experimental means, a programmable optical filter could be used to study the effect of a cascade of core and edge nodes and evaluate the number of nodes that can be crossed. Afterwards, as the OFDM signal offers the possibility to implement bit and power loading, it could be interesting to investigate the benefits brought by this technology over the number of core and edge nodes that can be cascaded and over the global data-rate that can be transported in the TISA network. The impact of the frequency detuning of the high resolution optical filters used in the TISA network node could be also particularly relevant. Furthermore an extensive performance comparison between different modulation formats such as Nyquist-WDM, Offset-QAM OFDM, and standard OFDM (as implemented in this thesis) could be performed in order to know if one or the other of these formats is better adapted to the constraints of the TISA network. Besides the experimental evaluation done here, numerical simulations could be carried out to give a clearer idea of the relevance to use the TISA approach for a wide-area optical transport network. The TISA approach would be certainly very interesting also in the context of intra data center or X-haul networks with simpler transmission techniques (i.e using for instance on-off keying modulation).

Moreover, the components and sub-systems used in the TISA test-bed are based on discrete devices, which involves performance limitation due for instance to insertion loss. The power consumption is also another parameter that has to be precisely controlled if we want that optical technologies be really competitive with respect to the electronic ones. It is the reason why the TISA approach would gain a lot to be integrated on Photonic Integrated Circuit (PIC). For example, the integration on PIC of fast tunable lasers, IQ modulators and separators could be very beneficial to a potential industrialization of the TISA solution.

TISA could also benefit from a simplification of the modulation technology used: indeed nothing stands in the way to use on-off keying modulation at 10 Gbps combined with direct detection. It would furthermore involve a non-negligible cost reduction of the TISA network.

Based on the experimental test-bed that we have implemented, an automatic control plane layer could be realized to automatically and remotely control all the devices of the TISA network. In this context, Software Defined Networking (SDN) could be of high interest to interface the TISA network. SDN should be able to provide some interesting functionalities such as service setup and teardown, dynamic network reconfiguration for the TISA solution to react for instance rapidly to network churn or new traffic demands.

Furthermore, we could imagine that when further progresses will have been achieved, the TISA solution works as an alternative to IP routers one day: packet switching would not require any

more optical-to-electrical conversions and would be supported entirely by the optical network layer. This idea constitutes a dream that could come true in a next future.

Publications

Papers

[1] L. Yi; W. Wei; Y. Jaouën; M. Shi; B. Han; M. Morvan; W. Hu, "Polarization-Independent Rectangular Microwave Photonic Filter Based on Stimulated Brillouin Scattering", in *Journal of Lightwave Technology*, vol. 34, no. 2, pp. 669-675, Jan.15, 15 2016.

[2] P. Gavignet, E. Le Rouzic, E. Pincemin, B. Han, M. Song, L. Sadeghioon "Time and Spectral optical Aggregation for Seamless Flexible Networks", Photonics in Switching, 2015.

[3] B. Han; P. Gavignet; E. Pincemin; T. Guillossou; M. Cresseaux; D. Le Brouster; B. Haentjens; Y. Jaouen, "Low phase noise CO-MB-OFDM optical burst transmitter for time and spectral optical aggregation," *2017 Optical Fiber Communications Conference and Exhibition (OFC)*, Los Angeles, CA, 2017, pp. 1-3

[4] B. Han, P. Gavignet and E. Pincemin, "Low phase noise optical burst transmitter for TIme and Spectral optical Aggregation solution," *2017 19th International Conference on Transparent Optical Networks (ICTON)*, Girona, 2017, pp. 1-6.

[5] B. Han, P. Gavignet and E. Pincemin, "First Experimental Demonstration of the Time and Spectral Optical Aggregation Solution, " *European Conference on Optical Communication (ECOC),* 2017.

[6] B. Han, P. Gavignet and E. Pincemin, "A Novel OFDM Training Sequence Strategy Based on a Sliding Window for Optical Burst Traffic, " *Optical Fiber Communications Conference and Exhibition (OFC), 2018*.

Patents

[1] B. Han, P. Gavignet, E. Pincemin and M.Song "Multi-wavelength coherent receiver for optical burst switching networks using colored bursts". PCT/FR2016/052001.

[2] B. Han, P. Gavignet and E. Pincemin, "Plan de commande pour un réseau optique de transmission de rafales multi-porteuses de données à adaptation dynamique de séquence d'apprentissage", FR1851325.

Réseaux de transport optique flexibles : apport de la combinaison des domaines temporel et spectral pour adapter la granularité des ressources optiques aux besoins de l'opérateur

RESUME :

Les demandes de trafic de plus en plus importantes lancent un grand défi aux opérateurs de télécommunications qui souhaitent augmenter toujours plus la capacité des réseaux tout en réduisant les coûts CAPEX et OPEX. Afin de répondre à ces défis, l'amélioration de la flexibilité de l'allocation des ressources réseau, possiblement associée avec un routage du trafic IP directement au niveau de la couche optique ont été identifiés comme un axe de recherche majeur. Il a été prouvé que les solutions de commutation optique sous la longueur d'onde ont la capacité d'améliorer la flexibilité du réseau et d'en réduire la consommation d'énergie notamment en supprimant les interfaces de conversion optique-électrique-optique. Elles peuvent être réalisées dans les domaines temporel et/ou spectral. L'un des objectifs de cette thèse était donc d'étudier la flexibilité apportée par la combinaison de ces deux types de solution. Dans ce contexte, l'approche « TIme and Spectral Optical Aggregation (TISA) » a été proposée. TISA permet d'effectuer une agrégation purement optique avec une granularité la plus fine possible grâce à la combinaison des domaines temporel et spectral. Le principal objectif de cette thèse était la réalisation en laboratoire de la preuve du concept TISA. Pour ce faire, nous avons conçu et réalisé un émetteur optique OFDM multi-bandes à haute pureté spectrale en utilisant un laser rapidement accordable. Ce laser est mis en œuvre en combinant des lasers à cavité externe à faible bruit de phase et des portes optiques à base d'amplificateurs à semi-conducteurs (SOAs). Cet émetteur est capable de générer des rafales aux formats DP-QPSK et DP-16QAM portés par la modulation OFDM tout en introduisant une petite pénalité sur la performance par rapport au mode continu. Ces signaux ont été analysés après transmission à travers un réseau TISA. Les taux d'erreurs binaires obtenus montrent une pénalité inférieure à 1 dB pour les deux formats de modulation. En effet, un récepteur cohérent conçu pour le trafic continu n'est pas parfaitement adapté au trafic en mode rafale ce qui entraîne une pénalité sur les performances système. Un nouvel estimateur de canal utilisant une fenêtre glissante a été proposé pour les trafics en rafales de signaux OFDM de type DP-16QAM. Les résultats expérimentaux montrent que le nouvel estimateur de canal et l'égaliseur associé apportent un gain significatif de performance et la suppression du plancher d'erreur. Ces résultats montrent la faisabilité de la solution TISA et sa capacité à effectuer une agrégation/désagrégation tout-optique et un routage transparent tout en offrant une granularité de sous-longueur d'onde dans les domaines temporel et spectral.

Mots clés : commutation optique, OFDM, commutation optique par rafales, communication optique, détection cohérente.

Flexible optical transport networks: benefits of the combination of time and spectral domains to adapt the granularity of optical resources to the needs of operators

ABSTRACT:

The ever increasing traffic demand is a big challenge for the operators in order to increase the network capacity while lowering CAPEX and OPEX costs. To address these challenges, it is expected to increase the flexibility of the network resources allocation while realizing directly the IP traffic routing in the optical layer. It has been proved that sub-wavelength optical switching solutions have the capability to improve the flexibility of the network as well as the potential to reduce the power consumption by removing the optical-electrical-optical conversion interfaces. Sub-wavelength optical switching solutions can be performed in time and/or spectral domains. One of the objectives of this thesis was to study the benefits brought by the combination of these two types of solutions. The "TIme and Spectral optical Aggregation (TISA)" approach has thus been proposed to allow a purely optical aggregation with the finest possible granularity thanks to the combination of temporal and spectral domains. The main objective of this thesis was to realize a proof of concept of the TISA concept to demonstrate experimentally the feasibility of the TISA solution. To accomplish this objective, we have designed and realized a multi-band OFDM optical burst transmitter with a narrow linewidth fast tunable laser. This laser has been implemented by combining external cavity lasers with semiconductor optical amplifier (SOA)-based optical gates. The transmitter is able to generate OFDM bursts in both DP-QPSK and DP-16QAM modulation formats while introducing a small penalty compared to the continuous flows configuration. We have performed the transmission of these bursts through the TISA network and have measured the bit error rates, which show less than 1 dB penalty for both modulation formats. Since the coherent receiver designed for continuous traffic is not suited for burst traffic, a penalty is observed in the system performance when transmitting DP-16QAM OFDM bursts. Therefore, a novel channel estimator/equalizer, using a sliding window, for the DP-16QAM OFDM bursts has been proposed: it brings a significant performance gain. Our results clearly show the feasibility of the TISA solution and demonstrate the ability to perform a purely optical aggregation/disaggregation and transparent routing while offering a sub-wavelength granularity in both time and spectral domains at the optical layer level.

Keywords: optical switching, OFDM, optical burst switching, optical communication, coherent detection.